The effect of fluorine substituents in conjugated polymers

Lvenich, Peter Wilfried

The Effect of Fluorine Substituents in Conjugated Polymers

Peter Wilfried Lövenich

A thesis submitted for the degree of Doctor of Philosophy at the University of Durham

Department of Chemistry
University of Durham

October 2001

Abstract

The Effect of Fluorine Substituents in Conjugated Polymers

Peter Wilfried Lövenich Ph.D. Thesis October 2001

A new route to a well-defined block copolymer with alternating PEO-solubilising groups and fluorinated distyrylbenzene units was established. The Horner Wittig reaction was used as the polycondensation reaction. The non-fluorinated analogue of this block copolymer was prepared via the Wittig reaction. Both polymers were soluble in chloroform and free-standing films could be cast from solution. The position of the HOMO and LUMO energy levels of these two materials were determined by a combination of cyclic voltammetry, UV photoelectron spectroscopy and UV/Vis absorption spectroscopy. The presence of fluorine substituents on the distyrylbenzene unit had no influence on the HOMO-LUMO band-gap (3.0 eV). However, the position of these two energy levels relative to the vacuum level was shifted to higher energies (0.85 eV shift) in the case of the fluorinated block copolymer. The photoluminescence quantum efficiency of the fluorinated block copolymer was 17%, that of the non-fluorinated block copolymer was 34%. The former was used as the electron conducting layer in a light emitting diode with poly(*p*-phenylene vinylene) as the emissive layer. The latter was used as the emissive layer in light emitting diodes. Luminances over 2000 cd/m^2 were observed for devices based on the non-fluorinated block copolymer using indium tin oxide as the anode and aluminium as the cathode. The luminescence efficiency of such devices was as high as 0.5 cd/A, corresponding to an internal quantum efficiency of 1.1%.

Furthermore, an oligo(*p*-phenylene vinylene) was synthesised that contained two terminal fluorinated benzene rings and two central non-fluorinated benzene rings, all connected by vinylene bridges. This material aggregated in a 'brickwall' motif, where each molecule overlaps with two halves of molecules in the row above and below. The structure of this J aggregate is due to aryl-fluoroaryl-interactions and was demonstrated by X-ray crystal structure analysis.

Memorandum

The work reported in this thesis has been carried out in the Interdisciplinary Research Centre in Polymer Science and Technology in the Department of Chemistry at the University of Durham, between October 1998 and October 2001. This work has not been submitted for any other degree and is the original work of the author, except where acknowledged by reference.

Some parts of this work have been published as joint publications:

1) W. James Feast, P. Wilfried Lövenich, Horst Puschmann and Carlo Taliani, *Chem. Comm.* **2001**, 505

2) Franco Cacialli, Richard H. Friend, W. James Feast, P. Wilfried Lövenich, *Chem. Comm.* **2001**, 1778

Statement of Copyright

Financial support

I gratefully acknowledge the funding provided by the European Union Research Training Networks SELOA and LAMINATE.

Acknowledgements

In 1998, when I left Germany to start a Ph.D. in Britain, some people were sceptical. However, the last three years at the Department of Chemistry at the University of Durham have been a very successful – both on a scientific and on a personal basis. I can recommend the experience to anybody who is considering this option. To a great extent this success has been due to the support of my supervisor *Professor W. James Feast*, of whom many have expressed their envy of my opportunity to work in his group! Also, I would like to acknowledge the support of all the members of the IRC in Polymer Science and Technology at Durham; many of them have become friends and I hope to stay in contact with them. I am grateful to many members of staff at the Chemistry department in particular *Dr. Alan Kenwright, Dr. Horst Puschmann, Prof. Randal Richards, Dr. Lian Hutchings, Dr. Dave Parker and Mrs Jarika Dostal.*

I am grateful to many collaborators in the LAMINATE network, in particular, *Dr. Franco Cacialli* and *Prof. Richard Friend* at the Cavendish Laboratory, Cambridge, for their help with device fabrication. I am also grateful to *Dr. Michele de Jong* and *Prof. William R. Salaneck* at Linköping University, Sweden, for the photoelectron spectroscopy measurements and *Prof. Carlo Taliani* at the Institute for Molecular Spectroscopy, Bologna, for fruitful discussions.

I would like to thank my parents; meinen Eltern danke ich für die Unterstützung während der letzten neun Jahre.

Finally, I would like to thank my girlfriend *Catherine* who has helped me with the editing of this work.

Table of Contents

1 Introduction

1.1 Conjugated Polymers

Traditionally, organic polymers have been considered as insulators. They are used in the electronics industry for the insulation of metallic conductors, since conventional polymers have a large band gap between the valence band and the conducting band.[1] However, polymers with a conjugated backbone have a much smaller band gap. This is due to the delocalisation of π-bonding and π^*-antibonding electron orbitals along the polymer backbone.[2] Conjugated polymers have low ionisation potentials (IPs) and high electron affinities (EAs) and can therefore be oxidised or reduced more easily than conventional polymers. Pure conjugated polymers are usually not conducting but can be converted to highly conducting materials by treatment with an oxidising or reducing agent; in analogy to inorganic semiconductors these conversions are also called p-doping or n-doping, respectively.

The simplest conjugated polymer is polyacetylene (PA)(*Figure 1.1.1a*). High molecular weight PA was first reported in 1958 by Natta *et al.*[3] It was prepared in the form of a black powder using an $Al(Et)_3/Ti(OPr)_4$ initiator system. Berets and Smith reported in 1968 that the doping of PA powder with oxygen or chlorine increases the conductivity.[4] In the 1970's Shirakawa *et al.* developed a synthesis for PA films using high concentrations of the $Al(Et)_3/Ti(OPr)_4$ type catalyst.[5,6] They were able to show that treatment of such films with halogens increased the conductivity by eight orders of magnitude.

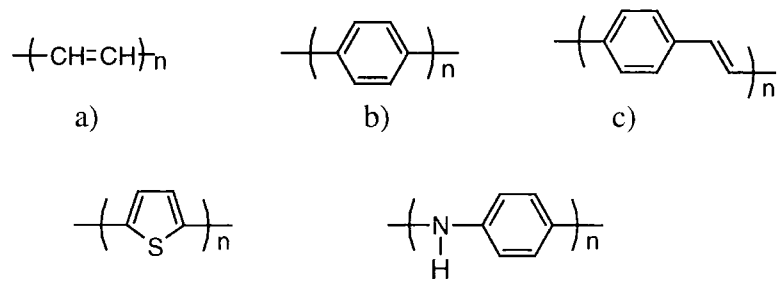

a) b) c) d) e)

Figure 1.1.1 Conjugated polymers. a) polyacetylene, b) poly(p-phenylene), c) poly(p-phenylene vinylene), d) polythiophene, e) polyaniline

In 1980 Edwards and Feast reported the synthesis of a soluble and well defined precursor polymer *via* the ring opening metathesis polymerisation (ROMP) which could be converted to PA films by thermal treatment (*Figure 1.1.2*).[7,8] In the so-called Durham precursor route, the precursor polymer could be purified and processed by conventional solution methods. During the thermal conversion hexafluoro-*o*-xylene was released and PA formed. The initially generated *cis* double bonds were isomerised to *trans* double bounds.

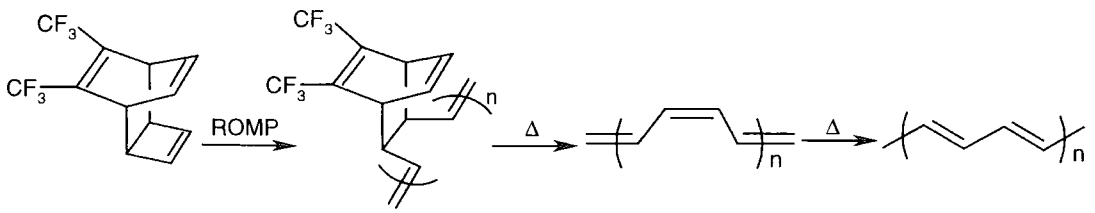

Figure 1.1.2 The Durham precursor route to PA.

Poly(*p*-phenylene vinylene) (PPV) was first prepared in 1960 by McDonald and Campbell *via* the Wittig reaction (*Figure 1.1.3*).[9] A 1:1 mixture of terephtalaldehyde and *p*-xylylene-bis(triphenylphosphonium chloride) was treated with base and gave a yellow powder. The molecular weight of PPV prepared by this route was low and the polymer insoluble.

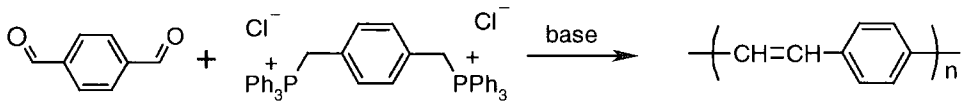

Figure 1.1.3 The Wittig route to PPV.

In 1966, Wessling and Zimmermann developed a precursor route, which allowed the preparation of oriented high molecular weight polymer films (*Figure 1.1.4*).[10,11] A bis-sulfonium salt was treated with base giving rise to a quinodimethane intermediate. The presence of radical trapping agents lowered the molecular weight of the precursor polymer, suggesting that the polymerisation proceeds radically but anionic propagation can not be excluded.[11] The precursor polymer with one sulfonium group per repeat unit could be isolated and purified by dialysis. The number average molecular weight of this precursor was determined to be at least 100,000 g/mol. The precursor could be oriented and converted thermally to PPV films. This route is generally referred to as the Wessling route.

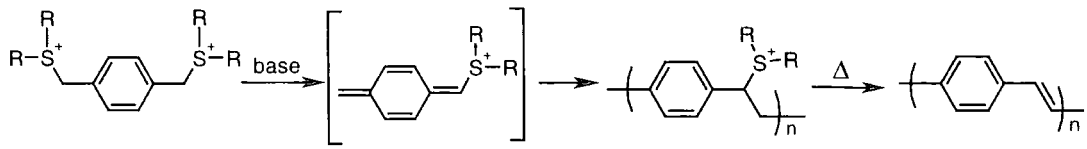

Figure 1.1.4 The Wessling route to PPV.

Also in 1966 Gilch and Wheelwright reported the synthesis of PPV based on the dehydrohalogenation of α,α'-dichloro-*p*-xylylene (*Figure 1.1.5*).[12] The reaction also proceeded *via* a quinodimethane intermediate, which polymerised to give poly(α-chloro-xylylene). This polymer intermediate could be isolated if a dilute solution of base is added slowly to an excess of α,α'-dichloro-*p*-xylylene. Using an excess of base or thermal treatment led to the fully conjugated polymer. This route is generally referred to as the Gilch route.

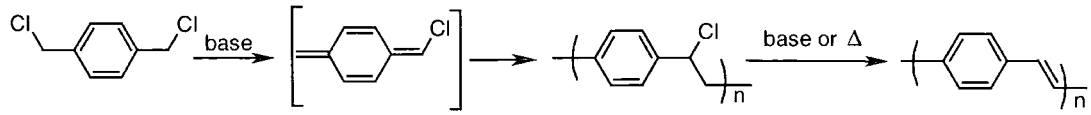

Figure 1.1.5 The Gilch route to PPV.

A large number of different conjugated polymers have been prepared including hydrocarbon polymers such as PA, poly(*p*-phenylene) (PPP) and PPV as well as heterocyclic polymers such as polythiophenes or polyaniline (*Figure 1.1.1*).[13] A range of applications for conjugated polymers are being investigated including their use in batteries, non-linear optics, field effect transistors and in photovoltaic and electroluminescent devices.[14]

1.2 Light emitting diodes

In 1990 Burroughes *et al.* demonstrated that conjugated polymers such as PPV are electroluminescent.[15] Since then much attention has been given to the synthesis and properties of PPV and the use of conjugated polymers in light emitting diodes (LEDs).[16] Today, LEDs based on polymers offer an alternative to the established

display technologies based on cathode-ray tubes and liquid-crystal displays, since polymer coating techniques are cheap and can be applied to large areas.

In a simple LED the fluorescent polymer is sandwiched between two electrodes.[17] A metal of low work function, such as aluminium or calcium, is usually used as the cathode. The work function of a solid describes the minimum energy that is required to remove an electron from the surface of the solid into the vacuum. The work functions of aluminium and calcium are 4.3 eV and 2.9 eV, respectively. These metals can donate electrons readily into the lowest unoccupied molecular orbital (LUMO) of the conjugated polymer. Indium-tin-oxide (ITO) is the most prevalent material used as the anode because of its high work function (4.5-5.1 eV) and its transparency in the visible region.

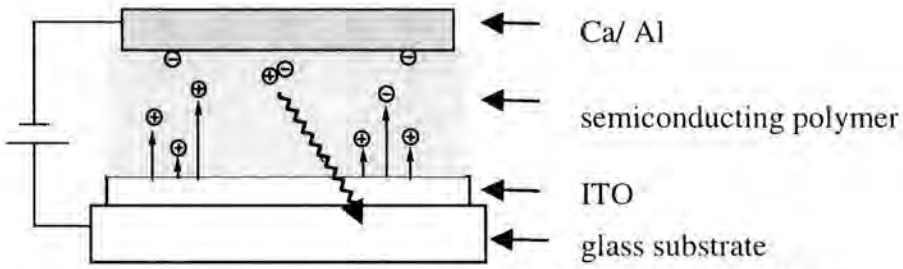

Figure 1.2.1 Schematic representation of a light emitting diode.

When the diode is biased sufficiently, positive and negative charges are injected from opposite electrodes. PPV is oxidised at the anode where radical cations ('holes') are created and it is reduced at the anode where radical anions ('electrons') are created. These radical cations and radical anions move towards the oppositely charged electrode. They can capture one another within one polymer chain and form a neutral bound electronically exited state. This so-called exciton is confined to the polymer chain. The spin wave-function of the exciton can be a singlet or a triplet. Spin allowed radiative emission is only from the singlet exited state.[2] Since the exchange energy between the singlet and the triplet state is large due to the confinement of the exciton the triplet excitons do not produce light emission. Only the singlet excitons give rise to electroluminescence.

A simple single layer device consisting of an emissive polymer sandwiched between an ITO glass substrate and a metal is denoted as ITO/polymer/metal. Offsets between the work function of the anode and the highest occupied molecular orbital (HOMO) of the polymer or between the work function of the cathode and the lowest unoccupied molecular orbital (LUMO) of the polymer lead to barriers for

hole-injection or electron-injection, respectively. *Figure 1.2.2 (left)* shows energy levels in the device ITO/PPV/Al. The levels are measured relative to the vacuum level. The values for these energy levels recorded in the literature vary slightly and errors of ±0.2 eV should be kept in mind.[2,18] However, it becomes clear that the HOMO of PPV aligns fairly well with the work function of ITO, whereas a large offset is found between the work function of aluminium and the LUMO of PPV. Therefore, the injection of holes predominates over the injection of electrons. If the injection rates of holes and electrons are unequal, the excess carriers of one sign pass through the polymer without recombination, contributing to the current but not to the emission.[17] The efficiency of the LEDs based on PPV with aluminium as cathode, as it was recorded in 1990, is of the order of 5×10^{-4} photons generated per electron injected.[15] This corresponds to an internal quantum efficiency of 0.05%.

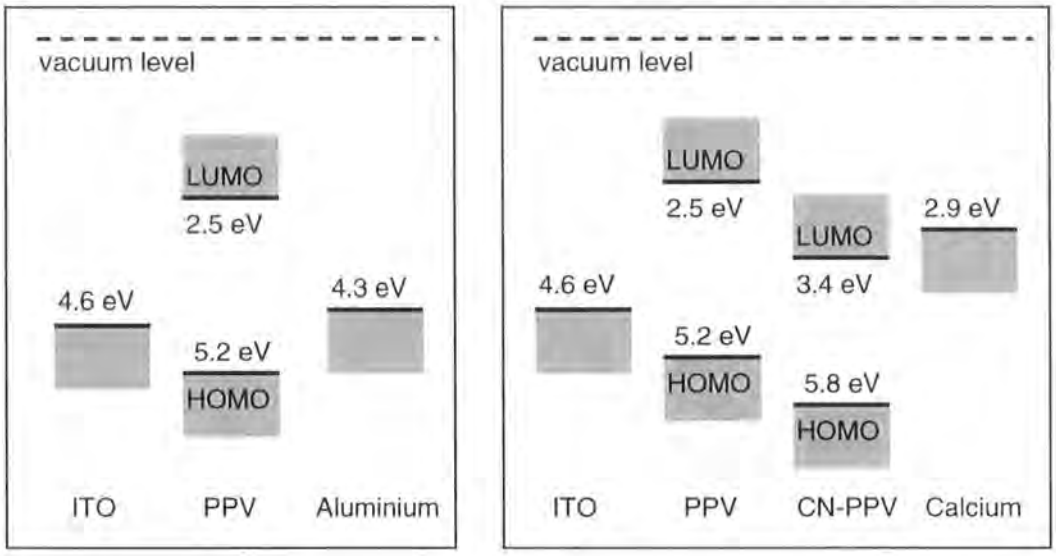

Figure 1.2.2 Energy levels for the device ITO/PPV/Ca (left) and ITO/PPV/CN-PPV/Ca (right). All values contain an error of ±0.2 eV.

To increase the efficiency of such a device, electron injection has to be boosted. This can be achieved by the introduction of an additional layer. For example the LUMO of a cyano-substituted PPV (CN-PPV, which will be explained in more detail in the next section) matches well with the work function of Ca. Very high efficiencies of 4% have been achieved for double layer devices such as ITO/PPV/CN-PPV/Ca.[2] *Figure 1.2.2 (right)* shows the energy levels of the two polymers and the work functions of the electrodes. The good match of the energy levels at the cathode and the anode becomes apparent. The use of a double layer

structure can have a further beneficial effect; recombination of the holes and electrons is likely to occur near the interface of the two polymers since one is a good hole carrier and the other one a good electron carrier and high densities of carriers are created on each side of the interface. This reduces the probability of exciton quenching by dissociation near the electrodes, which can reduce the efficiency of the device.[17]

Polymer LEDs are described in terms of the following characteristics:

- The electroluminescence (EL) spectrum together with the solid-state absorption and emission spectra of the polymer give an indication of the energy levels of the polymer. The colour of the emission is obviously an important factor for LEDs. The human eye has three sets of cells in the retina responding to blue (446 nm), green (555 nm) and red light (599 nm).[17] These three colours are required for a full-colour display.
- The photoluminescence (PL) quantum efficiency of the polymer is the ratio of emitted to absorbed photons when the polymer is irradiated with light.
- The internal quantum efficiency q_{int} is the ratio of the number of photons produced to the number of electrons flowing through the external circuit and is given by

  $$q_{int} = \gamma \, r \, \eta \, ,$$

  where γ is the ratio of excitons formed to the electrons flowing in the external circuit, r is the fraction of excitons formed as singlets and η is the efficiency of the radiative decay of the singlet excitons and therefore identical with the photoluminescence quantum efficiency.[19]
- The external quantum efficiency takes into account the fact that not all photons leave the device but some are internally reflected depending on the angle at which they hit the interface.[20] External efficiencies are therefore approximately a factor $2n^2$ smaller than internal efficiencies, where n is the refractive index of the polymer. In order to avoid the confusion between the two efficiencies and the uncertainty that is included when internal efficiencies are calculated from the measured external efficiencies, the value of brightness per unit of current (cd/A) instead of efficiencies is generally quoted in recent years, as it can be measured more reliably.

- The energy levels of the HOMO and the LUMO of the polymer together with the work functions of the electrodes determine the barriers for electron and hole injection.
- The brightness of the device is measured in candelas per square meters (cd/ m^2). A television screen typically has a brightness of about 100 cd/m^2.
- The turn-on voltage is the minimal voltage required to observe electroluminescence.
- The stability of LEDs is an important factor for consumer products. The shelf lifetime should be many years and the operational lifetime between 100 h and 10,000 h depending on the application.[21]

1.3 Derivatives of PPV

Changes in the chemical structure of PPV and its derivatives give rise to changes in the physical properties described in the previous section. The ability to tune these physical properties by manipulating the chemical structure of PPV has resulted in the synthesis of a great number of derivatives. Some examples of the different synthetic approaches to PPV derivatives and the resulting changes in the physical properties are given below.

PPV has an optical band gap of about 2.7 eV and emits in the yellow–green region of the visible spectrum with an emission maximum at 560 nm (2.2 eV). The solid state PL quantum efficiency of PPV is 27%.[22] The first report of electroluminescence by Burroughes *et al.* gives a quantum efficiency of 0.05%. Since then efficiencies of 0.1% have been reported for an ITO/PPV/Ca device.[23]

Shortly after the discovery of the electroluminescence of PPV in Cambridge, Heeger and Braun reported the use of a dialkoxy substituted PPV derivative in LEDs.[24] Poly[2-(2'ethylhexyloxy)-5-methoxy-1,4-phenylene vinylene] (MEH-PPV) was prepared *via* the Gilch route (*Figure 1.3.1*).[25] MEH-PPV is soluble in the conjugated form in organic solvents such as chloroform, THF or xylene. The EL and PL maxima of MEH-PPV are at 590 nm and therefore red-shifted relative to PPV. This is due to the electron-donating effect of the two alkoxy-groups. The PL

efficiency is 10 - 15%.[22] The authors report an internal quantum efficiency of 1% for a device of the form ITO/MEH-PPV/ Ca. This is a tenfold increase compared to the efficiency of PPV.

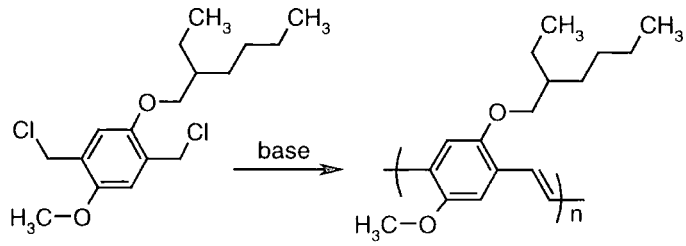

Figure 1.3.1 Synthesis of MEH-PPV via the Gilch-route.

A cyano-substituted PPV (CN-PPV) was first prepared by Hörhold *et al. via* the Knoevenagel reaction.[26] A terephtalaldehyde derivative is reacted with a benzene-1,4-diacetonitrile derivative. The resulting polymer is soluble due to the alkoxy side chains. The polymer has a much higher PL efficiency (48%) than PPV itself (27%).[22] The cyano-groups increase the electron affinity and the ionisation potential of the polymer (see *Figure 1.2.2*). Double layer ITO/PPV/CN-PPV/Ca devices of the form ITO/PPV/CN-PPV/Ca show the highest internal efficiencies (4%) recorded so far.

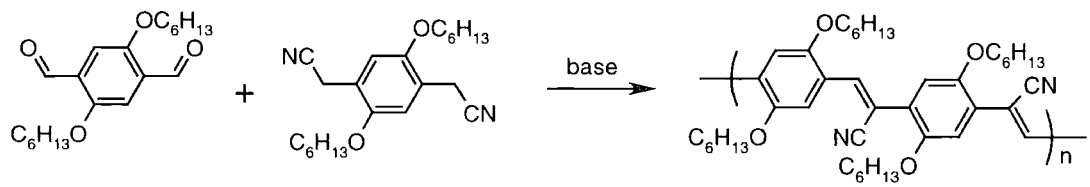

Figure 1.3.2 Synthesis of CN-PPV via the Knoevenagel reaction.

Processability of conjugated polymers can be achieved in several ways. So far the precursor route or the introduction of solubilising side chains on the conjugated polymer backbone have been discussed. It is also possible to use isolated chromophores in an otherwise non-conjugated polymer.[27] Such chromophores can be incorporated as side chains or within the polymer backbone. Fully conjugated polymers often contain a small amount of randomly distributed defects interrupting the conjugation and leading to a statistical distribution of conjugation lengths. In contrast, isolated chromophores have a precisely defined uniform length, which can be tailored to a specific emission wavelength. Polymers with isolated chromophores

are, strictly speaking, not conjugated polymers but they have similar characteristics such as a low band gap and good film forming properties; they have also been used successfully as the emissive layer in LEDs.

A very well defined polymer with oligo(phenylene vinylene) units as side chains was prepared by Lee *et al.* using ring opening metathesis polymerisation.[28] The polymer proved to be efficient as the emissive layer in a light emitting diode and a quantum yield of 0.3% was obtained when Ca was used as the cathode and ITO as the anode. The PL and EL maximum is at 475 nm. This is blue shifted relative to PPV due to the shorter conjugation length.

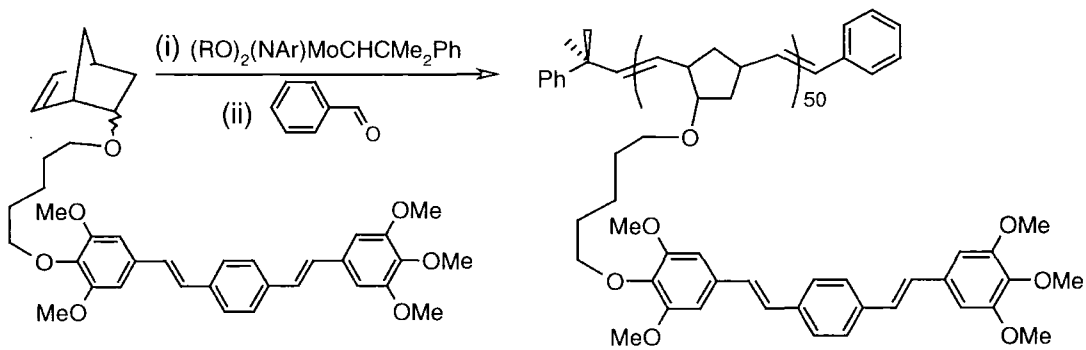

Figure 1.3.3 Synthesis of a well defined polymer with distyrylbenzene units in side chains (DSB Side) via ring opening metathesis polymerisation.

A variety of different approaches have been used to prepare polymers with isolated chromophores within the polymer backbone. In 1993 Karasz *et al.* reported the first block copolymer with alternating distyrylbenzene (DSB) units and non-conjugated flexible linkers.[29] The polymer is one of the first examples of a polymer emitting blue light. The EL maximum is at 465 nm. The Wittig reaction was used as the polycondensation reaction and the polymer consists of alternating DSB units and octane-1,8-diol units.

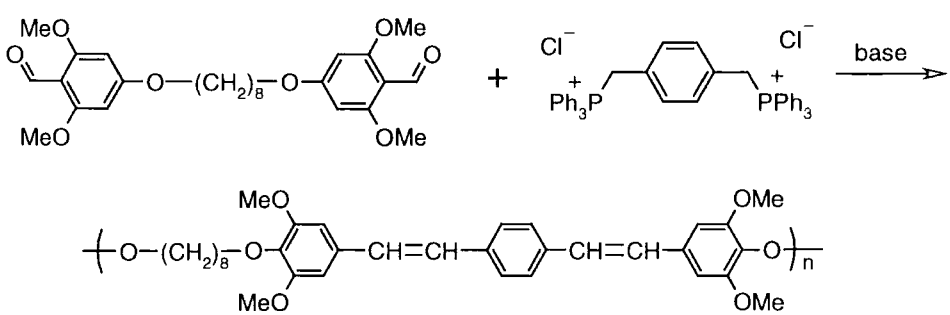

Figure 1.3.4 Synthesis of a block copolymer with DSB units and flexible linker units (DSB Block-A) via the Wittig reaction.

Benfaremo *et al.* have prepared a block copolymer of DSB and polyethylene oxide (PEO).[30] PEO with an average molecular weight of 900 (PEO_{900}) was activated as mesylate (methanesulfonate) and reacted with 4,4'-bis(4-hydroxystyryl)benzene. Due to the good solubility properties of the PEO unit no additional solubilising groups on the chromophore were required. The polymer is soluble in a range of organic solvents (THF, DMF, chloroform and acetonitrile). The polymer emits blue light but devices based on this polymer were not stable.

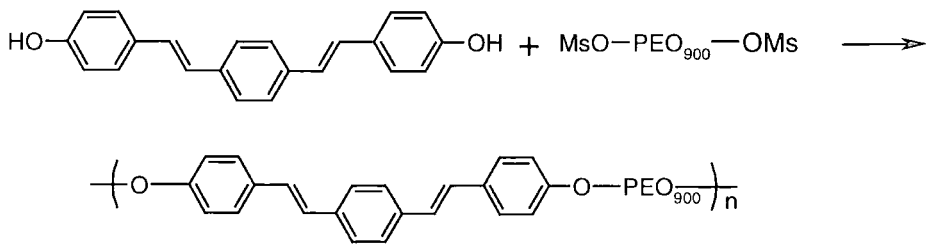

Figure 1.3.5 Synthesis of a block copolymer with DSB units and PEO units (DSB Block-B).

Li *et al.* have prepared a similar block copolymer based on DSB and oligo(ethylene oxide).[31] The Wittig reaction was used as the polycondensation reaction. The oligo(ethylene oxide) chain is much shorter than in the polymer prepared by Benfaremo *et al.* (DSB Block A) and two additional methyl groups on the central ring of the DSB unit aid solubility. The polymer is soluble in chloroform and shows blue photoluminescence. However, as in the previous case, LEDs based on this polymer were unstable.

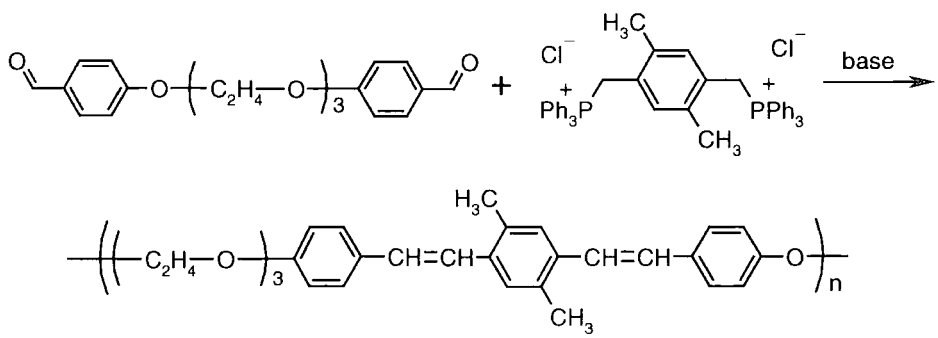

Figure 1.3.6 Synthesis of a block copolymer with DSB units and PEO units via the Wittig reaction (DSB-Block-C).

Recently, Karasz *et al.* have shown that the Heck reaction can be used as the polymerisation reaction to prepare segmented block copolymers (*Figure 1.3.7*).[32]

The authors selected the Heck reaction since it gives rise predominantly to *trans*-double bonds. Depending on the substituent R, the EL maximum is between 450 and 470 nm; long substituents lead to torsion of the chromophore and therefore a reduction of the effective conjugation length and a blue shift of the emission maximum. In the case of R = H, the polymer (DSB-Block-D) is very similar to Karasz' first block copolymer prepared by the Wittig reaction and only contains two additional methylene groups in the flexible linker. The authors report that yields and molecular weights of the polymers are high, but they do not report any EL quantum efficiencies for devices based on these polymers.

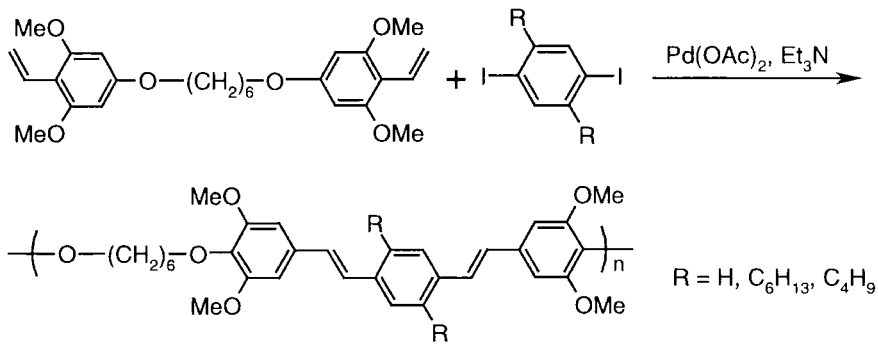

Figure 1.3.7 Synthesis of a block copolymer with DSB units via the Heck reaction (DSB-Block-D).

The Knoevenagel reaction has also been used to prepare block copolymers.[33] The electroluminescence maximum (505 nm) of the block copolymer with cyano groups is red shifted compared to that of the parent polymer 'DSB Block A' (*Figure 1.3.4*) since the cyano groups lower the LUMO energy level strongly. However, the authors mention difficulty with side reactions leading to cross-linking of the polymer and no efficiencies are reported.

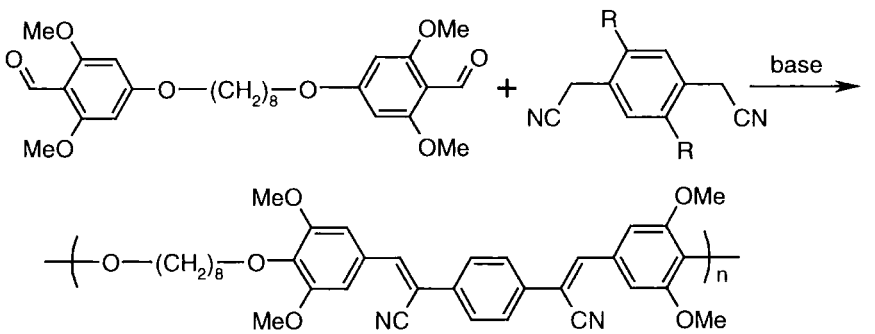

Figure 1.3.8 Synthesis of a block copolymer with cyano groups via the Knoevenagel reaction (DSB-CN).

Hay and Klavetter have prepared a block copolymer with alternating flexible linker units and conjugated units.[34] However, in this case the conjugated units have different lengths depending on the feed ratio of the three comonomers used. *Figure 1.3.9* shows the three different comonomers; terephtalaldehyde, *p*-xylylene-bis-(tripenylphosphonium chloride) and a comonomer with a central non-conjugated unit and two terminal aldehyde groups were cocondensed using the Wittig reaction. The absorption spectrum of the resulting polymer is an intermediate of the absorption spectrum of PPV and DSB-Block-A (*Figure 1.3.4*), as expected since the polymer contains DSB units as well as longer conjugated oligo(phenylene vinylene) units. However, the PL and EL spectra are very similar to those of PPV and show no resemblance to those of a DSB block copolymer. The authors assign this to an efficient intra- and intermolecular energy transfer from the shorter to the longer chromophores. The EL quantum efficiency for a device using ITO and Ca as electrodes was 0.8%.[35] This increase in the efficiency relative to PPV is due to a better confinement of the exciton.

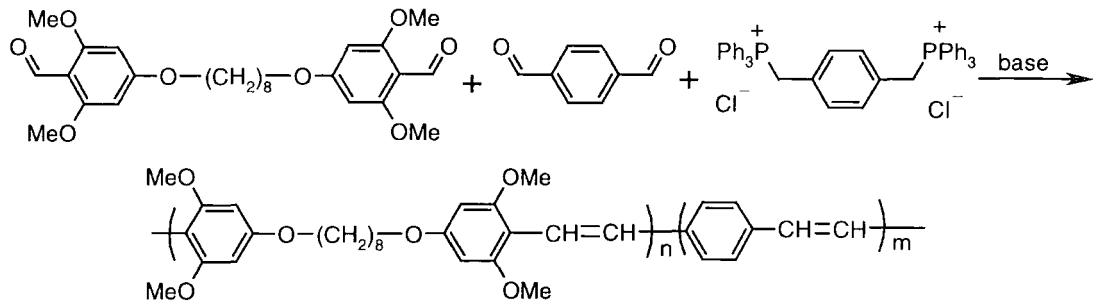

Figure 1.3.9 Synthesis of a block copolymer comprising conjugated units with a statistical distribution of conjugation length (PPV-Block).

The absorption maxima, the PL maxima and the EL maxima of the previously described polymers are compared in *Table 1.3.1*. In general, fully conjugated polymers have an absorption and emission maxima at higher wavelength than those containing DSB as chromophore, since a longer conjugation length results in a smaller optical band gap. Substituents can be used to tune the optical properties, for example alkoxy substituents on the aromatic rings lead to a red shift in absorption and emission. Some polymerisation methods lead to defects in the polymers and some polymers give rise to unstable LEDs. It is therefore very important that polymerisation method chosen leads to defect-free, well characterised polymers so

that the stable devices can be prepared and the device characteristics are not altered by impurities in the sample.

Polymer	Figure	λ_{max}(abs.)	λ_{max}(PL)	λ_{max}(EL)
PPV	*Figure 1.1.4*	450 nm	560 nm	560 nm
MEH-PPV	*Figure 1.3.1*	500 nm	590 nm	590 nm
CN-PPV	*Figure 1.3.2*	485 nm*	710 nm	-
DSB Side	*Figure 1.3.3*	362 nm	475 nm	475 nm
DSB-Block-A	*Figure 1.3.4*	356 nm	453 nm	474 nm
DSB-Block-B	*Figure 1.3.5*	330 nm*	485 nm*	-
DSB-Block-C	*Figure 1.3.6*	350 nm*	470 nm*	-
DSB-Block-D	*Figure 1.3.7*	370 nm*	470 nm*	470 nm*
DSB-CN	*Figure 1.3.8*	379 nm	497 nm	505 nm
PPV-Block	*Figure 1.3.9*	370 nm*	540 nm*	540 nm*

*Table 1.3.1 Solid state absorption maxima, PL maxima and EL maxima of the polymers described in this section. An asterisk * indicates that the value was not mentioned in the text of the corresponding article but was taken from a diagram; a relatively large error (± 5 nm) should therefore be kept in mind for these values.*

1.4 Fluorinated conjugated polymers

The fluorine atom is the atom with the second highest electron affinity (3.399 eV) in the periodic table after chlorine (3.617 eV).[36] While the electron affinity describes the energy gain of an atom when binding an electron, the electronegativity is, according to Pauling, the power of an atom in a molecule to attract electrons to itself.[37] The electronegativity is a less accurate measure than the electron affinity and different methods have been designed to determine it. However, all methods show that fluorine has the greatest power to attract electrons within a molecule followed by oxygen and chlorine. The strong electron withdrawing effect changes the character of organic molecules dramatically. For example most aromatic rings react readily under electrophilic attack while

fluorinated aromatic rings are almost inert under such conditions but react readily under nucleophilic attack.[38]

The fluorine atom is the smallest halogen. The van der Waal's radius of fluorine (1.35 Å) is only slightly bigger than that of hydrogen (1.2 Å).[39] Chlorine (1.80 Å) and bromine (1.95 Å) have distinctly larger van der Waal's radii. A fluorine atom therefore induces little steric effect when replacing a hydrogen atom in an organic molecule. A carbon-fluorine-bond is stronger than a carbon hydrogen bond. The bond strength of a C-F bond in C_2F_6 is 530 ± 8 kJ/mol compared with the C-H bond strength of 419 ± 8 kJ/mol in C_2H_6.[39] Polymers that are highly or completely fluorinated have properties beyond the limit of conventional polymers; they show stability at high temperatures, toughness and flexibility at low temperatures and non-adhesiveness. Many fluoropolymers are also resistant to corrosive chemicals.[40] Chemical stability and the high electronegativity are two of the reasons why the effect of fluorine on conjugated polymers has been studied previously. Some examples are given below.

Fluorine-substituted PPVs were first studied by McCoy *et al.*[41] The authors prepared poly(2-fluoro-1,4-phenylenevinylene) (1F-PPV) and poly(2,5-difluoro-1,4-phenylene vinylene) (2F-PPV) *via* the Wessling route (*Figure 1.4.1*). 1F-PPV showed a slight blue shift in the absorption spectrum relative to PPV. The maximum of the EL spectrum of a device using ITO and Al electrodes was unchanged when compared to the parent PPV polymer. However, the turn-on voltage was at least 7 V, whereas it was only 4 V for the corresponding device based on PPV,[42] which was attributed to an increase in the ionisation potential of 0.17 eV relative to PPV. Furthermore, the devices constructed with 1F-PPV showed an increase in efficiency.

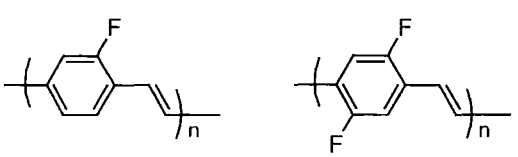

Figure 1.4.1 Poly(2-fluoro-1,4-phenylenevinylene)(1F-PPV) (left) and poly(2,5-difluoro-1,4-phenylene vinylene)(2F-PPV) (right).

The PPV derivative with two fluorine atoms per phenylene unit (2F-PPV) showed a red shift in the EL spectrum with a maximum at 600 nm.[43] The authors

found that such a red shift is typical for PPV derivatives with 2,5 substitution of π-donating, electron withdrawing groups such as chlorine, bromine as well as alkoxy substituents. The authors did not report efficiencies for devices based on 2F-PPV.

Benjamin *et al.* have prepared PPV analogues containing *p*-phenylenevinylene and 2,3,5,6-tetrafluoro-1,4-phenylenevinylene units *via* the Wessling route (*Figure 1.4.2*).[44] Two comonomers were reacted in different ratios resulting in polymers with a varying fluorine content. The yield of the polymer decreased as the content of fluorinated comonomer was increased; the polymer yield was only 25% when the reaction was conducted using a mixture of 60% fluorinated comonomer and 40% non-fluorinated comonomer. The photoluminescence intensity decreased sharply as the content of fluorinated monomer was increased. The authors were unable to prepare a fully fluorinated analogue of PPV. Also the electroluminescence was blue-shifted as the content of fluorinated comonomer was increased. However, it remained unclear whether this was due to the effect of fluorine on the optical band gap of the polymer or to the shortening of the conjugation length of homo-PPV blocks in the polymer, which were stronger emitters than the fluoro-analogues. The turn-on voltage of devices based on these polymers increased with increasing fluorine-content.

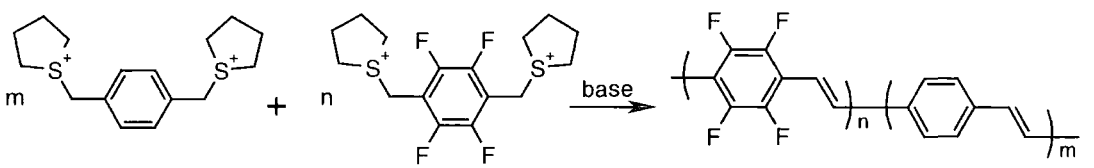

Figure 1.4.2 Synthesis of a copolymer with tetratrafluorophenylene vinylene units via the Wessling route (PPV/4F-PPV).

Holmes *et al.* prepared copolymers *via* the Gilch-route having 2,3,5,6-tetrafluoro-1,4-phenylene vinylene and 2,5-dialkoxy-1,4-phenylene vinylene units (*Figure 1.4.3*).[45] The authors incorporated between 7 and 19% of fluorinated monomer into the copolymer. The incorporation of fluorinated monomer led to a decrease in the yield and also a decrease in the solubility of the polymer. The electroluminescence spectra of all these copolymers were unchanged relative to that of the homopolymer MEH-PPV, the maximum emission for all polymers being at 590 nm. However, the photoluminescence efficiencies of the copolymers (4-7%)

were significantly lower than that of the MEH-PPV (14%). In these systems the EL efficiencies decreased and the turn-on voltages increased with increasing fluorine content.

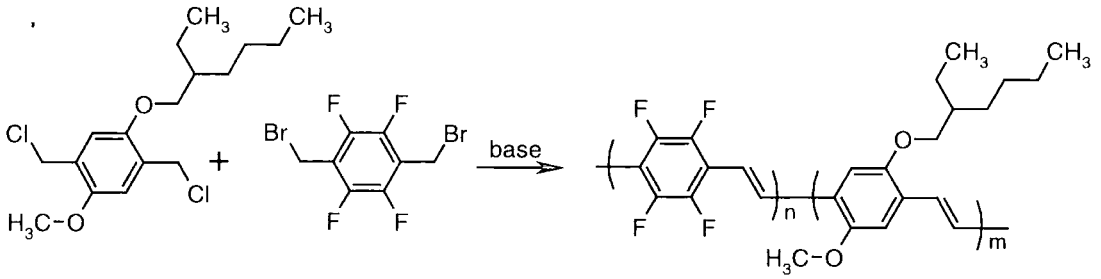

Figure 1.4.3 Synthesis of a copolymer with tetratrafluorophenylene vinylene units via the Gilch route (MEH-PPV/4F-PPV).

Efforts have been made to introduce fluorine atoms in side chains rather than directly on the aromatic ring. Grimsdale *et al.* have prepared poly(2-trifluoromethyl-1,4-phenylene vinylene) using the Gilch-route (*Figure 1.4.4*).[33,46] For this material absorption and emission spectra were blue shifted with respect to PPV and the solid state PL quantum efficiency was only 5%. The polymer gave poor, non-uniform electroluminescence in single layer devices.

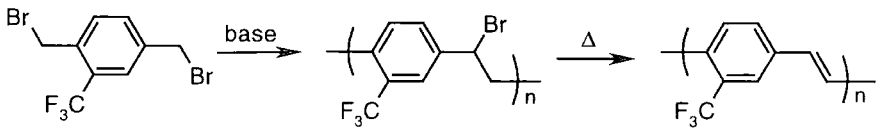

Figure 1.4.4 Synthesis of poly(2-trifluoromethyl-1,4-phenylene vinylene) via the Gilch route (CF_3-PPV 1).

Holmes *et al.* prepared polymers with trifluoromethyl-groups on the vinylene unit *via* the Horner-Wittig reaction.[47,48] The PL maximum was slightly red-shifted compared to PPV. The ionisation potential and the electron affinity were increased. The polymer was used in double layer devices in a similar fashion to CN-PPV in order to aid electron-injection and 'block' whole-injection.

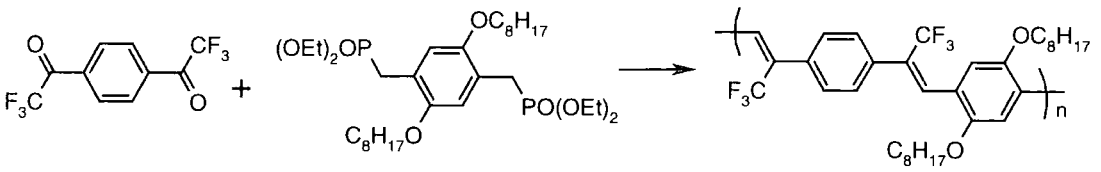

Figure 1.4.5 Synthesis of a PPV derivative with trifluormethyl-groups on the vinylene unit (CF_3 PPV 2).

Shim *et al.* prepared a PPV derivative with a perfluorobiphenyl substituent *via* the Wessling route (*Figure 1.4.6*).[49] The absorption maximum occurred at 400 nm and the PL and EL emission at 520 nm. All maxima were blue shifted relative to those of PPV. The IP of the polymer was increased by 0.4 eV relative to PPV. The authors found that the quantum efficiency was higher than that of PPV but the turn-on voltage was also increased.

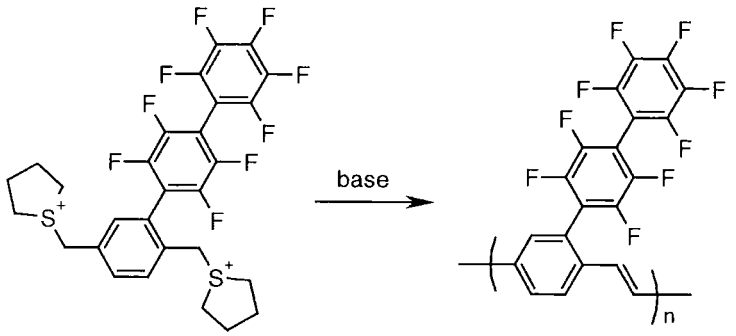

Figure 1.4.6 Synthesis of a PPV derivative with a perfluorbiphenyl side chain (PPFPV).

Sarker *et al.* prepared block copolymers with DSB units and non-conjugated flexible linkers,[50] in which the DSB units contained a central fluorinated benzene ring (*Figure 1.4.7*). The Horner-Wittig reaction was used as the polymerisation reaction.

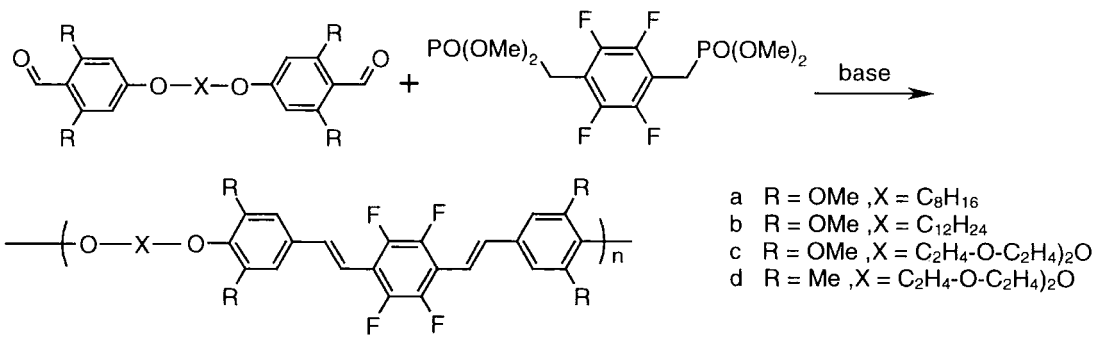

Figure 1.4.7 Synthesis of DSB block copolymers with a central fluorinated benzene ring via the Horner-Wittig reaction (F-DSB-Block-a, F-DSB-Block-b, F-DSB-Block-c, F-DSB-Block-d).

Three of the reported polymers had additional methoxy groups on the DSB units to aid solubility. These three polymers showed absorption maxima between 362 and 365 nm and PL emission maxima between 487 and 502 nm. A fourth polymer with methyl groups on the DSB unit had blue-shifted absorption and emission maxima (332 and 421 nm, respectively). This was attributed to the fact that the methyl

groups cause the conjugated system to be less planar. The PL quantum efficiencies of all four polymers were low and the authors believe this is due to highly ordered structures based on π-π-interactions between phenyl and perfluorophenyl groups and therefore regard such polymers as unattractive for LEDs.

The absorption, PL and EL maxima, the electron affinities and the ionisation potentials of fluorinated PPV derivatives are compared in *Table1.4.1.* The absorption maxima of the fluorinated polymers are either unchanged or show a small blue shift relative to the non-fluorinated equivalents. No general trend is observed for the PL and EL spectra but it is found that not only the electronegativity of the substituent but also the substitution pattern along the polymer affects the outcome.

Polymer	*Figure*	λ_{max}(abs.)	λ_{max}(PL)	λ_{max}(EL)	EA (HOMO)	IP (LUMO)
PPV	*Figure 1.1.5*	450 nm	560 nm	560 nm	2.5 eV	5.2 eV
CN-PPV	*Figure 1.3.2*	485 nm	710 nm	-	3.4 eV	5.8 eV
1F-PPV	*Figure 1.4.1*	422 nm	560 nm	560 nm	2.7 eV	5.4 eV
2F-PPV	*Figure 1.4.1*	420 nm	590 nm	600 nm	-	-
PPV/ 4F-PPV	*Figure 1.4.2*	350 nm	550 nm	525 nm/ 495 nm	-	-
MEH-PPV/ 4F-PPV	*Figure 1.4.3*	500 nm	590 nm	590 nm	-	-
CF_3-PPV 1	*Figure 1.4.4*	335 nm*	517 nm	-	-	-
CF_3-PPV 2	*Figure 1.4.5*	440 nm*	580 nm	-	3.1 eV	5.8 eV
PF-PPV	*Figure 1.4.6*	400 nm	520 nm	520 nm	2.9 eV	-
F-DSB-Block-a	*Figure 1.4.7*	365 nm	487 nm	-	-	-
F-DSB-Block-d	*Figure 1.4.7*	332 nm	421 nm	-	-	-

*Table 1.4.1 Absorption maxima, the PL maxima and the EL maxima of the polymers described in this section. The asterisks * indicate that these values were not mentioned in the text of the corresponding articles but were taken from diagrams in those articles; a relatively large error (± 5 nm) should therefore be kept in mind. The ionisation potential (IP) and the electron affinity (EA) are recorded relative to the vacuum level.*

While some reports suggest an improvement in device performance there are also many indications that the presence of fluorinated units or substituents has a negative effect on the emissive properties of the polymer and leads to a decrease in

EL efficiency. Some groups were unable to report any electroluminescence for single layer devices based on the fluorinated polymers due to poor device stability. However, several groups used the polymers to prepare highly efficient double layer LEDs, where the fluoro-polymer aids electron-transport and blocks hole-transport. The electron affinity of fluoro-polymers is always higher than that of their non-fluorinated analogous confirming that such polymers form good electron-transport layers. All structures reported have both hydrogens and fluorines along the polymer backbone. To our knowledge, nobody has so far prepared a fully fluorinated derivative of PPV.

1.5 Aim

The original aim of this work was to study the effect of fluorine on conjugated polymers. To this end various routes to fluorinated systems were investigated. A well characterised block copolymer with alternating fluorinated conjugated units and flexible linker units was synthesised. A copolymer with isolated chromophores bears the potential advantage over a polymer with a fully conjugated backbone in that the flexible linkers provide the solubility and no additional solubilising groups on the polymer backbone are required; in the case of PPV derivatives this means that all four available aromatic positions can be substituted with fluorine atoms. *Figure 1.5.1* shows a schematic representation of such a block copolymer.

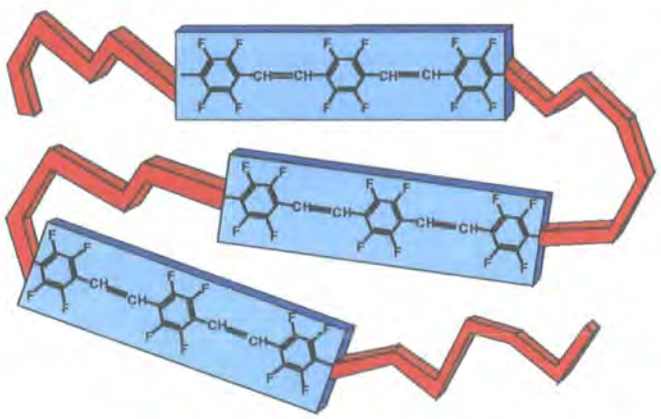

Figure 1.5.1 Schematic representation of a block copolymer with fluorinated conjugated units and non-conjugated flexible linkers.

The high electronegativity of fluorine was expected to aid electron injection and it was anticipated that a balance of charge carriers should lead to highly efficient electroluminescent polymers. In order to study the effect of fluorine, the non-fluorinated block copolymer was required as well as the fluorinated material.

Furthermore, fluorinated phenylene vinylene oligomers were synthesised in order to study the molecular packing in such molecules.

The use of polymers in LEDs is an area that requires expertise in both chemistry and physics. A network of European scientist in the area of organic semiconductors is currently funded through the EU commission as the LAMINATE (*L*arge *A*rea *M*olecular-electronics *I*nvolving a *N*ovel *A*pproach to *T*raining and *E*ducation) programme. The optoelectronic properties of the novel polymers will be studied in cooperation with these partners. The remainder of this thesis reports the synthesis, characterisation and investigation of the materials indicated above.

1.6 References

1. Mark, H. F. *Encyclopedia of Polymer Science and Engineering, Volume 5,* John Wiley & Sons, New York **1986**.
2. Friend, R. H.; Gymer, R. W.; Holmes, A. B.; Burroughes, J. H.; Marks, R. N.; Taliani, C.; Bradley, D. D. C.; Dos Santos, D. A.; Bredas, J. L.; Logdlund, M.; Salaneck, W. R. *Nature* **1999**, *397*, 121.
3. Natta, G.; Mazzanti, G.; Corraddini, P. *Atti Accad. Naz. Lincei Rend. Cl. Sci, Fis. Mat. Natur.* **1958**, *25*, 3.
4. Berets, D. J.; Smith, D. S. *J. Chem. Soc. Trans. Faraday* **1968**, *64*, 823.
5. Ito, T.; Shirakawa, H.; Ikeda, S. *J. Polym. Sci. Polym. Chem. Ed.* **1974**, *12*, 11.
6. Shirakawa, H.; Louis, E. J.; MacDiarmid, A. G.; Chiang, C. K.; Heeger, A. J. *Chem. Comm.* **1977**, 578.
7. Edwards, J. H.; Feast, W. J. *Polymer* **1980**, *21*, 595.
8. Edwards, J. H.; Feast, W. J.; Bott, D. C. *Polymer* **1984**, *25*, 395.
9. Campbell, T. W.; McDonald, R. N. *J. Org. Chem.* **1959**, *24*, 1246.
10. Wessling, R. A.; Zimmerman, R. G. *Patent US-B 3401152* **1968**.
11. Wessling, R. A. *J. Polym. Sci. Polym. Symp.* **1985**, *72*, 55.
12. Gilch, H. G.; Wheelwright, W. L. *J. Polym. Sci. Part A-1* **1966**, *4*, 1337.

13. Feast, W. J.; Tsibouklis, J.; Pouwer, K. L.; Groenendaal, L.; Meijer, E. W. *Polymer* **1996**, *37*, 5017.

14. Murray, M. M.; Holmes, A. B. Chapter 1 in *Semiconducting polymers by Hadziioannou and van Hutten,* Wiley-VCH, Weinheim **2000**.

15. Burroughes, J. H.; Bradely, D. D. C.; Brown, A. R.; Marks, R. N.; Mackay, K.; Friend, R. H.; Burns, P. L.; Holmes, A. B. *Nature* **1990**, *347*, 539.

16. Kraft, A.; Grimsdale, A. C.; Holmes, A. B. *Angew. Chem. Int. Ed. Engl.* **1998**, *37*, 402.

17. Scott, J. C.; Malliaras, G. G. Chapter 13 in *Semiconducting polymers* by Hadziioannou and van Hutten, Wiley-VCH, Weinheim **2000**.

18. Campbell, I. H.; Smith, D. L. Chapter 11 in *Semiconducting polymers* by Hadziioannou and van Hutten, *Wiley-VCH, Weinheim* **2000**.

19. Graupner, W.; Tasch, S.; Leising, G. Chapter 9 in *Semiconducting polymers* by Hadziioannou and van Hutten, *Wiley-VCH, Weinheim* **2000**.

20. Greenham, N. C.; Friend, R. H.; Bradley, D. D. C. *Adv. Mater.* **1994**, *6*, 491.

21. Gill, R. E.; van de Weijer, P.; Liedenbaum, C. T. H.; Schoo, H. F. M.; Berntsen, A.; Vleggaar, J. J. M.; Visser, R. J. *Optical Materials* **1999**, *12*, 183.

22. Greenham, N. C.; Samuel, I. D. W.; Hayes, G. R.; Phillips, R. T.; Kessener, Y. A. R. R.; Moratti, S. C.; Holmes, A. B.; Friend, R. H. *Chem. Phys. Lett.* **1995**, *241*, 89.

23. Brown, A. R.; Bradley, D. D. C.; Burroughes, J. H.; Friend, R. H.; Greenham, N. C.; Burn, P. L.; Holmes, A. B.; Kraft, A. *Appl. Phys. Lett.* **1992**, *61*, 2793.

24. Braun, H.; Heeger, A. J. *Appl. Phys. Lett.* **1991**, *58*, 1982.

25. Wudl, F.; Allemand, P. M.; Srdanov, G.; Ni, Z.; McBranch, D. *ACS Symp. Ser. 455* **1991**, 455.

26. Hörhold, H.-H.; Helbig, M. *Makromol. Chem. Macromol. Symp.* **1987**, *328*, 351.

27. Segura, J. L.; Martin, N. *J. Mater. Chem.* **2000**, *10*, 2403.

28. Lee, J. K.; Schrock, R. R.; Baigent, D. R.; Friend, R. H. *Macromolecules* **1995**, *28*, 1966.

29. Yang, Z.; Sokolik, I.; Karasz, F. E. *Macromolecules* **1993**, *26*, 1188.

30. Benfaremo, N.; Sandman, D. J.; Kumar, J.; Yang, K.; Rubner, M. F.; Lyons, C. *Macromolecules* **1998**, *31*, 3595.
31. Yang, C.; He, G.; Wang, R; Li, Y. *Mol. Cryst and Liq. Cryst.* **1999**, *337*, 473.
32. Pasco, S. T.; Lahti, P. M.; Karasz, F. E. *Macromolecules* **1999**, *32*, 6933.
33. Grimsdale, A. C.; Cacialli, F.; Gruener, J.; Li, X.-C.; Holmes, A. B.; Moratti, S. C.; Friend, R. H. *Synthetic Metals* **1996**, *76*, 165.
34. Hay, M.; Klavetter, F. L. *J. Am. Chem. Soc.* **1995**, *117*, 7112.
35. Hu, B.; Karasz, F. E. *Synthetic Metals* **1998**, *92*, 157.
36. Weast, R. C. *CRC Handbook of Chemistry and Physics,* 68th edition, 1987 - 1988, Florida , E 62.
37. Cotton, F. A.; Wilkinson, G. *Advanced Inorganic Chemistry,* Interscience, London **1962**.
38. Brooke, G. M. *J. Fluorine Chem.* **1997**, *86*, 1.
39. Weast, R. C. *CRC Handbook of Chemistry and Physics, 68th edition,* 1987 - 1988, Florida , F-178.
40. Johns, K.; Stead, G. *J. Fluorine Chem.* **2000**, *104*, 5.
41. McCoy, R. K.; Karasz, F. E.; Sarker, A.; Lahti, P. L. *Chem. Mater* **1991**, *3*, 941.
42. Kang, I.-N.; Shim, H.-K. *Chem. Mater.* **1997**, *9*, 746.
43. Gruge, R. M.; Sarker, A. M.; Lahti, P. M.; Hu, B.; Karasz, F. E. *Macromolecules* **1997**, *30*, 8286.
44. Benjamin, I.; Faraggi, E. Z.; Cohen, G.; Chayet, H.; Davidov, D.; Neumann, R.; Avny, Y. *Synthetic Metals* **1997**, *84*, 401.
45. Riehn, R.; Morgado, J.; Iqabal, R.; Moratti, S. C.; Holmes, A. B.; Volta, S.; Cacialli, F. *Macromolecules* **2000**, *33*, 3337.
46. Li, X.-C.; Grimsdale, A. C.; Cervini, R.; Holmes, A. B.; Moratti, S. C.; Yong, T. M.; Johannes, G.; Friend, R. H. *ACS Symposium Series*, **1997**, 322.
47. Lux, A.; Holmes, A. B.; Cervini, J. E.; Moratti, S. C.; Gruener, J.; Cacialli, F.; Friend, R. H. *Synthetic Metals* **1997**, *84*, 293.
48. Holmes, A. B.; Grimsdale, A. C.; Lux, A.; Li, X. C.; Cervini, R. *UK Patent 2 303 633* **1997**.
49. Jang, M.-S.; Song, S.-S.; Shim, H.-K. *Polymer* **2000**, *41*, 5675.
50. Sarker, A. M.; Strehmel, B.; Neckers, D. C. *Macromolecules* **1999**, 7409.

2 Syntheses of Fluorinated Conjugated Polymers *via* the McMurry Reaction

2.1 Introduction

This chapter describes the results of an investigation into the potential of McMurry coupling for the synthesis of fluorinated PPVs and related polymers. The reasons for attempting each approach are outlined together with the experimental results and the explanation of why the route was abandoned. Ultimately, the McMurry route was unsuccessful in our hands; nevertheless some interesting chemistry resulted which is reported in this chapter.

In the McMurry reaction aldehydes and ketones are dimerised to yield olefins under reductive conditions with low-valent titanium reagents.[1] The McMurry coupling has been of great use to organic chemists in both inter- and intramolecular reactions allowing the synthesis of sterically crowded olefins, small and large rings as well as a wide range of natural products.[2-4] The accepted mechanism involves an initial electron transfer from titanium to the carbonyl group (*Figure 2.1.1*).[5] Titanium is oxidised but the exact oxidation states can not be determined. (Changes from (0) to (II) or from (I) to (III) have been suggested.[2-4]) The ketyl radicals bound to a titanium particle then dimerise to the corresponding titanium bound pinacol. Deoxygenation of the bound pinacol occurs due to the large affinity of titanium for oxygen, leading to alkenes.

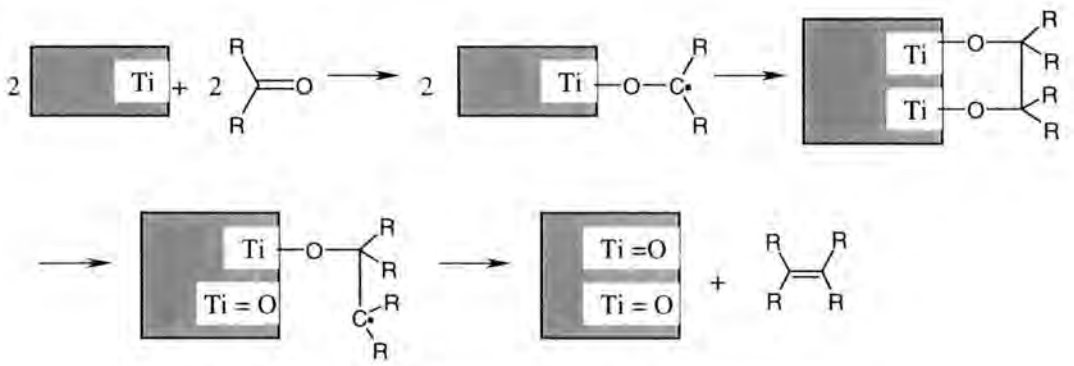

Figure 2.1.1 Mechanism of the McMurry reaction.

The McMurry reaction is compatible with a range of functional groups, including ethers, amines, saturated alcohols and halides.[6] The efficiency of the reaction depends on the specific reagents and conditions but yields of 98% have been reported repeatedly.[7,8] Such high conversions make the McMurry reaction attractive for polycondensation reactions. Indeed, Feast *et al.* and Schlüter *et al.* used the McMurry reaction to prepare soluble poly(*p*-phenylene vinylene)s.[9,10] Daik *et al.* have been able to polymerise 4,4'-di(benzoly)biphenyl via the McMurry reaction and obtained poly-(4,4'-diphenylene diphenylvinylene) of high molecular weight and high purity (*Figure 2.1.2*).[11,12] Also, Daik *et al.* were able to polymerise a fluorinated analogue where R= pentafluorophenyl. These findings encouraged further investigations into the McMurry reaction, which are described here.

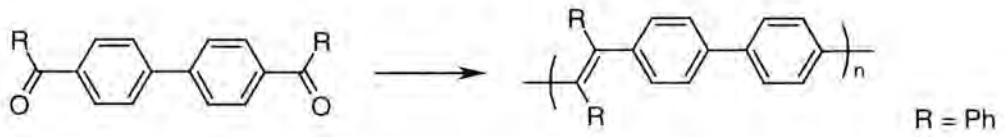

Figure 2.1.2 Synthesis of poly(4,4'-diphenylene diphenylvinylene).

It is expected that the McMurry reaction can also be used for the synthesis of copolymers when a mixture of comonomers is used. Given that all monomers have the same reactivity towards low-valent titanium, a statistical distribution of monomers within the polymer-chain can be anticipated.

2.2 Results and Discussion

Monomer syntheses

First, the use of the McMurry reaction as a condensation reaction for fluorinated aromatic ketones was examined. Small model compounds were chosen as analogues for the proposed polymerisation, in order to investigate the efficiency of the reaction and the occurrence of possible side-reactions. It was found that the reaction of pentafluorobenzophenone **1** with low-valent titanium gave the 9-pentafluorophenyl-

10-phenyl-1,2,3,4-tetraphenylpenanthrene **2** as the main product amongst at least eight other by-products. Compound **2** could be isolated in 30% yield and was fully characterised. Bis(pentafluorophenyl)diphenylethene **3** was not found in the product mixture (*Figure 2.2.1*). However, the second most abundant product identified by GC-MS and ^{19}F NMR was consistent with replacement of an *ortho*-fluorine atom by a hydrogen atom in structure **3** (see experimental section 2.4.2). Other products identified by GC-MS were consistent with further replacements of fluorine atoms by hydrogen in structures **2** and **3**.

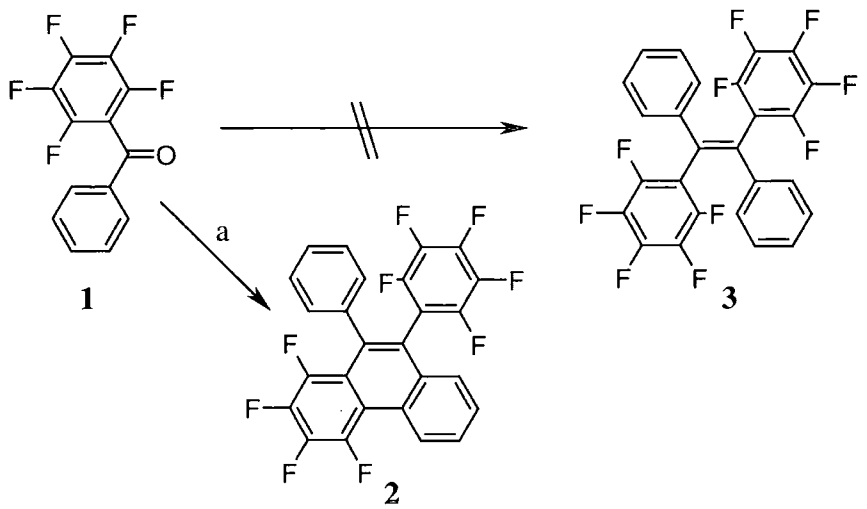

Figure 2.2.1 McMurry reaction of 2,3,4,5,6-pentafluorobenzophenone. a) $TiCl_3$, $LiAlH_4$, THF

Decafluorobenzophenone, the perfluorinated equivalent of **1**, reacted in a similar way with low-valent titanium; again a new carbon-carbon bond was formed between to adjacent rings giving rise to a phenanthrene ring system (reaction not shown). Such phenanthrene ring closures are undesired in polymer forming reactions since there is no control as to where they occur. Therefore, it was concluded that the McMurry reaction was unsuitable for the reductive coupling of fluorinated ketones and the products were not further investigated.

However, using fluorinated aldehydes no side reactions were found; for example pentafluorobenzaldehyde **4** reacts with low-valent titanium to give *trans*-decafluorostilbene **5** in good yield (89%)(*Figure 2.2.2*). No *cis*-isomer and no by-products were detected in the NMR spectra (^1H, ^{13}C, ^{19}F) of the crude product. This indicates that it is probably the steric crowding in the case of fluorinated ketones that

is responsible for the phenanthrene formation and side-reactions; since no *cis*-isomer was produced in the case of aldehydes, phenanthrene formation was not possible in this reaction.

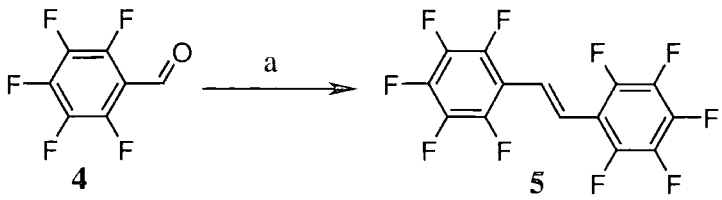

Figure 2.2.2 McMurry reaction of pentafluorobenzaldehyde. a) $TiCl_4$, Zn, dioxane

In order to use the coupling of aldehydes for polycondensation reactions a copolymer approach was investigated. The target copolymer consisted of alternating rigid oligo(tetrafluorophenylene vinylene) units and flexible solubilising units. The synthesis required two comonomers: one containing the flexible linker unit and the other one allowing the build up of the oligo(tetrafluorophenylene vinylene) units. Ideally, both monomers should have similar reactivities towards low-valent titanium. The first comonomer was prepared following the route shown in *Figure 2.2.3* and *Figure 2.2.4.*

Using pentafluorobenzaldehyde as the starting material, the aldehyde function was protected as an acetal (*Figure 2.2.3*).

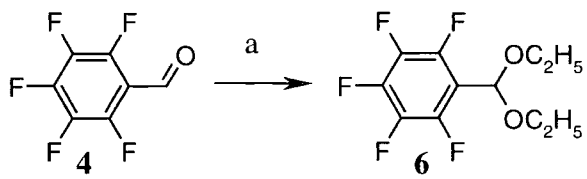

Figure 2.2.3 Protection of pentafluorbenzaldehyde as an acetal. a) C_2H_5OH, $CH(OC_2H_5)_3$, H_2SO_4

Nucleophilic substitution of pentafluorobenzaldehyde diacetal has been reported to occur selectively in the *para*-position.[13] Two protected aldehydes were connected by nucleophilic substitution with α,ω-diols. Three different α,ω-diols were investigated: sexi(ethylene oxide) **7**, neopentyl glycol **8** and 2-ethylhexane-1,3-diol **9**. [Compound **7** is termed sexi(ethylene oxide) (SEO) rather than hexa(ethylene oxide) (HEO) since the letter 'H' will be used at a later stage as abbreviation for

hydrogen.] Each α,ω-diol was deprotonated with *n*-butyllithium. Addition of pentafluorobenzaldehyde diacetal gave compounds **10**, **11** and **12** (*Figure 2.2.4*). Deprotection in aqueous acid gave the flexible linkers **13**, **14** and **15**, respectively. Each flexible linker consists of a central non-conjugated unit which promotes solubility and two terminal fluorinated aromatic aldehydes.

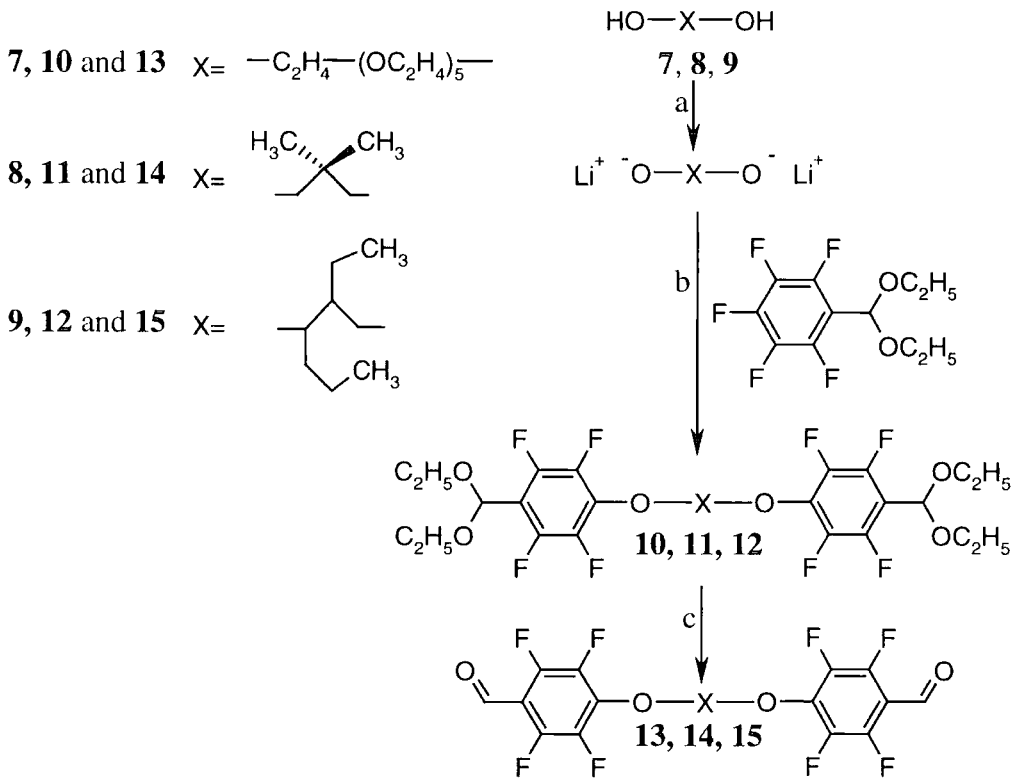

Figure 2.2.4 Synthesis of flexible linkers. a) BuLi, THF b) THF c) H_2O, THF, H_2SO_4

The second required comonomer is 2,3,5,6-tetrafluoroterephtalaldehyde **18** (if homopolymerised it would give rise to an insoluble and intractable fluorinated derivative of PPV). Several synthetic approaches, including reduction of the corresponding ester or nitrile, failed.[14,15] It was possible though to prepare 2,3,5,6-tetrafluoroterephtalaldehyde tetra-acetate **17** by oxidation of 2,3,5,6-tetrafluoroxylene **16** with chromium trioxide in the presence of acetic anhydride (*Figure 2.2.5*). Compound **17** was hydrolysed to give the desired 2,3,5,6-tetrafluoroterephtalaldehyde **18**.

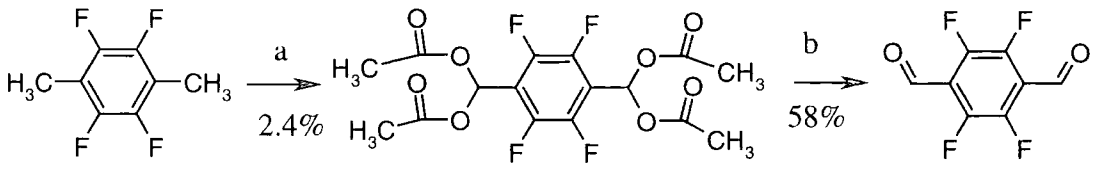

16 17 18

Figure 2.2.5 Synthesis of 2,3,5,6-tetrafluoroterephtalaldehyde. a) CrO_3, Ac_2O, AcOH b) C_2H_5OH, H_2O, H_2SO_4

However, the yield for the first step was very low (2.4%) and could not be improved. The overall yield starting from tetrafluoroxylene was only 1.4%. Since only small quantities (70 mg) of compound **18** could be prepared by this method in one batch, this route was unsatisfactory as a starting point for an investigation into new polymers.

The reaction of tetrafluoroxylene **16** with elemental bromine under irradiation with UV-light gave 1,4-bis(dibromomethyl)-2,3,5,6-tetrafluorobenzene **19** in good yield (69%). The reaction conditions were optimised and it was found that several additions of bromine and the use of a large reaction vessel were advantageous for the photolytic cleavage of bromine.[16] Although the reaction conditions were very harsh (excess of bromine, 160 °C, UV-light, 10 h) the C-F bonds stayed intact and no bromine substitution on the aromatic ring was observed by NMR or mass spectroscopy. Hydrolysis of compound **19** with concentrated sulphuric acid gave 2,3,5,6-tetrafluoroterephtalaldehyde **18**. The overall yield was improved to 24% and sufficient amounts of **18** (1 g) could be prepared to investigate polymerisations.

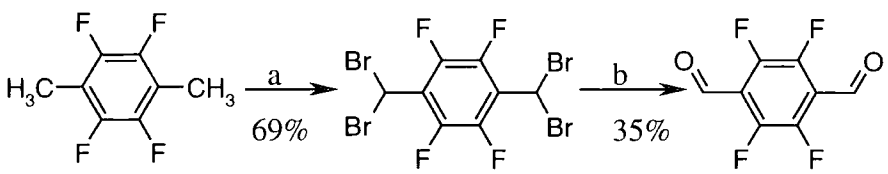

16 19 18

Figure 2.2.6 Synthesis of 2,3,5,6-tetrafluoroterephtalaldehyde. a) Br_2, hv b) H_2SO_4

Polymer syntheses

Initially, an attempt was made to homopolymerise the monomer **13**. However, the product could not be reprecipitated from chloroform into methanol. It was found that the McMurry reaction had produced a cyclic product **20** in 26% yield rather than a polymer (*Figure 2.2.7*) as shown by mass spectroscopy (m/z = 602) and NMR spectroscopy.

The ^{1}H NMR spectrum of **20** shows that the hydrogens in the sexi(ethylene oxide) unit are all shifted towards higher field compared to those in the linear compound **13**. Furthermore, the signals for the four central ethylene units are resolved in the case of **20** but they are not resolved in the case of **13**. These findings can be explained by the position these methylene units with respect to the aromatic rings and the influence of the ring-current on the shifts.

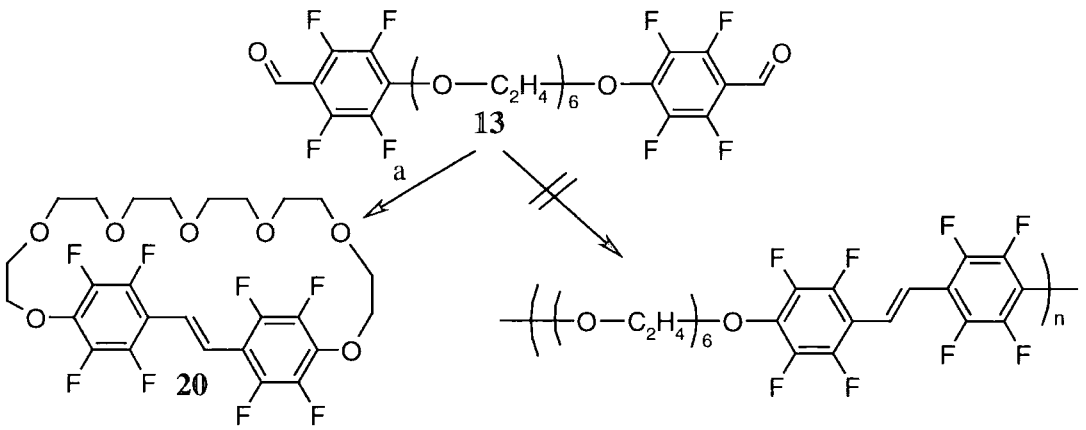

Figure 2.2.7 Polymerisation versus ring-closure in the reaction of compound **13** *with low-valent titanium. a) $TiCl_4$, Zn, THF*

This cyclisation is favoured by the fact that the McMurry reaction takes place on the surface of titanium particles and the two aldehyde groups are brought into close proximity. An increase in concentration in order to favour inter- over intramolecular reaction was not possible since the reaction mixture was a very viscous slurry of titanium in THF. Cyclisations of aromatic dialdehydes *via* the McMurry reaction to give stilbenes bridged by oligo(ethylene oxide) units have been reported previously by Fuerstner *et al.* and Gandour *et al.*.[4,17]

Using the monomer **13** and 2,3,5,6-tetrafluoroterephtalaldehyde **18** as comonomers (in molar ratio of 4:1), it was possible to prepare a mixture of polymer **21** and the cyclic product **20** (*Figure 2.2.8*). When a solution of the mixture in chloroform was reprecipitated into methanol the pure polymer was obtained.

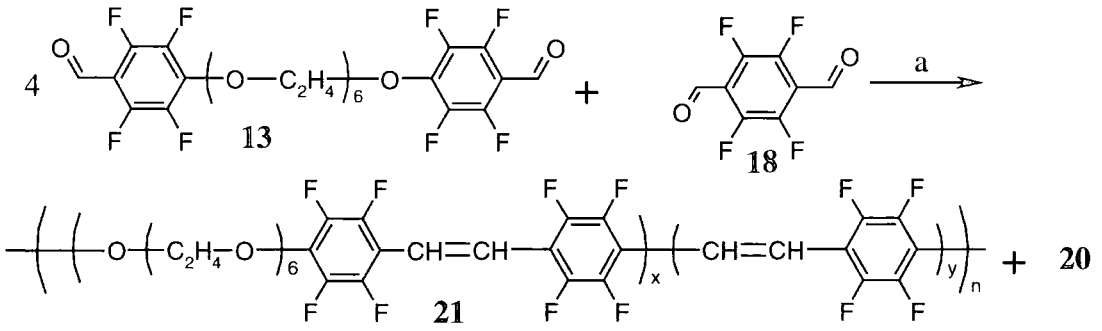

Figure 2.2.8 Synthesis of a fluorinated conjugated polymer via the McMurry reaction. a) $TiCl_4$, Zn, THF

The formation of polymers was due to the fact that in this reaction a range of conjugated units was formed. Stilbene units are formed when two aldehyde endgroups react, whereas if one molecule **18** is incorporated, a distyrylbenzene (DSB) unit is formed and when two molecules **18** are incorporated a distyrylstilbene (DSS) is formed; further incorporation of **18** results in longer conjugated sequences. With units such as DSB and DSS a cyclic product cannot be formed since the sexi(ethylene oxide) unit cannot bridge the larger units. The polymer **21** was characterised by ^{1}H NMR spectroscopy and Gel Permeation Chromatography (GPC), which indicated a M_n = 8,300 and a polydispersity of 3.2 with respect to polystyrene. Due to the formation of the cyclic compound **20** there was little control over the composition of the polymer with respect to relative incorporation of the two monomers; the polymer was expected to contain a higher fraction of **18** than was present in the starting mixture. Furthermore, analysis of the ^{1}H NMR spectrum of the polymer showed that some aldehydes had reacted incompletely and the polymer contained pinacol defects. For these reasons the synthesis of polymer **21** was not further investigated.

Monomer **12** which contains a shorter flexible linker was used in order to avoid a ring closure. When **12** was homopolymerised the obtained polymer was insoluble in non-chlorinated solvents and only very poorly soluble in chloroform or DCM

(reaction not shown). Since the neopentyl glycol unit was insufficient to render the polymer soluble, this reaction was also abandoned.

2-Ethylhexane-1,3-diol **9** is commercially available as a mixture of stereo-isomers. The long side chains and the disorder due to the isomeric mixture were expected to give rise to enhanced solubility. Like neopentyl-glycol **8** it is a 1,3-diol and the ring closure of the corresponding flexible linker **15** is not possible. Indeed, **15** and **18** could be copolymerised in the molar ratio x and y using the McMurry reaction.

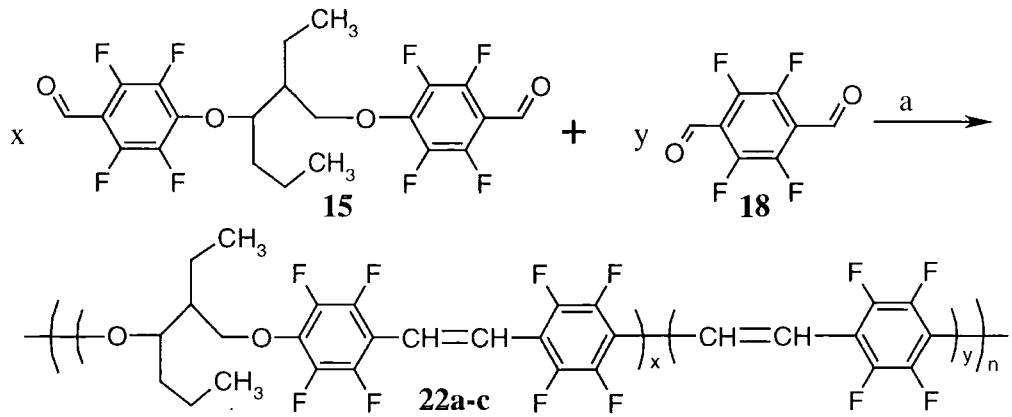

Figure 2.2.9 Synthesis of a fluorinated conjugated polymer via the McMurry reaction. a) $TiCl_4$, Zn, THF

The molar fraction of **18** (y) was varied between 0.1 and 0.3 (*Table 2.2.1*). The polymers obtained **22a, b** and **c** were soluble in chloroform and were characterised by NMR spectroscopy (^1H, ^{19}F), GPC and solution-state absorption and emission spectroscopy. The chloroform solution of polymer **22c** was slightly cloudy and GPC analysis was not possible. The ^1H NMR spectra of all polymers show that some aldehyde functions have reacted incompletely and all polymers contain pinacol defects.

Polymer	molar fraction x	molar fraction y	M_n	calculated fraction of stilbene units in the polymer	calculated fraction of DSB units in the polymer	calculated fraction of DSS units in the polymer
22a	0.9	0.1	3,500	90.0%	9.0%	0.9%
22b	0.8	0.2	7,500	80.0%	16.0%	3.2%
22c	0.7	0.3	--	70.0%	21.0%	6.3%

Table 2.2.1 Composition and molecular weight of polymers **22a, b** and **c**.

The solution state absorption spectra of the polymers **22a, b** and **c** show the typical absorption band for a stilbene unit as the main feature between 290 and 350 nm (*Figure 2.2.10*). The absorption band of longer conjugated units such as DSB and DSS can be found between 350 and 450 nm.[18,19]

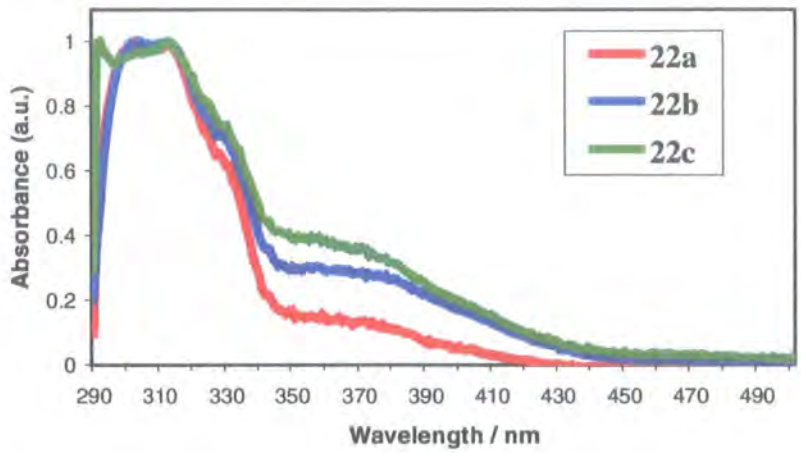

*Figure 2.2.10 Solution state absorption spectra of polymers **22a, b** and **c**.*

The theoretical distribution of stilbene, DSB, DSS and longer units within the polymer chain can be calculated according to the following equation:[20]

$$N(n) = P_{aa}^{(n-1)} P_{ab}$$

N is the probability that a sequence of n units of A (in this case **18**) occurs in the copolymer. P_{aa} and P_{ab} are the probabilities that a molecule A reacts with another molecule A or with a molecule B (in this case **15**), respectively. Assuming that both monomers have the same reactivity these probabilities can be replaced by the molar fractions of the comonomers (x and y). As the fraction of compound **18** in the reaction mixture is increased in polymers **22a, b** and **c** the calculated fraction of DSB and DSS in resulting polymers increases, too, as shown in *Table 2.2.1*. This increase can also be found in the absorption bands of DSB and DSS as shown in *Figure 2.2.11*, confirming the proposed structures. A quantitative analysis of the absorption spectrum was not possible since the polymers contain defects and the absorption coefficients are unknown.

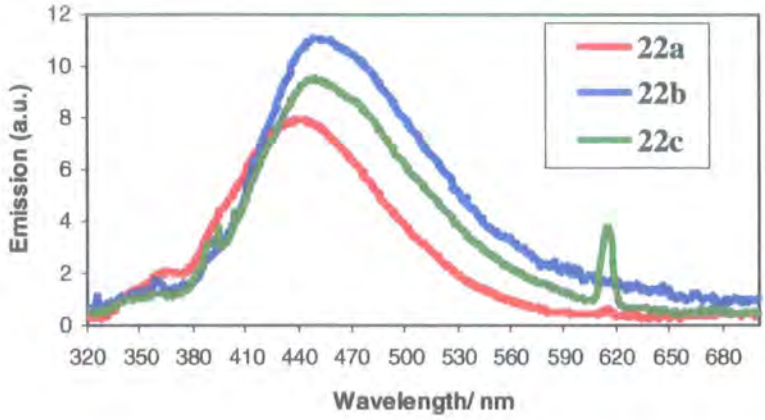

Figure 2.2.12 Solution state photoluminescence spectra of polymers ***22a, b*** *and* ***c*** *measured in 10 mg/l solutions in THF at an excitation wavelength of 308 nm.*

Hay and Klavetter have shown that the emission of a copolymer comprising conjugated units of different lengths stems from the longest conjugated units.[21] It was therefore expected that the emission maximum would be red-shifted as the length of the conjugated units increases from polymer **22a** to **22c**. Indeed, the emission maximum for polymer **22a** is found at 440 nm whereas the maxima for **22b** and **22c** are found at 450 nm (*Figure 2.2.12*).

However, it was not possible to prepare polymers with a comonomer **18** feed ratio higher than 30% because of the solubility problems already observed in the case of polymer **22c**. This limited the range of conjugated units, which could be prepared. Furthermore pinacol defects were found in all polymers prepared *via* the McMurry reaction. Therefore, the polymers were found unsuitable for the preparation of electroluminescent devices and not further investigated.

2.3 Conclusions

The McMurry reaction was found to be suitable for the coupling of fluorinated aromatic aldehydes but not for fluorinated aromatic ketones. Three comonomers with flexible linkers and fluorinated aromatic aldehyde end-groups were prepared as well as 2,3,5,6-tetrafluoroterephtalaldehyde. A range of polymers with moderate molecular weights (M_n 3,000 – 8,000) were synthesised on the basis of these

monomers. This copolymer approach allowed the variation of the length of conjugated units within those polymers.

However the solubility of the polymers with longer conjugated units was limited. Furthermore, all polymers showed pinacol defects. Therefore, the McMurry reaction was abandoned and different approaches to fluorinated block copolymers were investigated (Chapter 3).

2.4 Experimental

2.4.1 General

Apparatus

Melting points were obtained using an Electrothermal IA9200 series digital melting point apparatus. Elemental analysis data were recorded on an Exeter Analytical Elemental Analyser CE-440. Mass spectra were recorded using either a Micromass AutoSpec mass spectrometer or a Hewlett Packard Series II gas chromatograph with a HP1 GC column, attached to a Fisons Trio 1000 mass spectrometer. Calculated molecular weights are reported in g mol^{-1}. NMR-spectra were recorded using either a Varian Inova (^{1}H at 500 MHz and ^{13}C at 125 MHz), a Varian VXR400S (^{1}H at 399.95 MHz and ^{13}C at 100.58 MHz), a Varian Unity (^{1}H at 299.91 MHz and ^{13}C at 75.41 MHz) or a Varian Gemini (^{1}H at 200 MHz, ^{13}C at 50.2 MHz and ^{19}F at 188 MHz). Chemical shifts are reported in parts per million with respect to the solvent peak ($CDCl_3$ δ 7.27; TCE-d_2 δ 5.99; C_7D_8 δ 7.09, 7.00, 6.98, 2.09). The UV-lamp used was a Blak-Ray longwave UV-lamp (UVP inc., CA, 2 AMPS at 220 V). Molecular weights of polymers were determined using a Viscotek gel permeation chromatograph with refractive index detector using chloroform as eluent and polystyrene standards (3 x PL_{gel} mixed bed 5 μm columns). Absorption spectra were recorded using a Unicam UV/Vis spectrometer UV2. A FluroMax-2 spectrometer (ISA Instruments) was used for the emission spectra.

Chemicals

Reagents were supplied by Aldrich except pentaflurobenzaldehyde (Apollo), 2-ethylhexane-1,3-diol (Fluka) and lithium chloride (Lancaster). Deuterated solvents were used as supplied (Goss). THF was dried over alumina (EasyPure System).

2.4.2 9-Pentafluorophenyl-10-phenyl-1,2,3,4-tetraphenylpenanthrene (2)

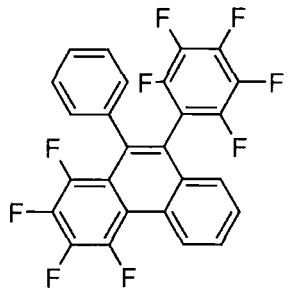

$TiCl_3$ (1.54 g, 10 mmol) and $LiAlH_4$ (0.19 g, 5 mmol) were placed in a flask under nitrogen. Dry THF (40 ml) was added at 0 °C. The mixture was refluxed for 1 h and cooled to room temperature. 2,3,4,5,6-Pentafluorobenzophenone (2.55 g, 9.4 mmol) was added. The mixture was refluxed for 20 h and quenched with 2 N hydrochloric acid (20 ml). The THF was removed under reduced pressure. The product did not dissolve in $CHCl_3$ (10 ml) as expected and 9-pentafluorophenyl-10-phenyl-1,2,3,4-tetraphenylpenanthrene (0.5 g) was collected by filtration. A further fraction was obtained by column chromatography (silica gel /hexane: chloroform 3:1) of the remaining solution. Combined yield of *9-pentafluorophenyl-10-phenyl-1,2,3,4-tetraphenylpenanthrene* (0.7 g, 30%) as a white powder, mp 272 °C. Found: C, 63.22%; H, 1.74%; M(MS, CI) 492 (M^+). Calculated for $C_{26}H_9F_9$: C, 63.43%; H, 1.84%; M 492. ^1H NMR (C_7D_8, 200 MHz) δ 7.6 –7.4 (m, 9H); ^{13}C NMR (C_7D_8, 100 MHz)[#] δ 144.93*, 143.75*, 142.49*, 141.71*, 138.89*, 138.52, 138.27*, 137.93*, 131.57, 131.40, 129.31, 128.42, 127.87, 127.33, 126.98, 123.85, 117.91, 117.87, 117.37, 117.28, 116.45, 113.31; ^{19}F NMR (C_7D_8, 188 MHz) δ –134.62 (t, J = 17.5 Hz, 1F), -139.69 (m, 2F), –145.33 (t, J = 17.5 Hz, 1F), –153.06 (t, J = 20.5 Hz, 1F), –155.82 (t, J = 17.5 Hz, 1F), -157.68 (t, J = 17.5 Hz, 1F), -161.59 (m, 2F) (see appendix page 130 and 131).

[#] The resonances that are marked with an asterix (*) were determined from ^{19}F decoupled ^{13}C NMR spectrum. The remaining resonances were determined from a ^1H decoupled ^{13}C NMR spectrum.

1,2-Diphenyl-1-pentafluorophenyl-2-(2,3,4,5-tetrafluorophenyl)ethene

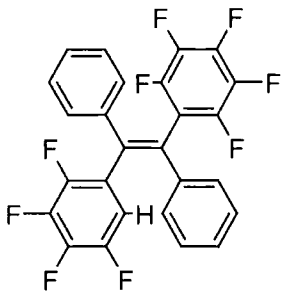

1,2-Diphenyl-1-pentafluorophenyl-2-(2,3,4,5-tetrafluorophenyl)ethane was found as the second most abundant product and characterised by GC-MS and ^{19}F NMR spectrum. M (MS, CI) 494 (M^+), ^{19}F NMR ($CDCl_3$, 188 MHz) δ -134.23 (ddd, J = 6Hz, 12Hz, 20Hz; 1F, C*F ortho* to CH), -139.44 (m, 2F, pentafluorophenyl), -139.84 (ddd, J = 4 Hz, 12Hz, 25 Hz, 1F, C*F ortho* to C=C), -152.46 (ddd, J = 4 Hz, 20 Hz, 20Hz, 1F, C*F meta* to C=C), -154.41 (ddd, J = 6 Hz, 20 Hz, 25 Hz, 1F, C*F meta* to CH), -154.65 (m, 1F, pentafluorophenyl), -161.89 (m, 2F, F_{12}, pentafluorophenyl) (see appendix page 132 and 133).

2.4.3 Decafluorostilbene (5)

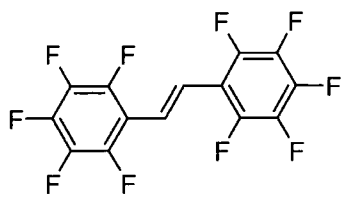

$TiCl_4$ (1.45 g, 0.85 ml, 7.65 mmol) was added to a suspension of Zn (1.0 g, 15.3 mmol) in dioxane (30 ml) at –10 °C under nitrogen. The mixture was refluxed for 1 h and cooled to room temperature. 2,3,4,5,6-Pentafluorobenzaldehyde (1.0 g, 5.1 mmol) was then added and the mixture refluxed for 14 h. The mixture was quenched with 2 N hydrochloric acid (5 ml) and all solvents removed under reduced pressure. The product was re-dissolved in diethyl ether, washed with 2 N hydrochloric acid and water and dried ($MgSO_4$) yielding, after evaporation of the solvent, decafluorostilbene (0.81g, 89%) as a white solid. As the melting point and the NMR spectra were in good agreement with those reported in the literature[22] no further analysis was carried out. mp 104 °C (lit.[23,24] 103-105 °C). ^1H NMR ($CDCl_3$,

200 MHz) δ 7.33 (s, 2H); ^{19}F NMR ($CDCl_3$, 188 MHz) δ –142.21 (m, 2F), -153.97 (t, J = 21 Hz, 1F), –162.44 (m, 2F).

2.4.4 Pentafluorobenzaldyde diethylacetal (6)

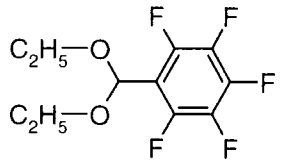

A mixture of pentafluorobenzaldehyde (20 g, 102 mmol), ethanol (20 ml), ethyl orthoformate (20 ml) and conc. H_2SO_4 (0.1 ml) were refluxed for 1.5 h. The solvent was removed under reduced pressure and diethyl ether (150 ml) was added. The organic layer was washed with water, aqueous $NaHCO_3$ and water, dried ($MgSO_4$) and the solvent removed under reduced pressure yielding pentafluorobenzaldyde diethylacetal (27 g, 98%) as a clear liquid. As the NMR spectra were in good agreement with those reported in the literature[25] no further analysis was carried out. ^{1}H NMR ($CDCl_3$, 200 MHz) δ 5.71 (s, 1H, C*H*O_2), 3.4-3.9 (m, 4H, OCH_2), 1.26 (t, J = 7 Hz, 6H, CH_3); ^{13}C {^{1}H} NMR ($CDCl_3$, 100 MHz) δ 144.86 (d, J = 250 Hz, *C*F), 141.18 (d, J = 250 Hz, *C*F), 137.49 (d, J = 250 Hz, *C*F), 113.21 (*C*-CHO_2), 96.50 (*C*HO_2), 63.71 (O*C*H_2CH$_3$), 14.95 (OCH$_2$*C*H$_3$); ^{19}F NMR ($CDCl_3$, 188 MHz) δ -142.91 (m, 2F), -154.48 (t, J = 20.5 Hz, 1F), –162.28 (m, 2F).

2.4.5 1,17-Bis(4-diethoxymethyl-2,3,5,6-tetrafluorophenyloxy)-3,6,9,12,15-pentaoxaheptadecane (10)

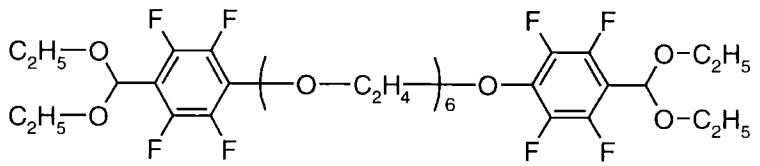

Hexa(ethylene glycol) (9.7 g, 34.3 mmol) was dissolved in dry THF (300 ml). *n*-Butyllithium in hexane (1.6M. 43.7 ml, 70 mmol) was added and the mixture stirred for 30 min under nitrogen. Then 2,3,4,5,6-pentafluorobenzaldehyde diethylacetal (18.5 g, 68.6 mmol) was added. The mixture was refluxed for 14 h. After the addition of water (20 ml) the volatile components were removed under reduced pressure. Diethyl ether (200 ml) was added and the organic phase was washed twice with brine, twice with water and dried ($MgSO_4$). The diethyl ether was removed

under reduced pressure and the product purified by column chromatography (silica gel, hexane: diethyl ether 1:1 followed by pure diethyl ether) yielding *1,17-bis(4-diethoxymethyl-2,3,5,6-tetrafluorophenyloxy)-3,6,9,12,15-pentaoxaheptadecane* (11.3 g, 42%) as a colourless oil. Found C: 52.26%; H, 5.95%; M(MS, CI) 800 (MNH_4^+). Calculated for $C_{34}H_{46}F_8O_{11}$: C, 52.17% H, 5.92%; M 782. ^{1}H NMR ($CDCl_3$, 200 MHz) δ 5.67 (s, 2H, acetal C*H*), 4.35 (t, J = 5 Hz, 4H, ar. COCH_2), 3.62 (m, 28H, OC_2H_4O and OCH_2CH_3), 1.23 (t, J = 7 Hz, 12H); ^{13}C {^{1}H} NMR ($CDCl_3$, 100 MHz) δ 144.77 (d, J = 260 Hz, ar. *C*F), 140.91 (d, J = 250 Hz, ar. *C*F), 137.95 (ar. *C*O), 111.46 (ar. *C*-CHO_2), 96.53 (*C*HO_2) 74.37, 71.05, 70.81, 70.79, 70.76, 70.29 (OC_2H_4O), 63.44 (OCH_2CH_3), 14.92 (OCH_2CH_3); ^{19}F NMR ($CDCl_3$, 188 MHz) δ -144.89 (m, 4F, C*F ortho* to CHO_2) -157.26 (m, 4F, C*F ortho* to OC_2H_4) (see appendix page 134).

2.4.6 1,3-Bis(4-diethoxymethyl-2,3,5,6-tetrafluorophenyloxy)-2,2-dimethylpropane (11)

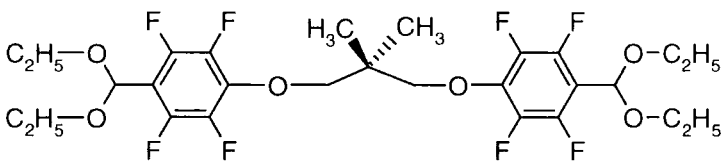

2,2-Dimethylpropane-1,3-diol (2.08 g, 20 mmol) was dissolved in dry THF (200 ml). *n*-Butyllithium in hexane (1.6 M, 25 ml, 40 mmol) was added and the mixture stirred for 30 min under nitrogen. Then 2,3,4,5,6-pentafluorobenzaldehyde diethylacetal (12 g, 44.4 mmol) was added. The mixture was refluxed for 14 h. After the addition water (20 ml) the volatile components were removed under reduced pressure. Diethyl ether (150 ml) was added and the organic phase was washed twice with brine, twice with water and dried ($MgSO_4$). The diethyl ether was removed under reduced pressure and the product purified by column chromatography (silica gel, hexane: diethyl ether 20:1) yielding *1,3-bis(4-diethoxymethyl-2,3,5,6-tetrafluorophenyloxy)-2,2-dimethylpropane* (3.38 g, 28%) as a colourless oil. Found: C, 53.41% H, 5.34% M(MS, EI) 604 (M^+). Calculated for $C_{27}H_{32}F_8O_6$: C, 53.64% H, 5.34%; M 604. ^{1}H NMR ($CDCl_3$, 200 MHz) δ 5.69 (s, 2H, acetal C*H*), 4.12 (s, 4H, ar. C-O-CH_2), 3.66 (m, 8H, O-CH_2CH$_3$), 1.25 (t, J = 7 Hz, 12H, O-CH$_2$CH_3), 1.14 (s, 6H, C(CH_3)$_2$); ^{13}C {^{1}H} NMR ($CDCl_3$, 100 MHz) δ 144.87 (d, J = 250 Hz,

ar. *C*-F), 140.82 (d, *J* = 250 Hz, ar. *C*-F), 138.04 (ar. *C*-O), 111.32 (ar. *C*-CHO_2), 96.58 (CHO_2), 79.21 (OCH_2CCH_3) 63.43 (OCH_2CH_3), 37.28 (OCH_2CCH_3), 21.03 (OCH_2CCH_3) 14.95 (OCH_2CH_3); ^{19}F NMR ($CDCl_3$, 188 MHz) δ -144.98 (m, 4F, C*F ortho* to CHO_2) -157.86 (m, 4F, C*F ortho* to OCH_2) (see appendix page 135).

2.4.7 1,3-Bis(4-diethoxymethyl-2,3,5,6-tetrafluorophenyloxy)-2-ethylhexane (12)

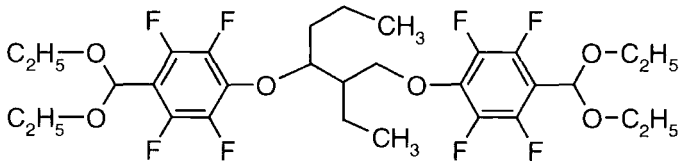

2-Ethylhexane-1,3-diol (2.92 g, 20 mmol) was dissolved in dry THF (200 ml). *n*-Butyllithium in hexane (1.6M, 25 ml, 40 mmol) was added and the mixture stirred for 30 min under nitrogen. Then, 2,3,4,5,6-pentafluorobenzaldehyde diethylacetal (11 g, 40.7 mmol) was added. The mixture was refluxed for 14 h. After the addition of water (20 ml) the volatile components were removed under reduced pressure. Diethyl ether (150 ml) was added and the organic phase was washed twice with brine, twice with water and dried ($MgSO_4$). The diethyl ether was removed under reduced pressure and the product purified by column chromatography (silica gel, hexane: diethyl ether 20:1) yielding *1,3-bis(4-diethoxymethyl-2,3,5,6-tetrafluorophenyloxy)-2-ethylhexane* (7.35 g, 57%) as a colourless oil. Found: C, 55.78%; H, 5.96%; M(MS, CI) 646 (M^+). Calculated for $C_{27}H_{32}F_8O_6$: C, 55.73%; H, 5.92%; M 646. ^1H NMR ($CDCl_3$, 200 MHz) δ 5.70 (s, 2H, acetal C*H*), 4.60 (m, 1H, OC*H*PrCHEtCH$_2$O), 4.30 (m, 2H, OCHPrCHEtC*H*$_2$O), 3.67 (m, 8H, O-C*H*$_2$CH$_3$), 2.06 (m, 1H, OCHPrC*H*EtCH$_2$), 1.68 (m, 6H, RC*H*$_2$CH$_3$), 1.26 (t, *J* = 7 Hz, 12H, O-CH$_2$C*H*$_3$), 0.98 (m, 6H, RCH$_2$C*H*$_3$); ^{13}C {^1H} NMR ($CDCl_3$, 100 MHz) δ 144.95 (d, *J* = 250 Hz, ar. *C*F), 141.40 (d, *J* = 250 Hz, ar. *C*F), 140.99 (d, *J* = 250 Hz, ar. *C*F), 137.69 (ar. *C*O), 136.78 (ar. *C*O), 111.32 (ar. *C*CHO$_2$), 96.60 (*C*HO$_2$), 84.87 (O*C*HPrCHEtCH$_2$O) 73.96 (OCHPrCHEt*C*H$_2$O), 63.50 (O*C*H$_2$CH$_3$), 43.92, 32.94, 19.52, 19.19, 18.93, 18.26 (aliph. *C*), 14.98 (OCH$_2$*C*H$_3$), 13.99, 13.92, 12.05, 11.69 (aliph. *C*); ^{19}F NMR ($CDCl_3$, 188 MHz) δ -144.83 (m, 4F, C*F ortho* to CHO_2), -156.56 (m, 2F, C*F ortho* to O-CH$_2$), -157.57 (m, 2F, C*F ortho* to O-CH$_2$) (see appendix page 136).

2.4.8 1,17-Bis(4-formyl-2,3,5,6-tetrafluorophenyloxy)-3,6,9,12,15-pentaoxaheptadecane (13)

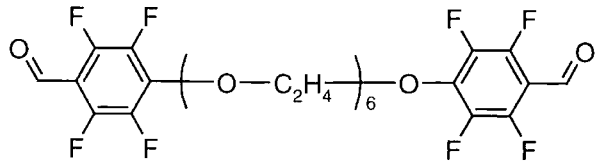

Bis(4-diethoxymethyl-2,3,5,6-tetrafluorophenyloxy)-3,6,9,12,15-pentaoxaheptadecane (11.3 g, 14.4 mmol) was dissolved in a mixture of THF and water (100 ml/ 50 ml) and conc. H_2SO_4 (1 ml) was added. The mixture was stirred over night at 55 °C. The THF was removed under reduced pressure and diethyl ether (100 ml) was added. The organic phase was washed with water, aqueous $NaHCO_3$ and twice with water. It was dried ($MgSO_4$) and the solvent removed under reduced pressure yielding *1,17-bis(4-formyl-2,3,5,6-tetrafluorophenyloxy)-3,6,9,12,15-pentaoxaheptadecane* (8.9 g, 97%) as a colourless oil. Found: C, 48.86%; H, 4.14%; M(MS, CI) 652 (MNH_4^+). Calculated for $C_{26}H_{26}F_8O_9$: C, 49.22%, H, 4.13%, M 634. ^{1}H NMR ($CDCl_3$, 200 MHz) δ 10.18 (s, 2H, C*H*O), 4.52 (m, 4H, ar. COCH_2), 3.83 (m, 4H, ar. COCH$_2$CH_2), 3.59 (m, 16H, OC$_2H_4$); ^{13}C {^{1}H} NMR ($CDCl_3$, 100 MHz) δ 182.09 (*C*HO), 147.52 (d, *J* = 260 Hz, ar. *C*F), 143.10 (ar. *C*O), 140.26 (d, *J* = 250 Hz, ar. *C*F), 108.90 (ar. *C*-CHO), 74.21, 70.80, 70.50, 70.44, 70.03, (OC$_2$H$_4$O); ^{19}F NMR ($CDCl_3$, 188 MHz) δ -146.75 (m, 4F, C-*F ortho* to CHO) -157.03 (m, 4F, C-*F ortho* to OC$_2$H$_4$) (see appendix page 137).

2.4.9 1,3-Bis (4-formyl-2,3,5,6-tetrafluorophenyloxy)- 2,2-dimethylpropane (14)

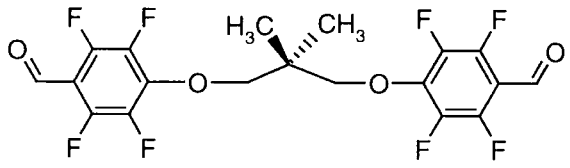

1,3-Bis(diethoxy-4-methyl-2,3,5,6-tetrafluorophenyloxy)-2,2-dimethylpropane (2.8 g, 4.6 mmol) was dissolved in a mixture of THF and water (60 ml/ 30 ml) and conc. H_2SO_4 (0.5 ml) was added. The mixture was stirred over night at 55 °C. The THF was removed under reduced pressure and diethyl ether (80 ml) was added. The organic phase was washed with water, aqueous $NaHCO_3$ and twice with water. It was dried ($MgSO_4$) and the solvent removed under reduced pressure yielding *1,3-bis*

(4-formyl-2,3,5,6-tetrafluorophenyloxy)-2,2-dimethylpropane (2.0 g, 95%) as a colourless oil. Found: C, 50.48%; H, 2.80%; M(MS, EI) 456 (M^+). Calculated for $C_{19}H_{12}F_8O_4$: C, 50.01%, H, 2.65%, M 456. ^{1}H NMR ($CDCl_3$, 200 MHz) δ 10.22 (s, 2H, C*H*O), 4.30 (s, 4H, ar. C-O-C*H*$_2$), 1.18 (s, 6H, C*H*$_3$) ^{13}C {^{1}H} NMR ($CDCl_3$, 100 MHz) δ 182.02 (*C*HO), 147.60 (d, *J* = 260 Hz, ar. *C*F), 143.06 (ar. *C*O), 140.20 (d, *J* = 250 Hz, ar. *C*F), 109.14 (ar. *C*-CHO), 79.02 (O*C*H$_2$CCH$_3$), 37.38 (OCH$_2$*C*CH$_3$), 21.01 (OCH$_2$C*C*H$_3$); ^{19}F NMR ($CDCl_3$, 188 MHz) δ -146.30 (m, 4F, C*F ortho* to CHO) -157.37 (m, 4F, C*F ortho* to O-C_2H_4) (see appendix page 138).

2.4.10 1,3-Bis(4-formyl-2,3,5,6-tetrafluorophenyloxy)-2-ethylhexane (15)

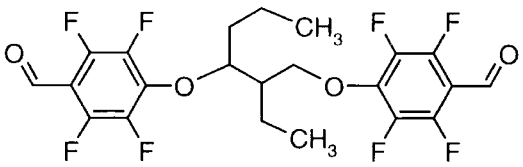

1,3-Bis(4-diethoxymethyl-2,3,5,6-tetrafluorophenyloxy)-2-ethylhexane (7.0 g, 10.8 mmol) was dissolved in a mixture of THF and water (200 ml/ 66 ml) and H_2SO_4 (1.5 ml) was added. The mixture was stirred overnight at 55 °C. The THF was removed under reduced pressure and diethyl ether (200 ml) was added. The organic phase was washed with water, aqueous $NaHCO_3$ and twice with water. It was dried ($MgSO_4$) and the solvent removed under reduced pressure yielding *1,3-bis(4-formyl-2,3,5,6-tetrafluorophenyloxy)-2-ethylhexane* (4.92 g, 91%) as a colourless oil. Found: C, 53.04%; H, 3.73%; M(MS, EI) 498 (M^+). Calculated for $C_{22}H_{18}F_8O_4$: C, 53.02%; H, 3.64%; M 498. ^{1}H NMR ($CDCl_3$, 200 MHz) δ 10.23 (s, 2H, C*H*O), 4.79 (m, 1H, OC*H*PrCHEtCH$_2$O), 4.52 (m, 2H, OCHPrCHEtC*H*$_2$O), 2.06 (m, 1H, OCHPrC*H*EtCH$_2$), 1.68 (m, 6H, RC*H*$_2$CH$_3$), 0.98 (m, 6H, RCH$_2$C*H*$_3$); ^{13}C {^{1}H} NMR ($CDCl_3$, 100 MHz) δ 182.01 (*C*HO), 147.91 (d, *J* = 260 Hz, ar. *C*-F), 143.02, 143.53 (ar. *C*-O), 140.91 (d, *J* = 250 Hz, ar. *C*-F), 140.43 (d, *J* = 250 Hz, ar. *C*-F), 109.41 (ar. *C*-CHO), 109.32 (ar. *C*-CHO), 85.32 (O*C*HPrCHEtCH$_2$O), 73.09 (OCHPrCHEt*C*H$_2$O), 44.09, 33.45, 33.16, 19.81, 18.92, 18.04, 13.90, 12.00, 11.36 (aliph. *C*); ^{19}F NMR ($CDCl_3$, 188 MHz) δ -146.26 (m, 4F, C*F ortho* to CHO), -156.26 (m, 2F, C*F ortho* to OCR), 157.25 (m, 2F, C*F ortho* to OCR) (see appendix page 139).

2.4.11 2,3,5,6-Tetrafluoroterephtalaldehyde tetra-acetate (17)

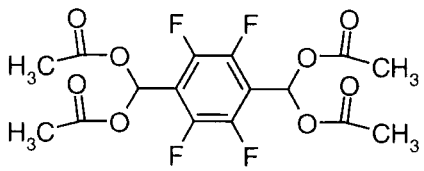

Tetrafluoro-*para*-xylene (2 g, 11.2 mmol) was dissolved in a stirred mixture of acetic acid (20 ml), acetic anhydride (40 ml) and sulfuric acid (3.3 ml, 6 g) and the mixture was cooled to 5 °C. Chromium trioxide (3.6 g, 36 mmol) was added gradually in order to keep the temperature of the cooled mixture between 5 and 7 °C. After 4.5 h the mixture was poured onto crushed ice (100 g) and left overnight. The product was filtered and washed twice with water. It was then dissolved in diethyl ether (30 ml), again washed twice with water, dried ($MgSO_4$) and recrystallised from ethanol (6 ml) yielding *2,3,5,6-tetrafluoroterephtalaldehyde tetra-acetate* (0.11 g, 2.4%) as a white solid, mp 182 °C. Found: C, 46.66%; H, 3.30%; M(MS, EI) 410 (M^+). Calculated for $C_{16}H_{14}F_4O_8$: C, 46.84%; H, 3.44%; M 410. ^1H NMR ($CDCl_3$, 200 MHz) δ 7.84 (s, 2H, CHO_2), 2.07 (s, 12H, CH_3); ^{13}C {^1H} NMR ($CDCl_3$, 100 MHz) δ 168.23, (*C*O), 82.96 (*C*HO_2), 20.53 (*C*H_3); ^{19}F NMR ($CDCl_3$, 188 MHz) δ -141.26 (s, 4F) (see appendix page 140).

2.4.12 2,3,5,6-Tetrafluoroterephtalaldehyde (18)

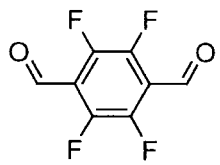

Starting from 2,3,5,6-tetrafluoroterephtalaldehyde tetra-acetate (**17**):

2,3,5,6-Tetrafluoroterephtalaldehyde tetra-acetate (0.24 g, 0.59 mmol) was added to a mixture of water (2 ml), ethanol (2 ml) and concentrated sulphuric acid (0.1 ml). The mixture was refluxed for 1.5 h and cooled to room temperature. All solvents were removed under reduced pressure and the mixture extracted with diethyl ether (5 ml), dried ($MgSO_4$) and the diethyl ether evaporated yielding 2,3,5,6-tetrafluoroterephtalaldehyde (0.07 g, 58%) as a white solid. NMR and mass spectra were identical to those described below.

Starting from 1,4-bis(dibromomethyl)-2,3,5,6-tetrafluorobenzene (**19**):

1,4-Bis(dibromomethyl)-2,3,5,6-tetrafluorobenzene (7.3 g, 14.7 mmol) was suspended in conc. H_2SO_4 (20 ml) and heated under vacuum increasing the temperature over 5 h from 100 °C to 140 °C. Further conc. H_2SO_4 (20 ml) was added and the mixture heated at 140 °C for 3 h. The mixture was cooled to room temperature and poured onto ice (100 g). The aqueous layer was extracted twice with diethyl ether (100 ml), the organic layer subsequently washed twice with water and dried ($MgSO_4$). The solvent was removed under reduced pressure and the product purified by column chromatography (silica gel, diethyl ether: hexane 1:1), yielding *2,3,5,6-tetrafluoroterephtalaldehyde* (1.05 g, 35%) as a white solid, mp 131 °C. Found: C, 46.50%; H, 0.98%: M(MS, EI) 206 (M^+). Calculated for $C_8H_2F_4O_2$: C, 46.62%; H, 0.98%; M 206. ^{1}H NMR ($CDCl_3$, 200 MHz) δ 10.37 (s, 2H); ^{13}C {^{1}H} NMR ($CDCl_3$, 100 MHz) δ 181.79 (*C*HO), 146.50 (d, J = 270 Hz, ar. *C*F), 118.63 (ar. *C*-C); ^{19}F NMR ($CDCl_3$, 188 MHz) δ -144.05 (s, 4F) (see appendix page 141).

2.4.13 1,4-Bis(dibromomethyl)-2,3,5,6-tetrafluorobenzene (19)

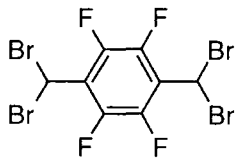

Tetrafluoro-*para*-xylene (4.0 g, 22.5 mmol) and elemental bromine (5.14 ml, 16.0 g, 100 mmol) were heated to 160 °C under nitrogen in a 250 ml two necked round bottomed flask equipped with a reflux condenser. The reflux condenser was connected to a bubbler followed by a scrubbing tower. The latter was filled with an aqueous solution of NaOH and $NaSO_3$. The reaction mixture was heated and irradiated with a UV lamp. After 4 h the mixture was cooled and a nitrogen inlet was connected to the flask. Nitrogen was blown through the flask and all HBr and excess bromine removed. More bromine (4.0 ml, 12.44 g, 0.78 mol) was added and the mixture heated and irradiated again for 2.5 h. It was cooled again, HBr and excess bromine were removed, and the procedure repeated three times (once with 4 ml bromine and twice with 1.2 ml bromine). The product was dissolved in $CHCl_3$ and washed with aqueous $NaHCO_3$ solution and twice with water yielding an off-white solid (7.7 g, 69%). The product was used in the next step without further purification. A small fraction (0.3 g) was recrystallised from acetic acid yielding *1,4-*

bis(dibromomethyl)-2,3,5,6-tetrafluorobenzene as a white solid, mp 93 °C. Found: C, 19.58%; H, 0.37%; M(MS, EI) 494 (M^+). $C_8H_2F_4Br_4$ requires C, 19.46%; H, 0.41%; M 494. ^{1}H NMR ($CDCl_3$, 200 MHz) δ 6.83 (s, 2H); ^{13}C {^{1}H} NMR ($CDCl_3$, 100 MHz) δ 143.05 (d, J = 260 Hz, ar. *C*F), 121.62 (ar. *C*), 20.02 (*C*HBr_2); ^{19}F NMR ($CDCl_3$, 188 MHz) δ -138.69 (s, 4F) (see appendix page 142).

2.4.14 5,6,28,29,30,31,32,33-Octafluoro-8,11,14,17,20,23,26-heptaoxa-tricyclo[22.2.2.2^{4,7}]tritriaconta-1(30),2,4(33),5,7(32),27(31),25-heptaene (20)

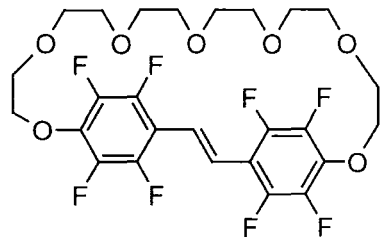

$TiCl_4$ (0.36 g, 0.21 ml, 1.9 mmol) was added to a suspension of zinc dust (0.25 g, 3.8 mmol) in THF (10 ml) and pyridine (0.15 ml) at 0 °C under nitrogen. The mixture was refluxed for 1 h and then cooled to room temperature. 1,17-Bis (4-formyl-2,3,5,6-tetrafluoro-phenyloxy)-3,6,9,12,15-pentaoxa-heptadecane (0.4 g, 0.63 mmol) was added. The mixture was refluxed for 24 h and then quenched with 2 N hydrochloric acid (10 ml). The mixture was extracted three times with diethyl ether (30 ml). The combined extracts were washed with $NaHCO_3$ solution, water, dried ($MgSO_4$) and the solvent removed under reduced pressure. The product was purified by column chromatography (silica gel /diethyl ether) yielding *5,6,28,29,30,31,32,33-octafluoro-8,11,14,17,20,23,26-heptaoxa-tricyclo[22.2.2.2^{4,7}]tritriaconta-1(30),2,4(33),5,7(32),27(31),25-heptaene* (0.10 g, 26%) as a white solid, mp 81-83 °C. Found: C, 51.66%; H, 4.37%; M(MS, EI) 602 (M^+). Calculated for $C_{26}H_{26}F_8O_7$: C, 51.83%; H, 4.35%; M 602. ^{1}H NMR ($CDCl_3$, 200 MHz) δ 7.40 (s, 2H, C*H*=C*H*), 4.46 (m, 4H, ar. COCH_2), 3.78 (m, $COCH_2CH_2$), 3.33 (m, 16H, OC_2H_4O); ^{13}C {^{1}H} NMR ($CDCl_3$, 100 MHz) δ 144.90 (d, J = 250 Hz, ar. *C*F), 141.91 (d, J = 250 Hz, ar. *C*F), 137.98 (ar. *C*O), 120.80 (*C*H=*C*H), 110.06 (ar. *C*-CH=CH) 73.13, 72.23, 70.81, 70.42, 69.78, 69.74 (OC_2H_4O); ^{19}F NMR ($CDCl_3$, 188 MHz) δ -145.01 (m, 4F, C*F ortho* to CH=CH) -157.44 (m, 4F, C*F ortho* to OC_2H_4) (see appendix page 143).

2.4.15 Polymerisation via the McMurry reaction

An illustrative example of a polymerisation reaction is given below. The choice of the flexible linker (**13, 14** or **15**) and the fraction (y) of 2,3,5,6-tetrafluoroterephtalaldehyde were varied.

$TiCl_4$ (0.72 g, 0.42 ml, 3.8 mmol) was added to a suspension of zinc dust (0.49 g, 7.6 mmol) in dry THF (20 ml) and pyridine (0.30 ml) at 0 °C under nitrogen. The mixture was refluxed for 1 h and then cooled to room temperature. 1,17-Bis-(4-formyl-2,3,5,6-tetrafluorophenyloxy)-3,6,9,12,15-pentaoxa-heptadecane (0.64 g, 1.0 mmol) and 2,3,5,6 tetrafluoroterephtalaldehyde (0.052 g, 0.25 mmol) were dissolved in dry THF (0.5 ml) and added to the mixture. Within 10 min the solution became so viscous that stirring with a magnetic stirrer ceased. The mixture was refluxed for 14 h and cooled to room temperature. DCM (20 ml) was added followed by 2 N hydrochloric acid (20 ml). The organic layer was washed with aqueous $NaHCO_3$ and brine, dried ($MgSO_4$) and the solvent removed under reduced pressure. The product was redissolved in chloroform and precipitated into ethanol. The polymer was characterised by GPC and ^1H NMR spectroscopy since the latter showed pinacol defects in the polymer. ^1H NMR ($CDCl_3$, 200 MHz) δ 7.39 (*trans* C*H*=C*H*), 6.74 (*cis* C*H*=C*H*), 5.34 (C*H*OHC*H*OH), 4.40 (ar. $COCH_2$), 3.83 ($COCH_2CH_2$), 3.63(OC_2H_4O); M_n = 8,300 g mol^{-1} M_w =27,000 g mol^{-1} PDI = 3.23. (see appendix page 144). The results of other polymerisation experiments are recorded in *Table 2.2.1* page 9.

2.5 References

1. Lenoir, D. *Synthesis* **1989**, 883.
2. Fürstner, A.; Bogdanovic, B. *Angew. Chem. Int. Ed. Engl.* **1996**, *35*, 2442.
3. Fleming, M. P.; McMurry, J. E. *Organic Synthesis* **1981**, *60*, 113.
4. Tirado-Rives, J.; Oliver, M. A.; Fronczek, F. R.; Gandour, R. D. *J. Org. Chem.* **1984**, *49*, 1627.

5. Dams, R.; Malinowski, M.; Westdorp, I.; Geise, H. *J. Org. Chem.* **1982**, *47*, 248.
6. McMurry, J. E. *Chem. Rev.* **1989**, *89*, 1513.
7. Mukaiyama, T.; Sato, T.; Hanna, J. *Chem. Lett.* **1973**, 1041.
8. McMurry, J. E.; Fleming, M. P. *J. Am. Chem. Soc.* **1974**, *96*, 4708.
9. Feast, W. J.; Millichamp, I. S. *Polym. Commun.* **1983**, *24*, 102.
10. Rehann, M.; Schlüter, A.-D. *Makromol. Chem. Rapid Commun.* **1990**, *11*, 375.
11. Cacialli, F.; Daik, R.; Feast, W. J.; Friend, R. H.; Lartigau, C. *Opt. Mat.* **1999**, *12*, 315.
12. Daik, R. *Ph.D. Thesis, University of Durham* **1997**.
13. Vysochin, V. I.; Barkhash, V. A.; Vorozhtsov, N. N. *Zh. Obshch. Khim* **1969**, *39*, 1607.
14. Cha, J. S.; Kwon, S. S. *J. Org. Chem.* **1987**, *52*, 5486.
15. Chapman, N. B.; Clarke, K.; Pinder, R. M.; Sawhney, S. N. *J. Chem. Soc. Part C* **1967**, 293.
16. Snell, J. M.; Weissberger, A. *Organic Sythesis Collective Volume 3* **1955**, 788.
17. Fuerstner, A.; Seidl, G.; Kopiske, C.; Krueger, C.; Mynott, R. *Liebigs Ann. Org. Bioorg. Chem.* **1996**, *5*, 655.
18. Siegrist, A. E.; Liechti, P.; Meyer, H. R.; Weber, K. *Helvetica Chimica Acta* **1969**, *52*, 2521.
19. Drefahl, G.; Plotner, G. *Chem. Ber.* **1961**, *94*, 907.
20. Alfrey, T.; Goldfinger, G. *J. Chem. Physics* **1944**, *12*, 205.
21. Hay, M.; Klavetter, F. L. *J. Am. Chem. Soc.* **1995**, *117*, 7112.
22. Brooke, G. M.; Mawson, S. D. *J. Fluorine Chem.* **1990**, *50*, 111.
23. Coates, G.; W., y.; Dunn, A. R.; Henling, L. M.; Ziller, J. W.; Lobkovsky, E. B.; Grubbs, R. H. *J. Am. Chem. Soc.* **1998**, *120*, 3641.
24. Rausch, M. D.; Gastinger, R. G. *Z. Naturforsch. B Anorg. Chem. Org. Chem.* **1979**, 700.
25. Puskina, L. N.; Stepanov, A. P.; Zhukov, V. S.; Naumov, A. D. *J. Org. Chem. USSR* **1972**, 592.

3 Synthesis of a Soluble Derivative of PPV and its Fluorinated Equivalent *via* the Wittig and Horner-Wittig Reactions

3.1 Introduction

The reaction of a phosphorus ylide with an aldehyde or ketone to yield olefins is generally referred to as the Wittig reaction.[1] The phosphorus ylide is usually prepared by treatment of a phosphonium salt with a base.

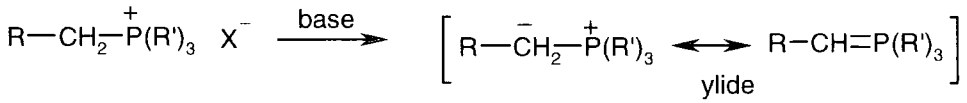

Figure 3.1.1 Synthesis of a phosphorus ylide.

The generally accepted mechanism of the Wittig reaction involves the formation of an oxaphosphetane that decomposes to give the alkene and phosphine oxide.[2] *trans*-Alkenes are obtained if the negative charge on the ylide carbon atom is stabilised by conjugation and the presence of electron-withdrawing groups such as COOR or CN. Fluorinated aromatic groups also give rise to *trans*-alkenes.[3] "Semistabilising" R-groups such as phenyl or allyl often give no great preference for *cis*- or *trans*-alkenes. Ylides with R-groups lacking any stabilising effect usually favour *cis*-alkenes.

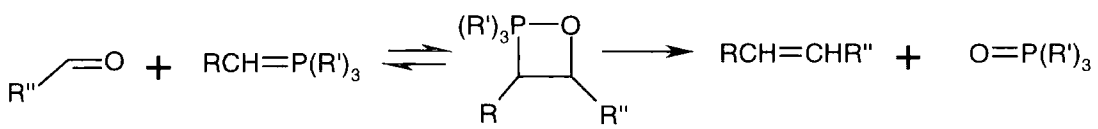

Figure 3.1.2 Mechanism of the Wittig reation.

The Horner-Wittig reaction uses phosphonate carbanions instead of ylides.[4] They are stronger nucleophiles since the negative charge is less stabilised than in the case of ylides. Hence phosphonate carbanions react with a wider variety of aldehydes and ketones and under milder conditions. The Horner-Wittig reaction

generally gives rise to *trans*-alkenes. The mechanism is similar to that of the Wittig reaction. High conversions make both the Wittig and Horner-Wittig reaction attractive for polycondensation reactions.[5] The use of both reactions will be examined for the preparation of fluorinated derivatives of PPV and their hydrogen equivalents.

3.2 Results and Discussion

Synthesis of fluorinated DSB block copolymers

The Wittig reaction has been widely used to prepare block copolymers of alternating DSB units and flexible linkers (see Chapter 1). The two double bonds of the DSB units are created during the polycondensation reaction. In contrast to the McMurry reactions described in Chapter 2, where polymers with conjugated units of varying length were prepared, this approach uses only DSB-units as the conjugated unit. When a flexible linker of a discrete length is used, rather than a mixture of oligomers, the structure of the polymer can be determined unambiguously.

In our first approach to block copolymers with fluorinated DSB units we prepared a comonomer with two terminal phosphonium groups and a central flexible linker unit. The synthesis started from the di-lithium salt of octane-1,8-diol **23** which was reacted with two equivalents of pentafluorotoluene **24** *(Figure 3.2.1)*. The product **25** was brominated with NBS and the bromine subsequently substituted by triphenylphosphine to give the bis-phosphonium salt **27**.

A soluble model compound **28** was prepared by reacting **27** with pentafluorobenzaldehyde. The model compound was fully characterised and the NMR spectra (^{1}H, ^{13}C and ^{19}F) show that all olefinic bonds have *trans*-configuration. The reaction of compound **27** with tetrafluoroterephtalaldehyde **18** gave a white polymer **29**. However, the polymer was only soluble in hot toluene or benzene and therefore not suitable for application in electroluminescent devices where solution

processing is desired. The polymer was characterised by NMR spectroscopy (^{1}H, ^{19}F) and not further investigated.

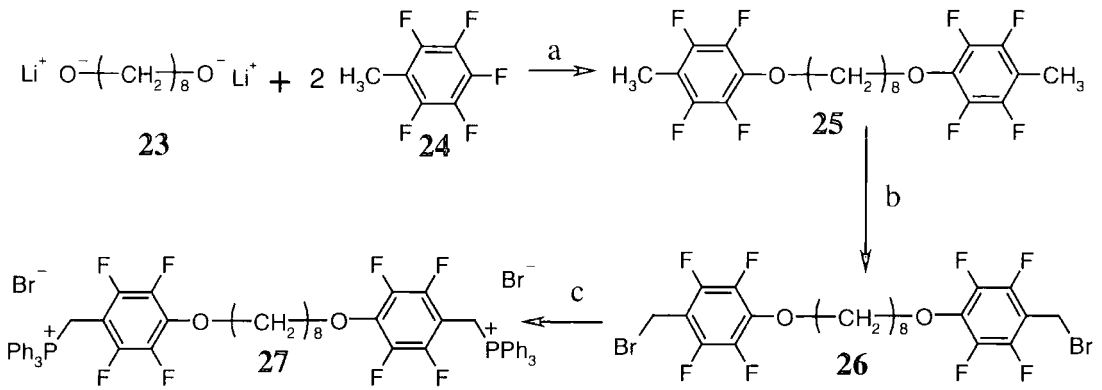

Figure 3.2.1 Synthesis a comonomer with two phosphonium end-goups. a) THF b) Br_2, hν, CCl_4 c) PPh_3, C_7H_8

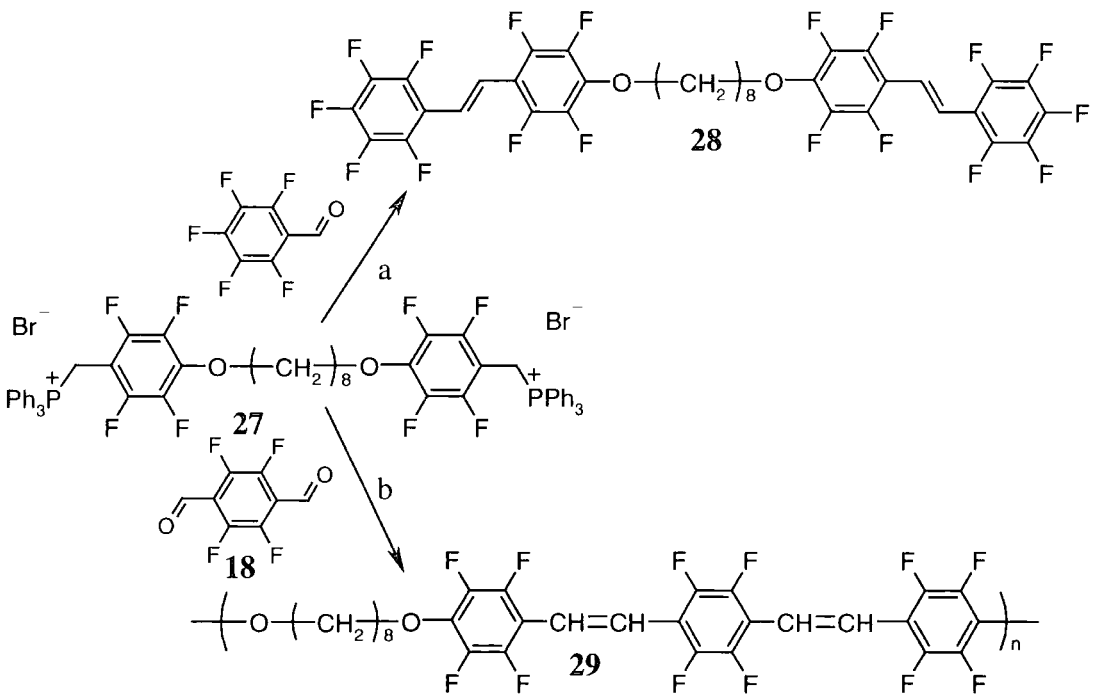

Figure 3.2.2 Synthesis of a DSB-octandiol-block copolymer and a model reaction for the polymerisation. a) LiCl, KO^{t}Bu, DMF b) LiCl, KO^{t}Bu, DMF

Since the octane-1,8-diol-spacer did not render the polymer soluble, hexa(ethylene glycol) was used in an analogous reaction sequence as a starting material to give polymers with enhanced solubility (*Figure 3.2.3*). Hexa(ethylene glycol) was deprotonated and reacted with pentafluorotoluene **24** to give compound

30. However, bromination of **30** with NBS was not selective for the methyl-groups but also occurred on the ethylene units of the sexi(ethylene oxide) spacer; the ^{1}H NMR spectrum of the product showed a decrease in the intensity for protons in the sexi(ethylene oxide) unit relative to compound **30** while additional signals were found at higher field which were assigned to protons adjacent to both oxygen and bromine in the ethylene oxide unit . Therefore, the route was abandoned.

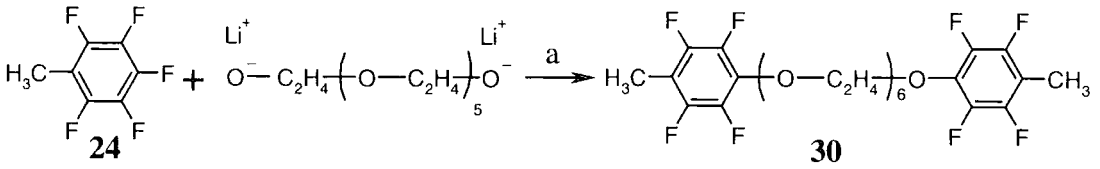

Figure 3.2.3 Synthesis of a flexible linker with a central sexi(ethylene oxide) unit. a) THF

The previous attempts to prepare block copolymers *via* Wittig reaction used comonomers, which contained a flexible linker and phosphonium end-groups. However, since such attempts were unsuccessful, a new approach starting from a comonomer comprising a flexible linker and aldehyde end-groups was investigated. A comonomer based on sexi(ethylene oxide) with aldehyde end-groups **13** could be prepared in sufficient quantity (11 g) as shown in Chapter 2. The second monomer required for a polymerisation *via* the Wittig reaction in this route is 2,3,5,6-tetrafluoroxylylen-1,4-bis(triphenylphosphonium bromide) **32** which could be prepared by bromination of tetrafluoroxylene **16** followed by substitution of bromine with triphenylphoshine (*Figure 3.2.4*).[6] However, the Wittig reaction of **32** with **13** did not result in a polymer that could be precipitated from chloroform into methanol. Instead, the ^{1}H NMR spectrum showed the presence of unreacted aldehyde end-groups, indicating a low conversion, so that this route was also abandoned.

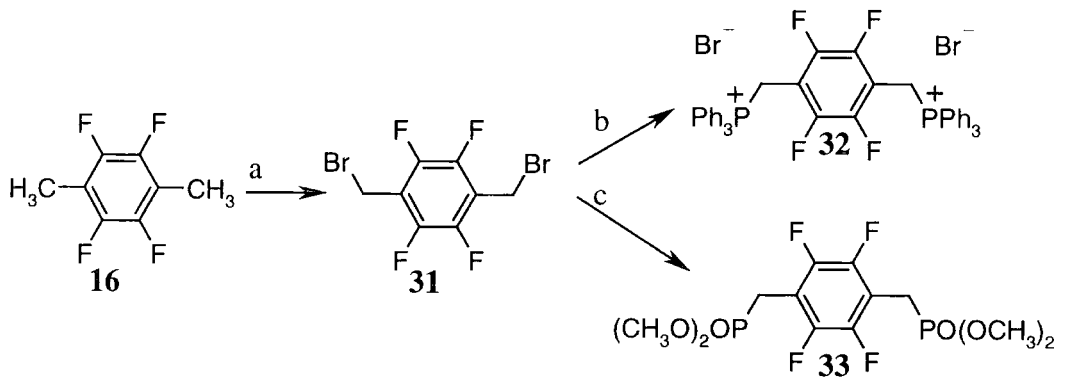

Figure 3.2.4 Synthesis of 2,3,5,6-tetrafluoroxylylen-1,4-bis(triphenylphosphonium bromide) and tetramethyl-2,3,5,6-tetrafluoroxylylene bisphosphonate. a) Br_2,hν b) PPh_3, toluene c) $P(OCH_3)_3$

In a new approach, the Horner-Wittig reaction was employed. Neckers *et al.* have shown the use of the Horner-Wittig reaction for the preparation of block copolymers (Chapter 1).[7] Tetramethyl-2,3,5,6-tetrafluoroxylylene bisphosphonate **33** can be prepared *via* the Arbuzov reaction of 1,4-bis(bromomethyl)-2,3,5,6-tetrafluorobenzene **31** with trimethylphosphite (*Figure 3.2.4).*[8] When the bisphosphonate **33** was reacted with the monomer **13** a soluble fluorinated block copolymer, poly(bis(2,3,5,6-tetrafluoro-*p*-phenylenevinylene)-2,3,5,6-tetrafluoro-*p*-phenylene-1,4,7,10,13,16,19-heptaoxanonadecane), (F-DSB-*block*-SEO) **34** was obtained (*Figure 3.2.5*).

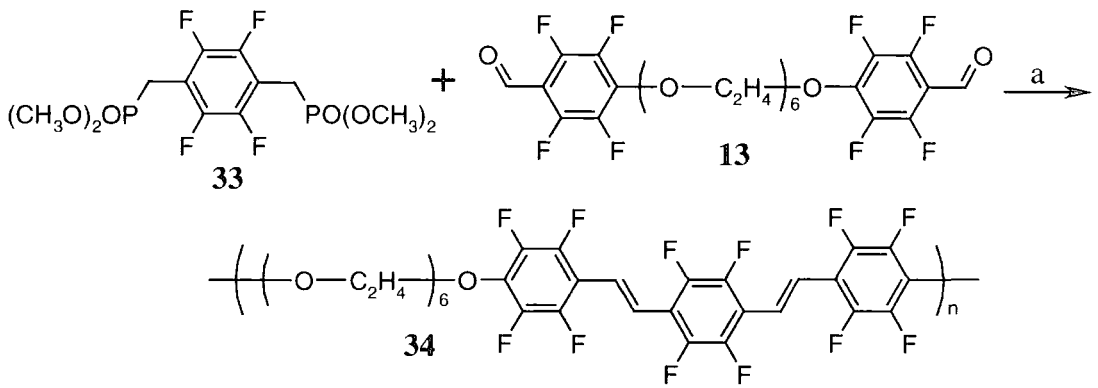

Figure 3.2.5 Synthesis of a block copolymer with fluorinated DSB units and sexi(ethylene oxide) linkers. a) THF, NaH

The reaction conditions differed greatly from those normally associated with Horner-Wittig reaction. Instead of stirring overnight at room temperature the reaction had to be kept close to the reflux temperature of THF (50 to 65 °C) for several days. This change in reactivity might be due to the electron-withdrawing effect of fluorine or to the low solubility of the intermediate oligomers in THF. It was found that reflux of the reaction mixture resulted in a side reaction which lead to a black product. Therefore a balance had to be found between increasing the rate of conversion by heating and minimising this side reaction. When the temperature was kept between 50 and 65 °C for 13 days a white polymer could be obtained in sufficient quantity (8 g).

F-DSB-*block*-SEO is soluble in chloroform and can be reprecipitated into methanol. Free-standing films can be cast from solution. The films are somewhat brittle and bending or stressing the films results in rupture. X-ray photoelectron

spectra and ^{1}H NMR spectra showed that the polymer was contaminated with silicon-grease (see also Chapter 4). When the polymer was reprecipitated into hexane the silicone was removed. Cleaned samples were used for further analysis.

The polymer was fractionated by gel chromatography (Bio-Beads S-X1 Beads, chloroform). Two fractions were obtained. Gel Permeation Chromatography (GPC) (Viscoteck, RI detector, we thank RAPRA Technology for this measurement) indicates for the first fraction a M_n of 12,600, a polydispersity of 3.5 and a degree of polymerisation of about 17 with respect to polystyrene. For the second fraction GPC shows a high content of oligomers, a M_n of 7,000, a polydispersity of 4.1 and a degree of polymerisation of about 9. *Figure 3.2.6* shows two traces for each fraction. The first fraction (3.5 g) was used for further analysis.

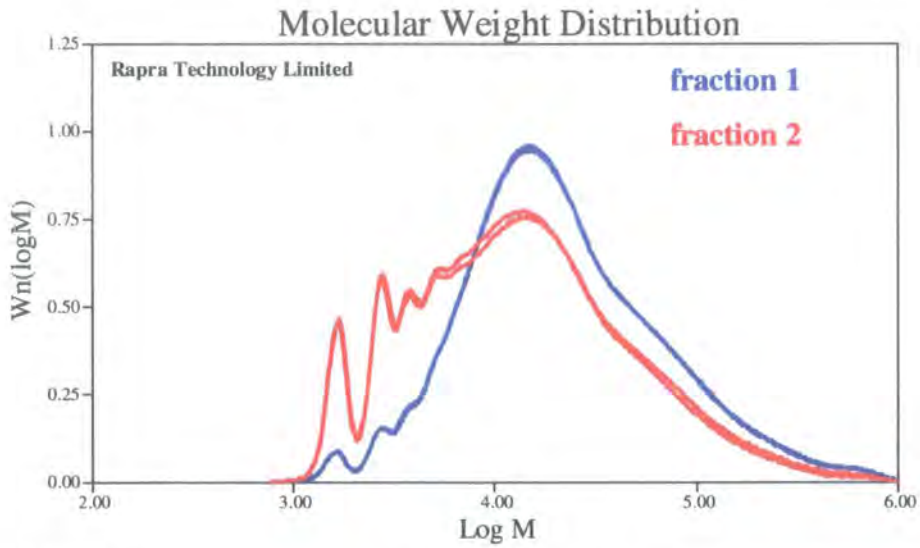

Figure 3.2.6 GPC analysis of F-DSB-block-SEO. Two traces for each fraction are shown.

The ion-content of the sample was analysed by extracting the polymer with boiling water. It was found that filtering the extracts lead to false results due to the ion content of the filter paper. When the extracts were decanted ion chromatography (Dionex, DX 120 Ion chromatograph) indicated the absence of any Na^+, K^+, Li^+ or Mg^{2+} ions and a trace (0.008%) of Ca^{2+} ions.

The ^{1}H NMR spectrum of F-DSB-*block*-SEO shows three resonances due to ethylene protons of the sexi(ethylene oxide) unit between δ 3.6 and 4.5 (ratio of integrals: 16H: 4H: 4H) (*Figure 3.2.7*). Next to the solvent peak (chloroform δ 7.27) a signal typical for an AB quartet is found at δ 7.38 (4H). The observed coupling constant is 16 Hz characteristic for *trans*-olefinic protons. Only a trace of a signal for *cis*-olefinic protons can be observed at δ 6.75. It is concluded that at least 95 % of all double bonds have a *trans*-configuration.

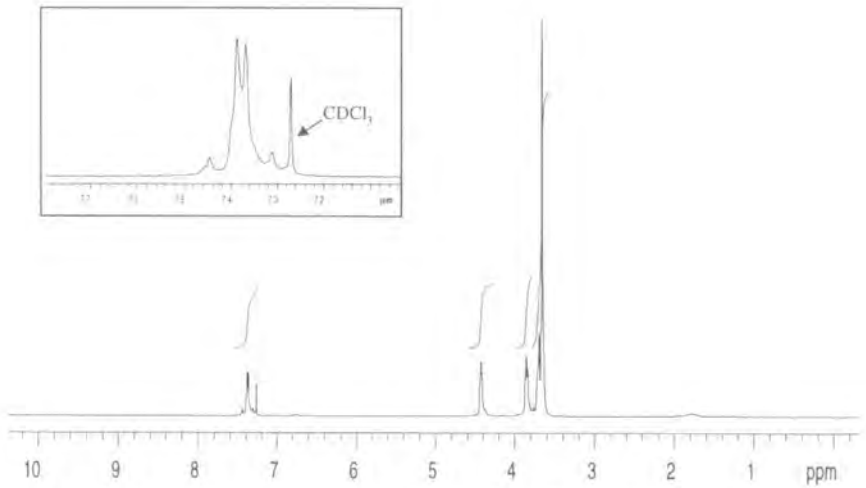

Figure 3.2.7 ^{1}H NMR spectrum of F-DSB-block-SEO. The inset shows the expanded region between δ7.1 and 7.7.

The ^{19}F NMR spectrum shows two signals in the ratio 4:8. The signal at δ -157.83 is due to the four fluorines in *ortho*-position to alkoxy groups. The resonances for the remaining eight fluorines coincide at δ -143.87. The fact that only one set of resonances is observed confirms that all DSB units have a *trans-trans*-configuration.

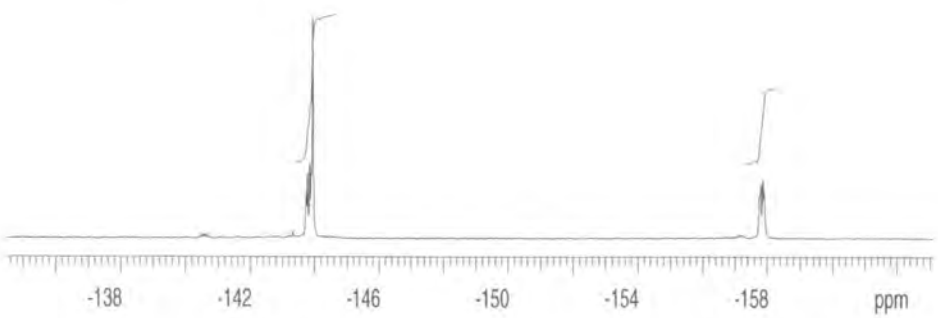

Figure 3.2.8 ^{19}F NMR spectrum of F-DSB-block-SEO.

Figure 3.2.9 shows the FTIR spectrum of F-DSB-*block*-SEO. The two strongest absorptions are due to the C=C stretching at 1483 cm^{-1} and the C-H out-of-plane deformation at 972 cm^{-1}. The latter is characteristic for a carbon-carbon double bond with two C-H bonds in the *trans*-position.[9] This very strong absorption confirms the finding from NMR spectroscopy that all or nearly all double bonds have *trans*-configuration. C-H out-of-plane deformations typical for double bonds with *cis*-configuration are generally found between 700 and 850 cm^{-1}.[10] It cannot be decided with certainty whether the small signals at 755 cm^{-1} and 860 cm^{-1} indicate the presence of a small percentage of *cis*-double bonds or whether they are due to CH_2-rocking. The absence of a signal at 1700 cm^{-1} indicates that the polymer is free of aldehyde end-groups.[11] The signal at 1650 cm^{-1} is due to an absorption of fluorinated aromatics (see appendix page 158).

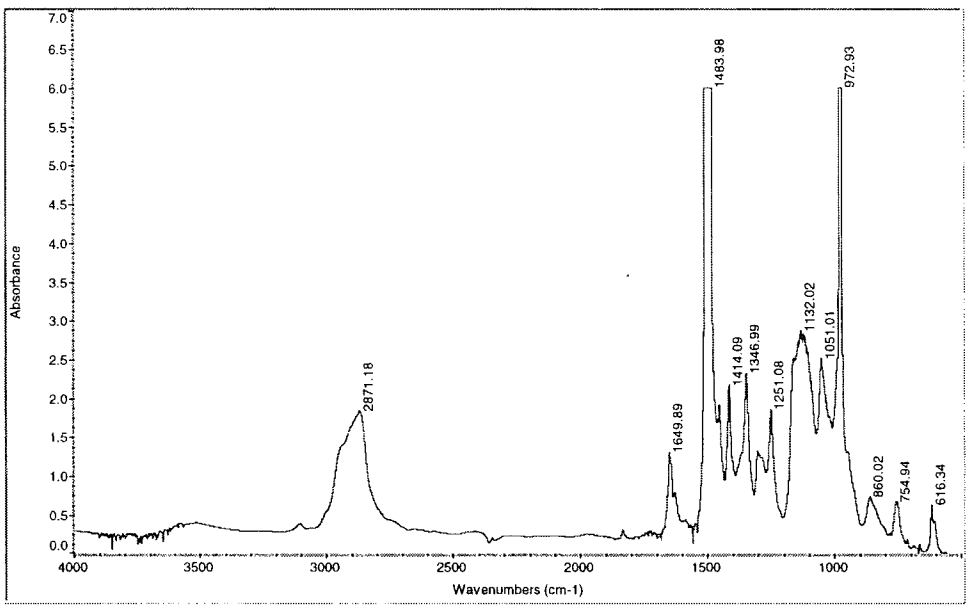

Figure 3.2.9 FTIR-spectrum of F-DSB-block-SEO (film). Since the polymer films were brittle it was not possible to prepare very thin film. The obtained films showed very intense absorption bands.

Differential Scanning Calorimetry (DSC) analysis of F-DSB-*block*-SEO shows three endothermic phase transitions at 78, 98 and 123 °C. These transitions indicate that the polymer contains some ordered structures at room temperature.

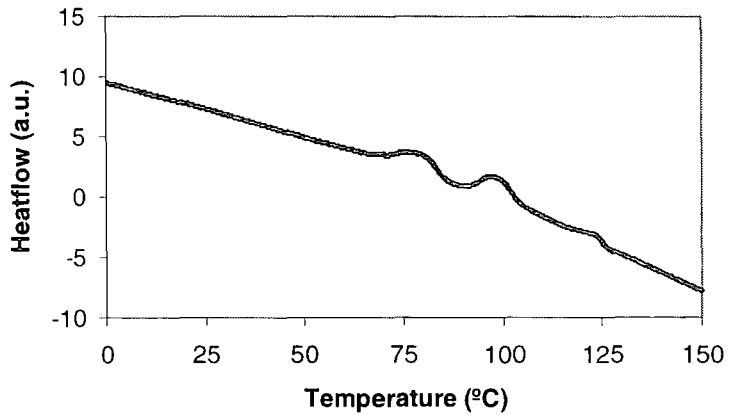

Figure 3.2.10 DSC trace of F-DSB-block-SEO.

Transitions between liquid crystalline phases have been reported for fluorinated DSBs. 1,4-Bis(2,3,4,5-pentafluorostyryl)benzene *(Figure 3.2.11 left)* shows three endothermic phase transitions though at higher temperature (194, 203 and 208 °C).[12] 1,4-Bis[(2,5-dihexyloxy)styryl]-2,3,5,6-tetrafluorobenzene *(Figure 3.2.11 right)* shows birefringent behaviour during a heating cycle and textures comparable to those of smectic and discotic mesophases during cooling.[13]

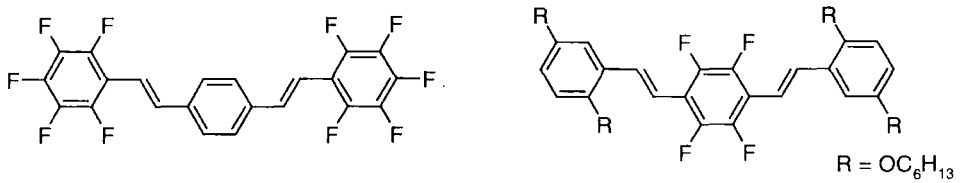

Figure 3.2.11 1,4-Bis(2,3,4,5-pentafluorostyryl)benzene (left) and 1,4-bis[(2,5-dihexyloxy)styryl]-2,3,5,6-tetrafluorobenzene (right) show liquid crystalline behaviour.

In conclusion the NMR spectra (^{1}H, ^{13}C and ^{19}F), FTIR spectra and elemental analysis of F-DSB-*block*-SEO are consistent with the assigned structure and no indications for defects such as pinacol or aldehyde groups are observed. The optical and electroluminescence properties of the polymer are described in Chapter 4.

Synthesis of a DSB block copolymer

Since the effect of fluorine on electroactive polymers was to be studied it was also necessary to prepare the hydrogen equivalent of F-DSB-*block*-SEO. Karasz *et*

al. have reported the use of the Wittig reaction to prepare copolymers with DSB units and flexible linkers.[14] In our approach sexi(ethylene oxide) was activated as bis-tosylate **35**. The reaction with two equivalents of *p*-hydroxybenzaldehyde **36** gave the monomer **37** (*Figure 3.2.12*). *p*-Xylylen-bis(triphenylphosphonium bromide) **38** was prepared by two-fold substitution of bromine on α,α'-dibromoxylene by triphenylphosphine. Wittig reaction of **37** and **38** gave poly(bis(*p*-phenylenevinylene)-*p*-phenylene-1,4,7,10,13,16,19-heptaoxanonadecane) (H-DSB-*block*-SEO) (*Figure 3.2.12*) **39**.

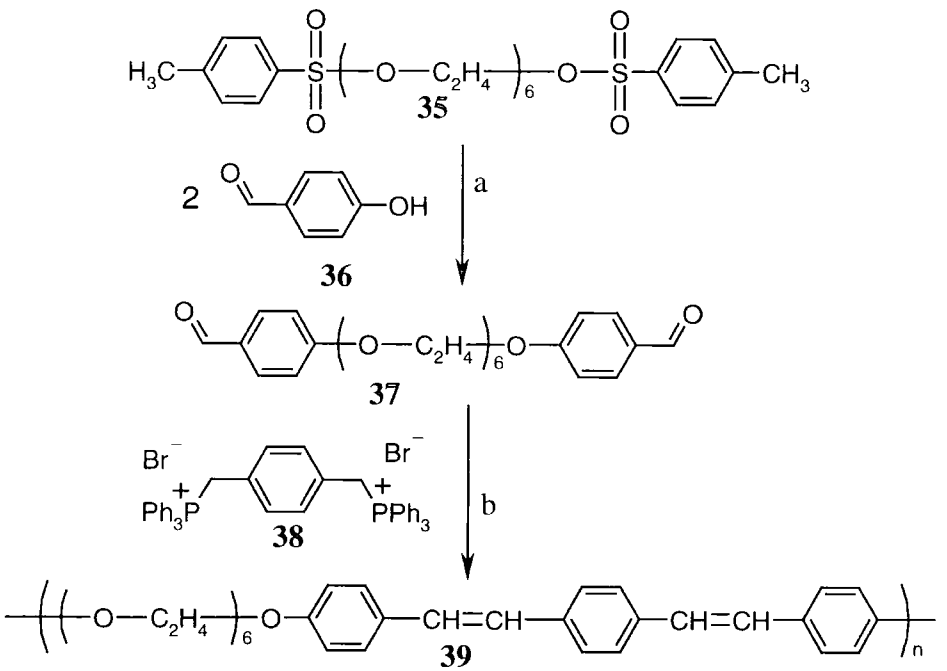

Figure 3.2.12 Synthesis of H-DSB-block-SEO. a) DMF, K_2CO_3 b) THF, KO^{t}Bu

Ion chromatography showed no traces of Na, K, Ca, Mg or Li. Two samples of H-DSB-*block*-SEO were analysed by GPC. Sample 1 was reprecipitated twice, sample 2 three times. Both samples indicated a M_n of 5600 g/mol, a polydispersity of 3.0 and a degree of polymerisation of 10 relative to polystyrene standard *(Figure 3.2.13).* H-DSB-*block*-SEO forms robust free-standing films cast from solution. Even though the average molecular weight is lower than in the case of F-DSB-*block*-SEO the films are stable when bent or stressed. Attempts to prepare the all-*trans* isomer by refluxing the polymer in toluene with traces of iodine failed and resulted in fragmentation of the polymer. The use of the Horner-Wittig reaction to prepare such an all-*trans* isomer also failed.

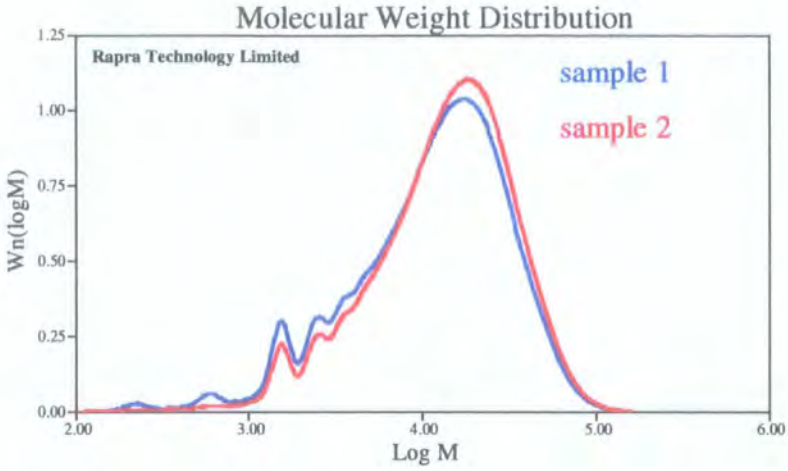

Figure 3.2.13 GPC analysis of H-DSB-block-SEO. Sample 1 was reprecipitated twice, sample 2 was reprecipitated three times.

The ^{1}H NMR spectrum shows three signals between δ 3.5 and 4.2 due to ethylene protons in the sexi(ethylene oxide) unit (integral ratio 16H: 4H :4H) *(Figure 3.2.14)*. The resonance at δ 6.5 is assigned to *cis*-olefinic protons (also see *Figure 3.2.15*).[9] The integration of this signal (2H) indicates that on average two out of the four olefinic protons per repeat unit have *cis*-configuration. The two signals at δ 6.8 (2H) and 6.9 (2H) can be assigned to aromatic protons in *ortho*-position to alkoxy-groups.[9] The fact that two resonances appear confirms that there are two different chemical environments, probably due to adjacent *cis*- or *trans*-double bonds. The resonance assigned to *trans*-olefinic protons at δ 7.0 (2H) overlaps with one of the aromatic signals. The sum of the two integrations is displayed in *Figure 3.2.14*. The remaining aromatic signals are found between δ 7.2 and 7.5 (8H).

The expansion of the region δ 6.4 – 7.1 shows the signals for olefinic protons in more detail (*Figure 3.2.15*). Two AB quartets with J_{AB} = 12 Hz are observed for the *cis*-vinylenes at δ 6.5. They are assigned to *cis-cis* and *cis-trans* DSB units. Two AB quartets with J_{AB} = 16 Hz are observed at δ 7.0 and assigned to *trans*-vinylenes in *trans-trans* and *trans-cis* DSB units. This findings are consistent with a 50:50 *cis*:*trans* distribution of double bonds. Geise *et al.* have reported similar *cis*:*trans* distributions for 4,4' dialkoxy substituted distyrylbenzene prepared by Wittig reaction.[9]

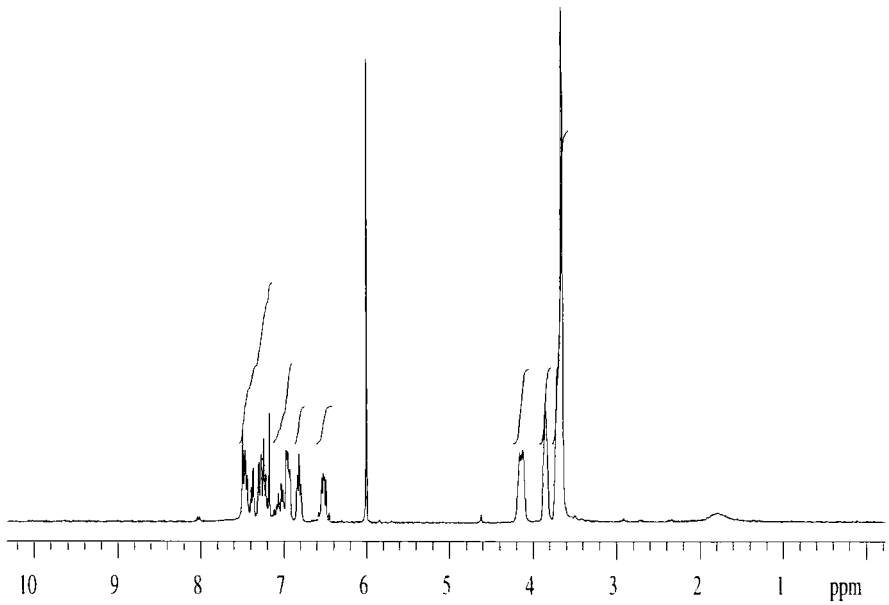

Figure 3.2.14 ^{1}H NMR spectrum of H-DSB-block-SEO in TCE-d_2.

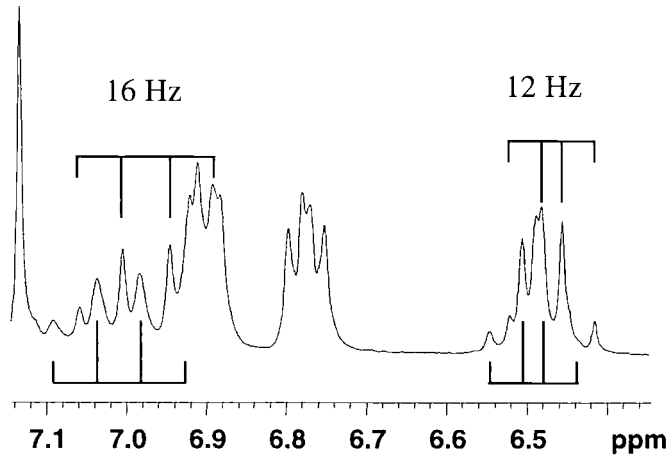

Figure 3.2.15 ^{1}H NMR spectrum of H-DSB-block-SEO in $CDCl_3$. Expansion of the region between δ6.4 and 7.1.

The ^{13}C NMR spectrum of H-DSB-*block*-SEO shows the two distinct sets of aromatic carbons (see appendix). This is expected to be due to the presence of *cis*- and *trans*-olefinic bonds adjacent to those aromatic rings. The FTIR spectrum of a thin film of H-DSB-*block*-SEO also shows the typical absorptions for *cis*- and *trans*-double bonds; the absorption band at 968 cm^{-1} can be assigned to (C-H) out-of-plane deformation in *trans*-double bonds. The absorption band at 837 cm^{-1} is characteristic

for *cis*-double bonds. The small band at 1710 cm^{-1} indicates the presence of a small amount aldehyde end-groups.[11] The DSC of H-DSB-*block*-SEO shows no exothermic or endothermic phase transitions between –150 °C and 220 °C degrees. The optical and electroluminescence properties of H-DSB-*block*-SEO are described in Chapter 4.

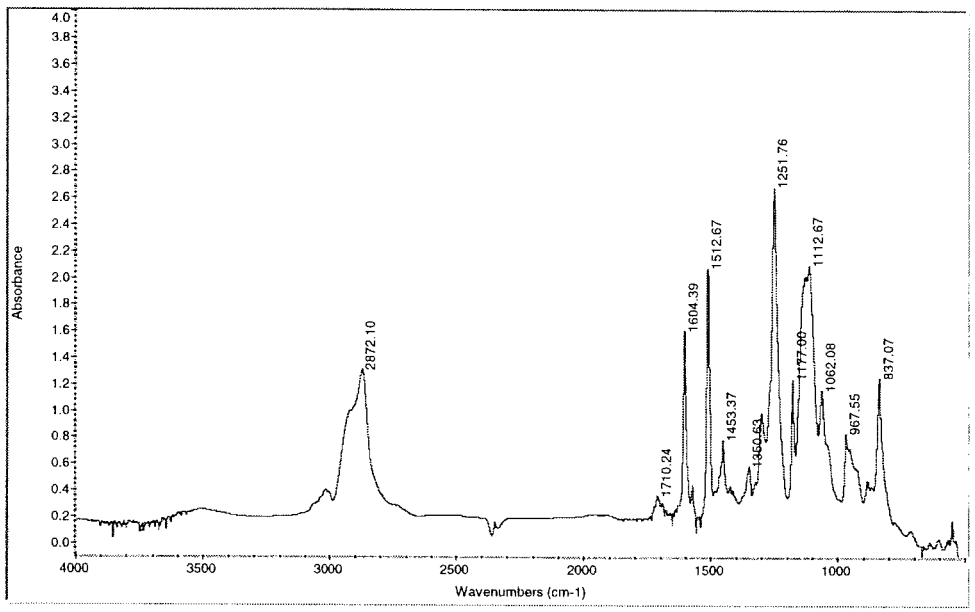

Figure 3.2.16 FTIR spectrum of H-DSB-block-SEO (thin film).

3.3 Conclusions

Attempts to prepare a block copolymer with fluorinated DSB units and a flexible linker *via* the Wittig reaction failed. However, a block copolymer with fluorinated DSB units and sexi(ethylene oxide) units could be prepared *via* the Horner-Wittig reaction. The polymer was fractionated by gel-chromatography. The first fraction shows a degree of polymerisation of 17. The FTIR and NMR spectra of the polymer indicate that all or nearly all the double bonds have *trans*-configuration.

A second block copolymer with DSB units and sexi(ethylene oxide) linker units, the hydrogen equivalent of the previous polymer, was prepared by the Wittig reaction. A degree of polymerisation of 10 was obtained. FTIR and NMR indicate a

50:50 *cis:trans* distribution of double bonds. Both polymers are soluble in chloroform and free-standing films can be cast from solution.

3.4 Experimental

3.4.1 1,8-Di-(4-methyl-2,3,5,6-tetrafluorophenyloxy)octane (25)

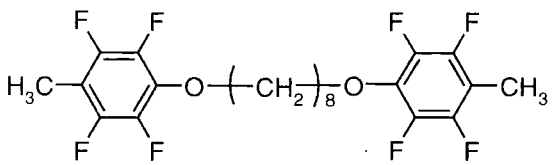

Octane-1,8-diol (10.0 g, 68.4 mmol) was dissolved in THF (500 ml). *n*-Butyllithium in hexane (1.6 M, 87 ml, 139 mmol) was added and the mixture was stirred for 10 min. 2,3,4,5,6-Pentafluorotoluene (31.7 g, 174 mmol) was added and the mixture refluxed for 5 days. After the addition of water (80 ml) the THF was evaporated. The mixture was washed three times with diethyl ether (200 ml). The combined extracts were washed with water (200 ml), dried ($MgSO_4$), concentrated under reduced pressure and purified by column chromatography (silica gel; hexane, diethyl ether 20:1), yielding *1,8-di-(4-methyl-2,3,5,6-tetrafluorophenyloxy)octane* (8.8 g, 27 %) as a colourless oil. Found: C, 56.37%; H, 4.80%; M(MS, CI) 488 (MNH_4^+). Calculated for $C_{22}H_{22}F_8O_2$: C, 56.17%; H, 4.71%; M 470. ^{1}H NMR ($CDCl_3$, 200 MHz) δ 4.15 (t, J = 7 Hz, 4H, CH_2O), 2.20 (t, J = 2 Hz, 6H, CH_3), 1.71 (m, 4H, CH_2), 1.40 (m, 8H, CH_2); ^{13}C {^{1}H} NMR ($CDCl_3$, 62.9 MHz) δ 145.21 (d, J = 245 Hz, C*F*), 140.66 21 (d, J = 245 Hz, C*F*), 135.50 (*C*CH_3), 109.15 (*C*O), 75.12 (*C*O), 29.72 (*C*H_2), 29.01 (*C*H_2), 25.36 (*C*H_2), 6.84 (*C*H_3); ^{19}F NMR ($CDCl_3$, 188 MHz) δ -145.54 (C*F ortho* to CCH_3), -158.84 (C*F ortho* to COR) (see appendix page 145).

3.4.2 1,8-Di-(4-bromomethyl-2,3,5,6-tetrafluorophenyloxy)octane (26)

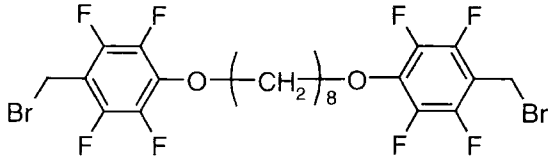

1,8-Di(4-methyl-2,3,5,6-tetrafluorophenyloxy)octane (6.3 g, 13.4 mmol) was dissolved in CCl_4 (50 ml). Bromine (4.7 g, 1.5 ml, 29 mmol) was added. The mixture was refluxed and irradiated with UV light for 4.5 h. The CCl_4 was removed by distillation and diethyl ether (100 ml) was added. The mixture was washed with water, dried ($MgSO_4$), concentrated under reduced pressure and purified by column chromatography (silica gel, hexane: diethyl ether 20:1), yielding *1,8-di-(4-bromomethyl-2,3,5,6-tetrafluorophenyloxy)octane* as a white powder (3.5 g, 42%) mp 54 °C. Found: C, 41.93%; H, 3.03%; M(MS, EI) 628 (M^+). Calculated for $C_{22}H_{20}Br_2F_8O_2$: C, 42.06%; H, 3.21%; M 628. ^{1}H NMR ($CDCl_3$, 200 MHz) δ 4.49 (s, 4H, CH_2Br), 4.24 (t, J = 6 Hz, 4H, CH_2O), 1.71 (m, 4H, CH_2), 1.40 (m, 8H, CH_2); ^{13}C {^{1}H} NMR ($CDCl_3$, 100 MHz) δ 145.14 21 (d, J = 248 Hz, C*F*), 141.07 21 (d, J = 248 Hz, C*F*), 138.39 (*C*CH_2Br), 109.83 (*C*O), 75.36 (*C*H_2O), 29.81 (*C*H_2), 29.04 (*C*H_2), 25.39 (*C*H_2), 17.03 (*C*H_2Br); ^{19}F NMR ($CDCl_3$, 188 MHz) δ -144.62 (C*F ortho* to CH_2Br), -157.13 (C*F ortho* to OR) (see appendix page 146).

3.4.3 1,8-Bis-(4-triphenylphosphoniummethylen-2,3,5,6-tetrafluoro-phenyloxy)octane dibromide (27)

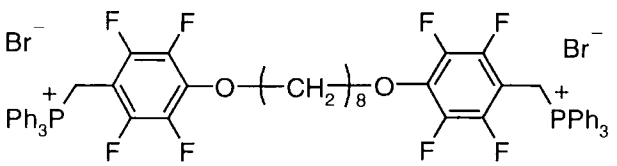

1,8-Di-(4-bromomethyl-2,3,5,6-tetrafluorophenyloxy)octane (0.50 g, 0.80 mmol) was dissolved in toluene (20 ml). Triphenylphosphine (2.07 g, 2.07 mmol) was added, the mixture refluxed under nitrogen for 150 min. The mixture was cooled to room temperature, filtered and the precipitate washed three times with cold toluene yielding *1,8-bis-(4-triphenylphosphoniummethylen-2,3,5,6-tetrafluorophenyloxy) octane dibromide* (0.76 g, 82 %) as a white powder. The product was characterised by ^{1}H NMR and ^{19}F NMR spectroscopy and used in the next step without further

purification. ^{1}H NMR ($CDCl_3$, 200 MHz) δ 7.6 – 7.9 (m, 30H, ar. C*H*), 5.44 (d, *J* = 13.5 Hz, 4H, CH_2P), 4.14 (t, *J* = 6 Hz, 4H, CH_2O), 1.66 (m, 2 H, CH_2), 1.33 (m, 4 H, CH_2); ^{19}F NMR ($CDCl_3$, 188 MHz) *δ* –138.91 (C*F ortho* to CH_2) -155.87 (C*F ortho* to OR) (see appendix page 147).

3.4.4 1,8-(Bis-2,3,4,5,6,2',3',4',5',6' nonafluorostilben-4-yloxy)octane (28)

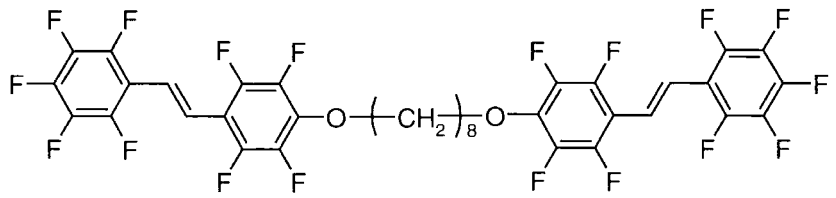

1,8-Bis-(4-triphenylphosphoniummethylen-2,3,5,6-tetrafluoro-phenyloxy)octane-dibromide (440 mg, 0.38 mmol) and LiCl (0.04 g) were dissolved in dry DMF (2 ml). KO^{t}Bu (1 M, 1.2 ml, 1.2 mmol) was added followed by 2,3,4,5,6-pentafluorobenzaldyde (165 mg, 0.84 mmol). After stirring for 6 h aqueous HCl (5%, 3 ml) was added. All solvents were removed under reduced pressure. The product was redissolved in chloroform, washed twice with water, dried ($MgSO_4$) and purified by column chromatography (silica gel/ hexane : diethyl ether 20 : 1) yielding *1,8-bis-(2,3,4,5,6,2',3',4',5',6'nonafluorostilben-4-yloxy)octane* (0.18 g, 58%) as a white powder, m.p. 93 - 94°C. Found: C, 52.38%; H, 2.60%; M(MS, EI) 826 (M^+). Calculated for $C_{36}H_{20}F_{18}O_2$: C, 52.31%; H 2.44%; M 826. ^{1}H NMR ($CDCl_3$, 200 MHz) *δ* 7.15 (d, 2H, *J* = 17 Hz, olef. C*H*), 7.12 (d, 2H, *J* = 17 Hz, olef. C*H*), 4.12 (t, 4H, *J* = 7 Hz, OCH_2), 1.65 (m, 4H, OCH$_2$CH_2), 1.27 (m, 8H, CH_2); ^{13}C {^{1}H} NMR ($CDCl_3$, 100 MHz) *δ* 146.5-136.5 (*C*F), 122.38, 119.71 (*CH*CH), 111.93, 109.57 (ar. *C*CHCH), 75.32 (O*C*H$_2$), 29.83, 29.04, 25.40 (*C*H$_2$); ^{19}F NMR ($CDCl_3$, 188 MHz) *δ* -142.54 (m, 4F, C*F ortho* to CHCH), -144.00 (m, 4F, C*F ortho* to CHCH), -154.80 (m, 2F, C*F para* to CHCH), -157.02 (m, 4F, C*F ortho* to OR), -162.63 (m, 4F, C*F meta* to CHCH) (see appendix page 148).

3.4.5 Poly(bis(2,3,5,6-tetrafluoro-p-phenylenevinylene)-2,3,5,6-tetrafluoro-p-phenylene-1,10-dioxodecane) (29)

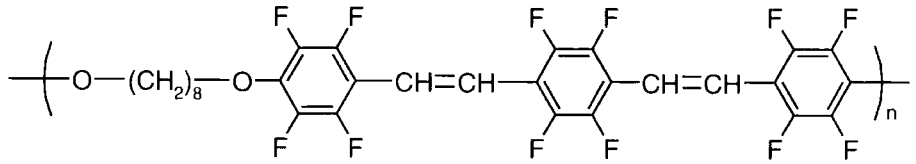

1,8-Bis-(4-triphenylphosphoniummethylen-2,3,5,6-tetrafluoro-phenyloxy)octane-dibromide (419 mg, 0.36 mmol) and LiCl (40 mg) were dissolved in DMF (3 ml). KO^{t}Bu (0.75 ml, 0.75 mmol) was added and the mixture stirred at room temperature for 3 h. 2,3,5,6-Tetrafluoroterephtalaldehyde (0.75 mg, 0.36 mmol) was added. After stirring for 18 h the mixture was quenched with aqueous HCl (5%, 3 ml). All solvents were removed under reduced pressure and the residue redissolved in toluene, filtered and dried ($MgSO_4$). It was suspended in $CHCl_3$ and precipitated into ethanol yielding *poly(bis(2,3,5,6-tetrafluoro-p-phenylenevinylene)-2,3,5,6-tetrafluoro-p-phenylene-1,10-dioxodecane)* (106 mg, 46%) as a white solid. The product was analysed by NMR (^1H,^{19}F) and not further investigated. ^1H NMR (C_7D_8, 400 MHz) δ 7.36 (d, J = 17 Hz, 2H, C*H*), 7.28 (d, J = 17 Hz, 2H, C*H*), 4.04 (m, 4H, OCH_2), 1.64 (m, 4H, CH_2),1.38 (m, 4H, CH_2), 1.27 (m, 4H, CH_2); ^{19}F NMR ($CDCl_3$, 188 MHz) δ -144.26 (m, 8F) -158.43 (m, 4F) (see appendix page 149).

3.4.6 1,17- Bis(4-methyl-2,3,5,6-tetrafluorophenyloxy)-3,6,9,12,15-pentaoxaheptadecane (30)

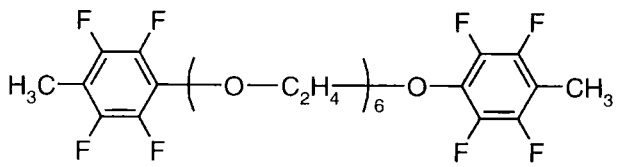

Sexi(ethylene oxide) (5.0 g, 17.7 mmol) was dissolved in dry THF (30 ml). *n*-Butyllithium (1.6 M, 23 ml, 36.8 mmol) was added and the mixture stirred for 1 h. The solvent was removed under reduced pressure and dry DMF (80 ml) was added. 2,3,4,5,6-Pentafluorotoluene (4.6 g, 25 mmol) was added and the reaction refluxed for 16 h. The DMF was removed under reduced pressure and the mixture redissolved in diethyl ether, washed twice with water, dried ($MgSO_4$) and purified by column chromatography yielding *1,17-bis(4-methyl-2,3,5,6-tetrafluorophenyloxy)-3,6,9,12,15-pentaoxaheptadecane* (2.3 g, 30%) as a viscous oil. Found: C, 51.61%;

H 5.06%; M(MS, CI) 607 (MH^+). Calculated for $C_{26}H_{30}F_8O_7$: C, 51.49%; H, 4.99%; M 606. ^1H NMR ($CDCl_3$, 200 MHz) δ 4.31 (t, J = 5 Hz, 4H, $COCH_2$), 3.81 (t, J = 5 Hz, $COCH_2CH_2$), 3.66 (m, 16H, C_2H_4), 2.19 (t, J = 2 Hz, 6H, CH_3); ^{13}C {^1H} ($CDCl_3$, 100 MHz) δ 145.05 (d, J = 250 Hz, ar. *C*F), 140.90 (d, J = 250 Hz, ar. *C*F), 135.09 (ar. COC_2H_4), 109.34 (ar. CCH_3), 73.99, 70.62, 70.41, 70.37, 69.98 (C_2H_4), 6.69 (CH_3); ^{19}F NMR ($CDCl_3$, 188 MHz) δ -145.45 (m, 4F, C*F ortho* to CH_3), -158.52 (m, 4F, C*F ortho* to OC_2H_4) (see appendix page 150).

3.4.7 1,4-Bis(bromomethyl)-2,3,5,6-tetrafluorobenzene (31)

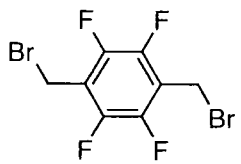

Tetrafluoro-*p*-xylene (10.0 g, 55.1 mmol) and elemental bromine (5.65 ml, 17.6 g, 110 mol) were dissolved in CCl_4 (100 ml) and refluxed for 3h under irradiation with UV-light. CCl_4 was removed by distillation and recovered. Diethyl ether (100 ml) was added to the reaction mixture and the solution was washed with dilute aqueous NaOH, aqueous $NaSO_3$ and water. The organic extracts were dried ($MgSO_4$). Evaporation of the solvent and recrystallisation of the product from ethanol (80 ml) gave 1,4-bis(bromomethyl)-2,3,5,6-tetrafluorobenzene (12.0 g, 64%) as white crystals. Elemental analysis, mass and NMR spectra were consistent with those reported in the literature.[15] Found: C, 28.60%; H, 1.15%; M(MS, EI) 336 (M^+). $C_8H_4F_4Br_2$ requires C, 28.60%; H, 1.20%; M 336. ^1H NMR ($CDCl_3$, 200 MHz) δ 4.52 (s, 2H); ^{13}C {^1H} NMR ($CDCl_3$, 100 MHz); δ ^{19}F NMR ($CDCl_3$, 188 MHz) δ -142.67 (s, 4F).

3.4.8 2,3,4,5-Tetrafluoroxylylene-1,4-bis(triphenylphosphonium bromide)(32)

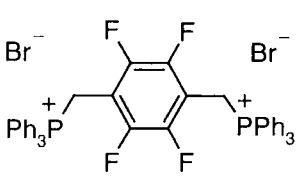

1,4-Bis(bromomethyl)-2,3,5,6-tetrafluorobenzene (0.48 g, 1.43 mmol) and triphenylphosphine (0.82 g, 3.14 mmol) were refluxed in DMF (15 ml) for 22 h. The reaction was cooled to room temperature and dry diethyl ether (30 ml) was added. The white precipitate was recovered by filtration, washed five times with dry diethyl ether (8 ml) and dried ($MgSO_4$) yielding *2,3,4,5-tetrafluoroxylylen-1,4-bis(triphenylphosphonium bromide)* (0.85 g, 69%) as a white solid, mp > 300 °C. ^{1}H NMR (DMSO-d_6, 300 MHz) δ 8.0-7.6 (ms, 30H, ar. C*H*), 5.30 (d, J = 14 Hz, 4H, CH_2); 3.26 (d, J = 20.4 Hz, 4H, CH_2); ^{13}C NMR (DMSO-d_6, 100 MHz) δ 135.57 (ar. *C*H), 134.09 (ar. C*H*), 130.17 (ar. *C*H), 116.60 (d, J = 87 Hz, CH_2); ^{19}F NMR (DMSO-d_6, 188 MHz) δ -137.26 (s, 4F) (see appendix page 151).

3.4.9 Tetramethyl-2,3,5,6-tetrafluoroxylylene bisphosphonate (33)

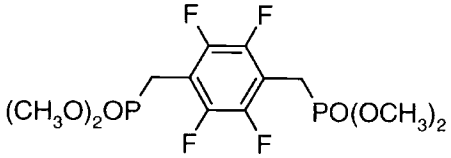

A mixture of 1,4-bis(bromomethyl)-2,3,5,6-tetrafluorobenzene (6.35 g, 18.9 mmol) and trimethylphosphite (7.0 g, 56.7 g) was heated to 90 °C for 16 h. The mixture was poured into hexane (100 ml) and allowed to solidify at 0 °C. The white solid was recrystallised from ethanol (8 ml) yielding tetramethyl-2,3,5,6-tetrafluoroxylylene bisphosphonate (3.35 g, 45%) as a white solid. As the melting point and ^{1}H NMR spectrum were in good agreement with those reported in the literature[7] no further analysis was carried out, mp 100 °C (lit. 96 °C), ^{1}H NMR ($CDCl_3$, 200 MHz) δ 3.77 (s, 6H, OCH_3), 3.73 (s, 6H, OCH_3), 3.26 (d, J = 20.4 Hz, 4H, CH_2).

3.4.10 F-DSB-block-SEO (34)

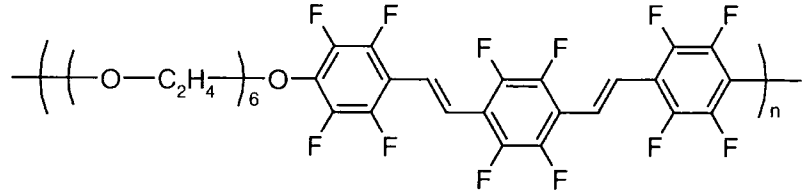

Tetramethyl-2,3,5,6-tetrafluoroxylylene bisphosphonate (6.46 g, 16.4 mmol) and NaH (3.8 g, 60% in oil, 95 mmol) were dissolved in dry THF (300 ml) under

nitrogen. The mixture was stirred for 30 min. 1,17-Bis (4-formyl-2,3,5,6-tetrafluorophenyloxy)-3,6,9,12,15-pentaoxa-heptadecane (10.4 g, 16.4 mmol) was dissolved in dry THF (40 ml) under nitrogen and added to the reaction mixture. The reaction temperature was increased from 50 °C to 65 °C over 13 days. The reaction was followed by NMR spectroscopy (^1H, ^{19}F). The solution was quenched with water (150 ml) and the THF removed under reduced pressure. Chloroform (500 ml) was added and the mixture washed with brine. The chloroform solution was filtered over Celite and concentrated (150 ml). The product was reprecipitated into methanol (450 ml) yielding *F-DSB-block-SEO* (8.0g, 62%) as white polymer. The polymer was fractionated by gel-chromatography (Bio-Beads S-X1, BIORAD, chloroform as eluent). Gel Permeation Chromatography (Viscoteck, RI detector, chloroform eluent, 2 x PL_{gel} mixed bed D 30 cm columns, polystyrene standards) fraction 1: M_n 12500 g/mol; M_w 44700 g/mol; PDI 3.6; fraction 2: M_n 7200 g/mol; M_w 32000 g/mol; PDI 4.4. Found: C, 51.76%; H, 3.63%. Calculated for $C_{34}H_{28}F_{12}O_7$: C, 52.59%; H 3.36%. ^1H NMR ($CDCl_3$, 300 MHz) δ 7.39 (d, J = 17 Hz, 2H, C*H*), 7.33 (d, J = 17 Hz, 2H, C*H*), 4.43 (t, J = 4.2 Hz, 4H, OCH_2), 3.86 (t, J = 4.2 Hz, 4H, OCH$_2$CH_2), 3.67 (m, 16H, OCH_2); ^{13}C {^1H} ($CDCl_3$, 100 MHz) δ 145.20 (d, J = 249 Hz, *C*F), 144.71 (d, J = 249 Hz, *C*F), 138.62 (d, J = 246 Hz, *C*F), 137.41 (ar.*C*O), 122.51 (*C*H), 120.79 (*C*H), 115.46 (ar. *C*CH), 109.99 (ar. *C*CH), 74.25 (*C*H$_2$), 70.84(*C*H$_2$), 70.58(*C*H$_2$), 70.13(*C*H$_2$); ^{19}F ($CDCl_3$, 188 MHz) δ –143.80 (m, 8F), -157.83 (m, 4F) (see appendix page 152).

3.4.11 Sexi(ethylene oxide) ditosylate (35)

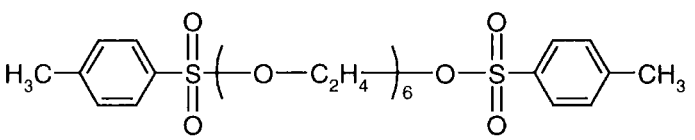

Sexi(ethylene oxide) (15.8 g, 56.0 mmol) was dissolved in DCM (300 ml) and pyridine (150 ml) and cooled to 10 °C. Tosyl chloride (55.5 g, 291 mmol) was dissolved in DCM (300 ml) and added dropwise while keeping the reaction temperature between 10 and 15 °C. After the addition was complete the mixture was stirred for 1 h at 10 °C and left to warm overnight. It was poured onto ice (750 g) and acidified with aqueous hydrochloric acid (2 M). The organic layer was washed twice with aqueous hydrochloric acid and five times with water, dried ($MgSO_4$) and

the solvent removed under reduced pressure yielding sexi(ethylene oxide) ditosylate (25.4 g, 77%) as a colourless oil. As the ^{1}H NMR spectrum was in good agreement with the literature[16] no further analysis was carried out. ^{1}H NMR ($CDCl_3$, 200 MHz) δ 7.80 (d, J = 8.4 Hz, 4H, ar. C*H*), 7.34 (d, J = 8.4 Hz, 4H, ar. C*H*), 4.17 (t, J = 5 Hz, 4H, OCH_2), 3.69 (t, J = 5 Hz, 4H, OCH_2CH_2), 3.62 (s, 8H, CH_2), 3.58 (s, 8H, CH_2), 2.45 (s, 6H, CH_3).

3.4.12 1,17-Bis (4-formylphenyloxy)-3,6,9,12,15-pentaoxaheptadecane (37)

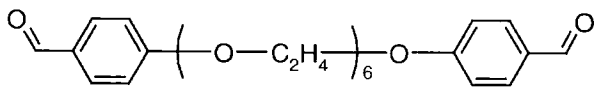

Sexi(ethylene oxide) ditosylate (25.0 g, 42.3 mmol), *p*-hydroxybenzaldehyde (11.0 g, 90.1 mmol) and K_2CO_3 (17 g, 123 mmol) were dissolved in DMF (70 ml) and heated at 90 °C for 48 h. The product was poured onto ice (100 g) and the solvent removed under reduced pressure. The product was redissolved in $CHCl_3$, dried ($MgSO_4$) and purified by column chromatography (silica gel, hexane: ethyl acetate 1:1 (800 ml), then ethyl acetate) yielding *1,17-bis(4-formylphenyloxy)-3,6,9,12,15-pentaoxa-heptadecane* (14.5 g, 70%) as a white solid, m.p. 43 - 45°C. Found: C, 63.49%; H, 7.07%; M(MS, EI) 490 (M^+). Calculated for $C_{26}H_{34}O_9$: C, 63.66%; H 6.99%; M 490. ^{1}H NMR ($CDCl_3$, 300 MHz) δ 9.87 (s, 2H, C*H*O), 7.81 (d, 4H, J = 9 Hz, ar. C*H*), 7.01 (d, 4H, J = 9 Hz, ar. C*H*), 4.20 (t, 4H, J = 4.5 Hz, OCH_2), 3.88 (t, 4H, OCH_2CH_2), 3.68 (m, 16H, CH_2); ^{13}C {^{1}H} NMR ($CDCl_3$, 63 MHz) δ 190.74 (*C*HO), 163.80 (*C*O), 131.89 (ar. *C*H), 130.01 (*C*CHO), 114.84 (ar. *C*H), 70.86 (OCH_2), 70.59, 69.41, 67.17 (CH_2) (see appendix page 153).

3.4.13 p-Xylylene-bis(triphenylphosphonium bromide) (38)

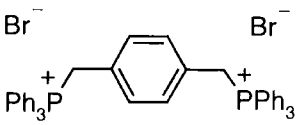

α,α'-Dibromoxylene (8.0 g, 30.3 mmol) and triphenylphosphine (17.7 g, 66.7 mmol) were refluxed in DMF (62 ml) for 3 h. The reaction was cooled to room temperature and dry diethyl ether was added (40 ml). The white precipitate was recovered by

filtration, washed three times with dry diethyl ether (20 ml) and dried ($MgSO_4$), yielding *p*-xylylenbis(triphenylphosphonium bromide) (0.85 g, 69%) as a white solid. As the melting point and ^1H NMR spectrum were in good agreement with those reported in the literature[17] no further analysis was carried out. mp > 300 °C (lit > 400 °C), ^1H NMR ($CDCl_3$, 300 MHz) δ 7.5 – 7.8 (m, 30H, ar. C*H*), 6.91 (s, 4H, ar. C*H*), 5.38 (d, J = 13 Hz, 4H, CH_2).

3.4.14 H-DSB-block-SEO (39)

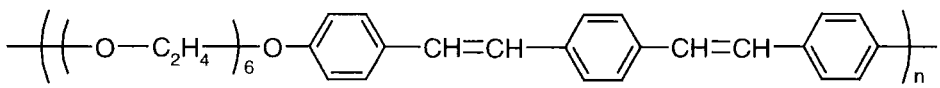

p-Xylylene-bis(triphenylphosphonium bromide) (7.96 g, 10.1 mmol) and LiCl were dissolved in DMF (60 ml). KO^{t}Bu (1.0 M, 29.6 ml, 29.6 mmol) was added and the mixture stirred for 1 h. 1,17-Bis(4-formylphenyloxy)-3,6,9,12,15-pentaoxaheptadecane (4.95 g, 10.1 mmol) was dissolved in DMF (10 ml) and added to the mixture. After stirring at room temperature for 6 h the mixture was quenched with aqueous HCl (2 M, 20 ml). All solvents were removed under reduced pressure. The product was redissolved in chloroform (200 ml) and washed with water. The chloroform solution was concentrated (10 ml) and the polymer precipitated into methanol (60 ml). The reprecipitation was repeated once more yielding *H-DSB-block-SEO* (3.8 g, 68%) as a yellow solid. Gel Permeation Chromatography (Viscoteck, RI detector, chloroform eluent, 2 x PL_{gel} mixed bed D 30 cm columns, polystyrene standards) M_n 5600 g/mol; M_w 16700 g/mol; PDI 3.0. Found: C, 71.69%; H, 7.11%. Calculated for $C_{34}H_{40}O_7$: C, 72.83%; H 7.19%. . ^1H NMR (TCE-d_2, 300 MHz) δ 7.5 – 7.1 (m, 8H, ar. C*H*), 7.01 (AB q, J = 16 Hz, 1H, C*H*=C*H*), 6.97 (AB q, J = 16 Hz, 1H, C*H*=C*H*), 6.90 (m, 2H, ar. C*H*), 6.77 (m, 2H, ar. C*H*), 6.49 (AB q, J = 12 Hz, 1H, C*H*=C*H*), 6.46 (AB q, J = 12 Hz, 1H, C*H*=C*H*), 4.13 (m, 4H, OCH_2), 3.84 (m, 4H, CH_2), 3.64 (m, 16H, CH_2) ^{13}C {^1H} NMR ($CDCl_3$, 100 MHz) δ 158.24, 157.60, 136.37, 135.89, 130.04, 130.00,129.76, 129.71, 129.56, 129.09, 128.55, 128.42, 127.79, 127.74, 127.66, 126.51, 126.15, 125.99, 114.77, 114.20, 114.15, 70.46, 70.21, 69.40, 67.31, 67.19 (see appendix page 154).

3.5 References

1. Wittig, G.; Geissler, G. *Liebigs Ann. Chem.* **1953**, *580*, 44.
2. Maryanoff, B. E.; Reitz, A. B. *Chem. Rev.* **1989**, *89*, 863.
3. Coates, G.; W.; Dunn, A. R.; Henling, L. M.; Ziller, J. W.; Lobkovsky, E. B.; Grubbs, R. H. *J. Am. Chem. Soc.* **1998**, *120*, 3641.
4. Boutagy, J.; Thomas, R. *Chemical Reviews* **1974**, *74*, 87.
5. McDonald, R. N.; Campbell, T. W. **1960**, *82*, 4669.
6. Campbell, T. W.; McDonald, R. N. *J. Org. Chem.* **1959**, *24*, 1246.
7. Sarker, A. M.; Strehmel, B.; Neckers, D. C. *Macromolecules* **1999**, 7409.
8. Brill; Landon *Chem. Rev.* **1984**, *84*, 577.
9. Ndayikengurukiye, H.; Jacobs, S.; Tachelet, W.; Van der Looy, J.; Pollaris, A.; Geise, H. J.; Claeys, M.; Kauffmann, J. M.; Janietz, S. *Tetrahedron* **1997**, *53*, 13811.
10. Williams, D. H.; Fleming, I. *Spectroscopic Methods in Organic Chemistry*, McGraw-Hill, 5th ed., Maidenhead, **1995**.
11. Huang, C.; Huang, W.; Guo, J.; Yang, C.-Z.; Kang, E.-T. *Polymer* **2001**, *42*, 3929.
12. Renak, M. L.; Bartholomew, G. P.; Wang, S.; Ricatto, P.; Lachicotte, R. J.; Bazan, G. C. *J. Am. Chem. Soc.* **1999**, *121*, 7787.
13. Strehmel, B.; Sarker, A. M.; Malpert, J. M.; Strehmel, V.; Seifert, H.; Neckers, D. C. *J. Am. Chem. Soc.* **1999**, *121*, 1226.
14. Yang, Z.; Sokolik, I.; Karasz, F. E. *Macromolecules* **1993**, *26*, 1188.
15. Filler, R.; Cantrell, G. L.; Wolanin, D.; Naqvi, S. M. *J. Fluorine Chem.* **1986**, 399.
16. Newcomb, M.; Moore, S.; Cram, D. J. *J. Am. Chem. Soc.* **1977**, 6405.
17. Griffin, C. E.; Gordon, M. *J. Organomet. Chem.* **1965**, 414.

4 Optical and Electroluminescence Properties of a Soluble Derivative of PPV and its Fluorinated Equivalent

This chapter deals with the optical and electroluminescent properties of the two polymers, H-DSB-*block*-SEO and F-DSB-*block*-SEO, the syntheses of which were described in Chapter 3. The properties were studied using several techniques: The binding energies of the valence bands (HOMOs) were measured by photoelectron spectroscopy (PES) and cyclic voltammetry. Furthermore, PES was used to study the chemical composition of the near-surface-region of the polymer films. The optical band gaps of the two polymers were determined using UV/Vis absorption spectroscopy. The absorption spectra were recorded in the solid state and in solution. Photoluminescence (PL) spectra and quantum yields were determined for thin films of the polymers. The changes in the absorption and emission spectra and in the electronic energy levels of these materials due to fluorine substitution will be discussed.

A variety of LEDs based on both polymers were prepared; single-layer devices were studied using different low work function metals (Al and Ca) and the effect of additional electron-conducting or hole-conducting layers was examined. The LEDs were characterised by their electroluminescence spectra, their stability and the dependence of current density and luminescence on the applied voltage. The polymer H-DSB-*block*-SEO was also used as emissive layer in light emitting cells (LECs) and the device characteristics were compared to those of an LED. The surface morphologies of several devices were studied by atomic force microscopy (AFM).

The various techniques used in this study are briefly described in the following sections along with the analysis of the data obtained from the samples under investigation.

4.1 Photoelectron Spectroscopy

Photoelectron spectroscopy (PES) is based on the photoelectric effect. The irradiation of a solid sample with photons of a sufficient energy gives rise to the ejection of inner-shell electrons in the case of X-ray photoelectron spectroscopy (XPS), or valence shell electrons in the case of UV photoelectron spectroscopy (UPS).[1] This photoionisation process can be represented by

$$M_0 + h\nu \rightarrow M^{+\bullet} * + e^- \qquad (4.1),$$

where M_0 represents the neutral molecule, hν is the ionising photon, $M^{+\bullet} *$ represents the radical cation of the molecule in the excited state and e^- the photoelectron which carries the kinetic energy. The energy balance for Eq. (4.1) is given by

$$E_0 + h\nu = E^{+\bullet} * + E_k \qquad (4.2),$$

where E_0 is the energy of the neutral molecule in the ground state, $E^{+\bullet} *$ is the energy of the radical cation and E_k is the kinetic energy of the electron. If the latter is measured at a fixed frequency ν the binding energy of the electron E_E can be determined as:

$$E_E = E^{+\bullet} * - E_0 = h\nu - E_k \qquad (4.3)$$

In a simple model the electronic structures of M_0 and $M^{+\bullet} *$ are described as single-electron states which means that the kinetic energy measured can be assigned to individual electronic levels.

Figure 4.1.1 shows a simple schematic of electrons in core or valence shells. The schematic diagram illustrates that the sum of the energy of the molecule in the ground state and the energy of the photon are equal to the energy of the radical cation of molecule in the excited state plus the kinetic energy of the emitted electron (Eq 4.2).

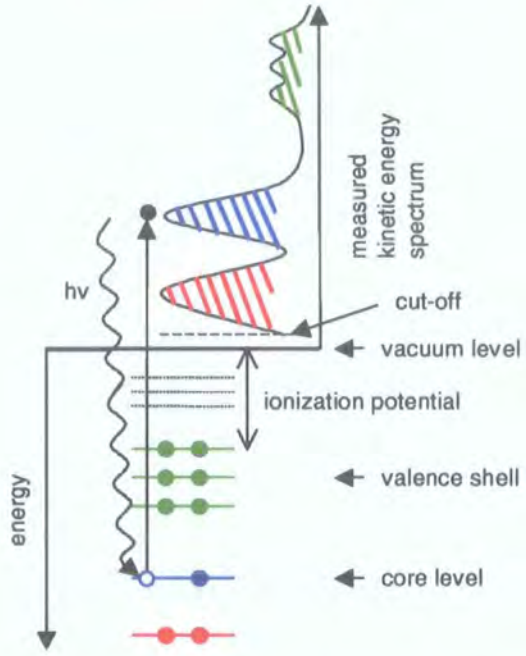

Figure 4.1.1 An idealised photoelectron spectrum (top) with the corresponding one-electron molecular levels (bottom).

The radiations used for XPS are the Al(K_α) and Mg(K_α) emission lines while a helium resonance lamp is used generally for UPS. The binding energies measured in XPS provide qualitative and quantitative analysis of the chemical composition of the near surface region of the sample; changes in the valence electron density of an atom are reflected in small, but significant shifts of the core level energies and are characteristic for a certain chemical environment of that atom. Consequently, XPS can provide structural information. The technique can be used for studies of the valence band, but the efficiency is approximately one order of magnitude lower than for core photoelectrons.[1] Studies of the valence band are gained more easily by UPS, since the photoionisation cross-section is higher for UV light. The PES measurements presented in this chapter were carried out by Dr. Michel de Jong and Prof. William R. Salaneck at Linköping University, Sweden, and we are grateful for their contribution to this work.

The XPS wide scan of a thin film of F-DSB-*block*-SEO on a gold substrate indicated the presence of a small amount of silicone impurity, probably silicone grease. Tilting the sample and thereby reducing the thickness of the region probed by the incident X-ray beam showed that the silicone was present predominantly on the surface of the sample. After the sample was rinsed with cyclohexane only the

expected signals for C, O and F were observed. All subsequent PES measurements were conducted using this cleaned sample. An XPS wide scan of H-DSB-*block*-SEO film only showed the presence of C and O, with no silicone contaminant.

The intensity of the binding energy signals of F(1s), O(1s) and C(1s)-electrons in thin films of F-DSB-*block*-SEO and H-DSB-*block*-SEO can be used to determine the relative abundance of those elements in the samples. The theoretically expected abundances can be calculated by counting the number of atoms per repeat unit. *Table 4.1.1* shows that the observed intensities are consistent with those calculated. The increase of fluorine content might be due to the tendency of fluorinated materials to migrate from the bulk to surface regions.

F-DSB-*block*-SEO					H-DSB-*block*-SEO		
	C(1s)	O(1s)	F(1s)			C(1s)	O(1s)
measured	0.61	0.13	0.26		measured	0.79	0.21
calc.	0.64	0.13	0.23		calc.	0.83	0.17

Table 4.1.1 Measured and calculated relative abundance of C, O and F in F-DSB-block-SEO and H-DSB-block-SEO according to the 1s-electron intensities in wide scan XPS spectra.

The XPS narrow scan of the 1s electrons of a specific element gives an indication of the chemical environments of that element; for instance a covalent bond to a highly electronegative atom will decrease the valence electron density around that atom and increase the binding energy for its 1s electrons.[2] Using reference compounds of known structure the observed binding energy can be related to a specific bonding environment. When several chemical environments for one type of atom are present within one molecule, the observed spectrum represents the sum of all signals due to these atoms. The individual binding energies and the relative abundance of the atoms can be determined using Gausian curves for each individual signal and fitting the sum of those signals to the measured spectrum.[3]

The XPS narrow scan of the C(1s) region of F-DSB-*block*-SEO shows three different binding energies (*Figure 4.1.2, left*). The dotted lines correspond to the fitted signals. The peak with the highest binding energy (287.2 eV) corresponds to C bonded to F, the middle peak (286.2 eV) corresponds to C bonded to O and the peak with the lowest binding energy (285.1 eV) corresponds to C bonded to C and H only. In the case of H-DSB-*block*-SEO only two signals are observed: one for C bonded to O at 285.7 eV and one for C bonded to C and H only at 283.8 eV (*Figure 4.1.2*

expected signals for C, O and F were observed. All subsequent PES measurements were conducted using this cleaned sample. An XPS wide scan of H-DSB-*block*-SEO film only showed the presence of C and O, with no silicone contaminant.

The intensity of the binding energy signals of F(1s), O(1s) and C(1s)-electrons in thin films of F-DSB-*block*-SEO and H-DSB-*block*-SEO can be used to determine the relative abundance of those elements in the samples. The theoretically expected abundances can be calculated by counting the number of atoms per repeat unit. *Table 4.1.1* shows that the observed intensities are consistent with those calculated. The increase of fluorine content might be due to the tendency of fluorinated materials to migrate from the bulk to surface regions.

F-DSB-*block*-SEO					H-DSB-*block*-SEO		
	C(1s)	O(1s)	F(1s)			C(1s)	O(1s)
measured	0.61	0.13	0.26		measured	0.79	0.21
calc.	0.64	0.13	0.23		calc.	0.83	0.17

Table 4.1.1 Measured and calculated relative abundance of C, O and F in F-DSB-block-SEO and H-DSB-block-SEO according to the 1s-electron intensities in wide scan XPS spectra.

The XPS narrow scan of the 1s electrons of a specific element gives an indication of the chemical environments of that element; for instance a covalent bond to a highly electronegative atom will decrease the valence electron density around that atom and increase the binding energy for its 1s electrons.[2] Using reference compounds of known structure the observed binding energy can be related to a specific bonding environment. When several chemical environments for one type of atom are present within one molecule, the observed spectrum represents the sum of all signals due to these atoms. The individual binding energies and the relative abundance of the atoms can be determined using Gausian curves for each individual signal and fitting the sum of those signals to the measured spectrum.[3]

The XPS narrow scan of the C(1s) region of F-DSB-*block*-SEO shows three different binding energies (*Figure 4.1.2, left*). The dotted lines correspond to the fitted signals. The peak with the highest binding energy (287.2 eV) corresponds to C bonded to F, the middle peak (286.2 eV) corresponds to C bonded to O and the peak with the lowest binding energy (285.1 eV) corresponds to C bonded to C and H only. In the case of H-DSB-*block*-SEO only two signals are observed: one for C bonded to O at 285.7 eV and one for C bonded to C and H only at 283.8 eV (*Figure 4.1.2*

right). The measured intensities for these signals are consistent with those calculated (*Table 4.1.2*).

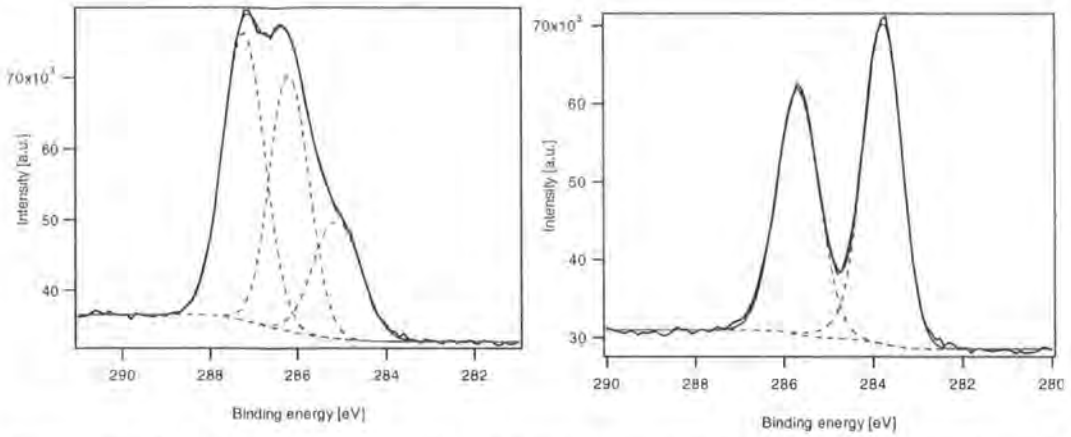

Figure 4.1.2 XPS narrow scan of the C(1s)region of F-DSB-block-SEO (left) and H-DSB-block-SEO(right).

C(1s) signal in F-DSB-*block*-SEO					**C**(1s) signal in H-DSB-*block*-SEO		
	C-F	**C**-O	**C**-H/**C**-C			**C**-O	**C**-H/**C**-C
measured	0.43	0.37	0.20		measured	0.45	0.55
calc.	0.35	0.41	0.24		calc.	0.41	0.59

Table 4.1.2 Measured and calculated relative abundance of C-F,C-O and C-H,C-C carbons in F-DSB-block-SEO and H-DSB-block-SEO according to the 1s-electron intensities in narrow scan XPS spectra.

Figure 4.1.3 shows the UPS spectrum of H-DSB-*block*-SEO and F-DSB-*block*-SEO. The electrons close to the valence band edge are found at the right-hand-side of the spectrum (see cartoon *Figure 4.1.1*). The binding energy of those electrons relative to the vacuum level is the ionisation potential (IP) and can be derived from UPS spectra using the cut-off of secondary electrons at the left hand side of the spectrum (not shown in *Figure 4.1.3*, but see cartoon *Figure 4.1.1*).[#] The IP for F-DSB-*block*-SEO is 6.3 ± 0.1 eV and for H-DSB-*block*-SEO is 5.3 ± 0.1 eV. The π-electron bands observed in both UPS spectra look similar to those observed for PPV.[1] However, the detailed interpretation of the form and position of these bands requires quantum-chemical calculations and was not undertaken during the course of this work.

[#] The UPS spectrum shows the electrons with the largest kinetic energy on the right-hand-side and those with almost no kinetic energy on the left-hand-side. These two positions are separated by an energy E_s. The IP can be calculated as $IP = h\nu - E_s$.

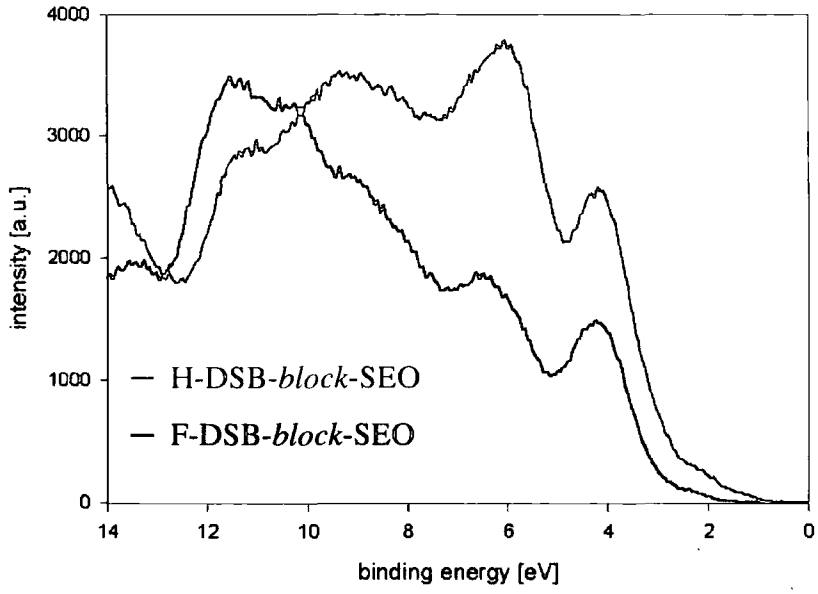

Figure 4.1.3 Comparison of the He(II) UPS valence band spectra of H-DSB-block-SEO and F-DSB-block-SEO. The binding energy is measured relative to the Fermi-level of the samples. It should not be confused with E_E (page 77).

The IPs of both polymers were also determined by cyclic voltammetry using ferrocene as the reference (see appendix page 159). According to cyclic voltammetry the IP for F-DSB-*block*-SEO was at 6.2 ± 0.1 eV and for H-DSB-*block*-SEO at 5.5 ± 0.1 eV. These values were consistent with those obtained by UPS measurements. The average values obtained from UPS and the cyclic voltammetry measurements were used in the further discussion (F-DSB-*block*-SEO: 6.25 ± 0.15 eV; H-DSB-*block*-SEO: 5.4 ± 0.20 eV).

The strong increase in the IP of F-DSB-*block*-SEO relative to H-DSB-*block*-SEO can be attributed to the effect of the high electron affinity of the fluorine substituents. Kang *et al.* found an increase of the IP of 0.17 eV when one hydrogen atom per aromatic ring of PPV was substituted by fluorine.[4] In our case four positions on each aromatic ring are substituted by fluorine and an increase of the IP of about 0.85 eV is observed; although F-DSB-*block*-SEO and H-DSB-*block*-SEO are copolymers with isolated chromophores and therefore somewhat different to Kang's fully conjugated PPV derivative, a similar increase in IP of about 0.2 eV per fluorine atom is found in both systems. The IPs will be further discussed in the context of the energy levels in LEDs.

4.2 UV/Vis Spectroscopy

Absorption spectra show transitions of electrons from the ground state to an excited state. The observed fine-structure is due to the vibrational structure of the excited state. The solution state UV/Vis spectra of H-DSB-*block*-SEO and F-DSB-*block*-SEO were recorded in chloroform. The spectrum of H-DSB-*block*-SEO shows a maximum at 354 nm for the π,π^*-transition (*Figure 4.2.2*). This maximum is slightly red-shifted with respect to the parent compound DSB (λ_{max} = 350 nm). A red shift is expected due to the effect of the two alkoxy-groups in the 4 and 4' positions, which extend the conjugation and therefore lower the band gap. A more pronounced red shift is observed in the case of 4,4'-diethoxy-distryrylbenzene (λ_{max} = 368 nm);[5] like H-DSB-*block*-SEO this molecule contains ca. 50% of double bonds in the *cis*-configuration and ca. 50% in the *trans*-configuration. The difference in the absorption maximum for these two compounds with identical chromophores might be explained by the fact that the absorption shows a vibronic fine-structure which is not well resolved. Different solvent conditions might lead to a better resolution and a different vibronic peak might be the maximum.

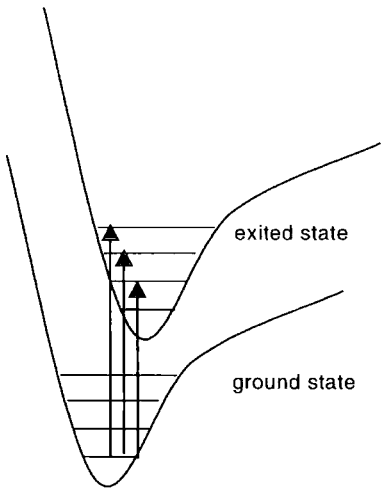

Figure 4.2.1 Schematic diagram of absorptions from the ground state to an excited state.

The vibronic fine-structure is more resolved in the case of F-DSB-*block*-SEO, which shows two maxima at 340 nm and 354 nm (*Figure 4.2.2*). Although the second maximum coincides with the maximum of H-DSB-*block*-SEO the spectrum is overall about 10 nm blue shifted relative to H-DSB-*block*-SEO.

Bazan *et al.* have studied the effect of fluorine substitution on DSB derivatives and found that the absorption maxima do not change more than a few nm (less than 10 nm) when between 2 and 12 fluorines are introduced on the aromatic rings.[6] However, their study does not include a DSB molecule with all 14 aromatic positions substituted by fluorine. This DSB derivative was synthesised during the course of this study and will be discussed in more detail in Chapter 5. In the

polymer F-DSB-*block*-SEO the DSB unit carries 12 fluorine atoms and a shift of 10 nm is observed.

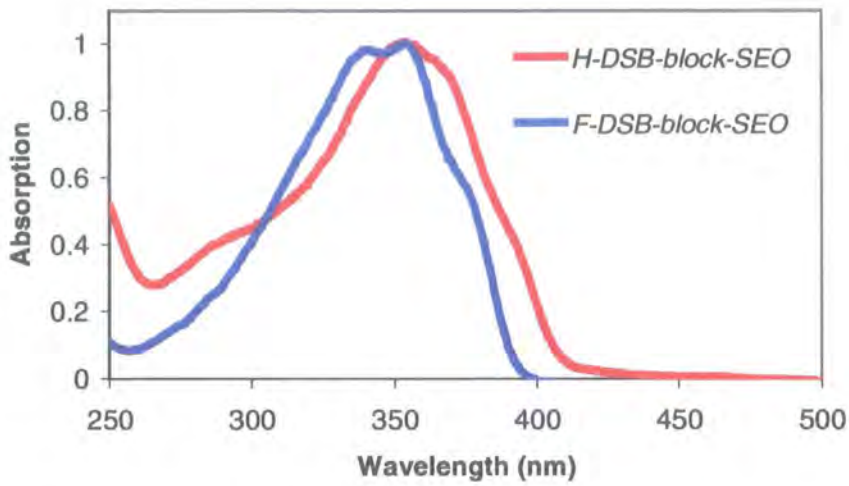

Figure 4.2.2 Absorption spectra of F-DSB-block-SEO and H-DSB-block-SEO in chloroform solution.

The onset of the absorption spectrum is a good measure of the HOMO-LUMO gap since it shows the minimum energy required to transfer an electron from the ground state to the excited state. The onset of absorption in the case of H-DSB-*block*-SEO is at 410 nm indicating a HOMO-LUMO gap of 3.0 eV. For F-DSB-*block*-SEO the onset is at 400 nm corresponding to a HOMO LUMO gap of 3.1 eV (*Table 4.2.3*).

The extinction coefficients of the DSB units within F-DSB-*block*-SEO and H-DSB-*block*-SEO are 4.0 and 3.6 x 10^4 l cm^{-1} mol^{-1}, respectively. Such values are typical for DSB units; for the case of 4,4'-dimethoxy-distryrylbenzene extinction coefficients of 2.3 and 6.8 x 10^4 l cm^{-1} mol^{-1} have been reported.[5,7]

Polymer	λ_{max} (solution)	ε (solution) /10^4 l cm^{-1} mol^{-1}	onset (solution)	λ_{max} (solid state)	onset (solid state)
H-DSB-*block*-SEO	354 nm (3.5 eV)	3.6	410 nm (3.0 eV)	334 nm (3.7 eV)	415 nm (3.0 eV)
F-DSB-*block*-SEO	354 nm (3.5 eV)	4.0	400 nm (3.1 eV)	301 nm (4.1 eV)	415 nm (3.0 eV)

Table 4.2.3 Solution state and solid state absorption characteristics of H-DSB-block-SEO and F-DSB-block-SEO

The solid state absorption spectra of both polymers were investigated since the polymers were used as thin films in LEDs. The absorption spectra of both polymers were blue shifted relative to their solution state spectra (*Figure 4.2.3*). This shift is particularly strong in the case of F-DSB-*block*-SEO. The first absorption maximum in the solid state is at 301 nm compared with the maximum at 354 nm in the solution state spectrum. This may be an indication of a strong aggregation in the solid state. The shape of the curve is typical for an H-aggregate. The main absorption in a H-aggregate is blue-shifted relative to the isolated chromophore. A second absorption is red-shifted but the transition is forbidden and appears only as a weak shoulder in the spectrum. Kilbinger *et al.* have reported strong blue shifts for aggregates of oligothiophene-PEO-block copolymers relative to molecularly dissolved molecules.[8] Similar results were found by Song *et al.* for stilbene-aggregates and Neckers *et al.* for block copolymers with partially fluorinated DSB units.[9,10]

The solid state absorption maximum for H-DSB-*block*-SEO is at 334 nm. The difference in absorption maximum in the solid state (334 nm) and the solution state (354 nm) for H-DSB-*block*-SEO is less pronounced than in the case of F-DSB-*block*-SEO indicating that the former might show less or less strong aggregation. Benfaremo *et al.* have prepared a similar block copolymer with all-*trans* DSB units and long PEO spacer units (see Chapter 1, *Figure 1.3.5*).[11] The solid state absorption maximum for this polymer (330 nm) is similar to that of H-DSB-*block*-SEO (334 nm); this shows that the different configurations of the double bonds (all-*trans* relative to 50% *cis* and *trans*) has little effect on the solid state absorption spectra.

The onset of absorption in the solid state is at 415 nm for F-DSB-*block*-SEO and H-DSB-*block*-SEO. Therefore, the HOMO-LUMO gap for both polymers in the solid state is 3.0 eV. It can be concluded that the replacement of hydrogens by fluorines in this type of block copolymer not only changes the IP (potential of the HOMO relative to the vacuum level) but also to the same extent the electron affinity (EA, potential of the LUMO relative to the vacuum level). The electron affinities of the polymers can now be calculated; for H-DSB-*block*-SEO the EA is 2.4 ± 0.2 eV and for F-DSB-*block*-SEO the EA affinity is at 3.25 ± 0.15 eV. The energy levels of the HOMO and the LUMO will be further discussed in the context of LEDs.

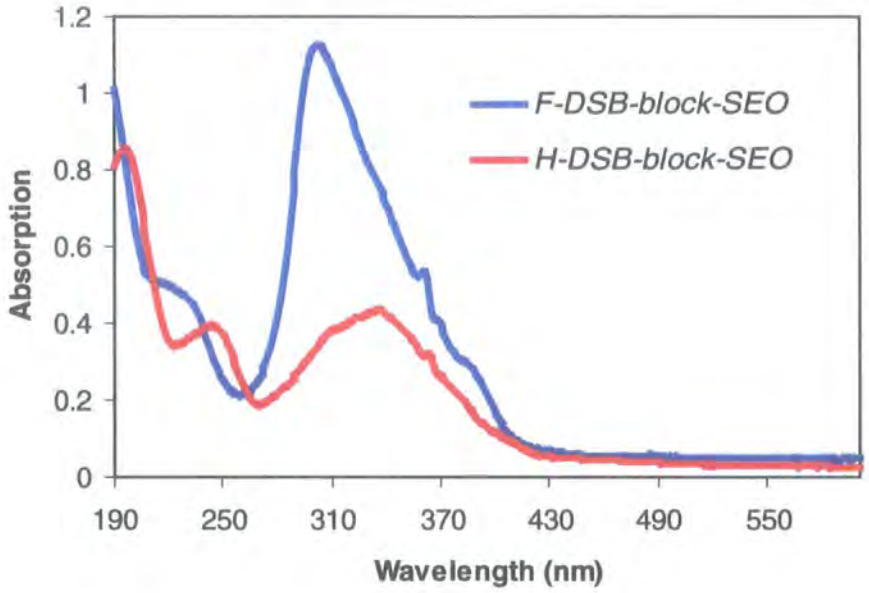

Figure 4.2.3 Absorption spectra of F-DSB-block-SEO and H-DSB-block-SEO thin films (ca. 100 nm thick) on spectrosil substrates (not normalised).

4.3 Photoluminescence

All photoluminescence (PL) and electro-luminescence (EL) measurements described in this chapter were conducted by the author in collaboration with Dr. Franco Cacialli at the Cavendish Laboratories in Cambridge. We are very grateful for his support of this work.

Photoluminescence spectra are emission spectra of samples, which have been excited by photons. The observed fine-structure is due the vibrational structure of the ground state. Luminescence in conjugated polymers is believed to be the result of the radiative decay of singlet excited states.[12] In the case of solid state photoluminescence the angular distribution of the emitted light is not uniform. In

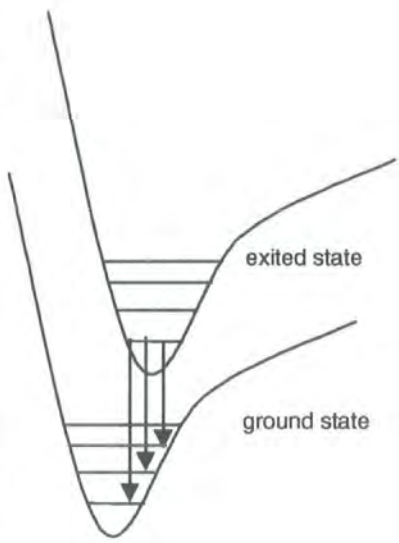

Figure 4.3.1 Schematic diagram of emissions from an excited state to the ground state.

order to obtain an average of the emission over all angles a hollow sphere (integrating sphere) is used which is coated on the inside with a reflecting material. A glass disk covered with the polymer film is placed in the centre of the integrating sphere. A laser beam is fired at the sample and the emission detected by a photodiode at a right angle relative to the incident laser beam. In our case a He-Cd laser with an emission wavelength of 325 nm was used.

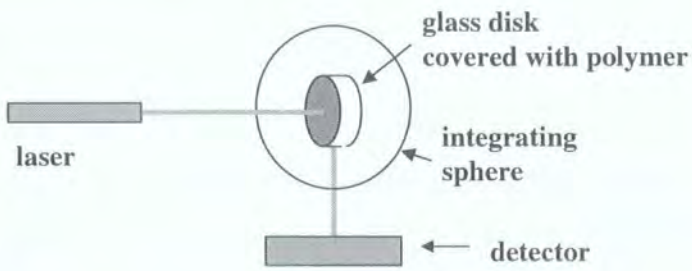

Figure 4.3.2 Schematic representation of the photoluminescence experiment.

The PL efficiency is the ratio of the emitted photons to the absorbed photons. To measure the PL efficiency three different experiments are used.[13] In the first experiment the sphere is empty and the laser beam is simply reflected at the wall of the sphere. In the second experiment the sample is placed in the sphere and the laser beam is aimed at the walls of the sphere. In a third experiment the laser is aimed at the sample. The loss in the intensity from the second experiment (L_b) to the third experiment (L_c) can be used to determine the absorption coefficient of the sample. The absorption coefficient (A) is the ratio of the photons that hit the sample to those absorbed and is given by:

$$A = (1 - L_c/L_b)$$

The intensity of the emission spectrum is measured in experiments two (P_b) and three (P_c). The photoluminescence efficiency η can then be calculated as

$$\eta = [P_c - (1 - A)\, P_b] / L_a A \,,$$

where L_a is the light intensity measured in the first experiment. A full derivation of this equation is given in the appendix (see page 129).

The photoluminescence efficiency of H-DSB-*block*-SEO is 34%, while the PL efficiency of F-DSB-*block*-SEO is 17%. These results are comparable to the PL efficiency of PPV, which is generally quoted as 27%,[14] but efficiencies as high as 80% have also been claimed.[15]

The solid state photoluminescence spectrum of H-DSB-*block*-SEO shows fine-structure with two maxima at 530 nm (2.34 eV) and 494 nm (2.50 eV) (*Figure 4.3.3*). The arrows on the spectra point towards the corresponding y-axes. The emission spectrum of the block copolymer with all-*trans* DSB units and PEO spacers prepared by Benfaremo *et al.* is reported to show two maxima at about 455 and 490 nm.[11] The similar separation of these maxima indicates that the ground states of both polymers have similar vibrational structures. The fact that the polymer with all-*trans* double bonds is blue shifted with respect to H-DSB-*block*-SEO, which contains a mixture of *cis*- and *trans*-double bonds, is surprising since steric hindrance and a decrease in conjugation and therefore a bigger optical band gap might be expected in the case of *cis*-double bonds. However, it is also possible that the entire emission of H-DSB-*block*-SEO arises from *trans-trans*-DSB units since the energy in the excited states of *cis-cis* and *cis-trans*-DSB units can be transferred to the *trans-trans*-DSB units, which are expected to have the smallest optical band gap. The reason for the blue-shift of the emission in the case of the polymers prepared by Benfaremo *et al.* remains unclear in particular since the absorption of this polymer is similar to that of H-DSB-*block*-SEO. These systems are not identical, though; in the Benfaremo-system the all *trans* DSB units constitute 24 wt.% of the total mass whereas in our system the *trans-trans*, *trans-cis* and *cis-cis* DSB units constitute 50 wt.%. The consequences of these differences merit further examination but this was not possible with the constraints of this study.

The Stokes' shift, which is the difference between the absorption maximum and the emission maximum, is 162 nm (*Figure 4.3.3*). For PPV the Stokes' shift is 110 nm. Stokes' shifts indicate differences between the excited state reached immediately after absorption and the excited state from which the emission occurs. These differences can be due to vibrational, electronic or geometric changes.[5]

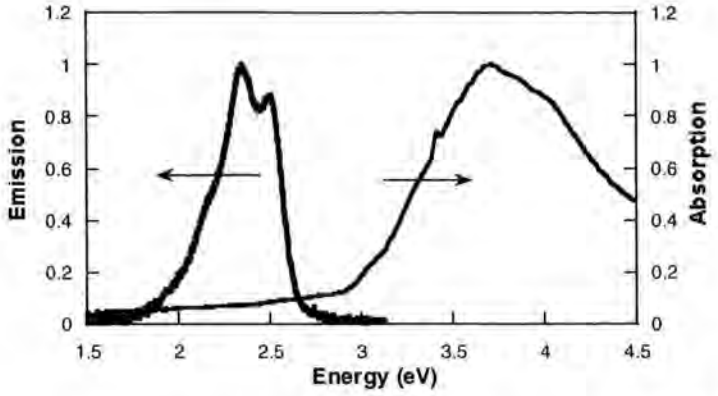

Figure 4.3.3 Photoluminescence and absorption spectra of H-DSB-block-SEO.

The emission spectrum of F-DSB-*block*-SEO shows no fine structure and is in the same region as the emission of H-DSB-*block*-SEO (*Figure 4.3.4*). The maximum is at 502 nm (2.47 eV). Due to the strong blue-shift of the solid state absorption maximum an even larger Stokes' shift (201 nm) is observed when the absorption and the emission spectra are compared.

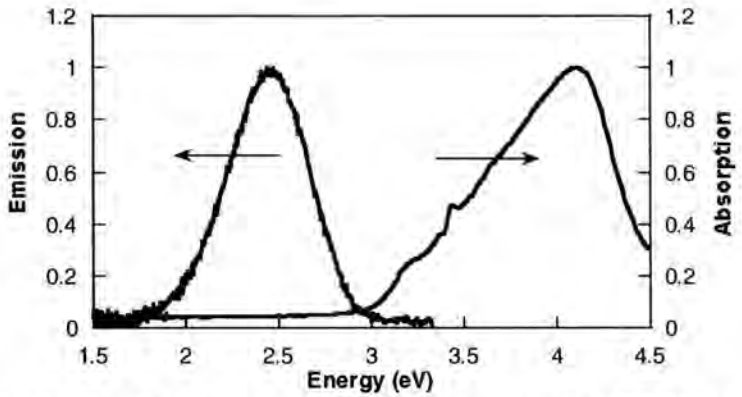

Figure 4.3.4 Photoluminescence and absorption spectra of F-DSB-block-SEO.

There is some disagreement in the literature about the effect of the *cis-trans* vinylene ratio in poly(arylene vinylene)s on the PL and EL efficiencies of devices. Feast *et al.* have prepared a range of poly(4,4'-diphenylene diphenylvinylene)s and related structures with varying *cis* and *trans* contents and shown that a maximum for the photoluminescence efficiency is reached at a *cis:trans* ratio of 1.[16-18] On the other hand Karasz *et al.* have reported that in the case of block copolymers optimum efficiencies are obtained when more than 90% of double bond configurations are *trans.*[19] However, they do not report any absolute values for their polymers. The results presented in this work show that polymers containing a mixture of *cis* and

trans double bonds can have high solid state PL efficiencies. There is also work on PPV obtained *via* the precursor route which shows that increasing the *cis*-vinylene content parallels increasing luminescence efficiency.[20]

Cornil, Heeger and Bredas have carried out quantum chemical calculations on dimers and trimers of stilbene as model compounds for PPV.[21] They found that in aggregates with high symmetry the absorption is blue shifted and luminescence is quenched. This blue shift in absorption along with the reduction in photoluminescence quantum efficiency is in agreement with the findings of the DSC analysis for F-DSB-*block*-SEO, which shows ordered structures. Cornil *et al.* also found that aggregates with lower symmetry and therefore less ordered structures did not show quenching of luminescence. The authors go on to suggest that high PL efficiencies can be expected for polymers with a supramolecular architecture that promotes different relative orientations of adjacent chains. Such disorder is certainly promoted in a polymer comprising a mixture of *cis* and *trans* vinylene units since the alignment of polymer chains is hindered by the different orientations of *cis* and *trans* double bonds.

It is not possible to make an unambiguous generalisation about the relationship between the *cis* and *trans* content of poly(arylene vinylene)s and PL efficiency. However, the wide spread view that all-*trans* configurations are generally beneficial is certainly questionable and it is clear that the outcome is related to the details of structure and organisation.

A blend of H-DSB-*block*-SEO and F-DSB-*block*-SEO (50 wt.%, 50 wt.%) prepared from solutions of both polymers shows a drop in solid state PL efficiency to 10%. This decrease might be due to a quenching process based on π,π-stacking of aromatic rings. π,π-stacking is a typical behaviour in mixtures of aromatics and perfluoroaromatics[22] and will be discussed in more detail in Chapter 5. In the case of photoluminescence, the stacking might lead to regions of high order where the excited state is quenched by non-radiative processes.

4.4 Light emitting diodes

Single-layer devices based on H-DSB-block-SEO

The principles of a polymer LED were described in Chapter 1. Indium-tin-oxide (ITO) is the most prevalent material used as the anode because of its high work function (4.5-5.1 eV) and its transparency in the visible region of light. Commercially available ITO-glass-substrates were treated first with an oxygen plasma, in order to increase the work function and surface energy of ITO.[23] After spin-coating with the emissive polymer, thin calcium or aluminium layers were deposited at a pressure below 10^{-7}mbar (see Experimental).

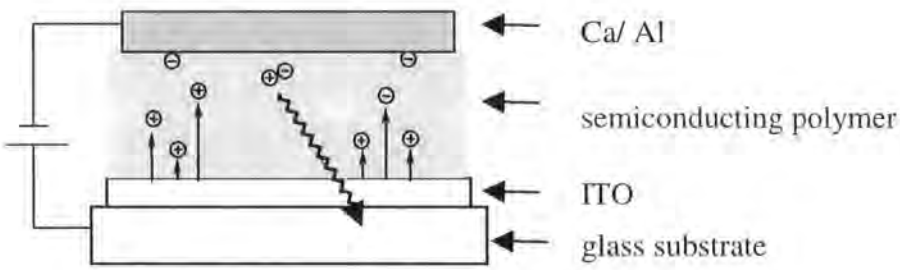

Figure 4.4.1 Schematic diagram of a light emitting diode.

First, single-layer devices with H-DSB-*block*-SEO as the emissive layer and calcium or aluminium as cathodes were prepared. These devices were then characterised by measuring the current density and luminescence relative to the voltage applied to the device. These so called current density/voltage/luminescence (IVL) curves show several characteristics of the device. The turn-on voltage is the minimum voltage required for electroluminescence. All IVL curves presented in this work show the luminescence on a logarithmic scale on the right hand axis of the graph. Due to the logarithmic scale the luminescence drops sharply to zero at the turn-on voltage, so that the turn-on voltage can be determined easily. The current density is shown on the left hand side of the IVL curves. *Figure 4.4.2* shows the IVL curves for the devices ITO/H-DSB-*block*-SEO/Ca and ITO/H-DSB-*block*-SEO/Al. For both devices current and luminescence increase steadily with increasing voltage. When Ca was used as the cathode the turn-on voltage was 6.5 V and when Al was used the turn-on voltage was 7.0 V. The devices were stable and

did not degrade over a period of ten minutes while a series of measurements was conducted. Maximum luminescences over 1000 cd/m^2 were observed at 24 V for a device with a Ca-cathode and luminescences over 2000 cd/m^2 were observed at 19 V in the case of an Al-cathode. The device structure with the Al-cathode was still capable of electroluminescence after storing in air for seven months.

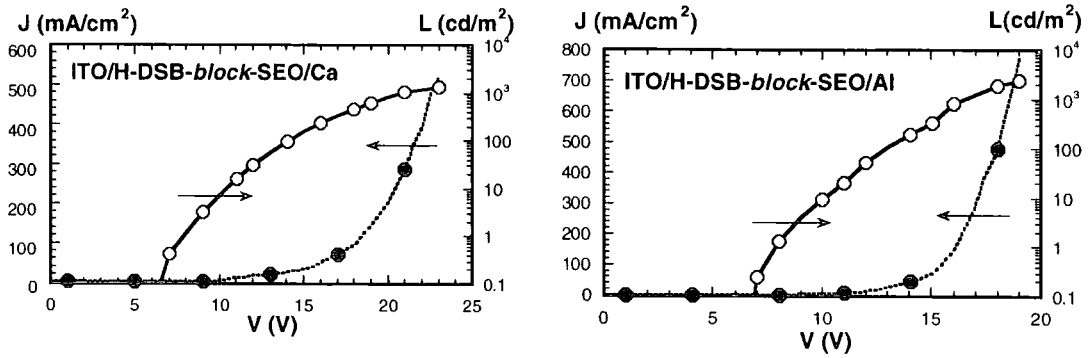

Figure 4.4.2 IVL curves for the devices a) ITO/H-DSB-block-SEO/Ca (left) and b) ITO/H-DSB-block-SEO/Al (right).

The average luminescence of a television screen is 100 cd/m^2 showing that the devices are very bright. Although the devices cannot be used over a prolonged period at 19 V, since degradation occurs at such high current densities, the devices were stable at lower voltages. These findings are particularly noteworthy with respect to polymers prepared by Benfaremo *et al.* and Li *et al.*.[11,24] These authors have prepared similar polymers but were unable to use them in electroluminescent devices due to their poor emission and stability characteristics. *Figure 4.4.3* shows the structures of the polymers prepared by Benfaremo *et al.* (left) and Li *et al.* (right). Possible reasons for the improved properties of H-DSB-*block*-SEO compared to these polymers include high purity, few defects and careful processing.

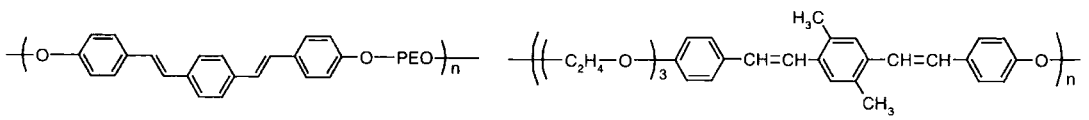

Figure 4.4.3 Polymers prepared by Benfaremo et al. (left) and Li et al. (right).

The maximum luminescence efficiency is about 0.5 cd/A for both devices. This corresponds to an internal quantum efficiency of 1.1%. Quantum efficiencies of up to 0.1% have been reported for PPV itself and up to 0.8% for block copolymers.[25,26] The high quantum efficiency of devices based on H-DSB-*block*-SEO confirms the excellent properties of the polymer as an emitter in LEDs.

The ionisation potential (IP) of H-DSB-*block*-SEO is 5.4 ± 0.2 eV and the electron affinity is 2.4 eV ± 0.2 eV. The work function of Ca is 2.9 eV and the work function of Al is 4.3 eV. *Figure 4.4.4* shows the energy levels of the polymer and the work functions of the electrodes. Without any barriers at either electrode the turn-on voltage should have a value close to the optical band gap i.e. 3.0 eV in the case of H-DSB-*block*-SEO. A small barrier is expected for the injection of electrons from Ca since its work function (2.9 eV) is close to the LUMO of H-DSB-*block*-SEO (2.4 eV). A larger barrier is expected for Al because of its higher work function (4.3 eV). Indeed, the turn-on voltage was slightly lower when Ca (6.5 V) was used instead of Al (7.0 V). However, due to the large difference between the two work functions a bigger difference in turn-on voltage and efficiency was originally expected.

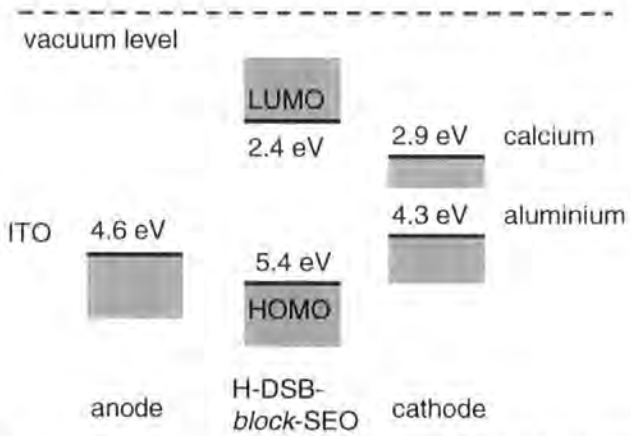

Figure 4.4.4 Electron energy level diagram of H-DSB-block-SEO and work functions of ITO, Ca and Al.

The EL spectra for the two single-layer devices are very similar (*Figure 4.4.5*). They show a fine-structure with two maxima at 2.37 eV and 2.51 eV, similar to those observed in the PL spectrum (2.34 eV and 2.50 eV). This confirms that the emission in photoluminescence and electroluminescence are based on the same excited states.

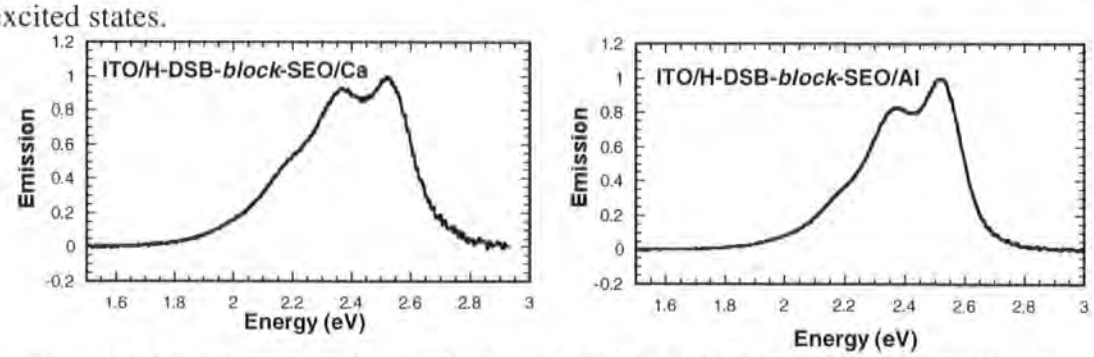

Figure 4.4.5 EL spectra for the devices a) ITO/H-DSB-block-SEO/Ca (left) and b)ITO/H-DSB-block-SEOAl (right).

Double-layer devices based on H-DSB-block-SEO and PEDOT:PSS

Poly(dioxyethylene thienylene) (PEDOT) doped with polystyrenesulfonic acid (PSS) is widely used as the hole-injection layer.[12] It has a high work function and thereby provides low barriers for hole-injection to the polymer. It is likely that some diffusion of the dopant PSS into the emissive polymer layer occurs during the processing which helps charge injection from the PEDOT into the emissive polymer.[12] However, the diffusion is restricted to the interface because of the polymeric nature of the dopant.

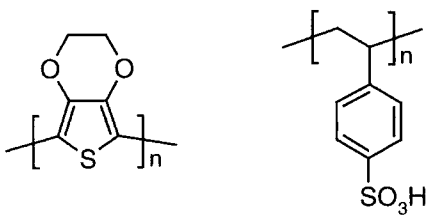

Figure 4.4.6 PEDOT and the dopant PSS provide a stable hole-injection layer.

An aqueous PEDOT:PSS solution was spun-cast onto ITO substrates and dried. H-DSB-*block*-SEO was spun-cast on top of this layer and the devices were completed by evaporation of Ca or Al cathodes. *Figure 4.4.7* shows the IVL curves for the double-layer devices ITO/PEDOT:PSS/H-DSB-*block*-SEO/Ca and ITO/PEDOT:PSS/H-DSB-*block*-SEO/Al. The onset of luminescence for both devices is 8.5 V. This increase compared to the single-layer devices is probably due to the increased thickness; the double-layer devices consist of a 100 nm-thick emissive layer plus a 90 nm-thick hole-conducting layer. The maximum efficiencies are 0.44 cd/A for the device with a Ca electrode and 0.39 cd/A for a device with an Al electrode, corresponding to internal quantum efficiencies of 1.1% and 1.0%, respectively. Both devices were stable over the period of measurements.

Hole-injection is facile from ITO to PPV and a similar situation can be expected for H-DSB-*block*-SEO because of the similarity in the energy levels. Since hole-injection is not the limiting factor for the efficiency of the device, the introduction of a hole-conducting layer does not improve the device characteristics, which is readily appreciated with the wisdom of hindsight.

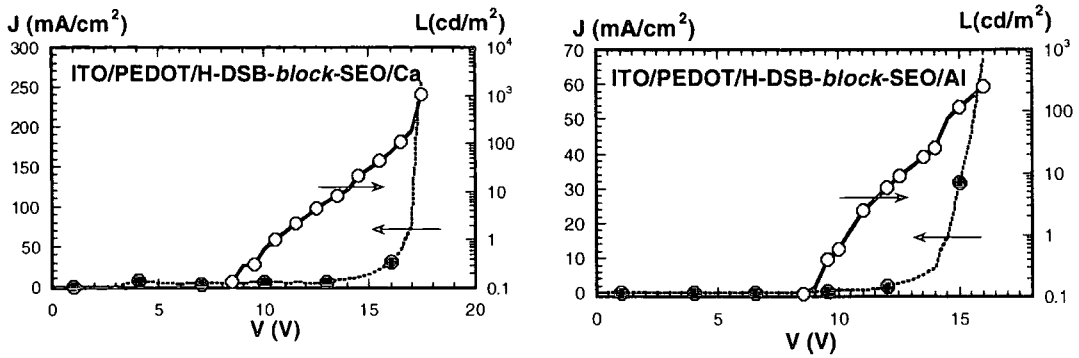

Figure 4.4.7 IVL curves the devices a) ITO/PEDOT:PSS/H-DSB-block-SEO/Ca (left) and ITO/PEDOT:PSS/H-DSB-block-SEO/Al (right).

Devices based on F-DSB-block-SEO

Single-layer devices with F-DSB-*block*-SEO as the emissive layer were prepared in the same way as those based on H-DSB-*block*-SEO. Calcium or aluminium was used as the cathode. In general, the devices based on F-DSB-*block*-SEO were disappointing with respect to their electroluminescence properties; the devices were unstable and the electroluminescence faded away within a few seconds after current was passed through the device; consequently, no luminescence vs. voltage curves could be recorded. The current density vs. voltage curves show that very little current passes through the devices; while a current of 500 - 700 mA/cm^2 at 19 V is observed in devices based on H-DSB-*block*-SEO the current is only between 3 and 5 mA/cm^2 for devices based on the fluorinated equivalent. The injection or transport of at least one charge carrier must therefore be hindered.

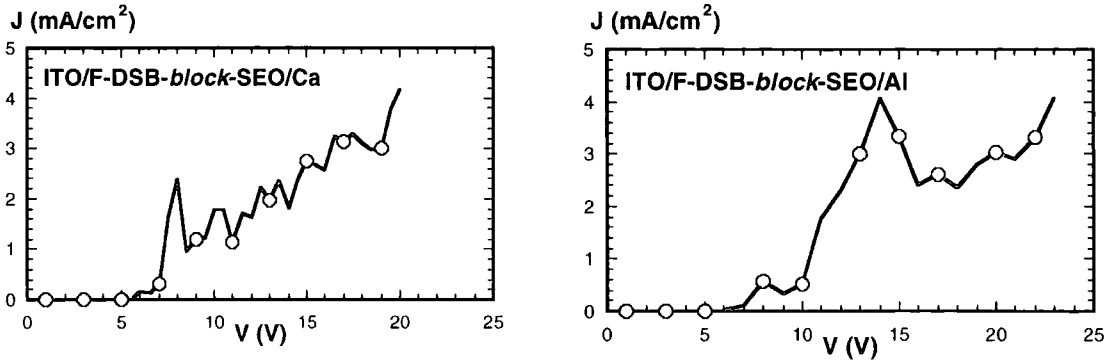

Figure 4.4.8 Current density vs. voltage curves for the devices a) ITO/F-DSB-block-SEO/Ca (left) and b) ITO/F-DSB-block/Al (right).

The EL spectrum for the device ITO/F-DSB-*block*-SEO/Al could be obtained, when several pixels were switched on successively and the individual emissions were summed. *Figure 4.4.9* shows EL spectrum with a maximum emission at 2.44 eV, similar to the PL maximum at 2.47 eV. No fine structure is observed. The similarity between the PL spectrum and the EL spectrum confirms that the emission originates from the same excited states.

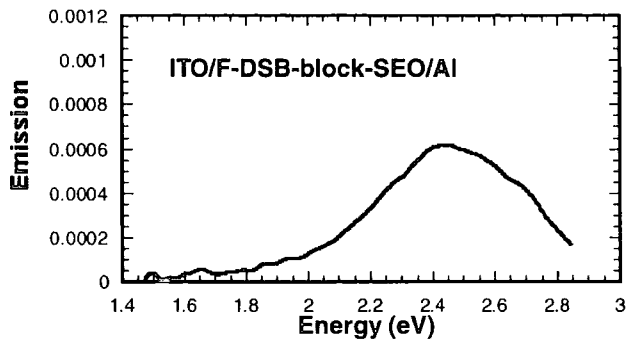

Figure 4.4.9 PL spectrum of the device ITO/F-DSB-block-SEO/Al.

Double-layer devices with PEDOT:PSS as the hole conducting layer were prepared. For these devices a much higher current was recorded, particularly when Ca was used as the cathode (*Figure 4.4.10*). However, the additional hole-conducting layer did not improve the electroluminescence properties. The increase in current indicates that there is a large barrier for hole-injection from ITO into F-DSB-*block*-SEO. This barrier can be bridged by a hole-conducting layer such as PEDOT:PSS.

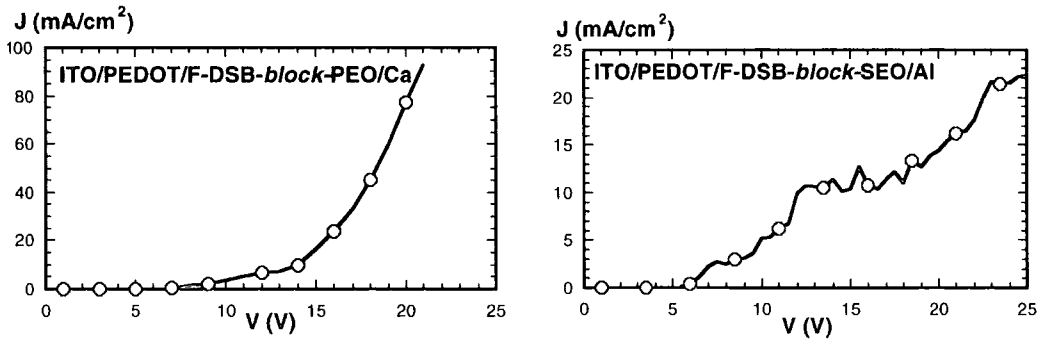

Figure 4.4.10 Current vs. voltage curves for the devices a) ITO/PEDOT:PSS/F-DSB-block-SEO/Ca (left) and b) ITO/PEDOT:PSS/F-DSB-block-SEO/Al (right).

The electron energy level diagram is shown in *Figure 4.4.11*. The IP of F-DSB-*block*-SEO is 6.25 eV and the EA is 3.25 eV. The large gap between the work function of ITO and the HOMO of F-DSB-*block*-SEO explains the hole-injection difficulty.

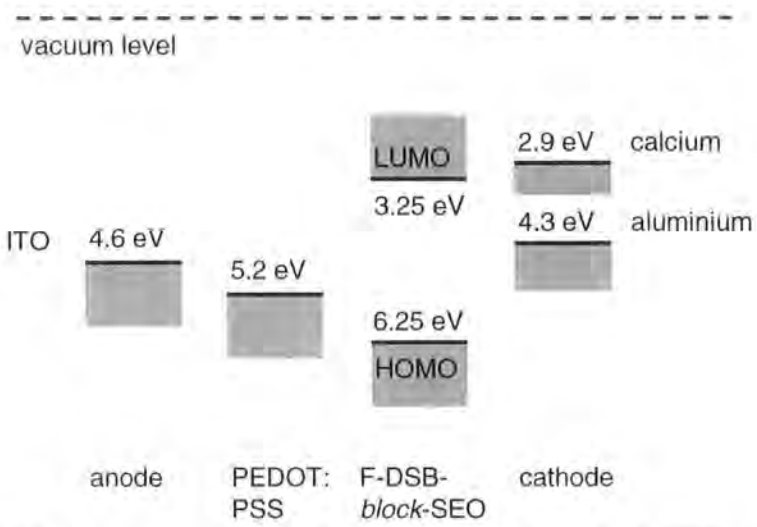

Figure 4.4.11 Electron energy level diagram of F-DSB-block-SEO and work functions of ITO, Ca and Al.

In order to examine the electron-conducting properties of F-DSB-*block*-SEO, a double-layer device was prepared with PPV as the emissive layer and F-DSB-*block*-SEO as the electron-conducting layer (ITO/PPV/F-DSB-*block*-SEO/Al). Its properties were compared to those of a single-layer device based on PPV (ITO/PPV/Al). The spectra of both devices were identical showing that indeed PPV was the emissive layer in both devices. The EL efficiency of both devices was also the same. This shows that F-DSB-*block*-SEO is a good electron-carrier and the increase in thickness of the device is compensated for by the beneficial effect of an additional electron-injection layer.

It can be concluded that fluorine has a strong effect on the energy levels of the block copolymer. The electron affinity of the polymers is increased and the polymer becomes a good electron-conducting material. However, the emissive properties of the polymer are poor; the PL efficiency is half that of H-DSB-*block*-SEO and the EL properties are very poor. Similar findings have been previously reported for fluorinated conjugated polymers (see Chapter 1). It appears that the substitution of hydrogen by fluorine not only changes the position of the energy levels but also

gives rise to new non-radiative processes, which are not present in the pure hydrocarbons.

Several further attempts were made to improve the properties of devices based on F-DSB-*block*-SEO. Blends of H-DSB-*block*-SEO and F-DSB-*block*-SEO were prepared in order to examine whether the good emissive properties of the former and the electron-conducting properties of the latter could be combined. Solutions of both polymers with equal concentrations were mixed and devices prepared in the usual manner using Al as the cathode. A very high current density (over 600 mA/cm^2) was observed for such devices at low voltages (3 V) but no electroluminescence was recorded. Rather than helping electron-injection, the blend provides an additional route for charge transport that is not found in either of the pure polymers. A possible explanation for this high current density could be the previously mentioned arene/perfluoroarene interactions, which could lead to alternating stacks of both chromophores. Such stacks would give rise to a quick charge transport across the polymer layer and not allow time for charge recombination.

A blend 95 wt.% of H-DSB-*block*-SEO and 5 wt.% of F-DSB-*block*-SEO (blend 2) was prepared in order to examine the properties of the fluoro-polymer as a dopant to aid electron-injection. The IVL curve of this polymer blend is shown in *Figure 4.4.12*. The onset of luminescence is at 8.0 V. The device is stable and luminescence efficiency is 0.17 cd/A. However, the device properties are not improved compared to single-layer devices based on pure H-DSB-*block*-SEO.

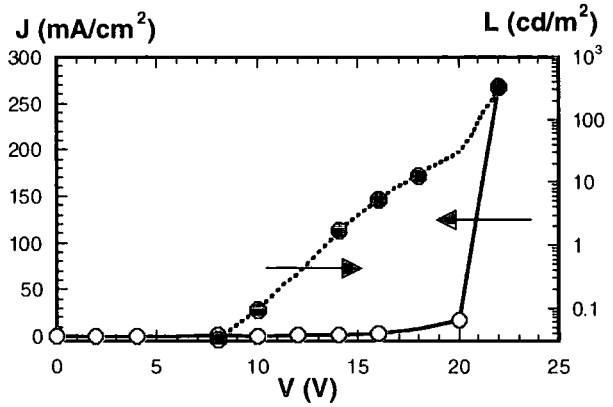

Figure 4.4.12 Current vs. voltage curves for the devices ITO/blend2/Al. Blend 2 consists of H-DSB-block-SEO(95 wt.%) and F-DSB-block-SEO(5%).

The use of an additional hole-conducting polymer, poly(9,9-dioctylfluorene-*co*-bis-N,N'-(4-butyphenyl)-bis-N,N'-phenyl-1,4-phenylenediamine (PFB) was examined (*Figure 4.4.13*). The ionisation potential of PFB is at 5.1 eV and it is often used in double-layer devices as hole-transporting layer.[27] However, a double-layer device of the form ITO/PFB/F-DSB-*block*-SEO/Ca could not be prepared since PFB is soluble in chloroform which is the only appropriate solvent for F-DSB-*block*-SEO. The solvent of the polymer forming the second layer has to be a non-solvent for the first layer to achieve a layered structure in the device. Therefore a single-layer device based on a blend of 60 wt.% F-DSB-*block*-SEO and 40 wt.% PFB was prepared using Ca as the cathode. However, the device showed very little luminescence (3 cd/m^2) and a high turn-on voltage (16 V) *(Figure 4.4.14 left).*

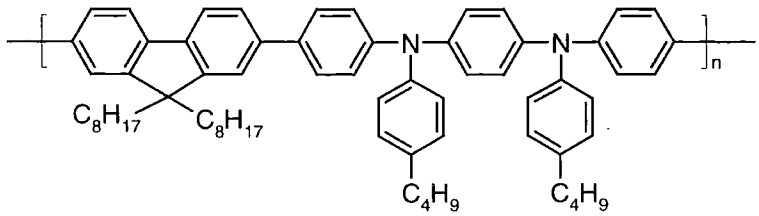

Figure 4.4.13 PFB, a hole-conducting polymer.

A device based on a blend of PFB (40 wt.%) and H-DSB-*block*-SEO (60 wt.%) and Ca as cathode was prepared. The IVL curve is shown in *Figure 4.4.14 (right).* The current density vs. voltage curve peaks at 5 V possibly due to a short-circuit. The onset of luminescence is at 8.5 V and a maximum luminescence of 100 cd/m^2 is obtained at 20 V. However, the device based on the blend has no improved properties compared with the device based on pure H-DSB-*block*-SEO and blends were therefore not further investigated as emissive layers in LEDs.

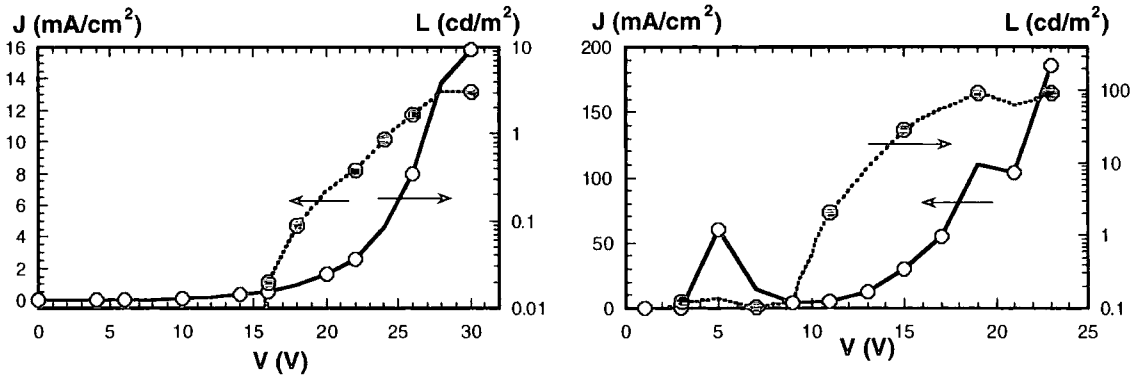

Figure 4.4.14 IVL curves for single-layer devices based on a) blend of F-DSB-block-SEO(60 wt.%) and PFB(40 wt.%) (left) and b) blend of H-DSB-block-SEO(60 wt.%) and PFB(40 wt.%) (right).

4.5 Light-emitting cells

In a light-emitting cell (LEC) an electroluminescent polymer mixed with a polymer electrolyte is sandwiched between two electrodes. LECs were first described by Pei *et al.* who used PPV as the electroluminescent polymer and a complex of poly(ethylene oxide) (PEO) and lithium trifluoromethanesulfonate (LiTf) as electrolyte.[28,29] When a voltage is applied, PPV near the anode is oxidised and PPV near the cathode is reduced. In contrast to LEDs, counter-ions from the electrolyte can move to compensate the charges created on the polymer chains. PPV is now p-doped at the anode and n-doped at the cathode. Due to the balance of charges and the relatively good electronic conductivity of PPV, the PPV/electrode interfaces are low-resistance contacts.

The current passing through the LEC consists of an ionic contribution and an electronic contribution. At an applied voltage an electrochemical equilibrium is established and the ionic current goes to zero. If the applied voltage is higher than the optical band gap of the polymer, holes in the HOMO move towards the cathode and the electrons in the LUMO move towards the anode. These p- and n-type carriers meet in a so-called p-n-junction to form an excited state, which can radiatively decay to the ground state (*Figure 4.5.1*). Such p-n-junctions are reversible. If the former cathode becomes the anode and the former anode the new cathode, a new equilibrium is established and the LEC can be used in reverse bias. The luminescence vs. voltage curve is therefore symmetric about zero bias. Due to the low resistant contacts the threshold voltages for electroluminescence in LECs are very close to the optical band gap of the luminescent polymer.

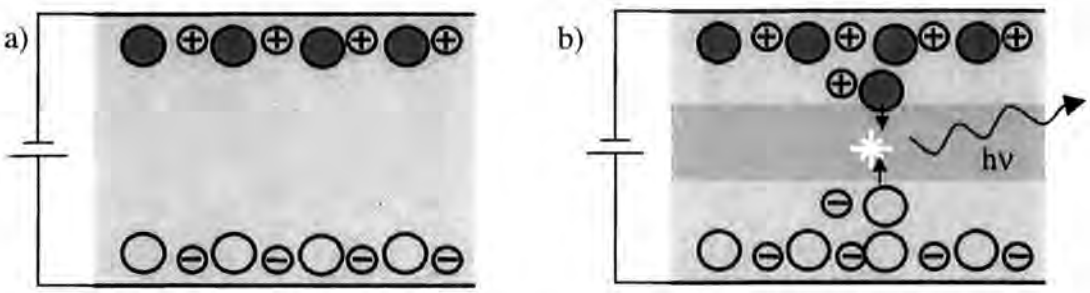

Figure 4.5.1 Schematic diagram of the EL process in a LEC. a) doping of the semi-conducting polymer as p-type or n-type. b) charge migration and radiative decay in the p-n junction.

The use of a blend of PPV and PEO in LECs can result in phase separation.[30] This can be overcome by incorporating oligo(ethylene oxide) units and oligo(phenylene vinylene) units into one polymer. Indeed, Huang *et al.* have prepared a conjugated polymer with a PPV backbone and two tri(ethylene oxide) side chains per aromatic ring (*Figure 4.5.2*).[30] The authors were able to demonstrate a low threshold voltage of 2.5 V and a luminescence vs. voltage curve symmetric about zero bias.

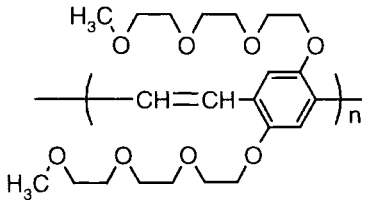

Figure 4.5.2 PPV derivative with tri(ethylene oxide) side chains.

H-DSB-*block*-SEO contains oligo(ethylene oxide) units as well as DSB units within its backbone and is therefore a good candidate to be used in LECs. H-DSB-*block*-SEO was complexed with lithium trifluoromethylsulfonate (LiTf) in a chloroform/methanol mixture and spin-coated onto ITO substrates. The Al anode was deposited by thermal evaporation. Under forward bias ITO was the anode and Al the cathode. An IVL curve conducted in forward bias is shown in *Figure 4.5.3*. The threshold for luminescence was at 3.8 V. This is still significantly higher than the optical band gap of 3.0 V but demonstrates a great improvement compared with the threshold of an LED based on H-DSB-*block*-SEO (6.5 V or 7.0 V). The luminescence increased sharply with increasing voltage; at 4.5 V a luminescence of 190 cd/m^2 was observed. However, the current density was high and at 4.5 V 2000 mA/cm^2 passed through the device. The prepared LEC devices were not as stable as the corresponding LEDs.

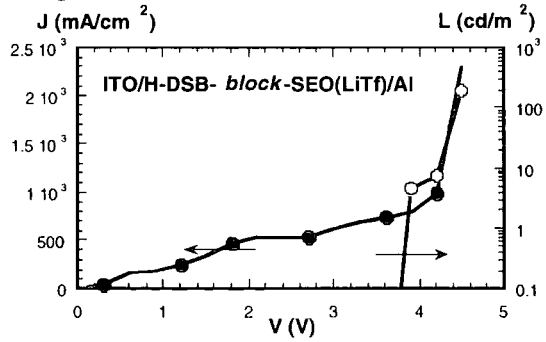

Figure 4.5.3 IVL curve of the LEC ITO/H-DSB-block-SEO(LiTf)/Al.

The device could also be used in reverse bias. Current and luminescence were recorded starting at –6.0 V and increasing the voltage to 4.5 V. The luminescence-voltage curve is approximately symmetrical about zero bias (slightly displaced towards reverse bias) with luminescence observed between -6.5 V and -4.0 V as well as between 3.8 V and 5.0 V. The current-voltage curve is antisymmetric about the origin similar to those reported by Pei *et al.*[29]

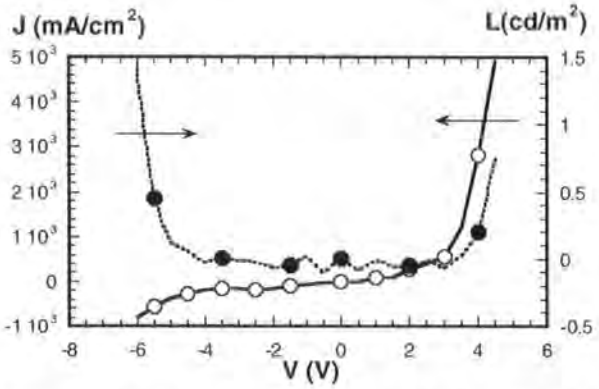

Figure 4.5.4 IVL curve of LEC based on a H-DSB-block-SEO(LiTf) complex in reverse and forward bias.

It was also possible to show that while the electrochemical equilibrium is established, the current density decreases over time at a constant voltage while the luminescence increases. *Figure 4.5.5* shows the decrease of the current density from 3.6 to 2.9 A/cm^2 and the increase of luminescence from 0 to 2.5 cd/m^2 over a period of 110 s at a constant voltage of 4 V. The two peaks in luminescence and current after 80 s and 95 s are probably due to local short circuits, which result in a sharp increase in current and luminescence.

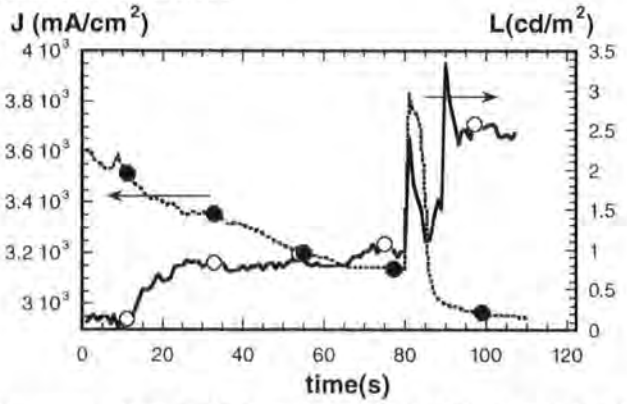

Figure 4.5.5 IVL curve of an LEC based on a H-DSB-block-SEO/ LiTf complex.

4.6 Atomic force microscopy

Atomic force microscopy (AFM) was used to analyse the surface morphology of the LED samples. Commercial atomic force microscopes consist of a piezoelectric scanner, a cantilever, an optical head and a base. The piezoelectric scanner controls the motion of the sample. The cantilever has a sharp tip and a soft spring. The sample is moved under the tip and features on the sample cause the cantilever to deflect. An optical system is used to determine the position of the tip relative to the sample; the beam of a laser is reflected off the back of the cantilever and detected by a photodiode. The differential signal of the photodiode provides a sensitive measure of the cantilever's deflection.

AFM studies of the thin polymer films of H-DSB-*block*-SEO and F-DSB-*block*-SEO as used in the corresponding single-layer devices showed a flat surface; no morphology is expected for a homogeneous polymer. In the case of blends of F-DSB-*block*-SEO and PFB the AFM studies revealed that phase segregation had occurred (*Figure 4.6.1*). Phase segregation can be beneficial in LEDs when it is controlled in a way which results in the electron-conducting polymer being in contact with the cathode and the hole-conducting polymer being in contact with the anode so that the current cannot pass through just one of the polymers. However, little control is gained in the case of blends of F-DSB-*block*-SEO and PFB. The aim of aiding hole-injection into the polymer and therefore improving the device properties was not achieved.

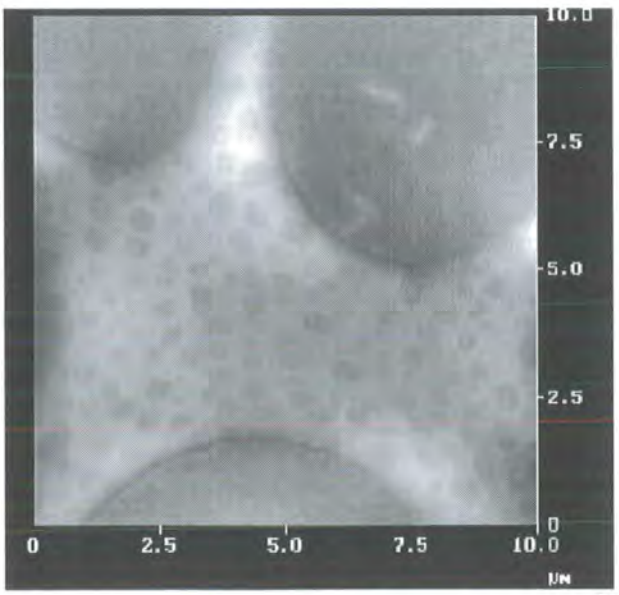

Figure 4.6.1 AFM study of a blend of F-DSB-block-SEO (60 wt.%) and PFB (40 wt.%).

In the case of LECs the AFM studies revealed demixing of H-DSB-*block*-SEO and LiTf (*Figure 4.6.2*). Holes with a diameter between 0.1 and 0.5 μm are found in the polymer layer and are probably due to the fact that LiTf particles deposit on the ITO substrate and prevent the polymer from covering these spots. The LiTf content of 10 wt.% corresponds to 2.5 sexi(ethylene oxide) units per LiTf ion pair. This ratio is probably too high to allow all LiTf ions to be fully complexed and demixing occurs. Further investigations should therefore include the reduction of the LiTf content.

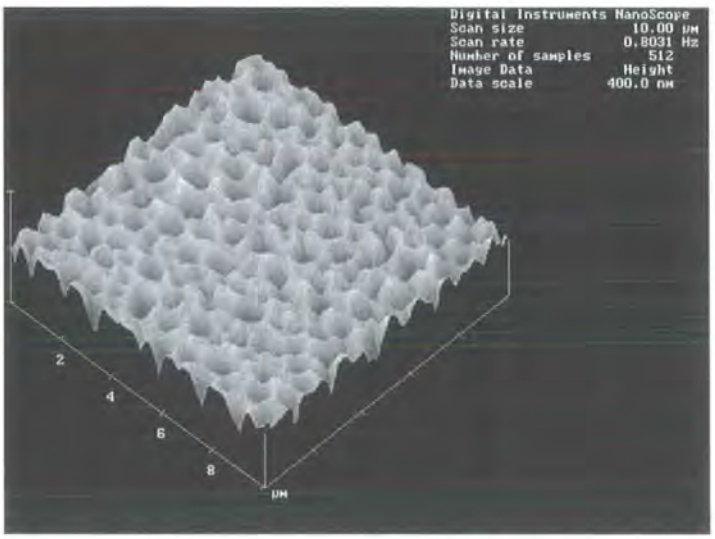

Figure 4.6.2 AFM study of a 100 nm thick film of H-DSB-block-SEO-LiTf complex

4.7 Conclusions

The energy levels of the HOMO and LUMO of H-DSB-*block*-SEO and F-DSB-*block*-SEO were determined by cyclic voltammetry, UPS and UV-absorption spectra. The IP and EA of H-DSB-*block*-SEO are 5.4 eV and 2.4 eV, respectively, and the IP and EA of F-DSB-*block*-SEO are 6.25 eV and 3.25 eV, respectively. The substitution of aromatic hydrogens by fluorines in the block copolymer did not change the size of the optical band gap (3.0 eV). However, this substitution increased the electron affinity and the ionisation potential by 0.85 eV.

The shape of the solid-state absorption spectrum of F-DSB-*block*-SEO indicates the presence of H-aggregates. The maximum of this spectrum is also strongly blue-shifted relative to the solution-state spectrum. Large Stokes' shifts between the solid state absorption and emission maxima are observed for both polymers.

H-DSB-*block*-SEO showed a high photoluminescence quantum efficiency (34%) and single-layer LEDs with aluminium as cathode exhibited luminescences

over 2000 cd/m^2. The luminescence efficiency was as high as 0.5 cd/A, corresponding to an internal quantum efficiency of 1.1%. The onset of luminescence was at 6.5 V. The polymer emitted in the yellow-green region of the visible spectrum. LEDs using calcium as the cathode showed very similar properties. A light emitting cell based on H-DSB-*block*-SEO complexed with lithium triflate showed a reduced threshold for luminescence (3.8 V).

A large barrier was found for the hole-injection from ITO to F-DSB-*block*-SEO. Although the hole-injection could be improved by adding a PEDOT:PSS layer, the fluoro-polymer generally showed very poor characteristics as an emissive layer in LEDs. However, the polymer proved to be a good electron-carrier due to its high electron affinity.

4.8 Experimental

Photoelectron Spectroscopy

In the case of XPS the photoelectrons were generated with Al (K_α) irradiation (1486 eV) and detected using a Scienta ESCA 200 hemisperical analyser (Gammadata-Scienta, Sweden). For UPS a He discharge lamp and monochromator (He II radiation, 40.8 eV) were used. The spectrometer for UPS was designed and constructed in Linköping, Sweden.

UV/Vis Spectroscopy

Solution state UV/Vis spectra of H-DSB-*block*-SEO and F-DSB-*block*-SEO were recorded in chloroform using a Unicam UV/Vis spectrometer UV2. Spectrosil substrates were used for solid state absorption experiments. Thin films of the polymer were prepared on these substrates by spin-coating (60 s, 2000 rpm) from a chloroform solution (approximately 2 wt.%, filtered through a Millipore membrane with a pore size of 1 μm). The solid state spectra were recorded using a Lambda 9 Perkin-Elmer double beam spectrometer.

Photoluminescence Spectroscopy

Samples were prepared on Spectrosil substrates as described under UV-Vis spectroscopy. The PL efficiency were determined in an integrating sphere, purged with nitrogen to avoid photo-oxidation using a He-Cd laser (325 nm).[13]

Light emitting diodes

Thin films of polymer were prepared by spin-coating (60 s, 2000 rpm) from chloroform solution (approximately 2 wt.%, filtered through a Millipore membrane with a pore size of 1 μm). Film thicknesses were determined with a Dektak IIa stylus profiler and concentrations adjusted so that 90-100 nm thick films were obtained. Commercially available ITO-coated glass substrates (Asahi) were used for the fabrication of LEDs. The ITO was patterned so that the metal electrodes on top of the polymer films could be contacted on the edge of the substrate without shorting (*Figure 4.8.1*). The ITO substrates were cleaned in an ultrasonic bath with acetone and 2-propanol, each for 15 min and then treated for 10 min with oxygen plasma at approximately 300 W. For double-layer LEDs with PEDOT:PSS (Bayer AG), the commercially available PEDOT:PSS was spun-cast from an aqueous suspension. It was dried and cross-linked by thermal treatment for 1 h at 100 °C under nitrogen.[31] A thin calcium or aluminium layer was subsequently deposited over the substrate through a shadow mask at a pressure below 10^{-7}mbar. The pixel size was determined by the overlap of the ITO and the cathode patterns yielding an area of about 2 x 10^{-2} cm^2. The calcium layer was covered with an aluminium layer in the same way in order to protect the anode from oxidation and improve the mechanical integrity of the device for the measurements. All processing of LEDs was carried out in a glove box under a nitrogen atmosphere with less than 20 ppm residual water vapour and 5 ppm oxygen.

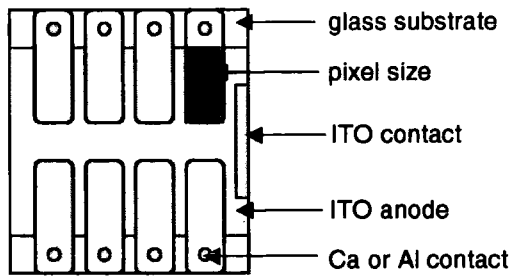

Figure 4.8.1 Schematic diagram of a 1 cm x 1 cm LED test device.

Measurements were carried out in a sample holder specially designed to allow the transfer of the sample from the glove box to the measuring station without exposure to air. The luminous output was measured with a calibrated silicon photodiode, and the EL efficiency calculated by taking into account the refraction and reflection at the interfaces. Spectral characterisation was performed by means of an Oriel CCD-matrix spectrograph, with a spectral resolution better than 5 nm.

Atomic force microscopy

AFM investigations were carried out with a Nanoscope IIIa Dimension 3100 (Digital Instruments Inc., Santa Barbara).

4.9 References

1. Lögdlund, M.; Salaneck, W. R. Chapter 5 in *Semiconducting polymers by Hadziioannou and van Hutten,* Wiley-VCH, Weinheim **2000**.
2. Ghosh, P. K. *Introduction to Photoelectron Spectroscopy,* John Wiley & Sons, New York **1983**.
3. West, A. R. *Molecular spectroscopy, Heyden&Son*, London **1977**.
4. Kang, I.-N.; Shim, H.-K. *Chem. Mater.* **1997**, *9*, 746.
5. Ndayikengurukiye, H.; Jacobs, S.; Tachelet, W.; Van der Looy, J.; Pollaris, A.; Geise, H. J.; Claeys, M.; Kauffmann, J. M.; Janietz, S. *Tetrahedron* **1997**, *53*, 13811.
6. Renak, M. L.; Bartholomew, G. P.; Wang, S.; Ricatto, P.; Lachicotte, R. J.; Bazan, G. C. *J. Am. Chem. Soc.* **1999**, *121*, 7787.
7. Siegrist, A. E.; Liechti, P.; Meyer, H. R.; Weber, K. *Helvetica Chimica Acta* **1969**, *52*, 2521.
8. Kilbinger, A. F. M.; Feast, W. J. *J. Mater. Chem.* **2000**, *10*, 1777.
9. Song, X.; Geiger, C.; Leinhos, U.; Perlstein, J.; Whitten, D. G. *J. Am. Chem. Soc.* **1994**, *116*, 10340.
10. Sarker, A. M.; Strehmel, B.; Neckers, D. C. *Macromolecules* **1999**, 7409.
11. Benfaremo, N.; Sandman, D. J.; Kumar, J.; Yang, K.; Rubner, M. F.; Lyons, C. *Macromolecules* **1998**, *31*, 3595.
12. Friend, R. H.; Gymer, R. W.; Holmes, A. B.; Burroughes, J. H.; Marks, R. N.; Taliani, C.; Bradley, D. D. C.; Dos Santos, D. A.; Bredas, J. L.; Logdlund, M.; Salaneck, W. R. *Nature* **1999**, *397*, 121.
13. de Mello, J. C.; Wittmann, H. F.; Friend, R. H. *Advanced Materials* **1997**, *9*, 230.
14. Greenham, N. C.; Samuel, I. D. W.; Hayes, G. R.; Phillips, R. T.; Kessener, Y. A. R. R.; Moratti, S. C.; Holmes, A. B.; Friend, R. H. *Chem. Phys. Lett.* **1995**, *241*, 89.

15. Carter, J. C.; Grizzi, I.; Heeks, S. K.; Lacey, D. J.; Latham, S. G.; May, P. G.; de los Panos, O. R.; Pichler, K.; Towns, C. R.; Wittmann, H. F. *Appl. Phys. Lett.* **1997**, *71*, 34.

16. Cacialli, F.; Daik, R.; Feast, W. J.; Friend, R. H.; Lartigau, C. *Opt. Mat.* **1999**, *12*, 315.

17. Feast, W. J.; Cacialli, F.; Koch, A. T. H.; Daik, R.; Lartigau, C.; Friend, R. H.; Beljonne, D.; Bredas, J. L. *Macromolecules* **2001**, accepted for publication.

18. Daik, R. *Ph.D. Thesis, University of Durham* **1997**.

19. Pasco, S. T.; Lahti, P. M.; Karasz, F. E. *Macromolecules* **1999**, *32*, 6933.

20. Son, S.; Dobabalapur, A.; Loveniger, A. J.; Galvin, M. E. *Science* **1995**, *269*, 376.

21. Cornil, J.; Heeger, A. J.; Bredas, J. L. *Chem. Phys. Lett.* **1997**, *272*, 463.

22. Coates, G. W.; Dunn, A. R.; Henling, L. M.; Dougherty, D. A.; Grubbs, R. H. *Angew. Chem. Int. Ed. Engl.* **1997**, 248.

23. Kim, J. S.; Friend, R. H.; Cacialli, F. *J. Appl. Phys.* **1999**, *86*, 2774.

24. Yang, C.; He, G.; Wang, R.; Li, Y. *Mol. Cryst and Liq. Cryst.* **1999**, *337*, 473.

25. Brown, A. R.; Bradley, D. D. C.; Burroughes, J. H.; Friend, R. H.; Greenham, N. C.; Burn, P. L.; Holmes, A. B.; Kraft, A. *Appl. Phys. Lett.* **1992**, *61*, 2793.

26. Hu, B.; Karasz, F. E. *Synthetic Metals* **1998**, *92*, 157.

27. Redecker, M.; Bradley, D. D. C.; Inbasekaran, M.; Wu, W. W.; Woo, E. P. *Advanced Materials* **1999**, *11*, 241.

28. Pei, Q.; Klavetter, F. *US Patent Appl. No. 08/268763, June 28* **1994**.

29. Pei, Q.; Yang, Y.; Yu, G.; Zhang, C.; Heeger, A. J. *J. Am. Chem. Soc.* **1996**, *118*, 3922.

30. Huang, C.; Huang, W.; Guo, J.; Yang, C.-Z.; Kang, E.-T. *Polymer* **2001**, *42*, 3929.

31. Riehn, R.; Morgado, J.; Iqabal, R.; Moratti, S. C.; Holmes, A. B.; Volta, S.; Cacialli, F. *Macromolecules* **2000**, *33*, 3337.

5 Molecular Organisation in Fluorinated Oligo(phenylene vinylene)s

5.1 Introduction

This chapter deals with the molecular organisation of two fluorinated oligo(phenylene vinylene)s. The understanding of the molecular organisation in small molecules provides useful information about these specific compounds as well as guidelines, which may be relevant to related structures such as polymers. The structures of aggregates of organic materials have profound effects on their optical properties; this has been shown in the case of sexithiophene, for instance, where different morphologies give rise to different fluorescence spectra.[1]

Oligo(phenylene vinylenes)s have been studied as model compounds for PPV. Hadziioannou *et al.* have prepared 1,4-bis(*p*-styrylstyryl)benzene, studied the crystal structure and measured optoelectronic properties (*Figure 5.1.1*).[2] Like PPV this model compound crystallises in a herringbone structure. The absorption maximum and the absorption edge of the model compound are 0.2 eV blue-shifted relative to PPV indicating that the effective conjugation length of PPV exceeds that of the model. The authors were able to prepare LEDs based on the model compound but the turn-on voltage for such devices was high (18 V).

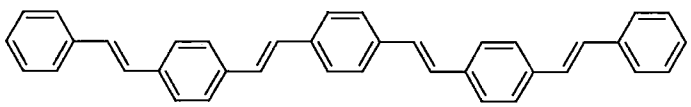

Figure 5.1.1 1,4-Bis(p-styrylstyryl)benzene, a model compound for PPV.

Fluorinated aromatics show strong interaction with non-fluorinated aromatics. This was first discovered by Patrick and Prosser in 1960,[3] who demonstrated that benzene (mp 5.5 °C) and hexafluorobenzene (mp 4 °C) form a stable 1:1 complex (mp 24 °C), consisting of a face-to-face stack of alternating benzene and hexafluorobenzene molecules. The origin of this stable arrangement is thought to lie in the quadrupolar interaction between the two molecules;[4] both molecules have large molecular quadrupole moments but of opposite sign. *Figure 5.1.2* shows

schematic representations of the quadrupole moments of benzene *(a)* and hexafluorobenzene *(b)*. While benzene has a high electron density in the centre and a low electron density on the outside, the situation is exactly opposite in the case of hexafluorobenzene. The face-to-face stacking of alternating benzene and hexafluorobenzene rings in a 1:1 mixture of the two compounds is shown in *Figure 5.1.2 (d)*. Recent work suggests that van der Walls interactions also play an important role in this interaction.[5] Benzene and hexafluorobenzene on their own crystallise in a herringbone structure, where one molecule is orientated perpendicular to its neighbour, shown for benzene in *Figure 5.1.2 c*.

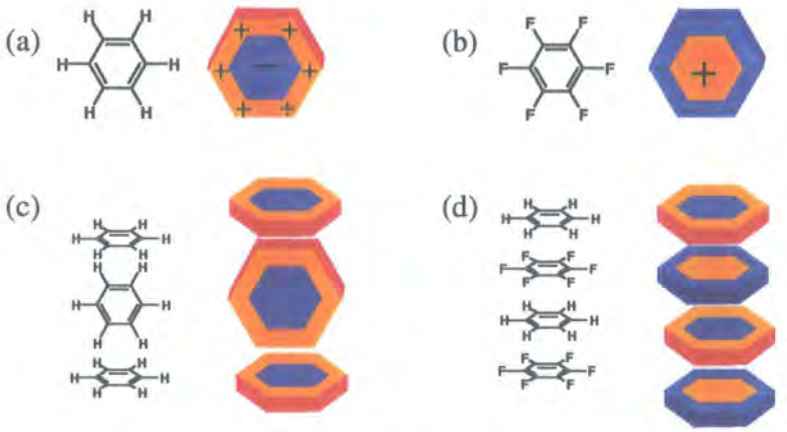

Figure 5.1.2 Schematic representations of the quadrupole moments of benzene (a), hexafluorobenzene (b) and the crystal structures of benzene(c) and a 1:1 mixture of benzene and hexafluorobenzene (d).

Grubbs *et al.* have studied the aggregation of fluorinated stilbenes and DSBs. They found that 2,3,4,5,6-pentafluorostilbene (PFS) crystallises in stacks with an alternating orientation of the molecules.[6] *Figure 5.1.3 (left)* shows two molecules in such a stack. Each phenyl ring is sandwiched between two pentafluorophenyl rings and *vice versa*. Photodimerisation occurs when the crystals are irradiated with UV light. The authors obtained X-ray crystal structures for PFS and the cyclobutane adduct. The PFS molecules are paired in the stack in the sense that one molecule is slightly closer to its neighbour above than the one below. The distances between the double bonds are 3.700 Å and 3.707 Å. The authors suggest that this pairing leads to 100% conversion in the [2+2] photodimerisation. In general, solid-state photodimerisations give less than 100% yield because some olefins are isolated between cyclobutane molecules in the crystal matrix.

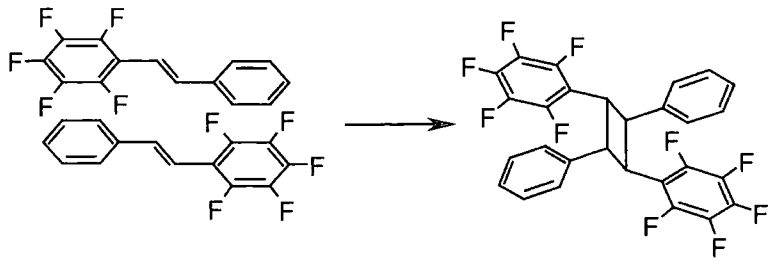

Figure 5.1.3 Solid-state photodimerisation of trans-pentafluorostilbene.

Grubbs *et al.* also investigated the molecular packing of 1,4-distyryl-2,3,5,6-tetrafluorobenzene (*Figure 5.1.4*).[6] The molecule crystallises in stacks in which each tetrafluorobenzene ring is sandwiched between two phenyl rings. However, the phenyl rings can only π-stack on one side since the molecule contains two phenyl rings for each fluorinated benzene ring. The photodimerisation leads to a polymer since each molecule contributes to the formation of two cyclobutane rings. The authors obtained a X-ray crystal structure of 1,4-distyryl-2,3,5,6-tetrafluorobenzene. The presence of a polymer was demonstrated by GPC and NMR spectroscopy.

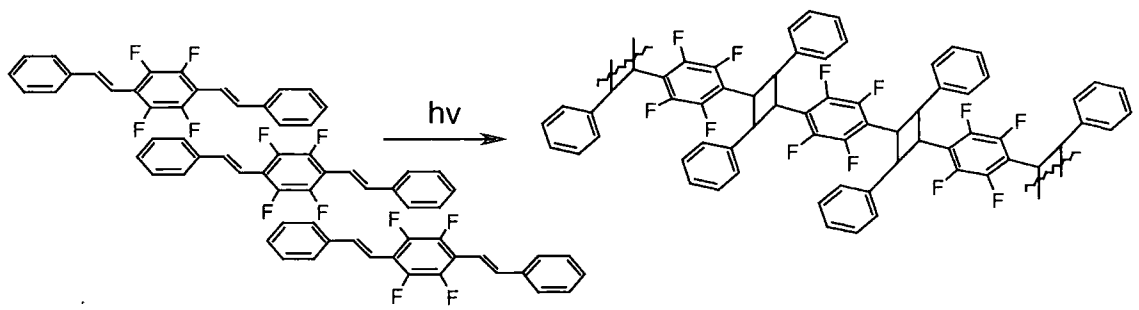

Figure 5.1.4 Solid state photopolymerisation of 1,4-distyryl-2,3,5,6-tetrafluorobenzene.

5.2 J aggregates

This project was carried out in collaboration with Prof. Carlo Taliani at the Institute of Molecular Spectroscopy in Bologna. As part of the EU LAMINATE Network we became interested in using the directing effect of phenyl-pentafluorophenyl interactions to prepare J aggregates of large aromatic chromophores suitable for optoelectronic applications. J aggregates are characterised by a narrow and intense absorption band that shows a bathochromic shift relative to the single isolated molecule. They were first described by Jelly who observed a strong absorption for the case of cyanine dyes.[7] A possible arrangement for J aggregates is the simple 'brickwall' motif, in which each brick or molecule is situated over the gap between the bricks in the row below (*Figure 5.2.1*).

Figure 5.2.1 'Brickwall' motif.

The red shift in absorption can be understood using a simple model. The underlying principles are explained for the case of stilbene, a simple conjugated rod-like molecule. The absorption of a photon by an isolated stilbene molecule is shown on the left-hand side of *Figure 5.2.2*. The ground state of stilbene has no dipole moment. The absorption of a photon requires a change in the dipole moment of the molecule and the excited state can be represented by a structure, which has a negative charge on one side and a positive charge on the other side of the molecule. In *Figure 5.2.2* this excited state is also represented by a simple rod with a positive and a negative sign on opposite sides. The absorption in the case of a J aggregate is shown on the right-hand side of *Figure 5.2.2*. For the case of two molecules in a 'brickwall' motif two excited states are possible. In one case the dipole moments point in the same direction resulting in an attractive interaction between the negative charge on one molecule with the positive charge on the other. Due to this attractive interaction the excited state is lower in energy than the excited state of the isolated molecule. If the dipole moments of the two molecules point in opposite directions the excited state is higher in energy since two equal charges are in proximity. Furthermore, the net dipole moment of these two excited states is zero so that the transition to this state is in fact forbidden.

This simple model shows why J aggregation leads to a red shift in absorption. This so-called excitonic coupling leads to narrow and intense absorption and fluorescence bands.

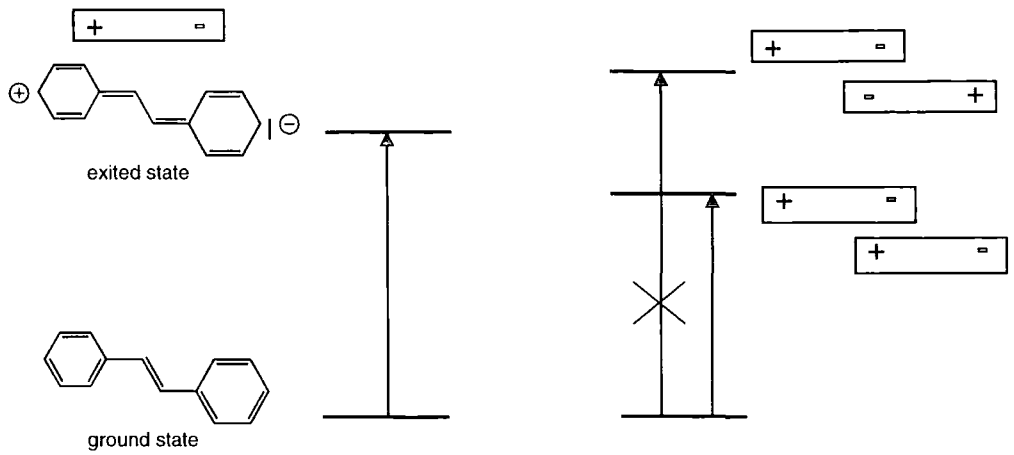

Figure 5.2.2 Energy diagrams for the absorption in isolated stilbene molecules (left) and stilbene molecules in J aggregates (right).

5.3 Results and discussion

4,4'-Bis(2,3,4,5,6-pentafluorostyryl)stilbene

Our first target molecule was an oligo(phenylene vinylene) which forms a J aggregate on the basis of phenyl-perfluorophenyl-interactions. An oligo(phenylene vinylene) containing four benzene rings was chosen in which the two terminal benzene rings were fully fluorinated. The synthesis started from *p*-tolylaldehyde **40** which was coupled in a McMurry reaction to give *trans*-4,4'-dimethylstilbene **41** (*Figure 5.3.1*). The two methyl groups were mono-brominated with NBS yielding 4,4'-bis(bromomethyl)stilbene **42**. Substitution of the bromine with triphenylphosphine gave the bis(phosphonium salt) **43**. A Wittig reaction with two equivalents of pentafluorobenzaldehyde gave 4,4'-bis(2,3,4,5,6-pentafluorostyryl) stilbene **44**. Compound **44** is a yellow solid and was prepared on a scale of 2.2 g.

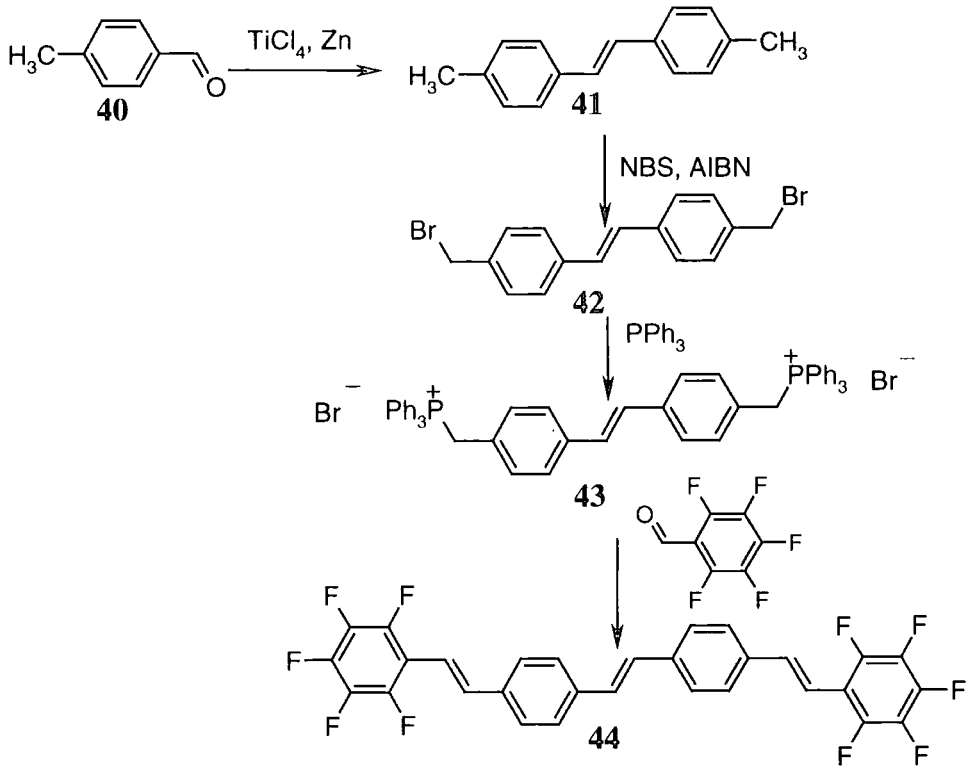

Figure 5.3.1 Synthesis of bis(2,3,4,5,6-pentafluorostyryl)stilbene.

The ^{1}H NMR spectrum of **44** shows three resonances for olefinic protons in a 1:1:1 intensity ratio; a singlet at δ 7.17 and an AB quartet with δ_A 7.00, δ_B 7.43 and a coupling constant of 16.5 Hz typical for a *trans*-vinylene configuration. The singlet signal for aromatic protons is observed at δ 7.57.

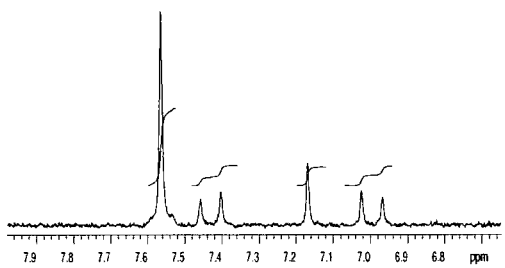

Figure 5.3.2 ^{1}H NMR spectrum of bis(2,3,4,5,6-pentafluorostyryl)stilbene.

Crystals of **44** suitable for X-ray structure analysis were obtained both by sublimation in a thermal gradient oven and from a solution in *trans*-stilbene. The latter technique was described by Hadziioannou *et al.* to prepare crystals of 1,4-bis(*p*-styrylstyryl)benzene (*Figure 5.1.1*); in this method *trans*-stilbene (mp 125 °C) is used as a high boiling solvent. The crystallisation occurs between 270 and 170 °C

and the *trans*-stilbene is removed at 170 °C by filtration. Both techniques lead to identical crystals indicating one predominant form of aggregation. The crystal structure shows that all double bonds have a *trans*-configuration, confirming the ^{1}H NMR analysis (*Figure 5.3.3*). The centre of each molecule is an inversion centre so that only half the molecule is crystallographically unique. The planes of the fluorinated and the non-fluorinated rings are twisted very slightly relative to each other (2.2°) and the two central rings are twisted with an angle of 3°. This almost planar arrangement allows strong π-π interactions.

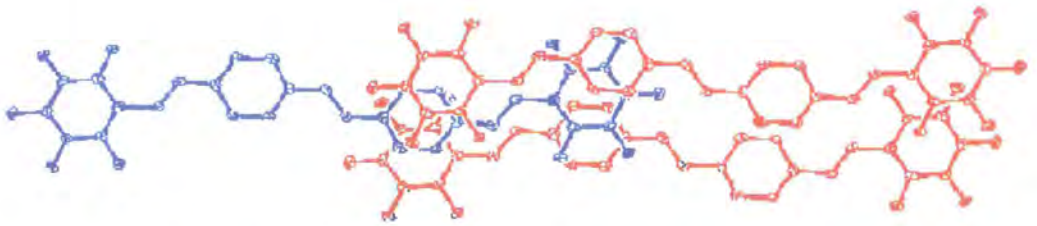

Figure 5.3.3 Crystal structure of **44** *–top view.*

The molecules aggregate in a simple 'brickwall' motif in which each molecule overlaps with two halves of neighbouring molecules in the row below and above it. Thereby, each central aromatic ring is sandwiched between two terminal fluorinated aromatic rings of neighbouring molecules and *vice versa*. The distance between the mean planes of all the atoms in the molecules is 3.41 Å. However, the situation is further complicated by the fact that there is some lateral slippage between the aromatic rings which results in successive rows of the 'brickwall' being slightly offset with respect to each other; analogous structures have been reported and described as 'molecular staircases'.[8] This slippage is not equally distributed between all aromatic rings but the molecules are paired in the sense that one ring overlaps more with its fluorinated counterpart above than the one below or *vice versa*. As a consequence of this the two olefinic carbons of the central molecule in *Figure 5.3.3* and *Figure 5.3.4* are closer to their counterparts below (3.659 Å) than to the one above (3.869 Å).

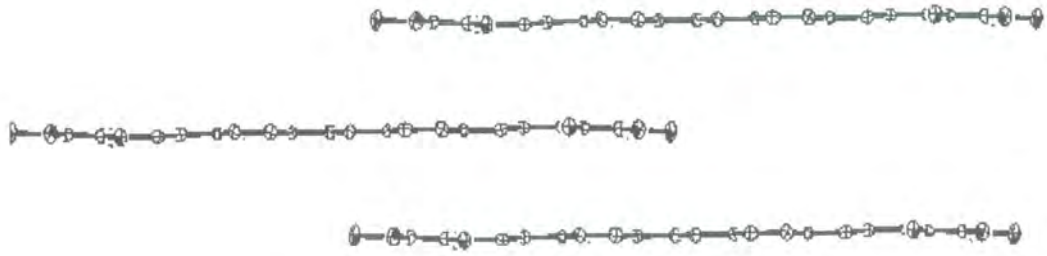

Figure 5.3.4 Crystal structure of **44** *- side view.*

The unit cell of **44** is shown in *Figure 5.3.5*. Each unit cell contains one molecule (Z=1).

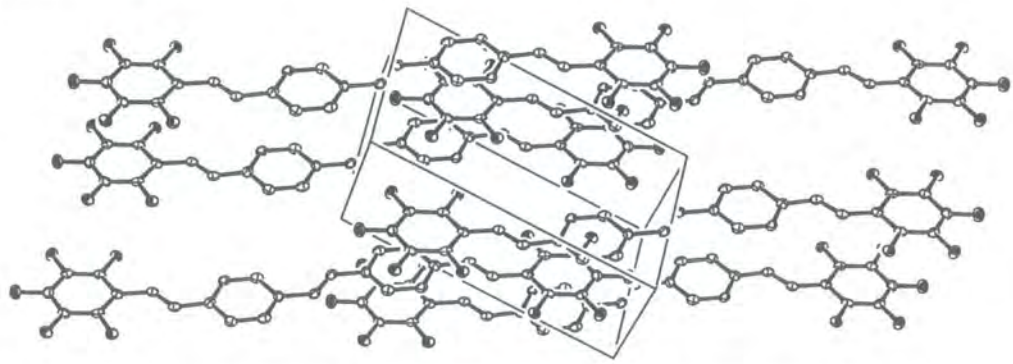

Figure 5.3.5 Crystal structure of **44** *- the unit cell.*

In addition to the face-to-face π-stacking the molecular packing is associated with intermolecular C-F···H-C interactions. Four such interactions are observed on each ring resulting in 16 per molecule. The H···F distances determined in this X-ray study are 2.390, 2.467, 2.480 and 2.595 Å, derived using the neutron normalised C-H distance of 1.083 Å. The corresponding C-H···F angles are 159.4°, 157.4°, 132.1° and 122.9°. The distance between the terminal fluorine atoms in the 4-positions of edge-to-edge neighbours is short (2.676 Å).

The packing of compound **44** is similar to that of 2,3,4,5,6-pentafluorostilbene (PFS) (see section 5.1). The densities of both compounds are very similar (1.635 g cm^{-3} for **44**, 1.641 g cm^{-3} for PFS). Molecules of PFS in the crystal are also paired but the pairing is less obvious than in the case of compound **44**. Because of these similarities we expected photochemically induced [2+2] reactions for the double bonds in the crystal. UV irradiation of a thin film of **44** resulted in a colour change from yellow to almost colourless consistent with the loss of conjugation. ^{1}H NMR

spectroscopy of the product shows a new signal at δ 4.88 for cyclobutane hydrogens and the ^{19}F NMR spectrum shows three new resonances at δ -142.11, -156.11 and -162.98 with concomitant reduction in the intensity of the initial signals at δ -143.81, -157.47 and -163.75. These findings indicate that a photochemically induced [2+2] reaction occurs in the solid state of compound **44**. *Figure 5.3.6* shows the photochemical [2+2] reaction of two molecules of **44**. In a crystal with many millions of unit cells this reaction would lead to polymers similar to the case of 1,4-distyryl-2,3,5,6-tetrafluorobenzene.

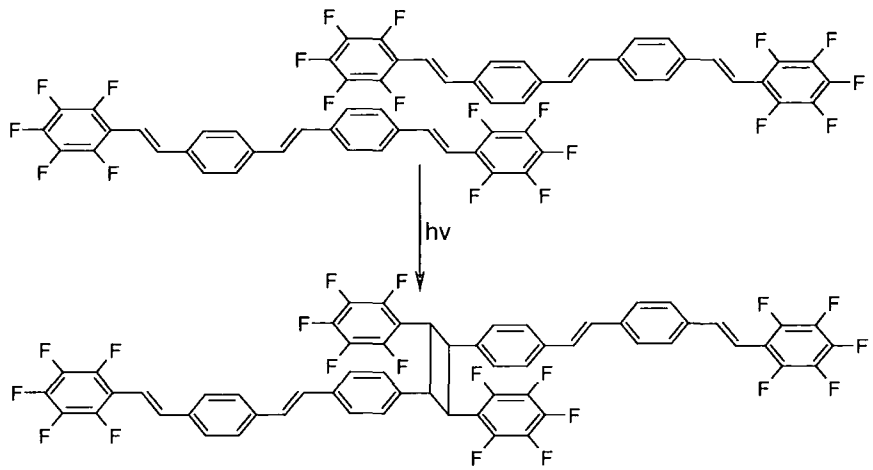

Figure 5.3.6 Photochemically induced [2+2] reaction in the solid state of **44**.

The electronic and optical properties of compound **44** are currently under investigation in the Institute of Molecular Spectroscopy in Bologna.

1,4-Bis(2,3,4,5,6-pentafluorostyryl)-2,3,5,6-tetrafluorobenzene

Our second target molecule was a DSB derivative in which all aromatic positions are substituted with fluorine. Fluorinated DSBs have been studied as model compounds for fluorinated conjugated polymers. Bazan *et al.* have prepared a series of DSB derivatives via the Wittig and Heck reactions.[9] 1,4-Bis(pentafluorostyryl)-2,5-difluorobenzene was the DSB derivative containing the most fluorine atoms prepared in this study (*Figure 5.3.7*).

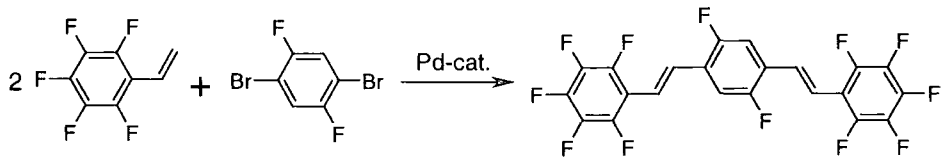

Figure 5.3.7 Synthesis of 1,4-bis(pentafluorostyryl)-2,5-difluorobenzene via the Heck reaction.

Oligo(*p*-tetrafluorophenylene vinylene)s have been prepared previously by Brooke *et al.* in a reaction of pentafluorostryryl lithium with hexafluorobenzene (*Figure 5.3.8*).[10] A series of oligomers was prepared in this reaction (n = 1-6). 1,4-Bis(2,3,4,5,6-pentafluorostyryl)-2,3,5,6-tetrafluorobenzene (n = 2) was one of the products and was characterised by NMR and mass spectroscopy. However, because of the low yield (12 mg) this route was not attractive for a further investigation into this DSB derivative.

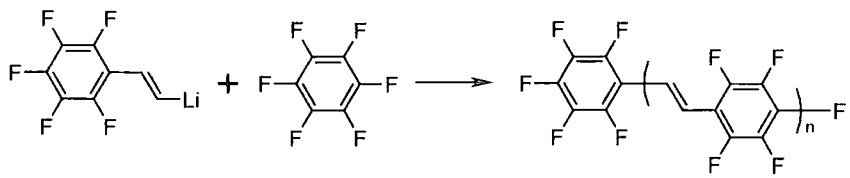

Figure 5.3.8 Synthesis of oligo(p-tetrafluorophenylene vinylene)s.

The Wittig reaction of 2,3,5,6-tetrafluoroxylylen-1,4-bis(triphenylphosphonium bromide) **32** with pentafluorobenzaldyde **4** was examined as a more selective route to 1,4-bis(2,3,4,5,6-pentafluorostyryl)-2,3,5,6-tetrafluorobenzene **45**. However, the reaction was unsuccessful and no DSB derivative was obtained.

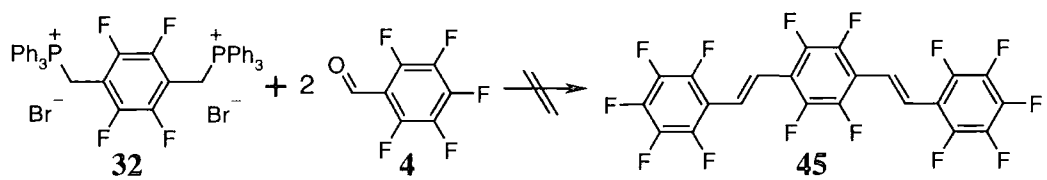

*Figure 5.3.9 Attempted Wittig reaction of compound **4** and **32**.*

The synthesis of tetrafluoroterephtalaldehyde **18** (as described in chapter 2) opened an alternative route to compound **45** (*Figure 5.3.10*). While the previous reaction required the formation of two ylides on the central benzene ring, in this approach the ylides are formed on the terminal rings. 2,3,4,5,6-(pentafluorobenzyl)triphenylphosphonium bromide **46** could be prepared by the reaction of pentafluorobenzylbromide and triphenylphosphine. The Wittig reaction

between **46** and **18** gave 1,4-bis(2,3,4,5,6-pentafluorostyryl)-2,3,5,6-tetrafluorobenzene **45** in acceptable yield (57%).

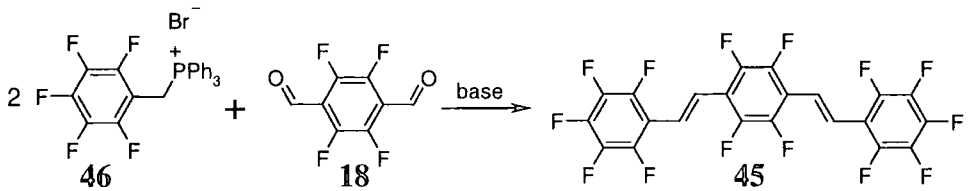

Figure 5.3.10 Synthesis of 1,4-bis(2,3,4,5,6-pentafluorostyryl)-2,3,5,6-tetrafluorobenzene.

The NMR spectra (^{1}H, ^{19}F) of compound **45** show that all double bounds have *trans*-configuration. The UV absorption spectrum of **45** in chloroform shows a maximum at 342 nm. This is slightly blue shifted with respect to the absorption maximum of DSB itself (350 nm). Such a small shift is in good agreement with results reported by Bazan *et al.*[9] These authors found that the absorption maxima of DSB derivatives with a varying number of fluorine substituents all show all very similar absorption maxima with shifts smaller than 10 nm.

Attempts were made to prepare 1:1 cocrystals of compound **45** and DSB. Yellow crystals could be obtained from an equimolar solution of the two compounds, but the crystals were unsuitable for X-ray structure analysis and only a few oval shaped reflections were observed.

However, the solubilities of compound **45** and DSB show that aggregation is occurring. The solubilities of **45** and DSB in toluene are 6.8 x 10^{-3} mol l^{-1} and 3.2 x 10^{-3} mol l^{-1}, respectively. When both are mixed in a molar ratio of 1:1 the solubility decreases to 0.28 x 10^{-3} mol l^{-1} (with respect to each component).

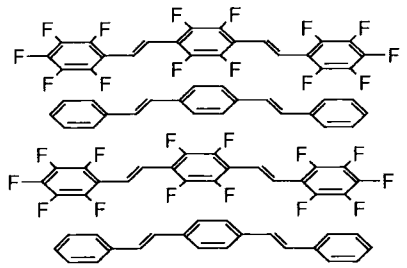

Figure 5.3.11 Proposed structure of the aggregate of **45** *and DSB.*

A possible structure for the stacking of the two compounds is shown in *Figure 5.3.11* in which DSB and the fluorinated derivative alternate. No charge transfer band was observed.

5.4 Conclusions

A self-assembling J aggregate based on aryl-fluoroaryl interactions was synthesised. The molecule contains two terminal fluorinated benzene rings and two central non-fluorinated benzene rings, all connected by vinylene bridges. The X-ray crystal structure shows the packing of the molecules in a 'brickwall' motif and 16 H···F interactions per molecule. A photochemically induced [2+2] reaction in the solid state was demonstrated.

An efficient synthetic route to the fluorinated DSB derivative 1,4-bis(2,3,4,5,6-pentafluorostyryl)-2,3,5,6-tetrafluorobenzene has been demonstrated. An equimolar mixture of this fluorinated derivative and DSB itself shows evidence for aggregation.

5.5 Experimental

5.5.1 4,4'-Dimethylstilbene (41)

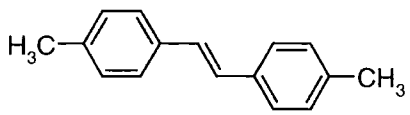

$TiCl_4$ (16.6 g, 9.6 ml, 87.4 mmol) was added to a suspension of Zn (11.4 g, 175 mmol) in THF (400 ml) at 0 °C under nitrogen. The mixture was refluxed for 1 h and cooled to room temperature. *p*-Tolualdehyde (7.1 g, 59 mmol) was then added and the mixture refluxed for 14 h. The mixture was quenched by addition of aqueous hydrochloric acid (40 ml, 2 N) and the THF was removed under reduced pressure. The product was redissolved in diethyl ether (300 ml), washed three times with water (200 ml) and dried ($MgSO_4$) yielding, after evaporation of the solvent, 4,4'-dimethylstilbene (5.9 g, 96%) as a white solid. As the melting point and the ^1H NMR spectrum were in good agreement with those reported in the literature[11] no further analysis was carried out, mp 181 °C (lit.[11,12] 180-182 °C). ^1H NMR ($CDCl_3$,

200 MHz) δ 7.42 (m, 4H, ar. C-*H*), 7.18 (m, 4H, ar. C-*H*), 7.07 (s, 2H, C*H*=C*H*), 2.39 (s, 6H, CH_3).

5.5.2 4,4'-Bis(bromomethyl)stilbene (42)

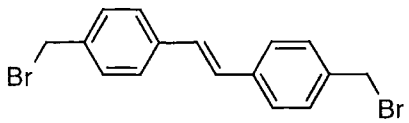

4,4'-Dimethylstilbene (6.0g, 28.8 mmol) and N-bromosuccinimide (15.0 g, 84 mmol) were dissolved in chloroform (600 ml). AIBN (0.06 g, 0.36 mmol) was added and the mixture refluxed. Two further additions of AIBN (0.06 g, 0.36 mmol) were made after 2 h and 4 h, respectively. After a total of 8 h of reflux the mixture was washed five times with water (200 ml) and dried ($MgSO_4$). The solution was concentrated to 90 ml, warmed to 65 °C and then cooled slowly to room temperature to allow crystallisation. The white crystals were recovered by filtration and the product was recrystallised once more from a hexane/ toluene mixture (1:1) yielding 4,4'-bis(bromomethyl)stilbene (3.1 g, 30%) as white crystals. As the melting point and the ^{1}H NMR spectrum were in agreement with those reported in the literature[13-15] no further analysis was carried out. mp 187 °C (lit.[14,15] 188-193 °C). ^{1}H NMR ($CDCl_3$, 200 MHz) δ 7.50 (m, 4H, ar. C-*H*), 7.39 (m, 4H, ar. C-*H*), 7.11 (s, 2H, C*H*=C*H*), 4.53 (s, 4H, CH_2Br).

5.5.3 4,4'-bis(methyltriphenylphosphonium bromide)stilbene (43)

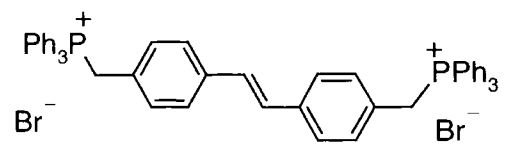

4,4'-Bis(bromomethyl)stilbene (3.1 g, 8.47 mmol) and triphenylphosphine (5.04 g, 19.2 mmol) were dissolved in DMF (35 ml) and the resulting mixture was refluxed for 4 h. The mixture was cooled to room temperature. The white precipitate was collected by filtration and washed with toluene (50 ml) and diethyl ether (50 ml) yielding 4,4'-bis(methyltriphenylphosphonium bromide)stilbene (6.64g, 88%) as a white solid. The product was used in the next step without further purification.

5.5.4 4,4'-bis(2,3,4,5,6-pentafluorostyryl)stilbene (44)

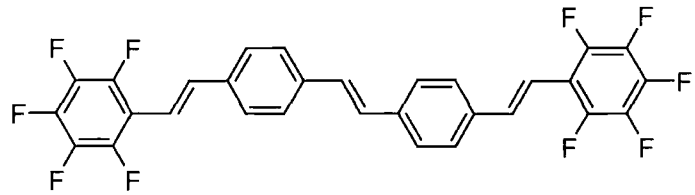

A mixture of LiCl (0.9 g) and 4,4'-bis(methyltriphenylphosphonium bromide)stilbene (6.6 g, 7.41 mmol) was dissolved in DMF (57 ml). KO^{t}Bu (14.8 ml, 14.8 mmol) was added and the mixture stirred for 2 h. Pentafluorobenzaldehyde (3.5 g, 17.8 mmol) was added and the mixture stirred at room temperature for 6 h. The reaction was quenched by addition of water (10 ml) and a yellow powder collected by filtration. The product was washed with diethyl ether (20 ml) and dried under vacuum yielding *4,4'-bis(2,3,4,5,6-pentafluorostyryl)stilbene* (2.24 g, 54%) as a yellow solid. Found C: 63.68%; H, 2.46%; M(MS, EI) 564 (M^+). Calculated for $C_{30}H_{14}F_{10}$: C, 63.84% H, 2.50%; M 564. ^{1}H NMR (TCE-d_2, 300 MHz) δ 7.57 (s, 8H, ar. C-*H*), 7.43 (d, J = 16.5 Hz, 2H, C*H*=C*H*), 7.17 (s, 2H, C*H*=C*H*), 7.00 (d, J = 16.5 Hz, 2H, C*H*=C*H*); ^{19}F NMR (C_7D_8, 188 MHz) δ -163.75 (m, 4F), -157.47 (t, J = 21 Hz, 2F), -143.81 (m, 4F) (see appendix page 155).

Crystal-preparation from solution in stilbene

A U-shaped glass tub was prepared with a pore-3-sinter in the middle (*Figure 5.5.1*). 4,4'-bis(2,3,4,5,6-pentafluorostyryl)stilbene (80 mg) was thoroughly mixed with stilbene (800 mg) and placed in one side of the glass-tube. The glass-tube was place in a high temperature oil-bath and heated to 260 °C for 10 min. The oil-bath was then cooled at a rate of 0.5 °C per minute to 170 °C and kept at 170 °C for 10 h. A small pressure of nitrogen gas was applied to the side of the glass-tube containing the mixture so that the melt was forced through the filter. The remaining crystals of 4,4'-bis(2,3,4,5,6-pentafluorostyryl)stilbene were washed out of the tube with diethyl ether and washed three times with diethyl ether. These crystals were suitable for X-ray crystal structure analysis.

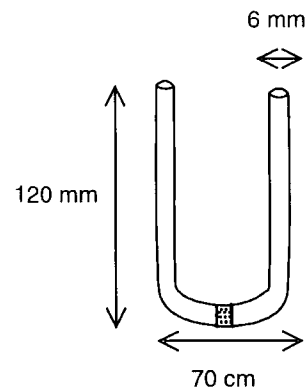

Figure 5.5.1 Sketch of a U-shaped glass tube

Crystal-preparation by sublimation

4,4'-bis(2,3,4,5,6-pentafluorostyryl)stilbene (300 mg) was placed in a Carius-tube and evacuated overnight. The tube was sealed and placed in a thermal gradient oven with a maximum temperature between 180 – 210 °C. After 7 days the tube was cooled to room temperature and opened carefully. Small crystals of 4,4'-bis(2,3,4,5,6-pentafluorostyryl)stilbene were obtained. The crystals were suitable for X-ray crystal structure analysis.

Crystallographic data for 4,4'-bis(2,3,4,5,6-pentafluorostyryl)stilbene

M_r = 564, space group P1, a = 6.0624, b = 7.4468, c = 13.0565, β = 82.972, γ = 85.693°, U = 572.378 Å^3, T = 100 K, Z = 1, μ(Mo-Kα) = 0.152 mm^{-1}, 2604 reflections measured, 2604 unique (R_{int} = 0.0797) which were used in all calculations and 1486 greater than $2\sigma(I)$ The final R(F) was 0.0853 ($I>2\sigma(I)$ data) and the $wR(F^2)$ was 0.1885 (all data). The relatively large R factor is due to the small crystals available, 0.20 x 0.10 x 0.05 mm^3. See http://www.rsc.org/suppdata/cc/b1/b100002k/ for crystallographic files in .cif formats.

[2+2] reaction of 4,4'-bis(2,3,4,5,6-pentafluorostyryl)stilbene

A thin film of 4,4'-bis(2,3,4,5,6-pentafluorostyryl)stilbene in a quarz-tube was irradiated with a UV-lamp. The colour changed from yellow to white. ^{19}F NMR (C_7D_8, 188 MHz) δ -142.11, -143.81, -156.11, -157.47, -162.98, -163.75 (see appendix page 156).

5.5.5 1,4-Distyrylbenzene

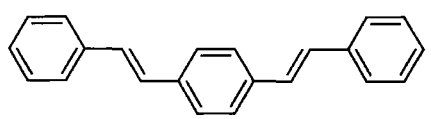

p-Xylylene-bis(triphenylphosphonium bromide) (21.0g, 26.6 mmol) and benzaldehyde (6.2 g, 58 mmol) were dissolved in dry ethanol (400 ml). Lithium ethoxide (1M, 54 ml, 54 mmol) was added and the mixture was stirred at room temperature for 4 h. Water (200 ml) was added and the product collected by filtration. The product was recrystallised from toluene (250 ml) in the presence of a trace of iodine yielding 1,4-distyrylbenzene (6.0 g, 80%) as colourless crystals. As the melting point and the ^{1}H NMR spectrum were in agreement with those reported

in the literature[9,16] no further analysis was carried out, mp 263 °C (lit.[16] 268 °C) ^{1}H NMR ($CDCl_3$, 200 MHz) δ 7.55 (m, 8H), 7.35 (m, 6H), 7.14 (s, 4H).

5.5.6 (2,3,4,5,6-Pentafluorobenzyl)triphenylphosphonium bromide (46)

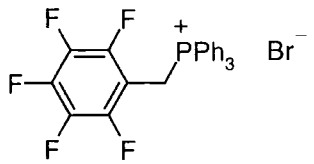

Triphenylphosphine (2.02 g, 7.7 mmol) and pentafluorobenzylbromide (2.0 g, 7.7 mmol) were dissolved in dry toluene (50 ml) and heated for 1.5 h. The mixture was allowed to cool and a white solid collected by filtration. The product was washed twice with toluene (5 ml) and dried under vacuum yielding (2,3,4,5,6-pentafluorobenzyl)triphenylphosphonium bromide (3.45 g, 85%) as a white solid. As the elemental analysis and the ^{19}F NMR spectrum were in agreement with those reported in the literature[17] no further analysis was carried out. Found C 57.37%, H 3.21% $C_{25}H_{17}BrF_5P$ requires C 57.38%, H 3.27%. ^{19}F NMR ($CDCl_3$, 188 MHz) δ -136.41 (m, 2F), -151.14 (m, 1F), -160.10 (m, 2F).

5.5.7 1,4-Bis(2,3,4,5,6-pentafluorostyryl)-2,3,5,6-tetrafluorobenzene (45)

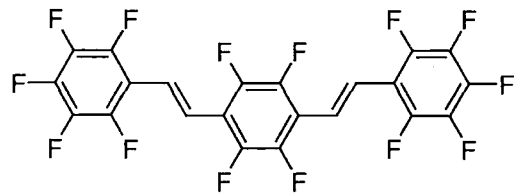

(2,3,4,5,6-Pentafluorobenzyl)triphenylphosphonium bromide (1.2 g, 2.3 mmol) and LiCl (0.2 g) were dissolved in DMF (10 ml). KO^{t}Bu (1 M, 2.3 ml, 2.3 mmol) was added. After stirring for 3.5 h tetrafluoroterephtalaldehyde (0.24 g, 1.15 mmol) was added. The mixture was stirred for further 15 h at room temperature and quenched by addition of aqueous hydrochloric acid (2 M, 2 ml). All solvents were removed under reduced pressure and the product redissolved in chloroform (200 ml). The mixture was washed with aqueous hydrochloric acid (2 M, 100 ml) and the aqueous layer extracted with chloroform (100 ml). The combined organic fractions were washed three times with water (100 ml) and dried ($MgSO_4$). The $MgSO_4$ was rinsed with toluene (30 ml). The solvents were removed under reduced pressure. The

product was purified by column chromatography (silica gel, toluene: hexane 1:20) yielding *1,4-bis(2,3,4,5,6-pentafluorostyryl)-2,3,5,6-tetrafluorobenzene* (0.35 g, 57%) as a light yellow powder. Column chromatography with hexane only (a large amount of solvent (2 L) was required) gave a white powder, mp 190-192 °C. Found C, 50.28%; H, 1.09%; M(MS, EI) 534 (M^+). Calculated for $C_{22}H_4F_{14}$: C, 49.46% H, 0.75%; M 534. ^{1}H NMR (C_7D_8, 300 MHz) δ 7.20 (s, 4H, C*H*=C*H*); ^{19}F NMR (C_7D_8, 188 MHz) δ -142.95 (m, 4F), -143.93 (s, 4F), -154.70 (m, 2F), 162.96 (m, 4F) (see appendix page 157).

5.6 References

1. Lunedei, E.; Moretti, P.; Murgia, M.; Muccini, M.; Biscarini, F.; Taliani, C. *Synth. Met.* **1999**, *101*, 592.
2. van Hutten, P.; Wildeman, J.; Meetsma, A.; Hadziioannou, G. *J. Am. Chem. Soc.* **1999**, *121*, 5910.
3. Patrick, C. R.; Prosser, G. S. *Nature* **1960**, 1021.
4. Williams, J. H. *Acc. Chem. Res.* **1993**, *26*, 593.
5. Lorenzo, S.; Lewis, G. R.; Dance, I. *New. J. Chem.* **2000**, *24*, 295.
6. Coates, G. W.; Dunn, A. R.; Henling, L. M.; Ziller, J. W.; Lobkovsky, E. B.; Grubbs, R. H. *J. Am. Chem. Soc.* **1998**, *120*, 3641.
7. Jelley, E. E. *Nature* **1936**, 1009.
8. Vishweshwar, P.; Nangia, A.; Lynch, V. M. *Acta Cryst.* **2000**, *C56*, 1512.
9. Renak, M. L.; Bartholomew, G. P.; Wang, S.; Ricatto, P.; Lachicotte, R. J.; Bazan, G. C. *J. Am. Chem. Soc.* **1999**, *121*, 7787.
10. Brooke, G. M.; Mawson, S. D. *J. Fluorine Chem.* **1990**, *50*, 111.
11. Traylor, T. G.; Stewart, K. J. *J. Am. Chem. Soc.* **1986**, *108*, 6977.
12. Westman, G.; Wennerstorm, O.; Raston, I. *Tetrahedron* **1993**, *49*, 483.
13. Younes, S.; Tchani, G.; Baziard-Mouysset, G.; Stigliani, J. L.; Payard, M. *Eur. J. Med. Chem.* **1994**, *29*, 87.
14. Drefahl, G.; Ploetner, G. *Chem. Ber.* **1958**, *91*, 1274.
15. Brown, T. M.; Carruthers, W.; Pellatt, M. G. *J. Chem. Soc. Perkin Trans. 1* **1982**, 483.
16. Campbell, T. W.; McDonald, R. N. *J. Org. Chem.* **1959**, *24*, 1246.
17. Wheaton, G. A.; Burton, D. J. *J. Org. Chem.* **1983**, *48*, 917.

6 Overall Conclusions and Proposal for Future Work

6.1 Conclusions

Several synthetic routes to fluorinated conjugated polymers were investigated. The McMurry reaction was found unsuitable for this aim since it led to side reactions and defects in the case of fluorinated aromatic aldehydes and ketones. The Horner Wittig reaction was used successfully to prepare a fluorinated block copolymer, which consisted of alternating oligo(ethylene oxide) units and fluorinated distyrylbenzene units. The polymer was fractionated and the high molecular weight fraction showed a degree of polymerisation of 17. All double bonds in the conjugated unit had a *trans*-configuration. To our knowledge this is the first example of a poly(*p*-phenylene vinylene) derivative in which all four available aromatic positions are substituted with fluorine atoms.

In order to study the influence of fluorine substituents on conjugated polymers the non-fluorinated equivalent was synthesised. The Wittig reaction was used as polycondensation method. 50% of the double bonds in the distyrylbenzene unit had a *cis*-configuration and 50% had a *trans*-configuration. The degree of polymerisation was 10. Both polymers were soluble in chloroform and free-standing films could be cast from solution.

The electron affinity and the ionisation potential in both polymers were determined by a combination of cyclic voltammetry, UV photoelectron spectroscopy and UV-absorption spectroscopy. The substitution of hydrogen by fluorine in the block copolymer increased the electron affinity and the ionisation potential by 0.85 eV. However, the optical band-gap was the same in both polymers (3.0 eV). The photoluminescence quantum efficiency of the fluorinated and the non-fluorinated block copolymers were 17% and 34%, respectively.

Light emitting diodes based on both devices were prepared. Indium tin oxide was used as the anode in these devices and aluminium or calcium was used as the cathode. The fluorinated block copolymer showed very poor characteristics as emissive layer in light emitting devices. However, the polymer proved to be a good electron-carrier due to its high electron affinity.

Single layer LEDs based on the non-fluorinated block copolymer exhibited luminances over 2000 cd/m^2. The luminescence efficiency was as high as 0.5 cd/A, corresponding to an internal quantum efficiency of 1.1%. The onset of luminescence was at 6.5 V. The polymer emitted in the yellow-green region of the visible light. A light emitting cell based on a complex of this polymer with lithium triflate showed a reduced threshold for luminescence.

In a further project a self-assembling J aggregate based on aryl-fluoroaryl interactions was synthesised. The molecule contained two terminal fluorinated benzene rings and two central non-fluorinated benzene rings, all connected by vinylene bridges. This oligo(p-phenylene vinylene) aggregated in a 'brickwall' motif as shown by X-ray crystal structure analysis. 16 H···F interactions per molecule were observed in the crystal structure. A photochemically induced [2+2] reaction in the solid state was demonstrated.

6.2 Future Work

Several aspects of this work deserve further investigation. The preparation of non-fluorinated block copolymers with varying content of *cis*- and *trans*-double bonds is desirable in order to investigate the effect of the conformation on the optical and electronic properties. The effect of such conformational changes on the photoluminescence and electroluminescence efficiency is of particular interest. Such polymers could be prepared by isomerisation of the described block copolymer or by new synthetic routes (e.g. Heck reaction).

Some further work on light emitting cells is required in order to increase the stability of the devices. Since demixing of the polymer and lithium triflate occurred under the concentration used, whether or not lower concentrations of lithium triflate lead to increased stability and a further decrease in turn-on voltage should be examined.

The organisation in the fluorinated block copolymers should be further investigated. X-ray diffraction might show the degree of crystallinity in the polymer.

Finally, the optical properties of the oligo(*p*-phenylene vinylene) derivative with two fluorinated terminal aromatic ring need to be investigated. A thin film of the

material needs to be prepared in which the molecules aggregate in the 'brickwall' motif. A narrow and intense absorption and emission is expected for a J aggregate.

Appendix

Determination of the Photoluminescence Quantum Efficiency

The quantum efficiency η is the ratio of the number of photons emitted and the number of photons absorbed.[#] Three different experiments are used to determine the photoluminescence. In the first experiment the integrating sphere is empty. In the second experiment the sample is place in the sphere and the laser beam is aimed at the wall of the sphere. In the third experiment the laser is aimed at the sample. In each experiment the intensity of light at the excitation wavelength is measured (L_a, L_b, L_c). Also, in the second and third experiment the intensities of the emitted light are determined (P_b, P_c).

When a photon hits the sample it can be absorbed, transmitted or reflected. The absorption coefficient A is the ratio of the number of photons that are absorbed by the sample to the total number of photons hitting the sample. In the case of experiment three the intensity L_c is decreased relative to the intensity in experiment two L_b due to the absorption by the sample. The absorption coefficient can therefore be calculated in the following way:

$$L_c = L_b (1 - A)$$

And therefore:

$$A = 1 - L_c / L_b$$

The total number of photons that hit the detector in experiment three is given by $P_c + L_c$. Two parts contribute to this: The first part is the number of photons that are emitted from the sample, which is the product of the quantum efficiency, the intensity of the incident beam and the absorption coefficient. $\eta L_a A$. The second part is due to the light that is reflected or transmitted by the sample. This part can be calculated by using the intensities measured in experiment two since the beam is not aimed at the sample in this case $(1\text{-}A)(L_b + P_b)$

and therefore:

$$L_c + P_c = (1\text{-}A)(L_b + P_b) + \eta L_a A.$$

which can be rearranged to:

$$L_c + P_c = L_c + (1\text{-}A)\, P_b + \eta L_a A.$$

$$\eta = [P_c - (1\text{-}A)\, P_b] / L_a A$$

[#] de Mello, J.C; Wittman, H. F; Friend, R. H. *Advanced Materials* 9, **1997**, 230

9-Pentafluorophenyl-10-phenyl-1,2,3,4-tetraphenylpenanthrene (**2**)

^{1}H NMR spectrum

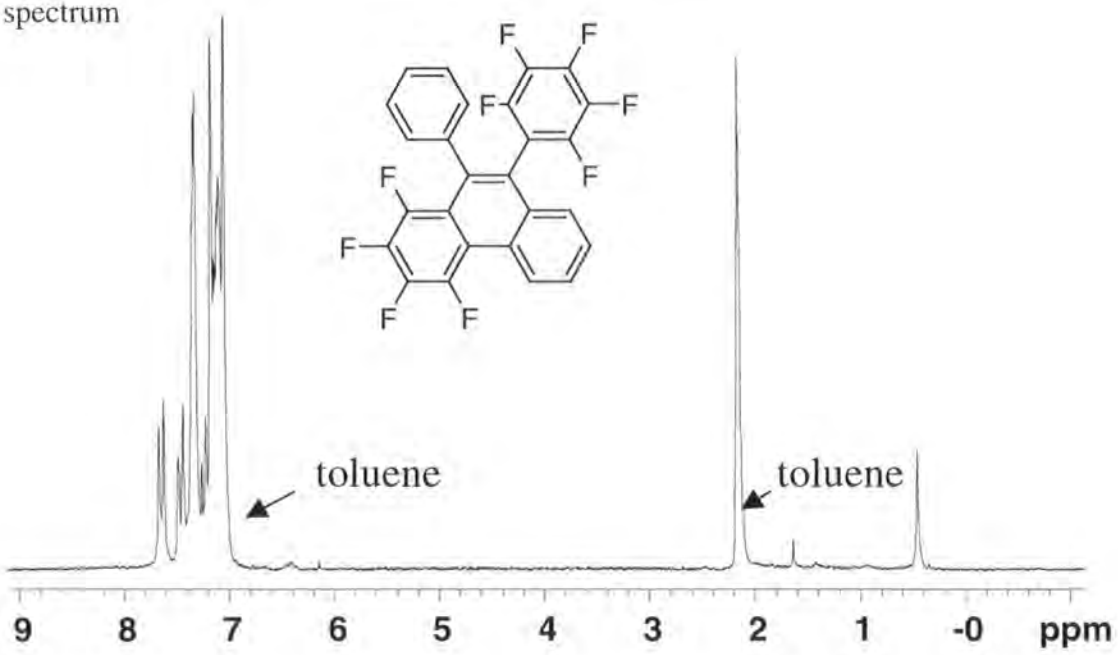

^{13}C NMR spectrum (^{1}H decoupled)

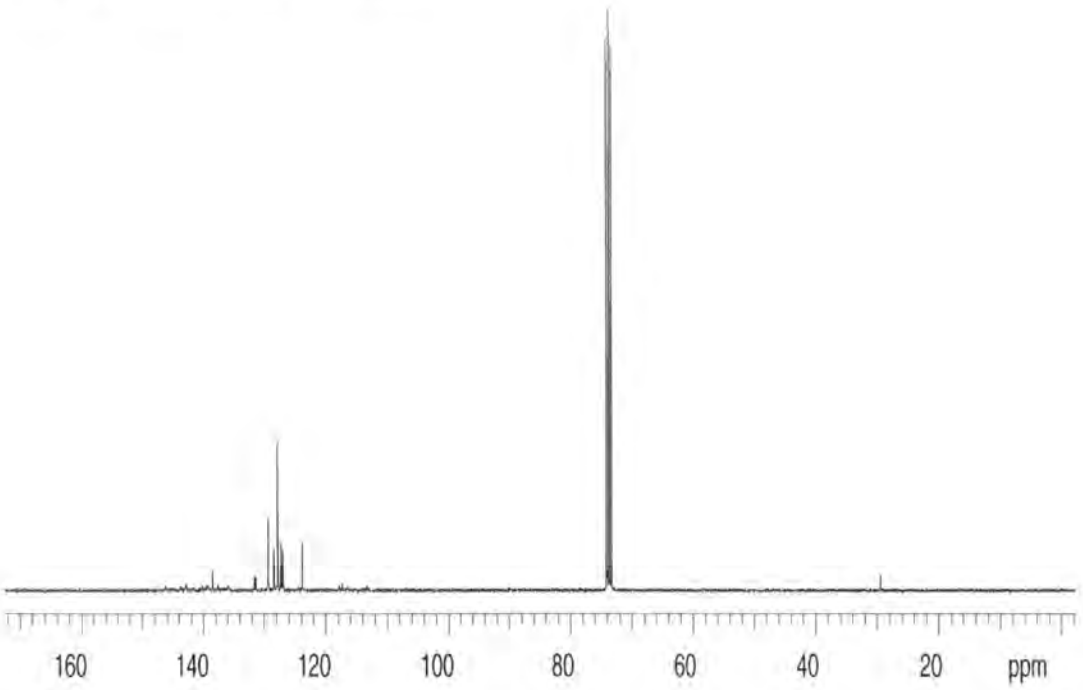

9-Pentafluorophenyl-10-phenyl-1,2,3,4-tetraphenylpenanthrene (**2**) (cont.)

^{13}C NMR spectrum (^{19}F decoupled)

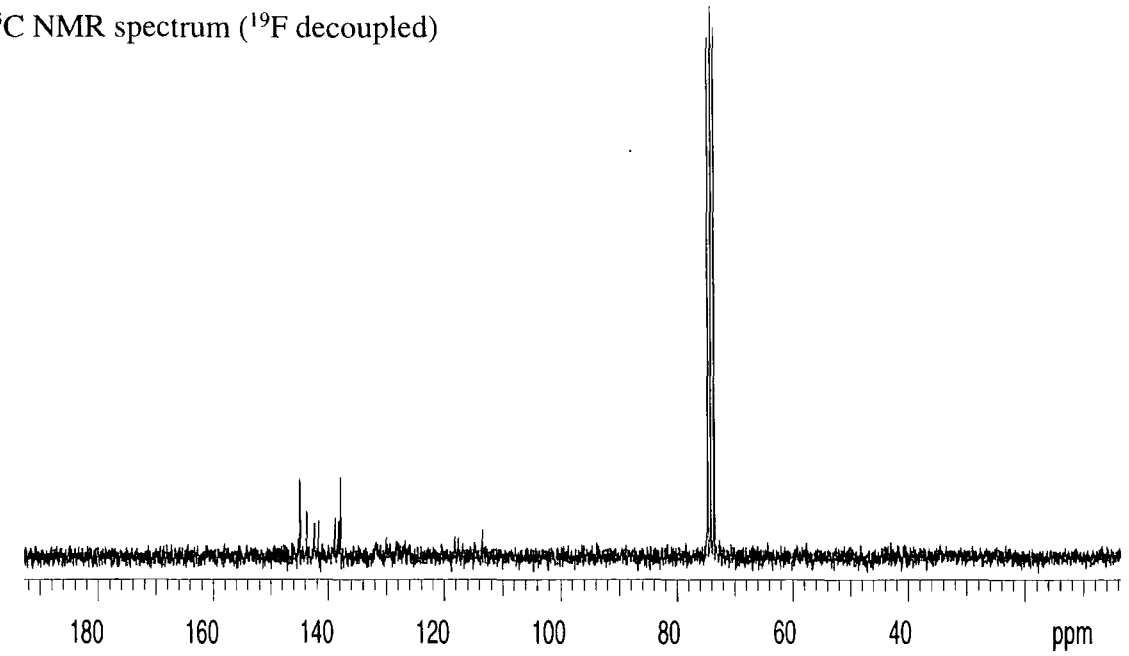

^{19}F NMR spectrum

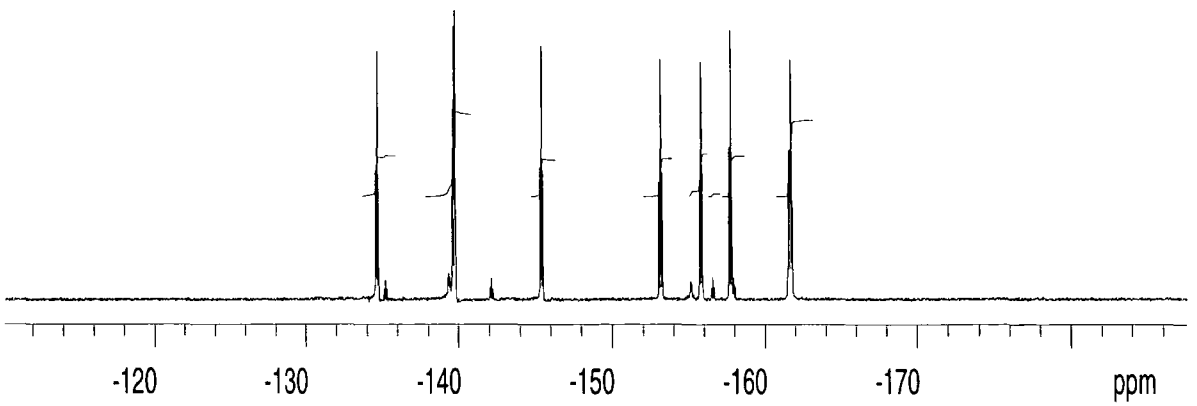

1,2-Diphenyl-1-pentafluorophenyl-2-(2,3,4,5-tetrafluorophenyl)ethene
(mixed with pentafluorobenzophenone)

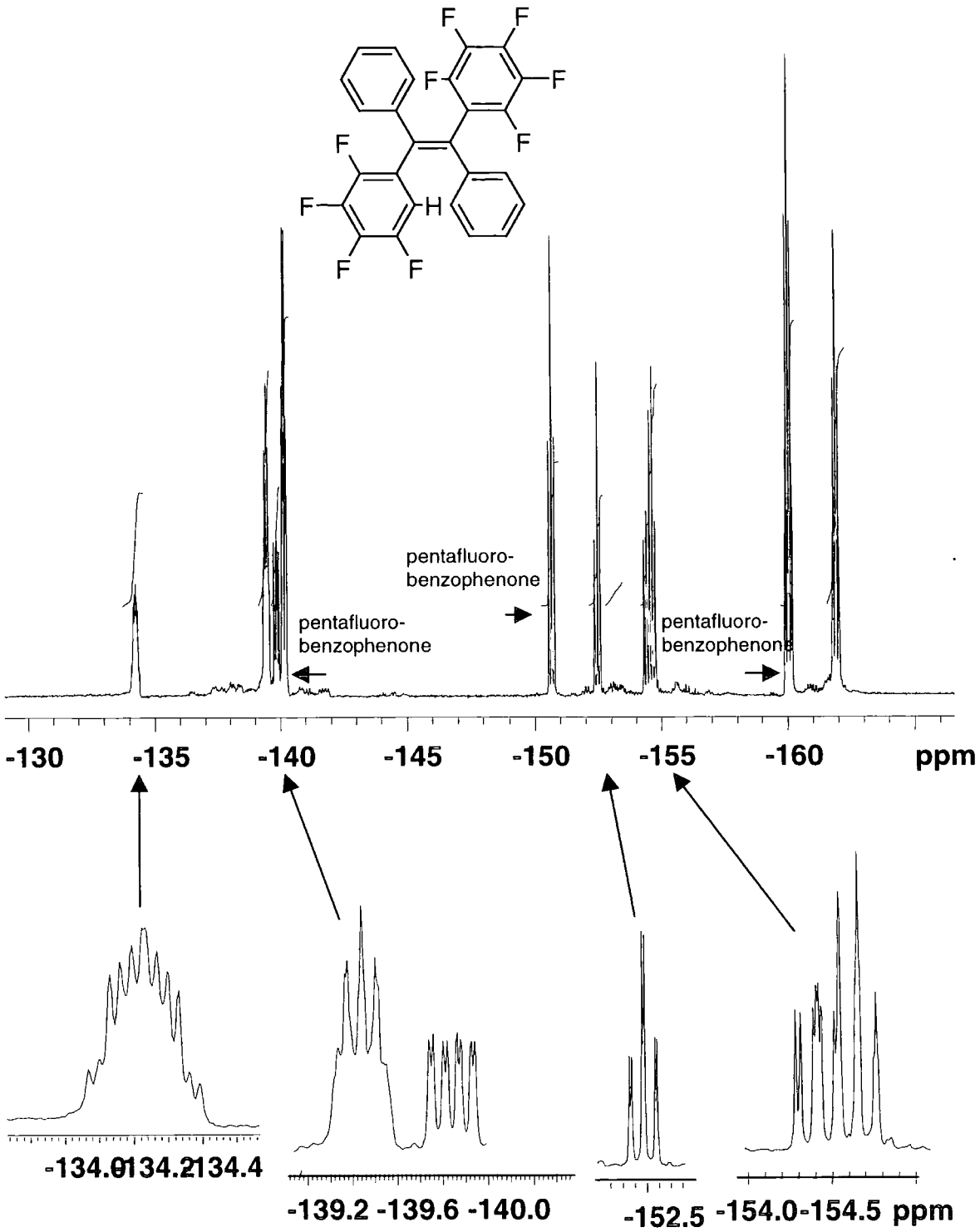

GC-MS results for reaction 2.4.2 showing
9-pentafluorophenyl-10-phenyl-1,2,3,4-tetraphenylpenanthrene (2) and
1,2-diphenyl-1-pentafluorophenyl-2-(2,3,4,5-tetrafluorophenyl)ethene

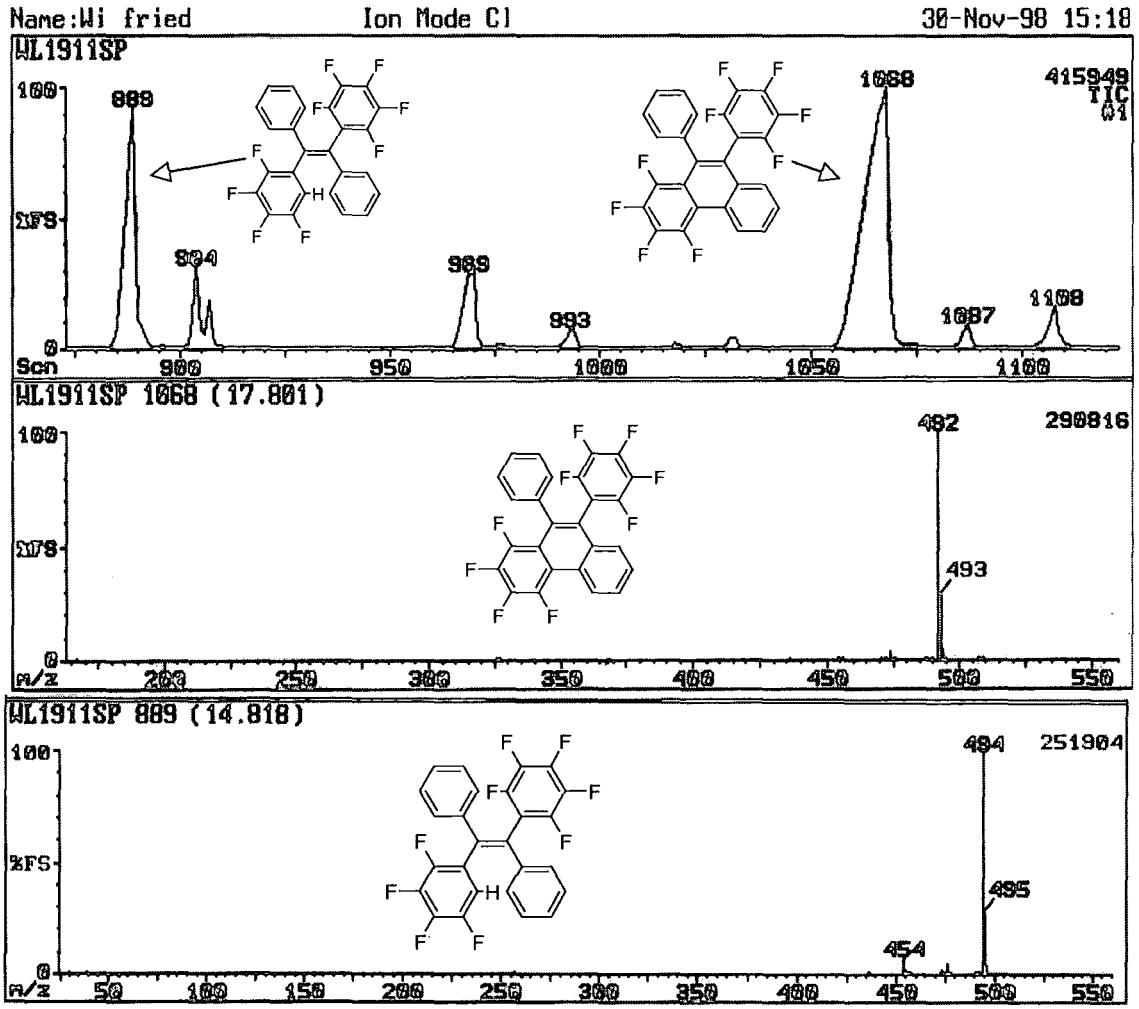

1,17-Bis(diethoxy-4-methly-2,3,5,6-tetrafluorophenyloxy) - 3,6,9,12,15-pentaoxaheptadecane (**10**)

^{1}H NMR spectrum

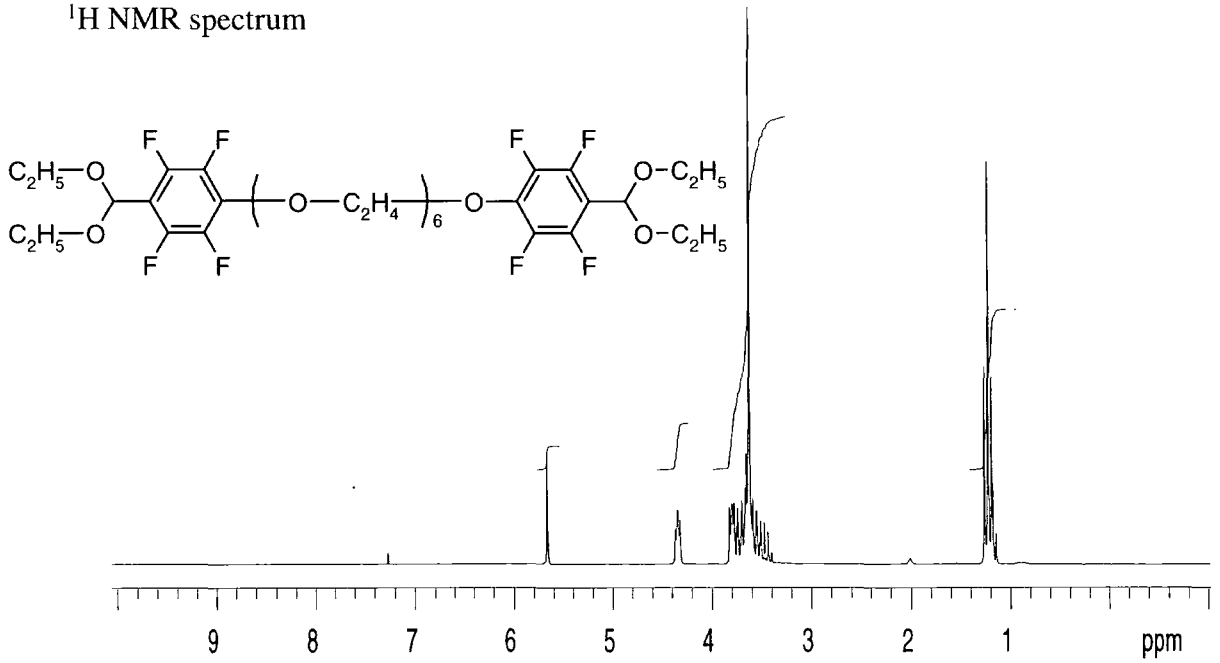

^{13}C NMR spectrum

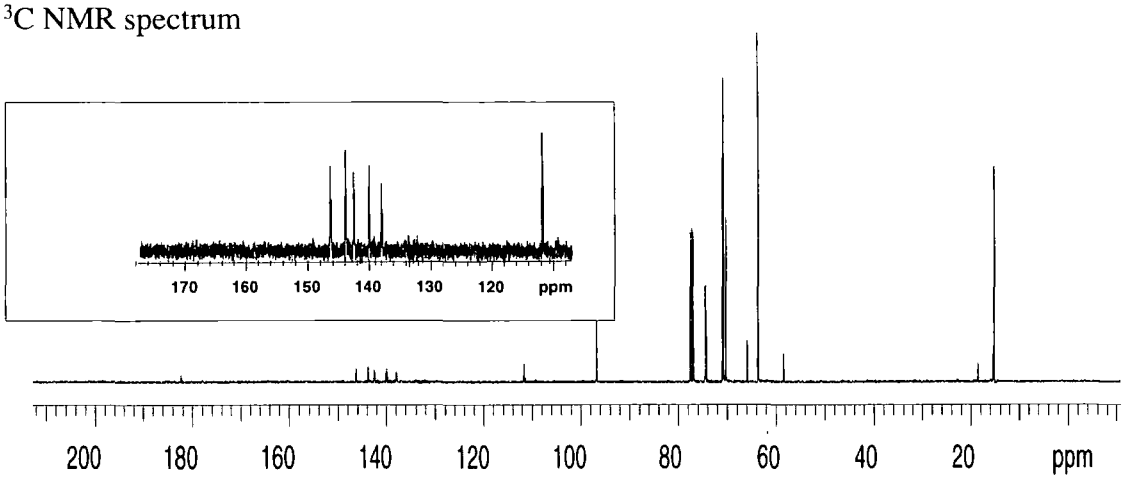

^{19}F NMR spectrum

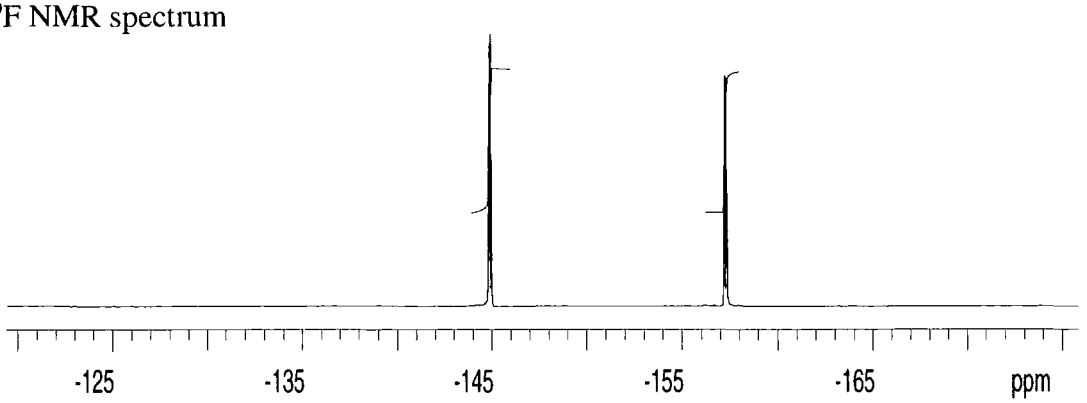

1,3-Bis(diethoxy-4-methly-2,3,5,6-tetrafluorophenyloxy)-2,2-dimethylpopane (11)

^{1}H NMR spectrum

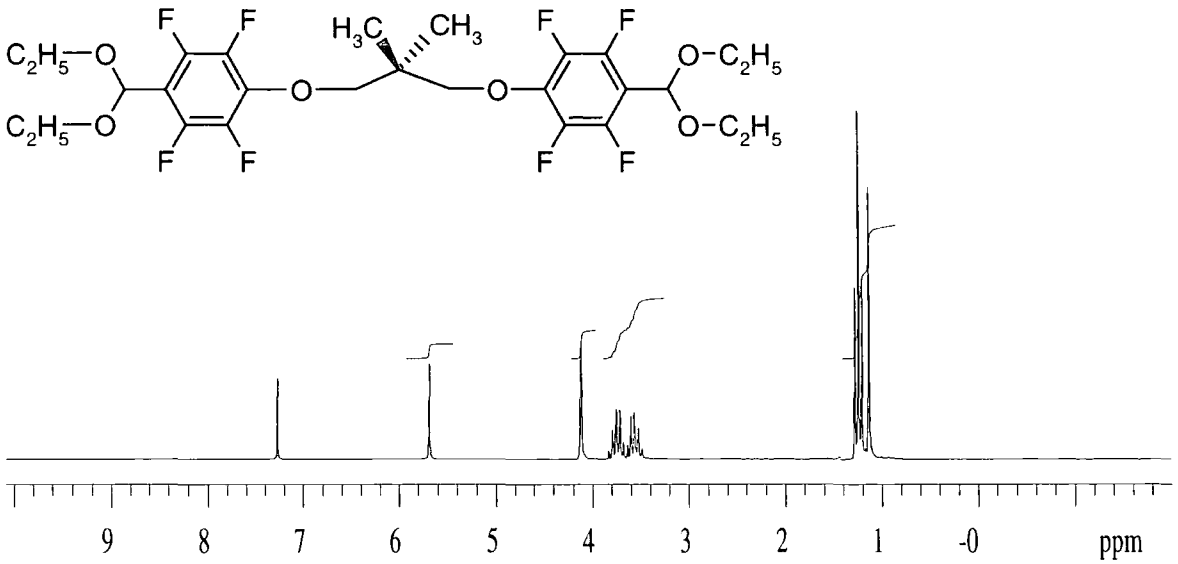

^{13}C NMR spectrum

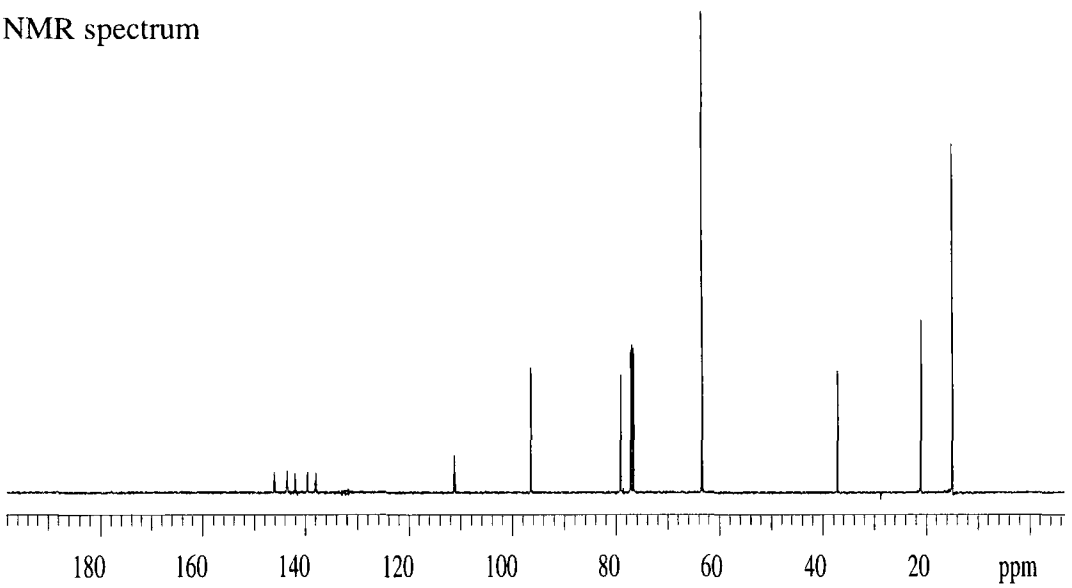

^{19}F NMR spectrum

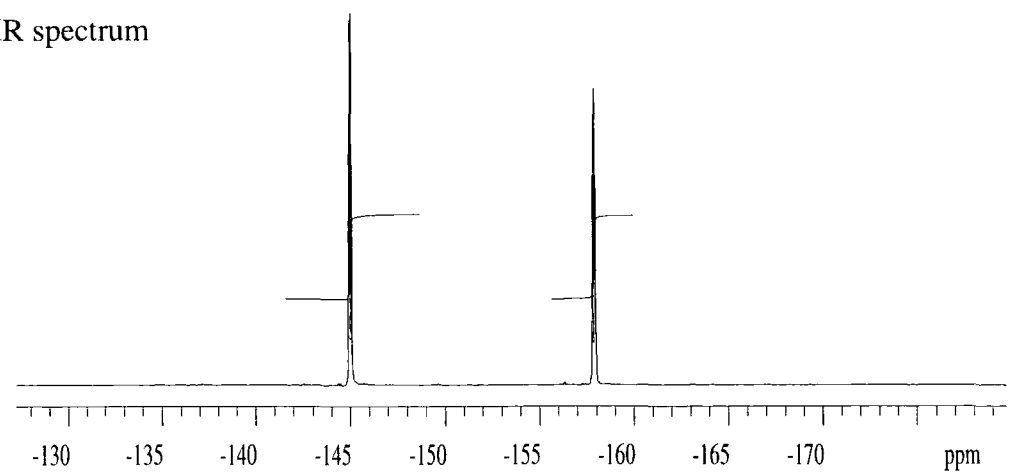

1,3-Bis(diethoxy-4-methly-2,3,5,6-tetrafluorophenyloxy)-2-ethylhexane (12)

^{1}H NMR spectrum

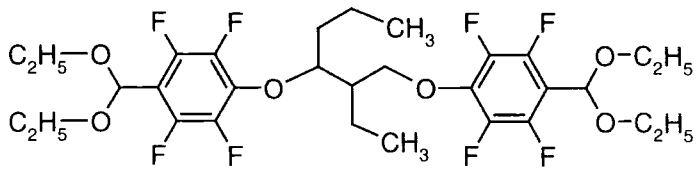

^{13}C NMR spectrum

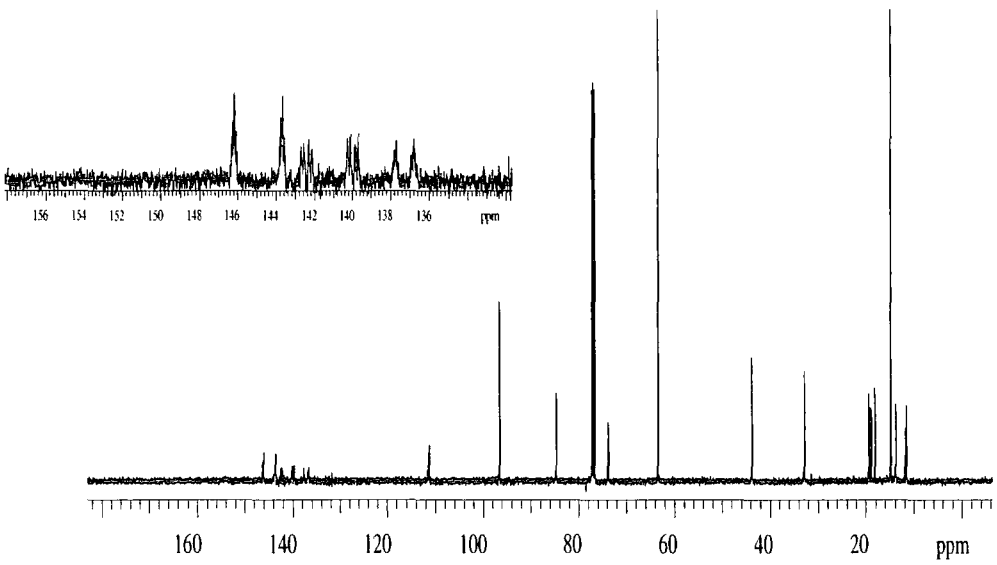

^{19}F NMR spectrum

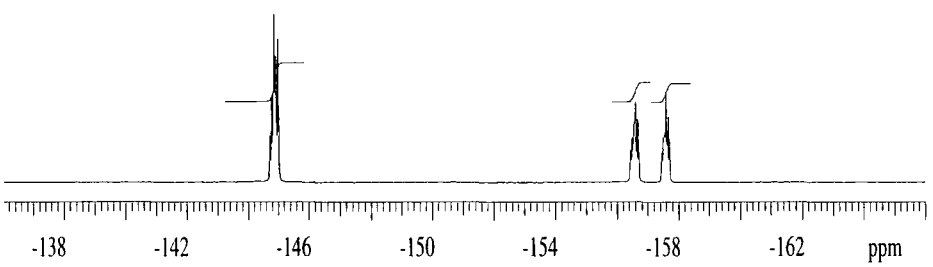

11,17-Bis(4-formyl-2,3,5,6-tetrafluorophenyloxy) -3,6,9,12,15-pentaoxaheptadecane (**13**)

^{1}H NMR spectrum

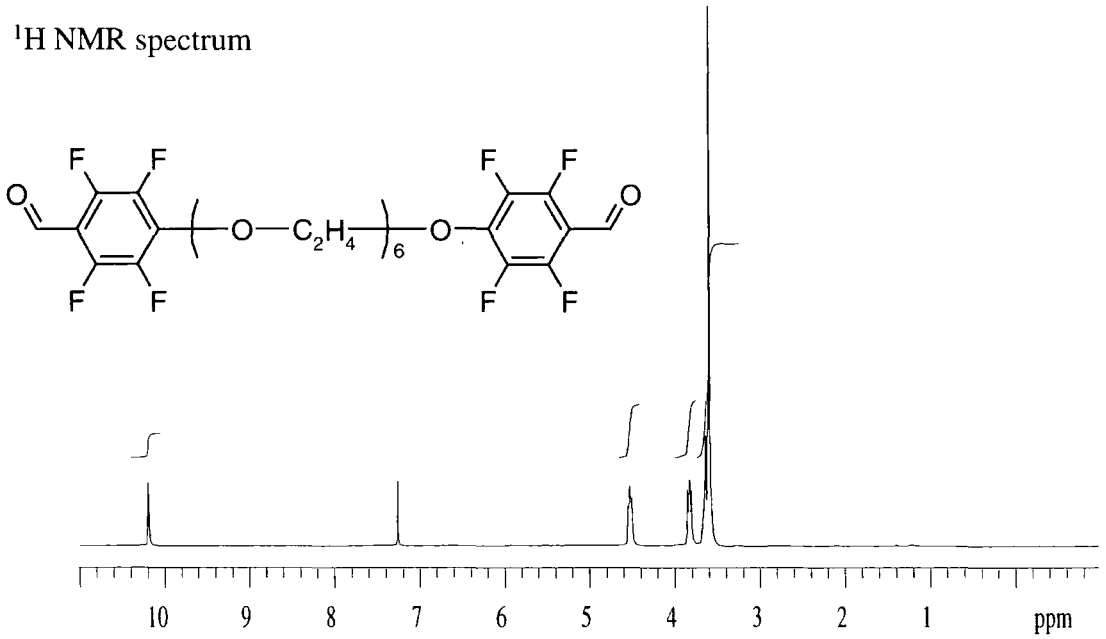

^{13}C NMR spectrum

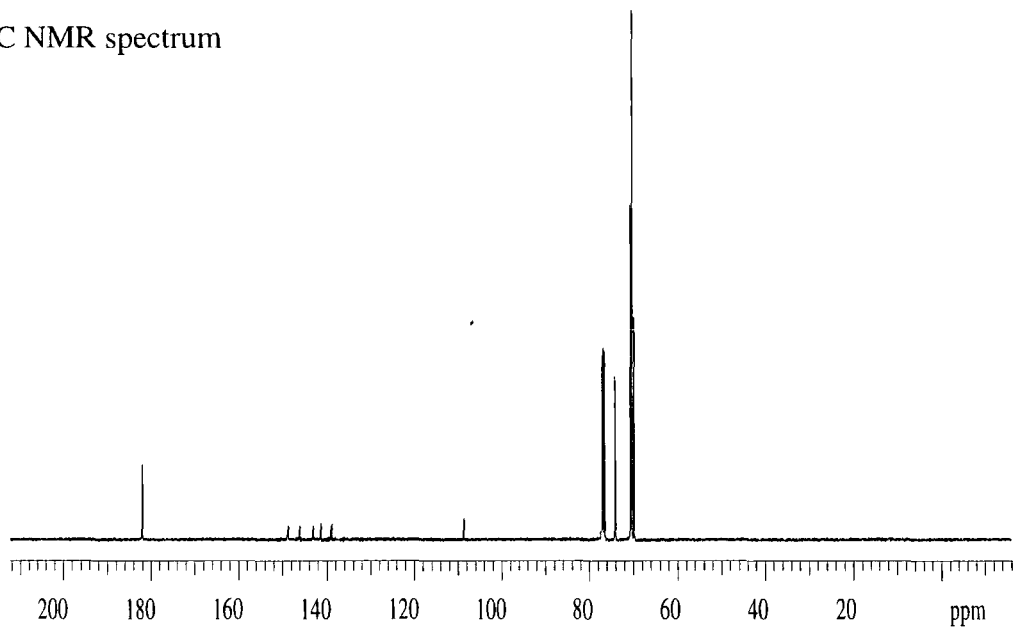

^{19}F NMR spectrum

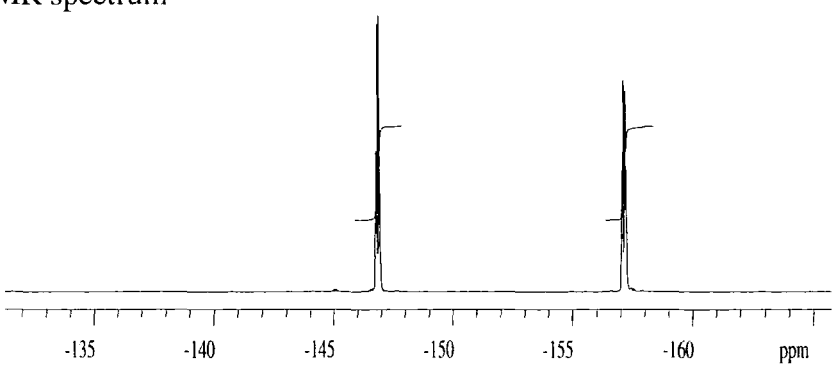

1,3-Bis (4-formyl-2,3,5,6-tetrafluorophenyloxy)- 2,2-dimethylpopane (**14**)

^{1}H NMR spectrum

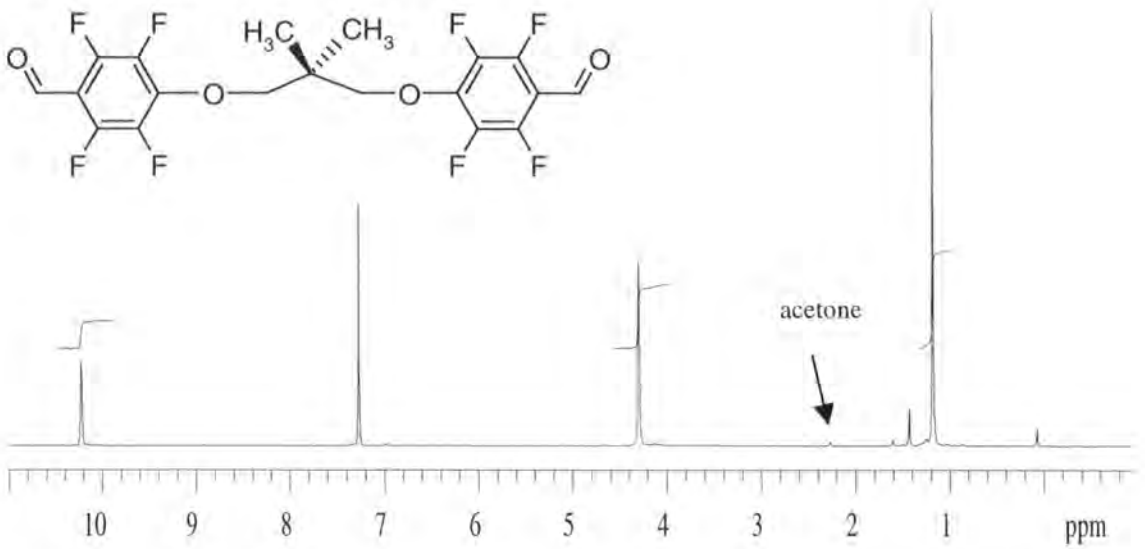

^{13}C NMR spectrum

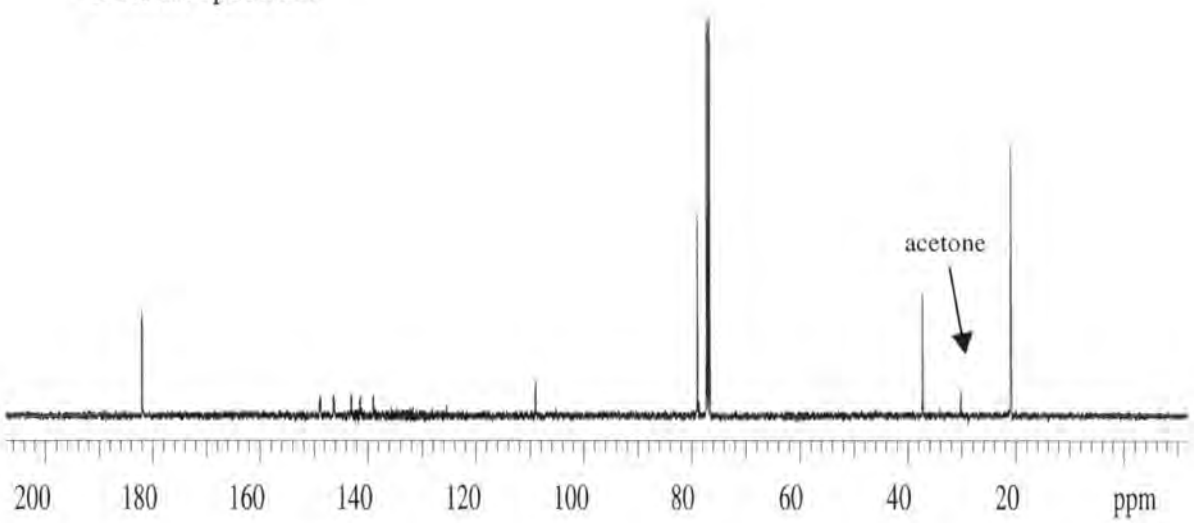

^{19}F NMR spectrum

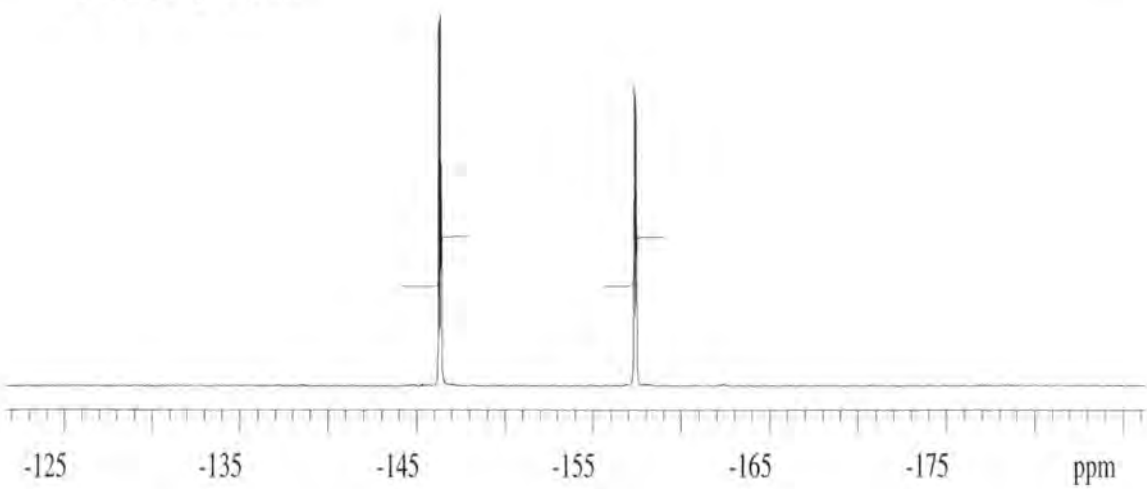

1,3-Bis(4-formyl-2,3,5,6-tetrafluorophenyloxy)-2-ethylhexane (15)

^{1}H NMR spectrum

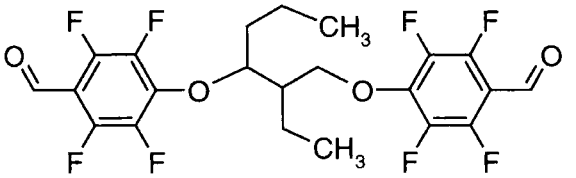

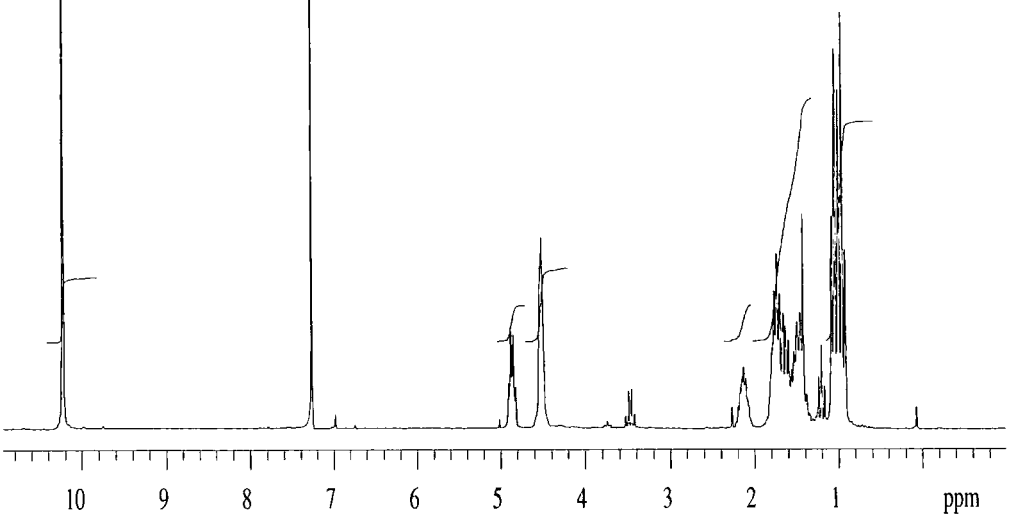

^{13}C NMR spectrum

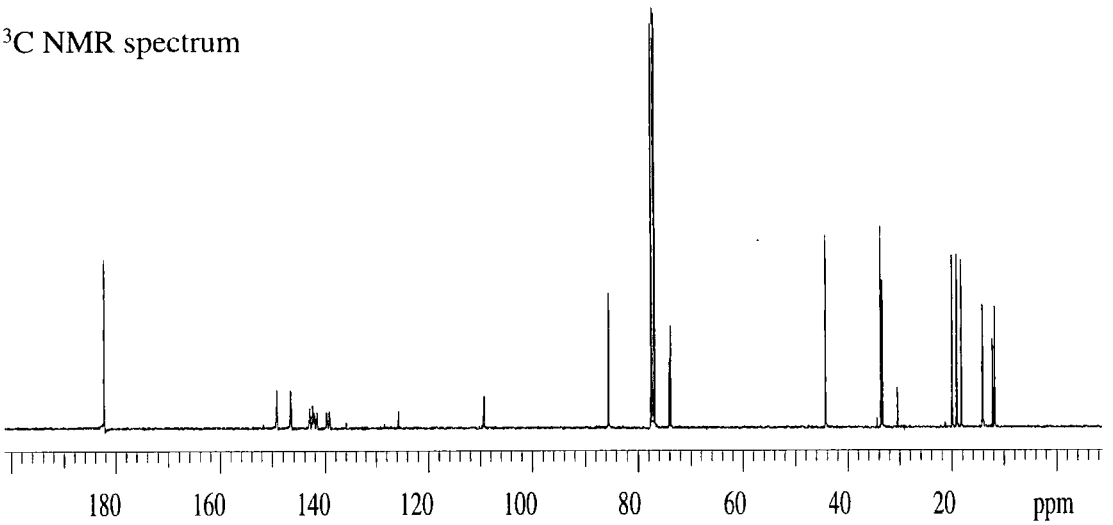

^{19}F NMR spectrum

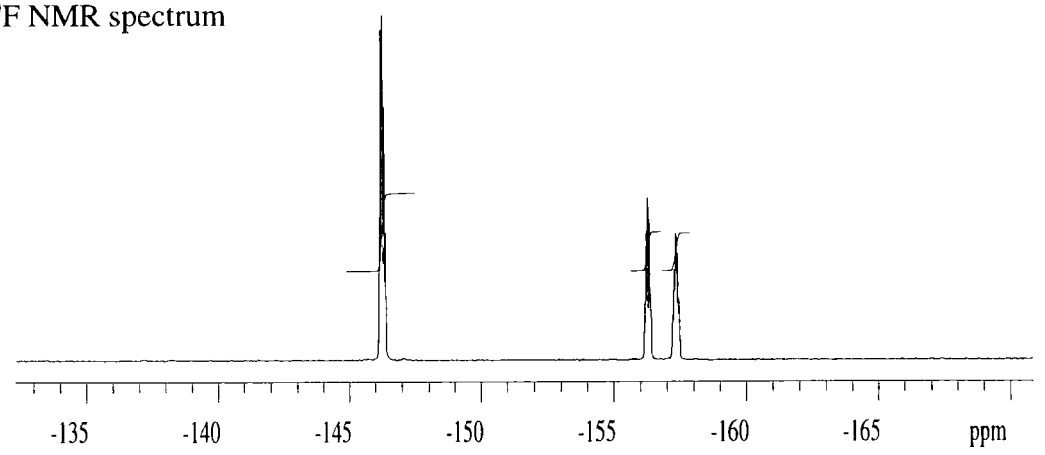

2,3,5,6-Tetrafluoroterephtalaldehyde tetra-acetate (17)

^{1}H NMR spectrum

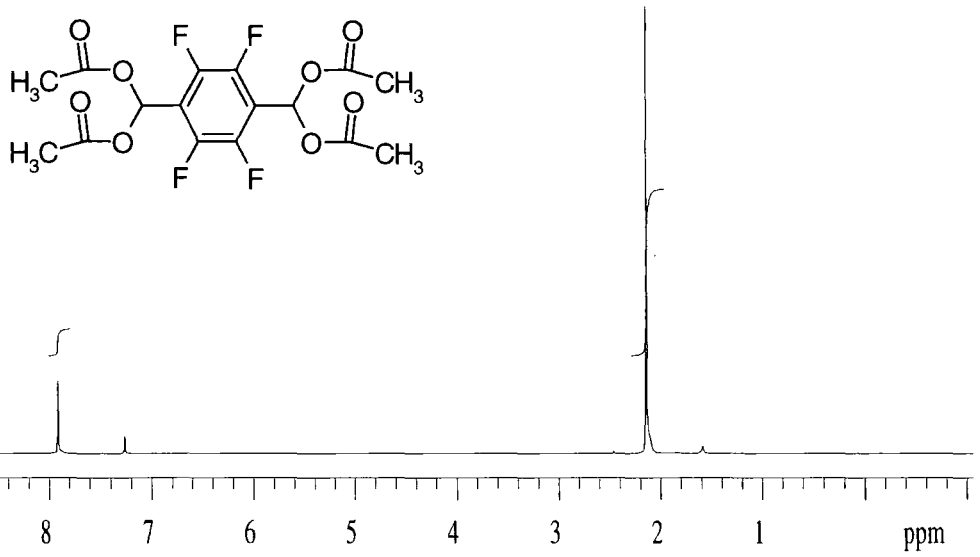

^{13}C NMR spectrum

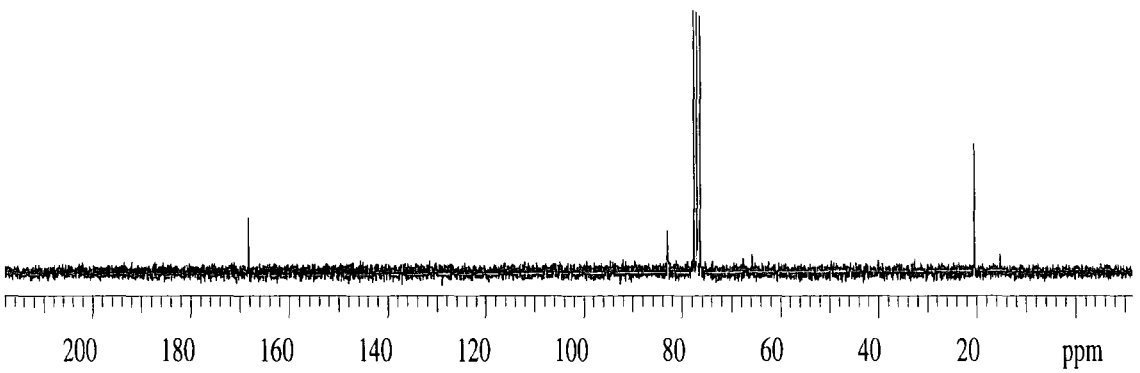

^{19}F NMR spectrum

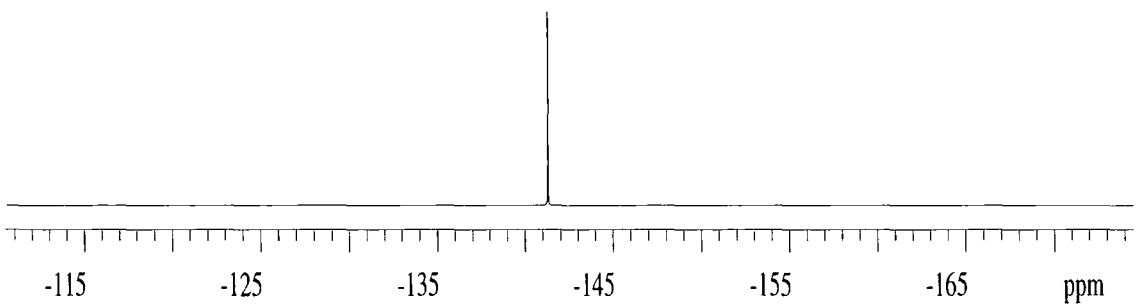

2,3,5,6-Tetrafluoroterephtalaldehyde (**18**)

^{1}H NMR spectrum

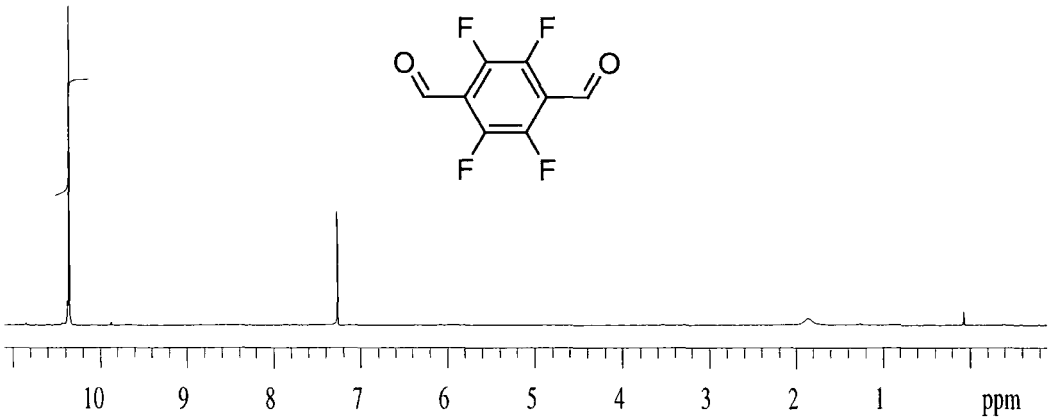

^{13}C NMR spectrum

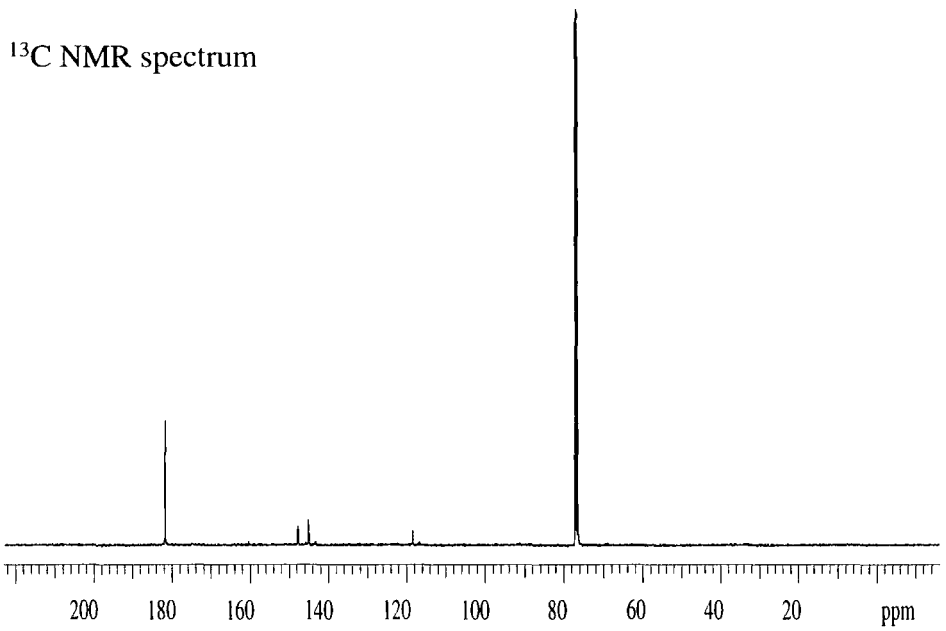

^{19}F NMR spectrum

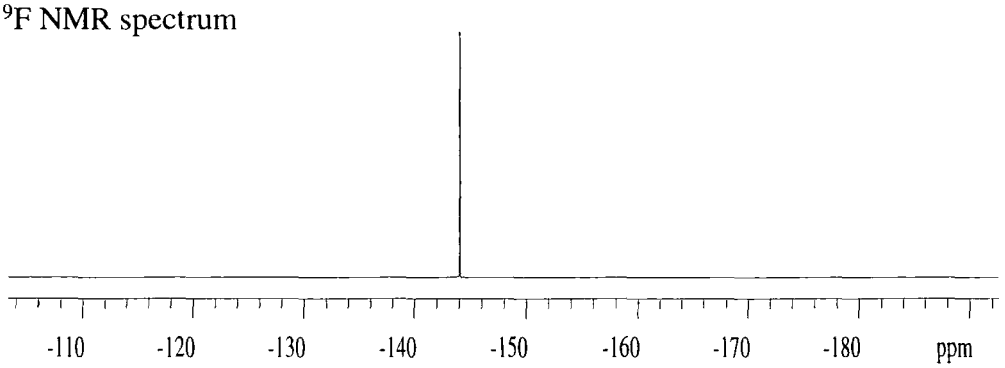

1,4-Bis(dibromomethyl)-2,3,5,6-tetrafluorobenzene (19)

^{1}H NMR spectrum

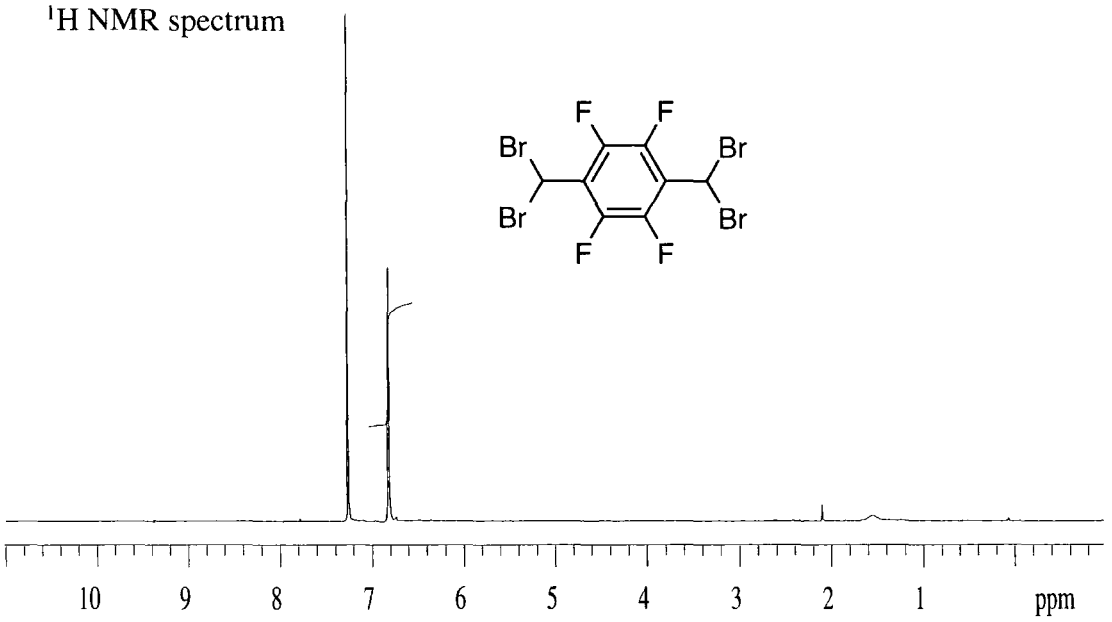

^{13}C NMR spectrum

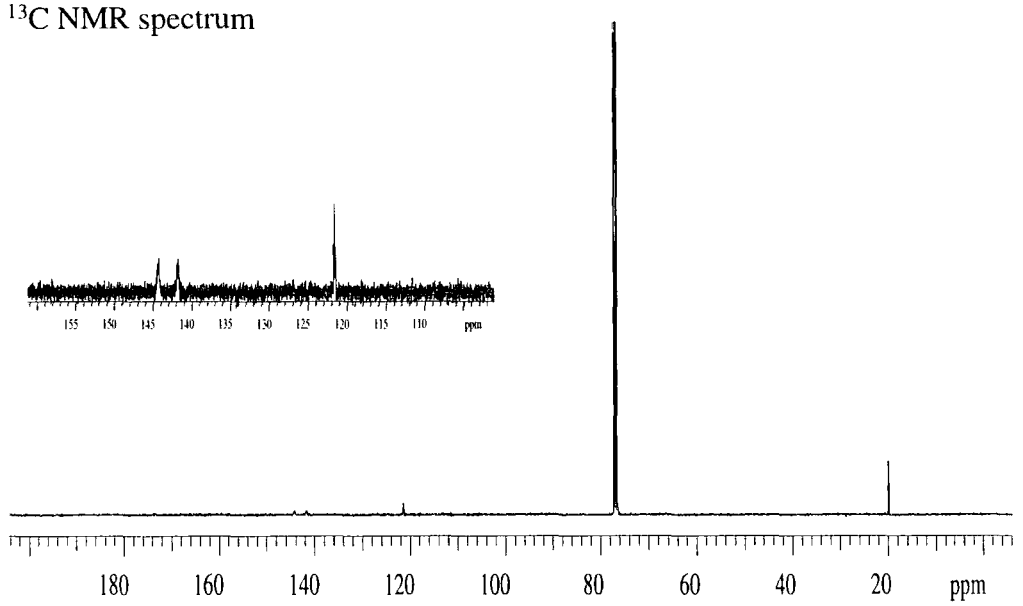

^{19}F NMR spectrum

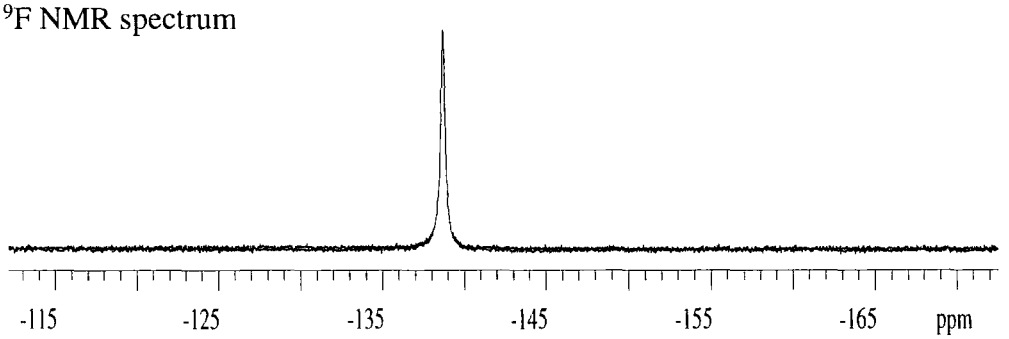

5,6,28,29,30,31,32,33-Octafluoro-8,11,14,17,20,23,26-heptaoxa-tricyclo[22.2.2.2^{4,7}]tritriaconta-1(30),2,4(33),5,7(32),27(31),25-heptaene (**20**)

^{1}H NMR spectrum

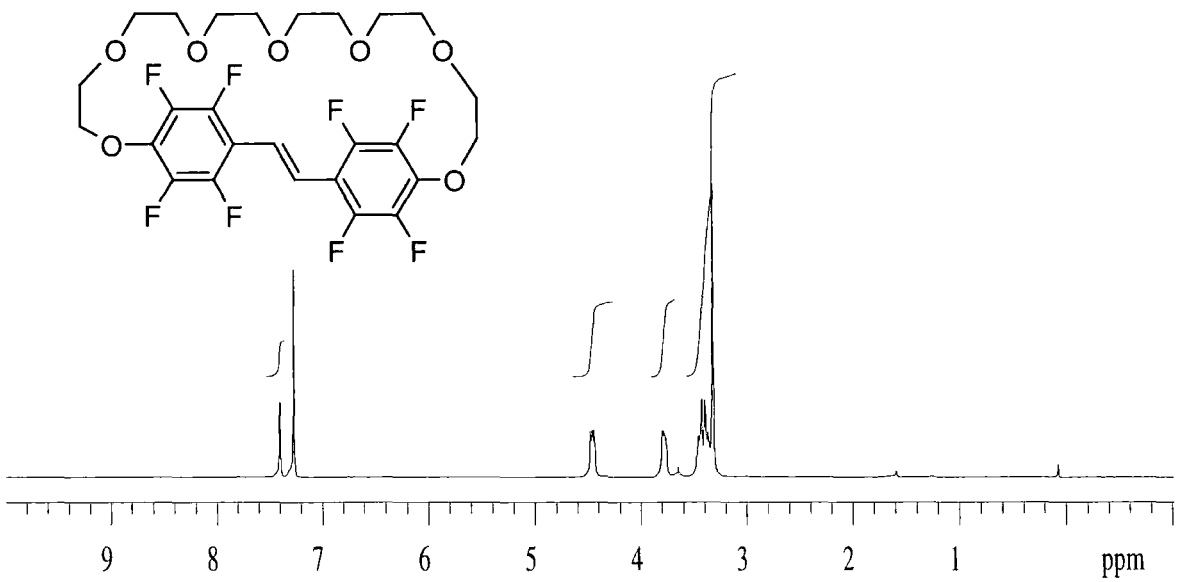

^{13}C NMR spectrum

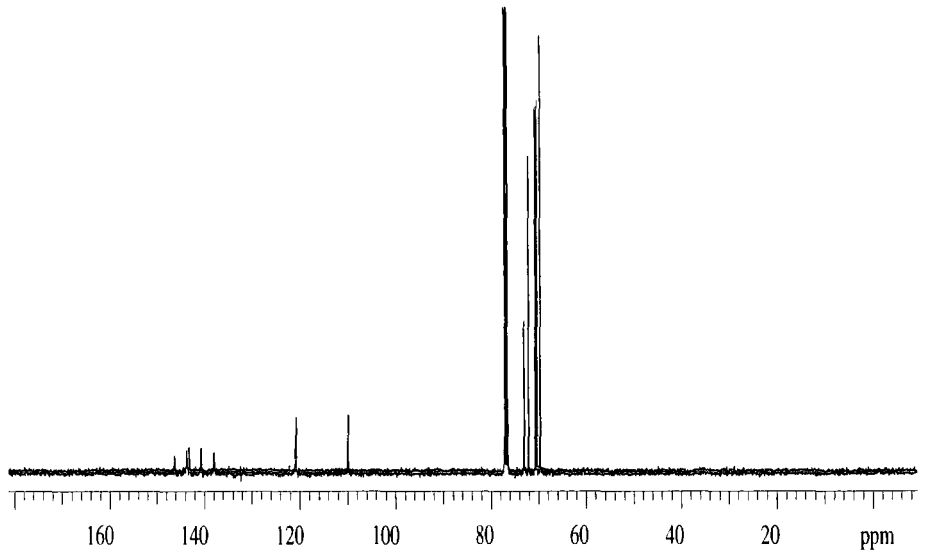

^{19}F NMR spectrum

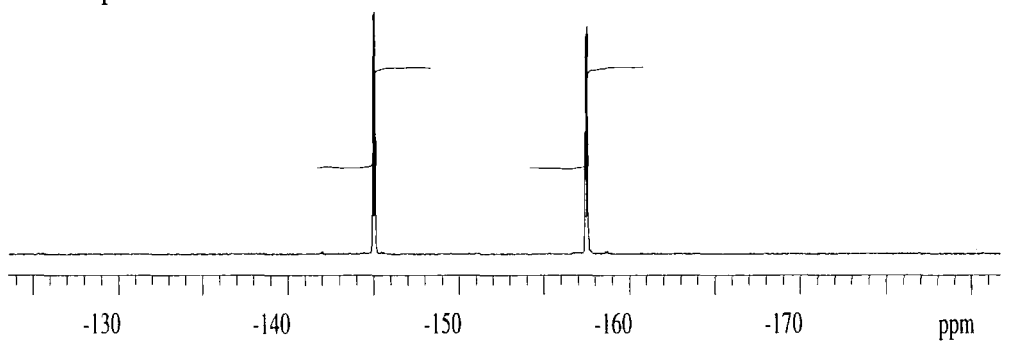

Polymerisation via the McMurry reaction

^{1}H NMR spectrum

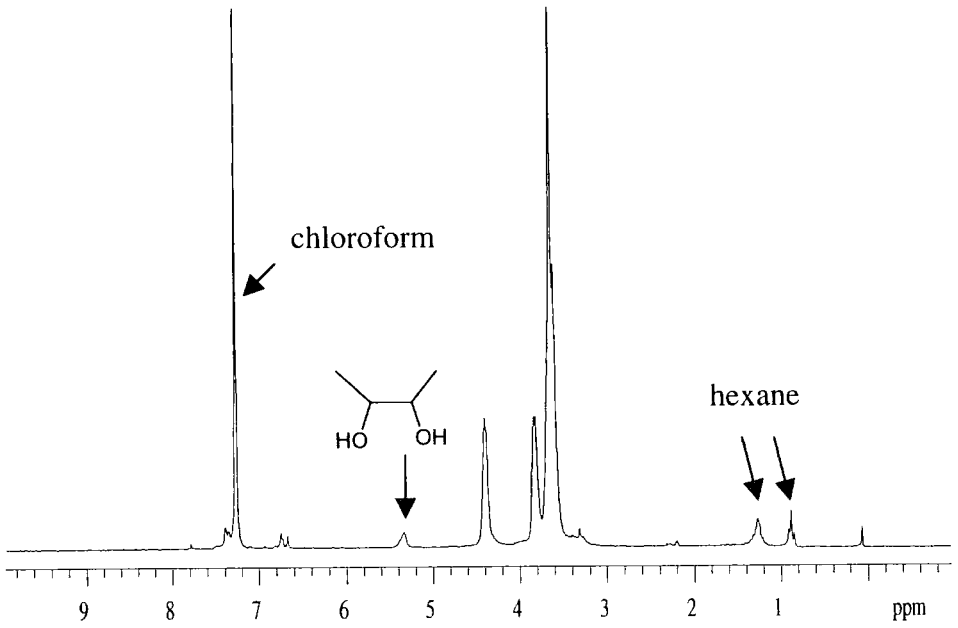

1,8-Di-(4-methly-2,3,5,6-tetrafluorophenyloxy)octane (25)

^{1}H NMR spectrum

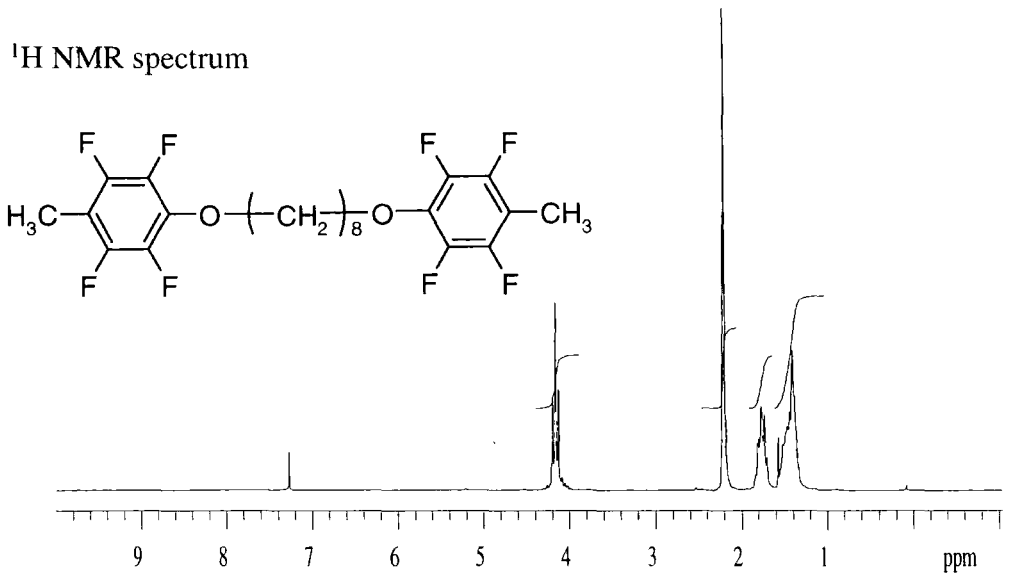

^{13}C NMR spectrum

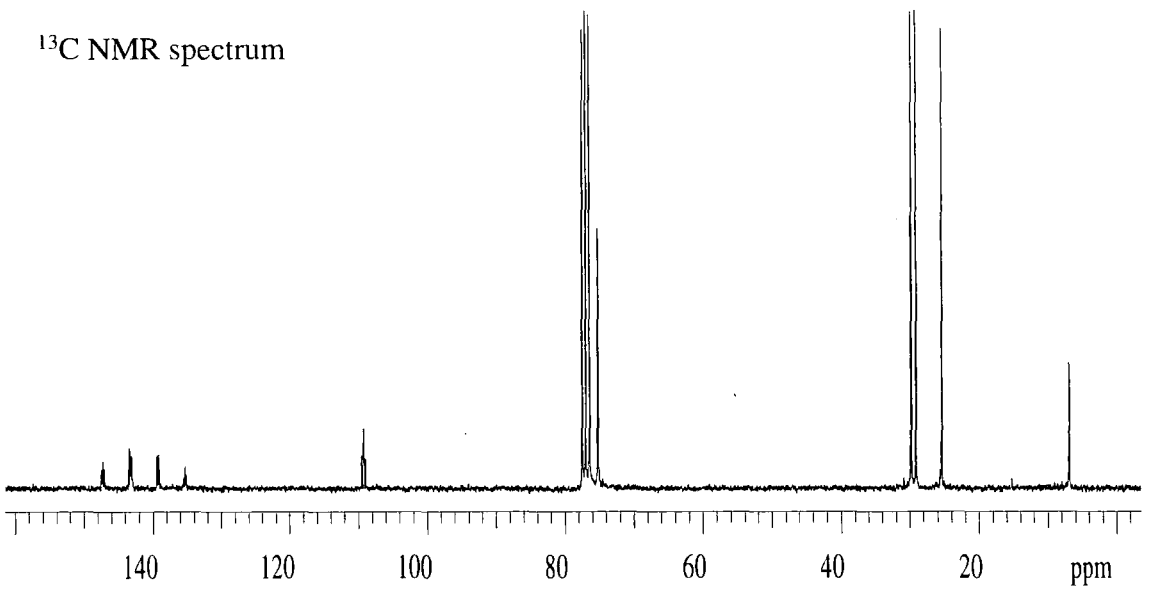

^{19}F NMR spectrum

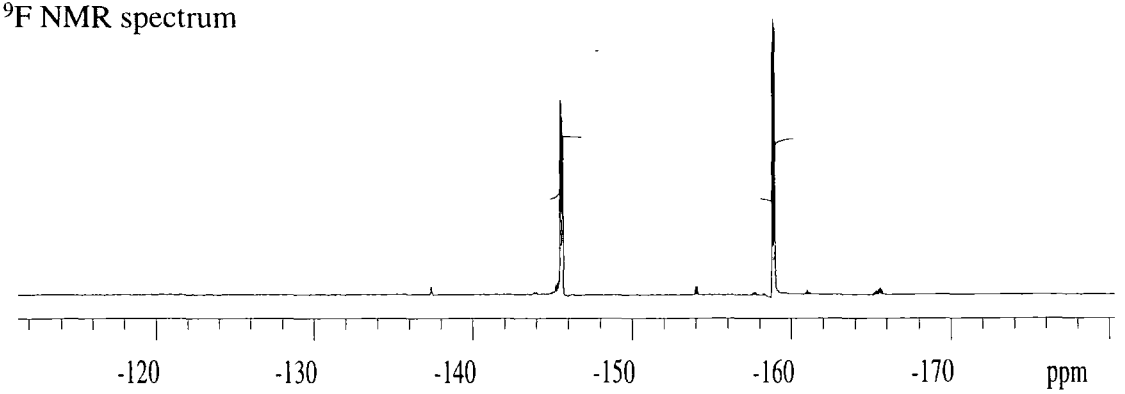

1,8-Di-(4-bromomethyl-2,3,5,6-tetrafluorophenyloxy)octane (26)

^{1}H NMR spectrum

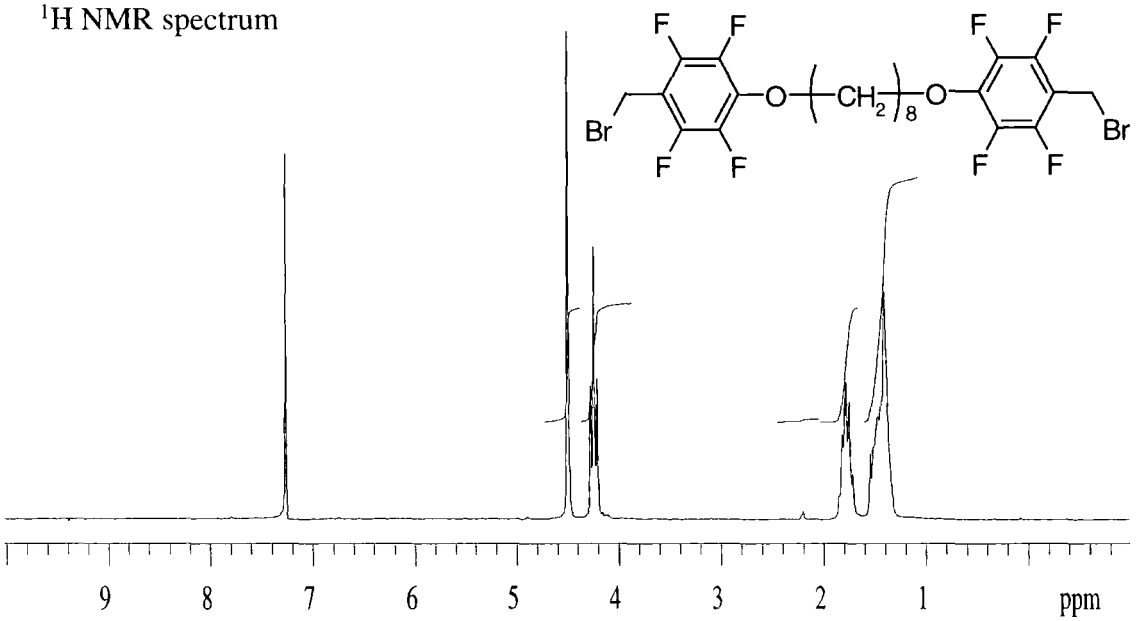

^{13}C NMR spectrum

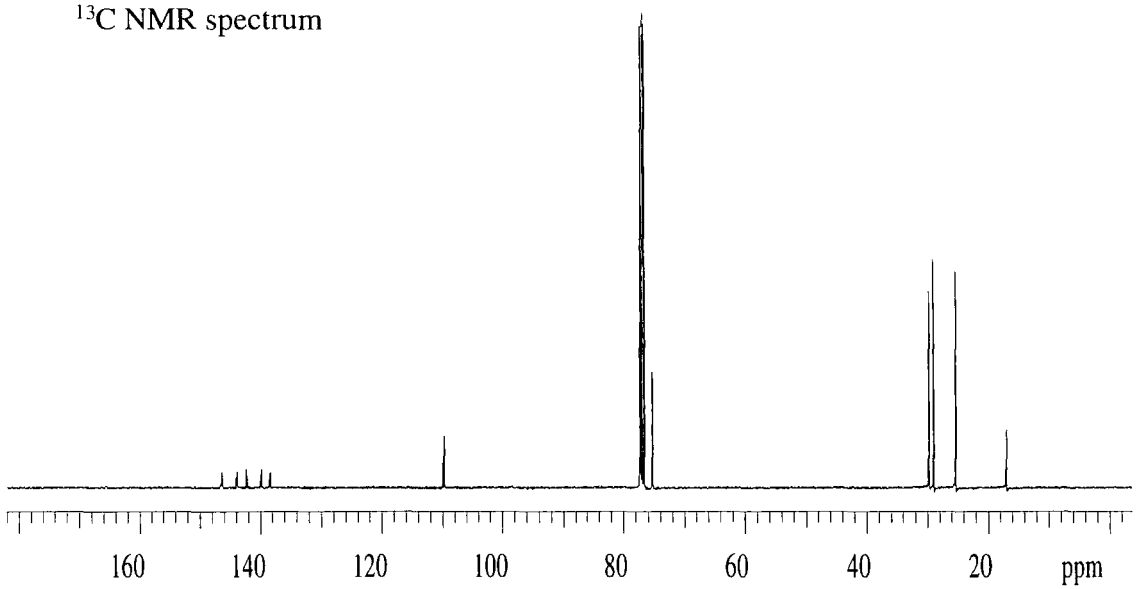

^{19}F NMR spectrum

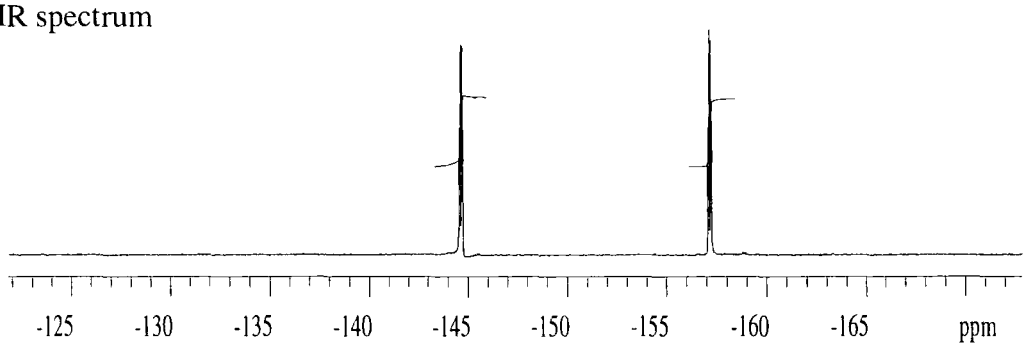

1,8-Bis-(4-triphenylphosphoniummethylen-2,3,5,6-tetrafluoro-phenyloxy) octane dibromide (**27**)

^{1}H NMR spectrum

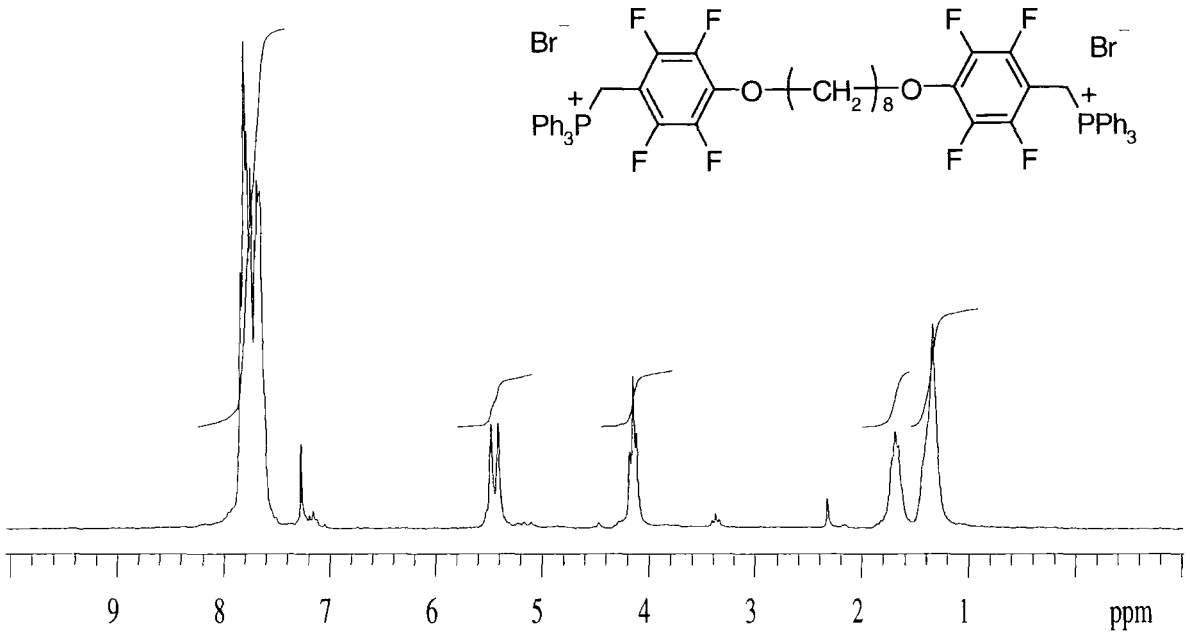

^{19}F NMR spectrum

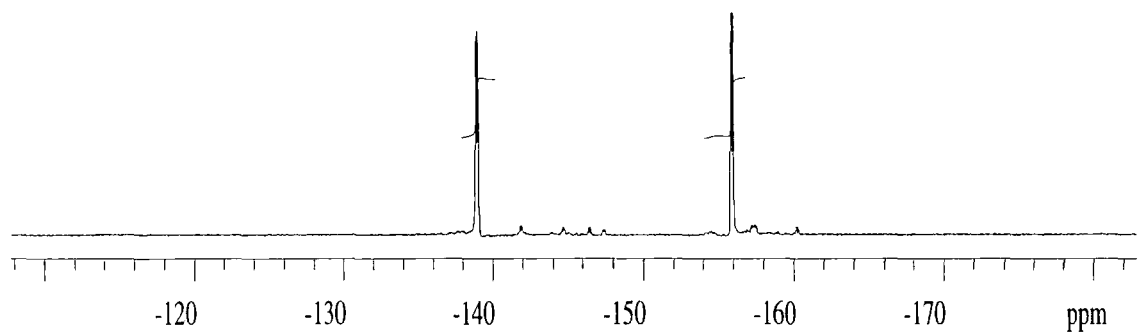

1,8-(Bis-2,3,4,5,6,2',3',4',5',6' nonafluorostilben-4-yloxy)octane (28)

^{1}H NMR spectrum

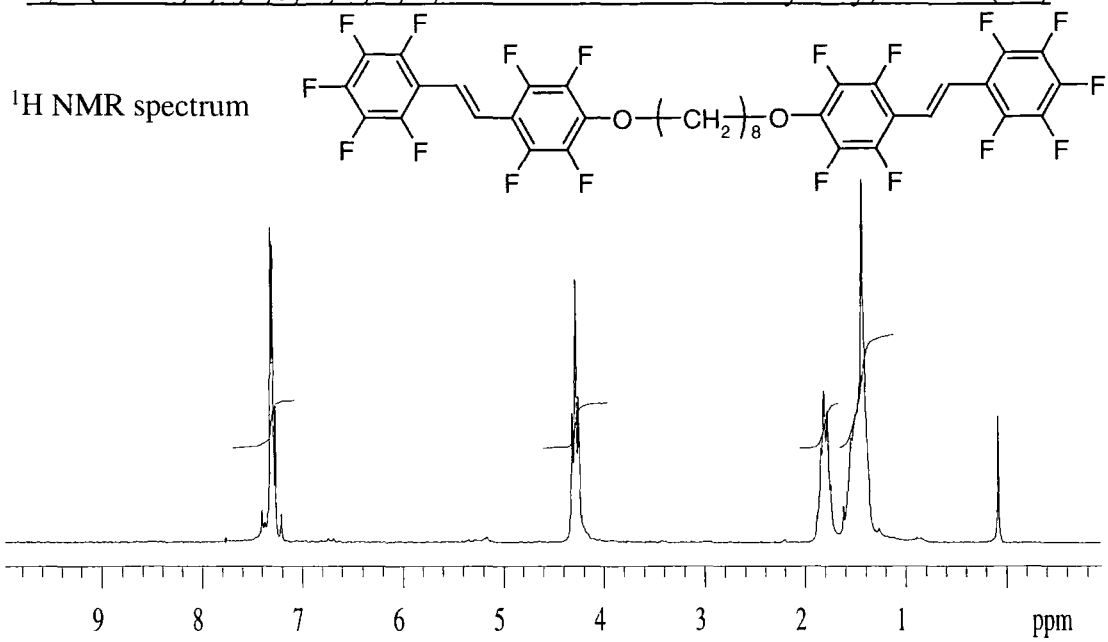

^{13}C NMR spectrum

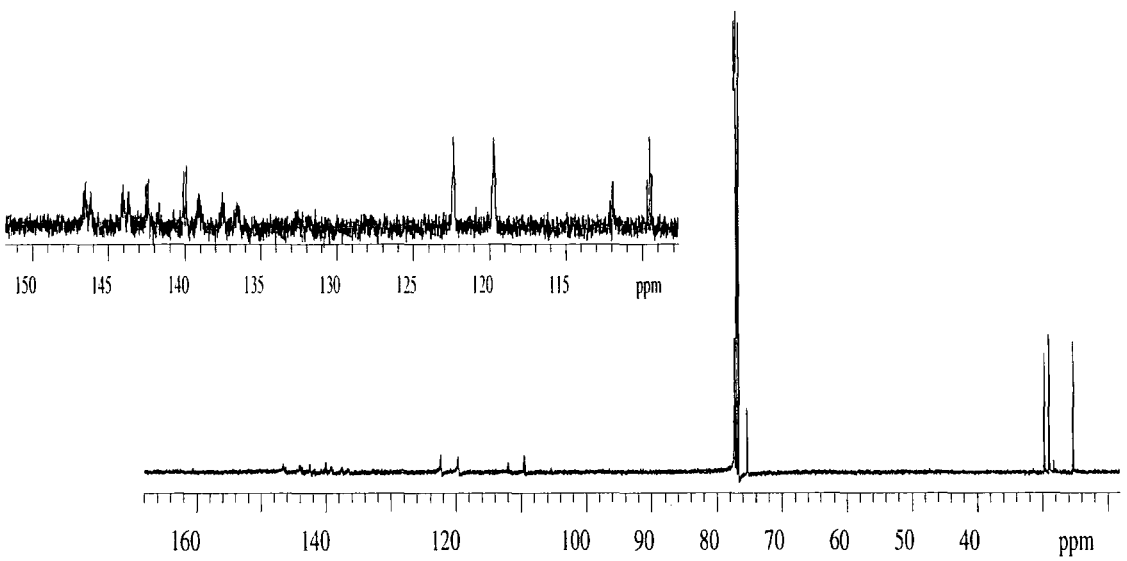

^{19}F NMR spectrum

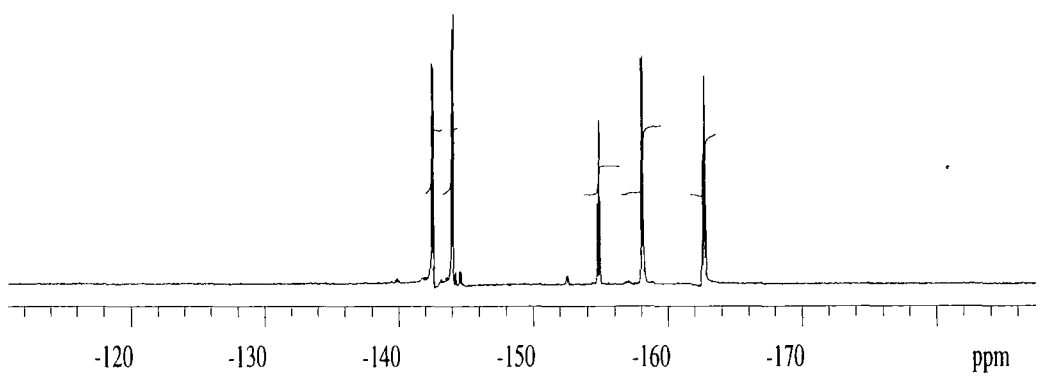

Poly(bis(2,3,5,6-tetrafluoro-p-phenylenevinylene)-2,3,5,6-tetrafluoro-p-phenylene-1,10-dioxodecane) (29)

^{1}H NMR spectrum

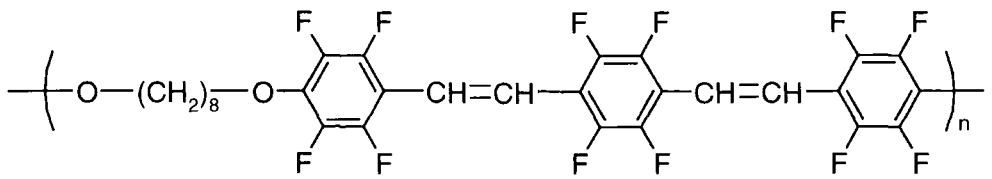

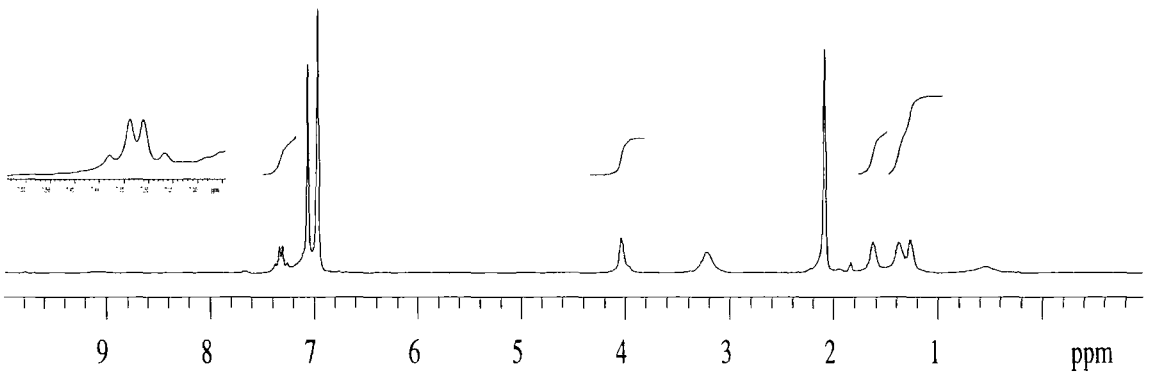

^{19}F NMR spectrum

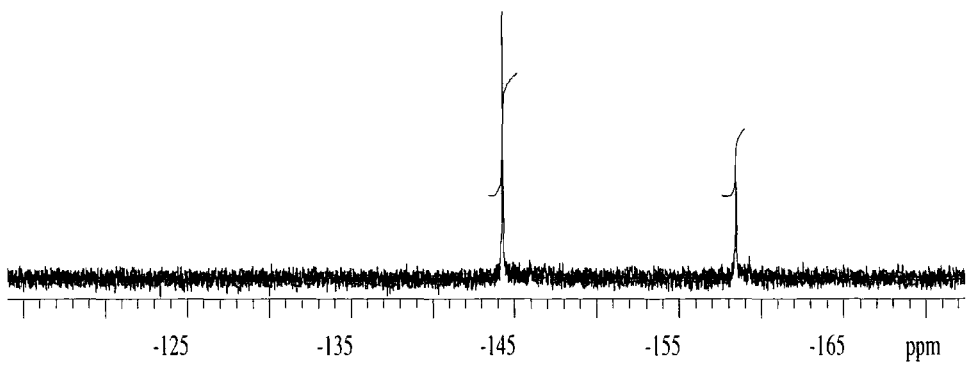

1,17- Bis(4-methly-2,3,5,6tetrafluorophenyloxy)-3,6,9,12,15-pentaoxaheptadecane (**30**)

^{1}H NMR spectrum

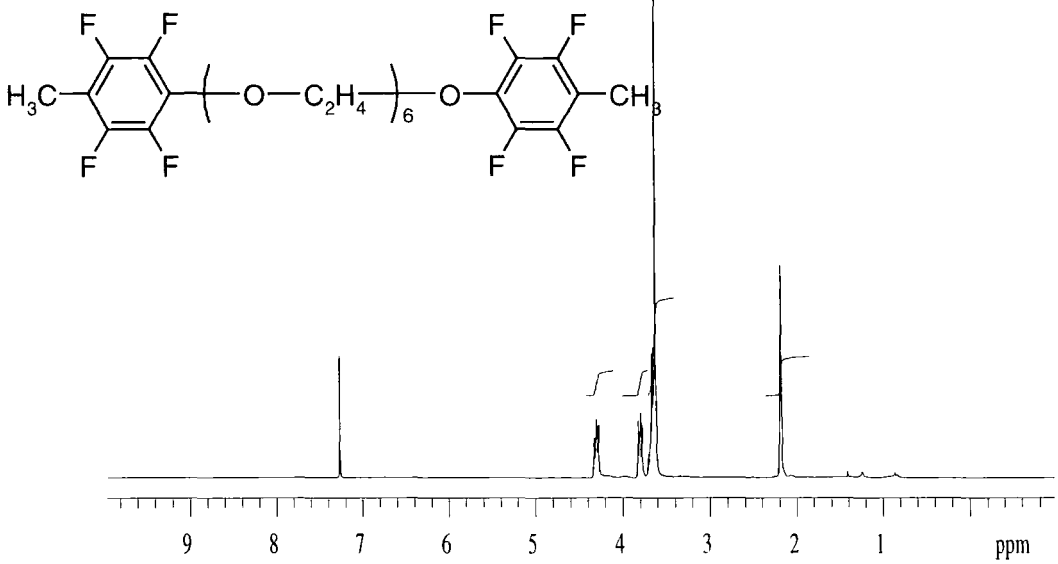

^{13}C NMR spectrum

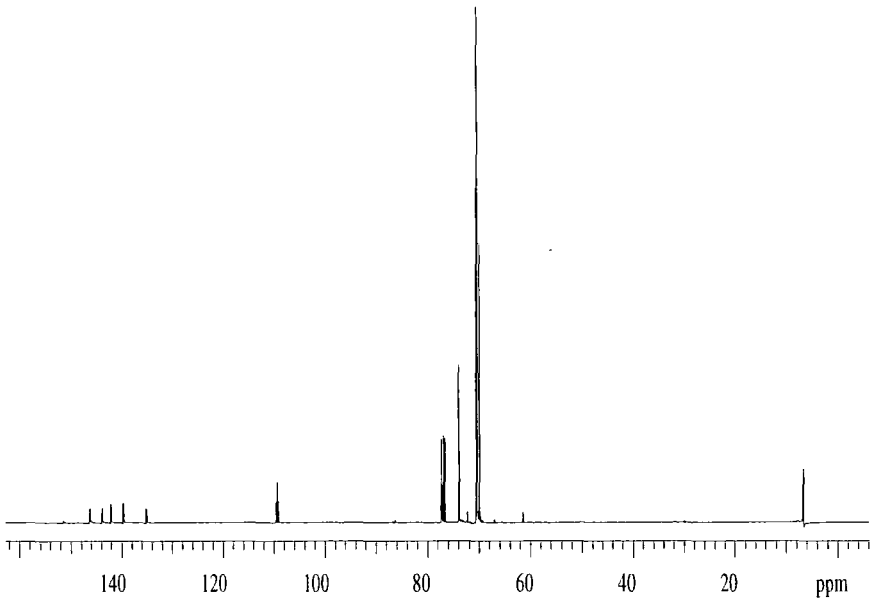

^{19}F NMR spectrum

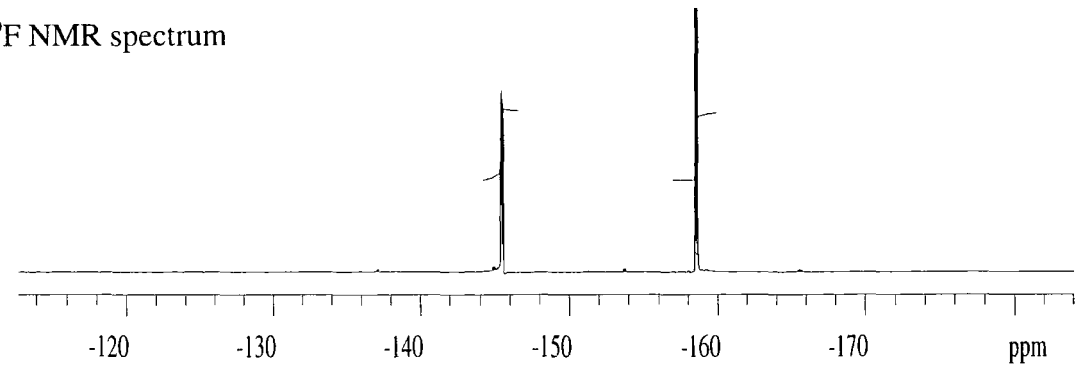

2,3,4,5-Tetrafluoroxylylen-1,4-bis(triphenylphoshomium bromide)(**32**)

^{1}H NMR spectrum

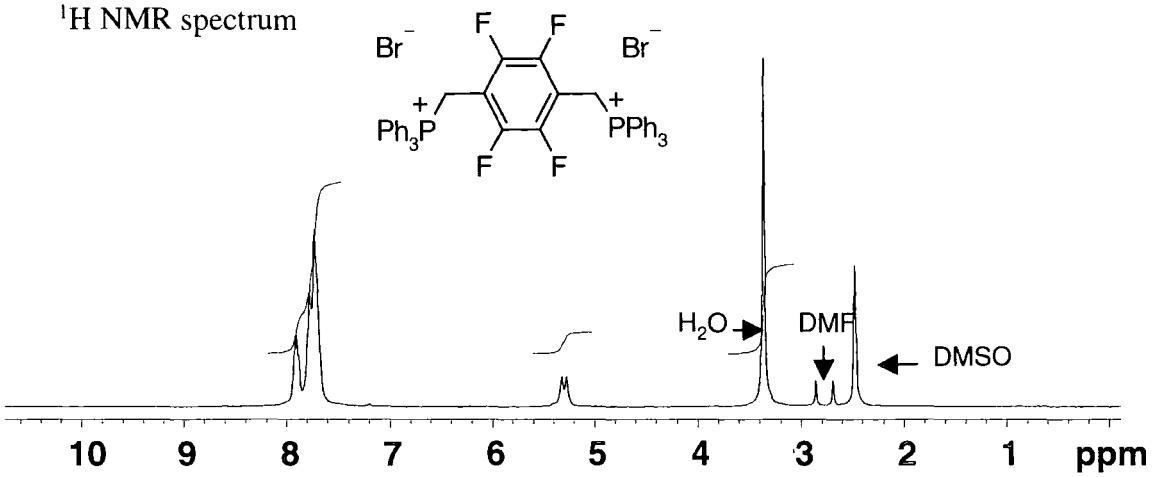

^{13}C NMR spectrum

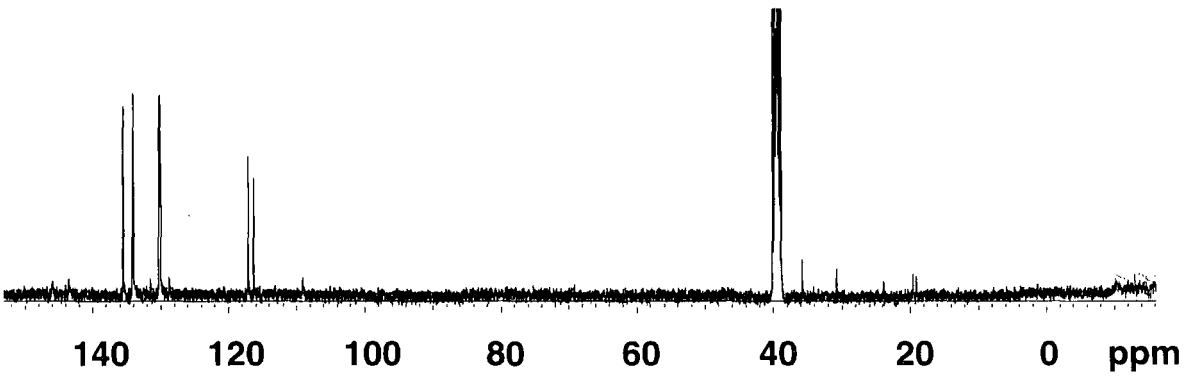

^{19}F NMR spectrum

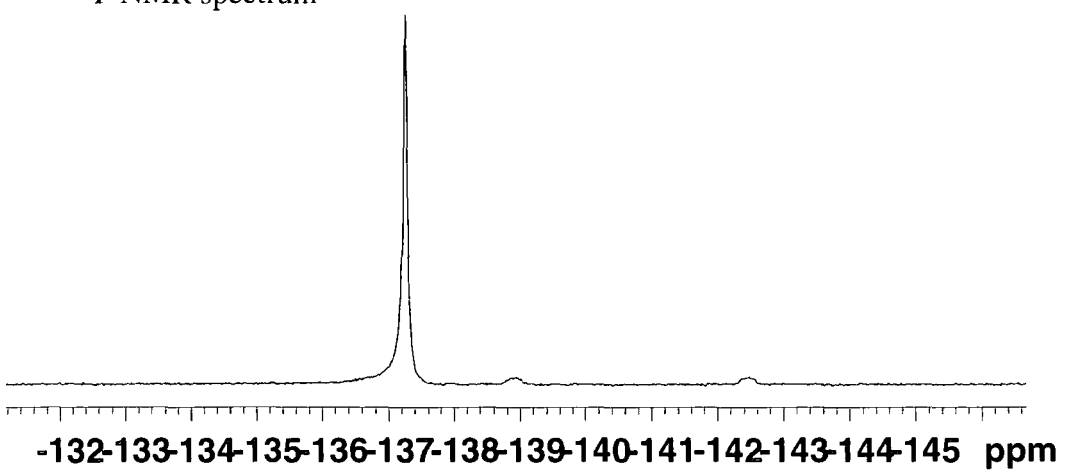

F-DSB-*block*-SEO (34)

^{1}H NMR spectrum

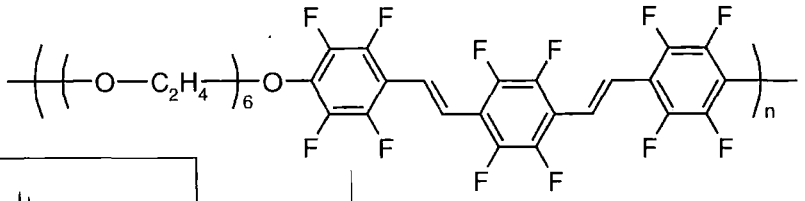

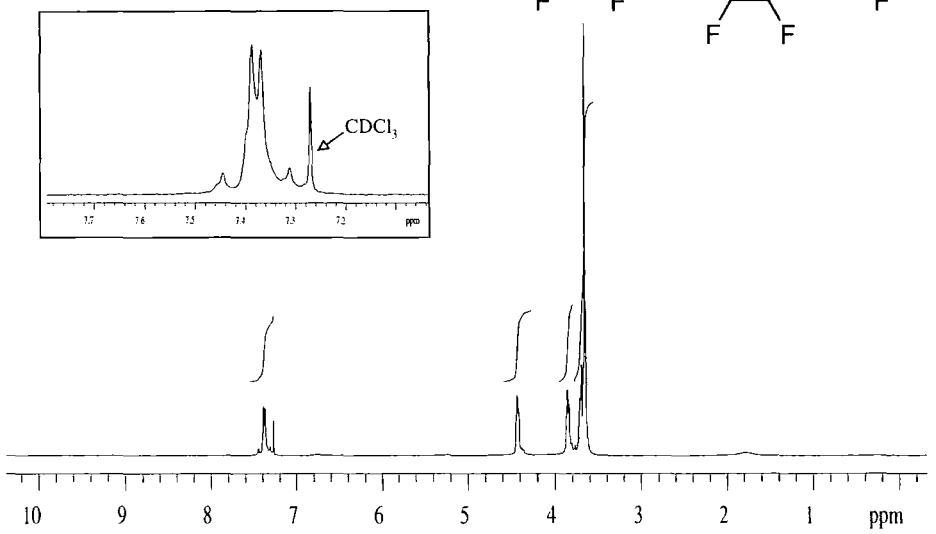

^{13}C NMR spectrum

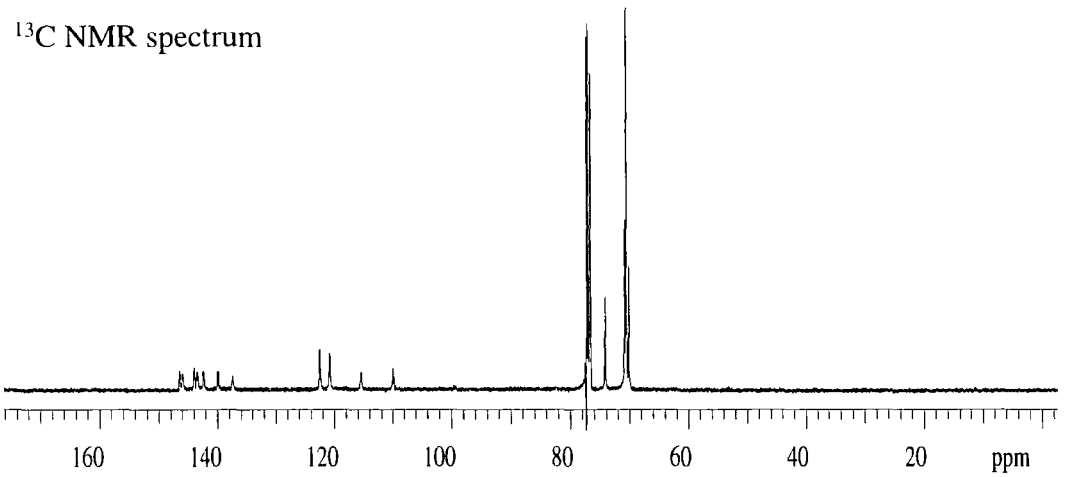

^{19}F NMR spectrum

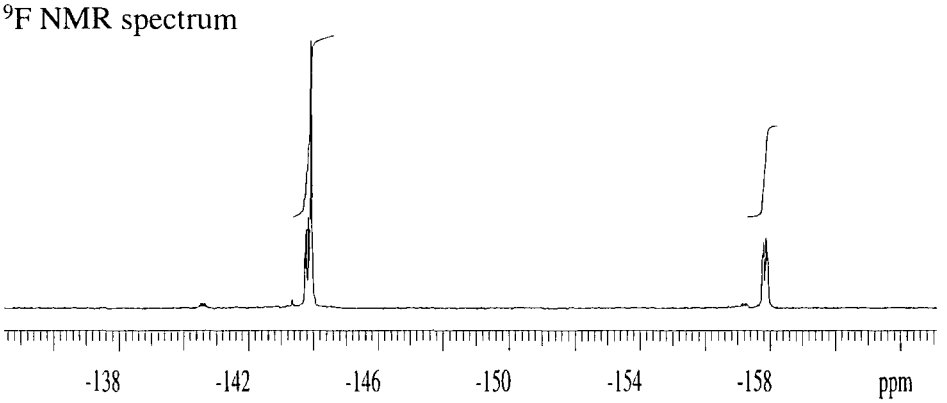

1,17-Bis (4-formylphenyloxy)-3,6,9,12,15-pentaoxaheptadecane (**37**)

^{1}H NMR spectrum

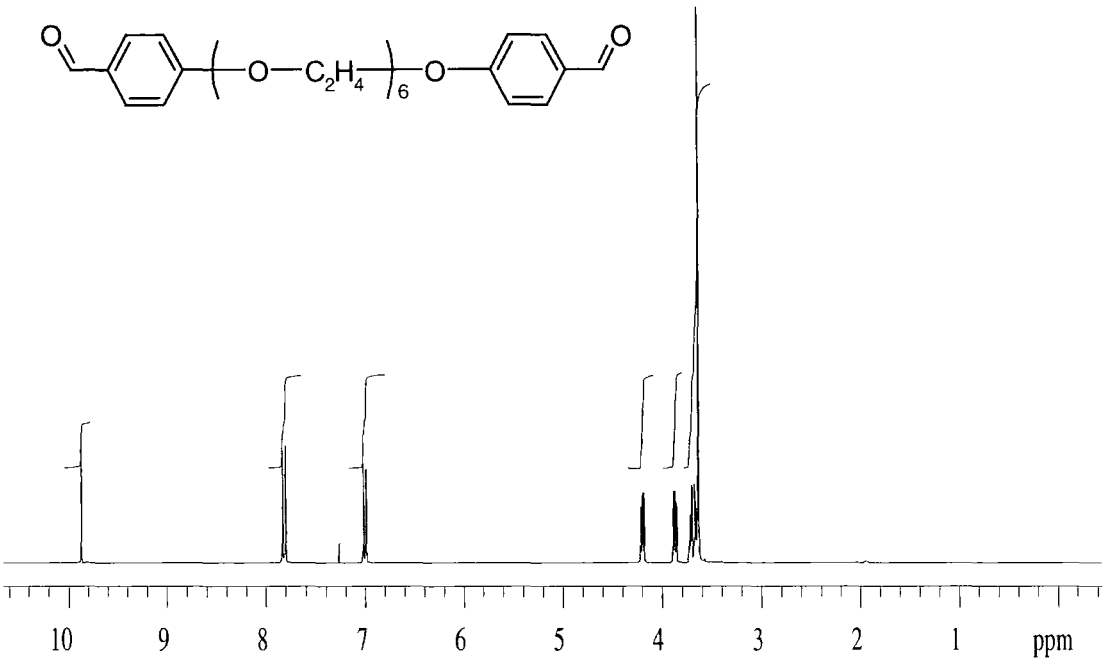

^{13}C NMR spectrum

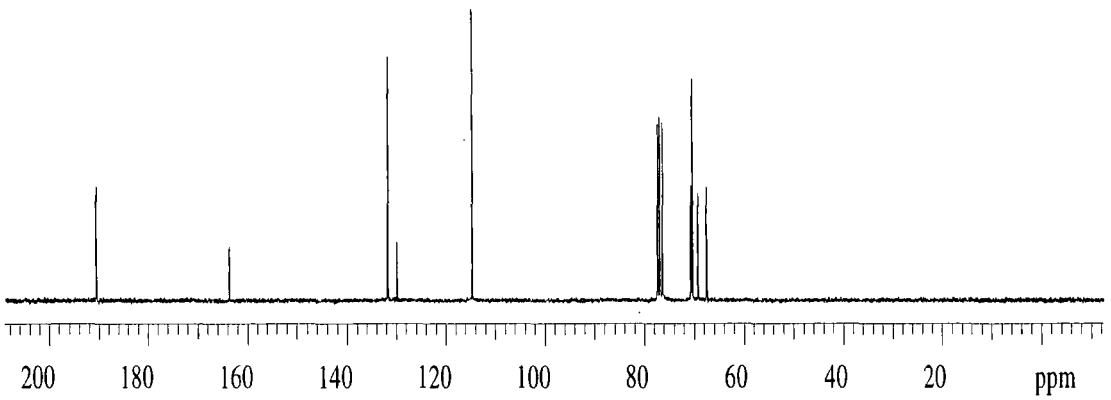

H-DSB-*block*-SEO (39)

^{1}H NMR spectrum

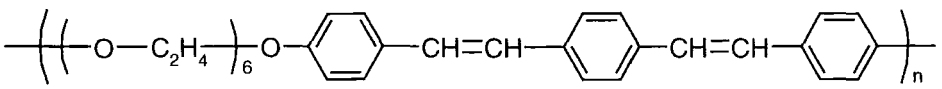

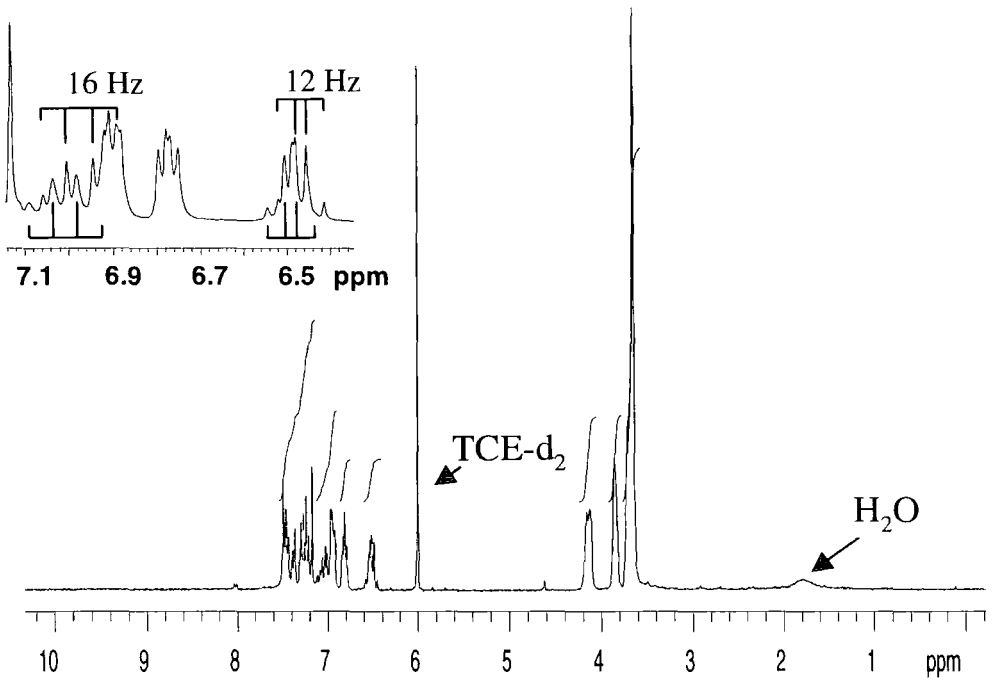

^{13}C NMR spectrum

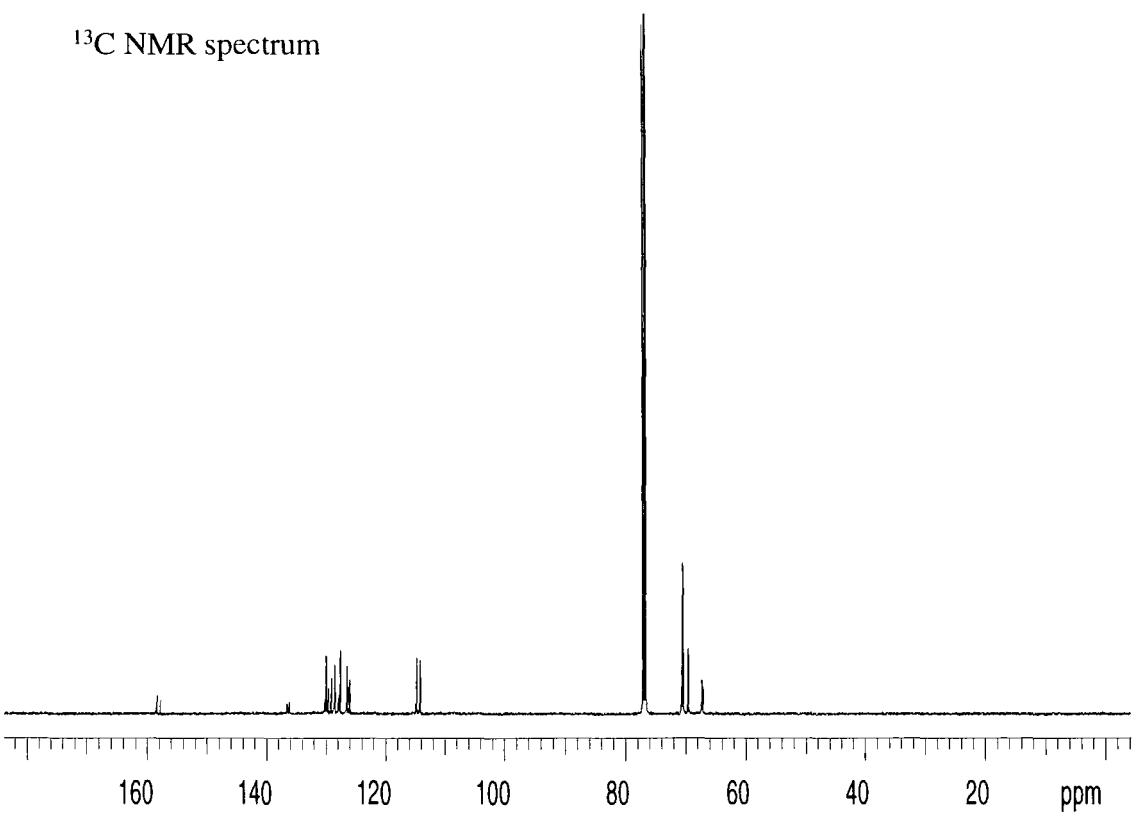

4,4'-bis(2,3,4,5,6-pentafluorostyryl)stilbene (44)

^{1}H NMR spectrum

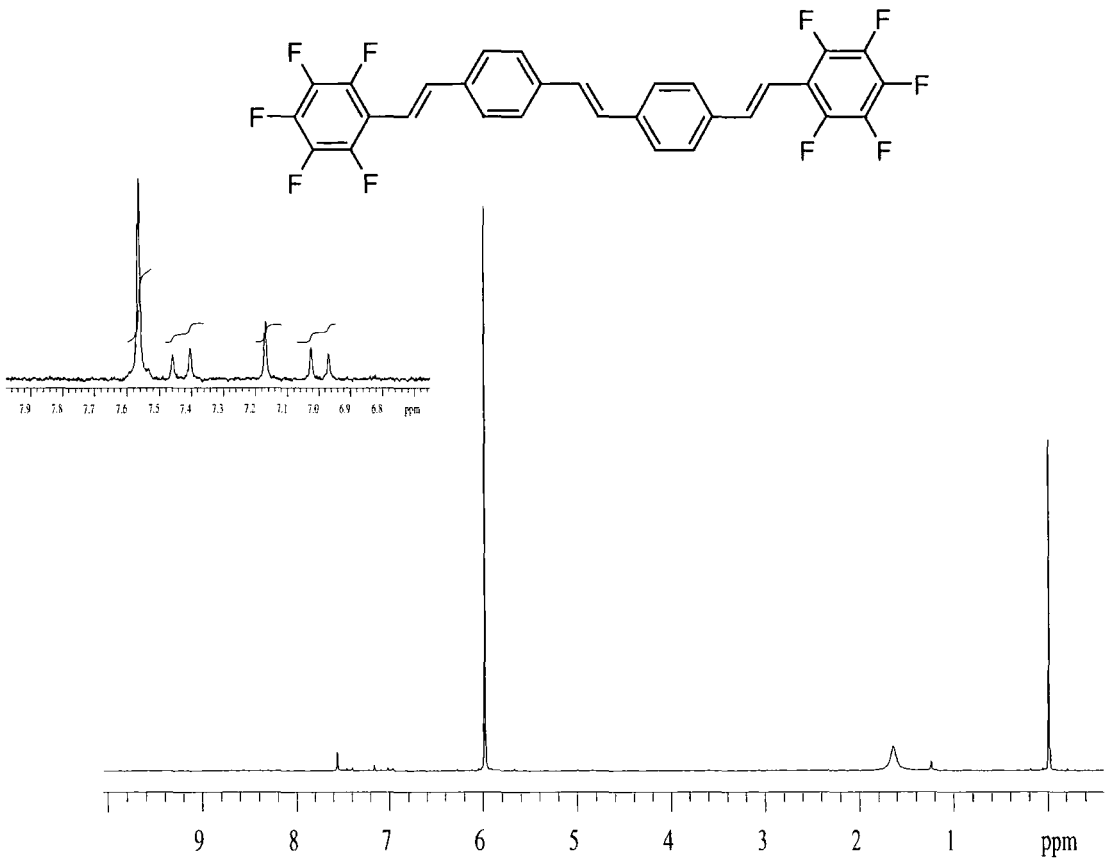

^{19}F NMR spectrum

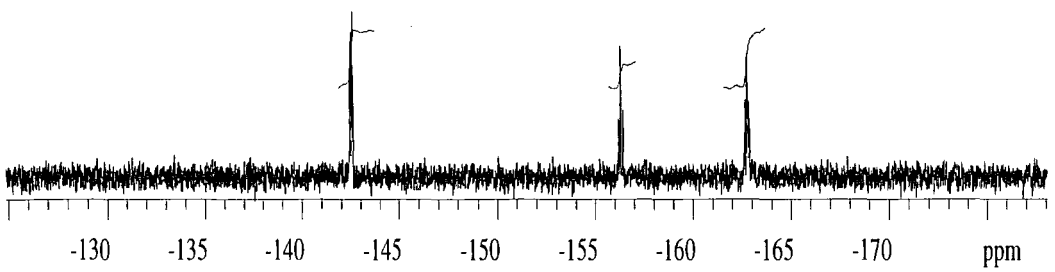

Photochemical [2+2] reaction of
4,4'-bis(2,3,4,5,6-pentafluorostyryl)stilbene (**44**)

^{1}H NMR spectrum

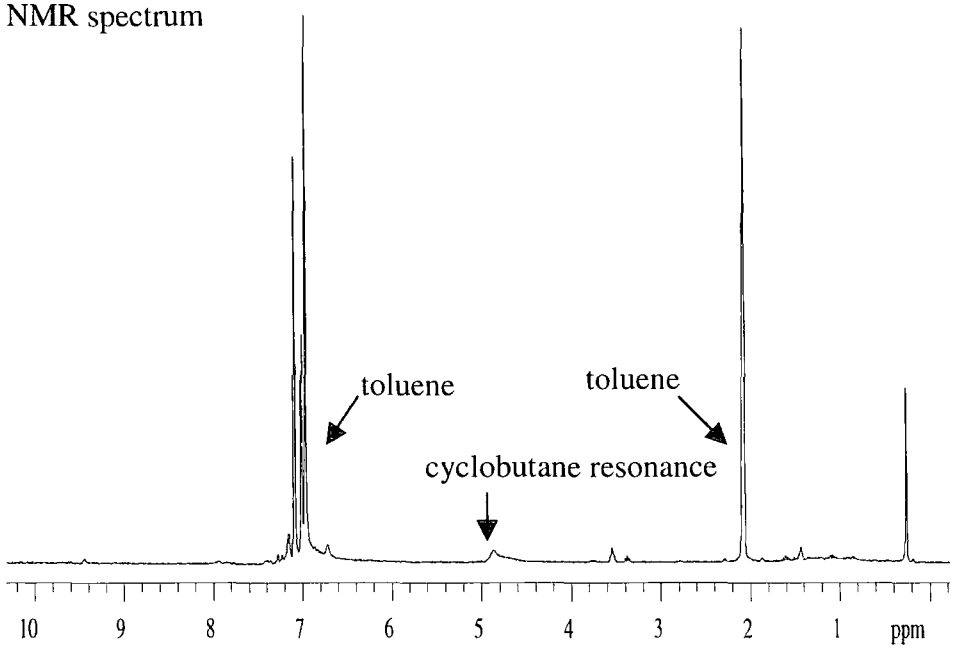

^{19}F NMR spectrum

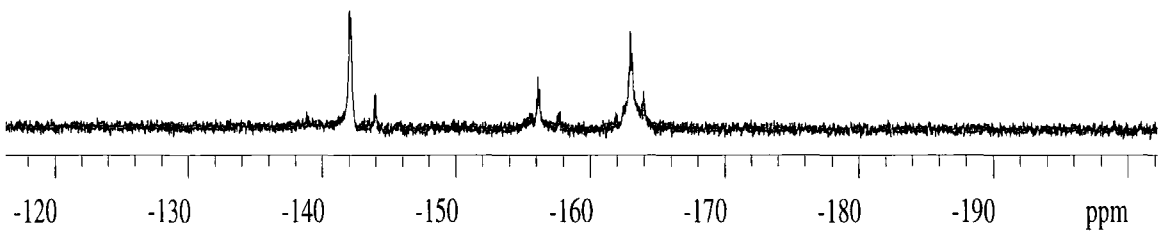

1,4-Bis(2,3,4,5,6-pentafluorostyryl)-2,3,5,6-tetrafluorobenzene (45)

^{1}H NMR spectrum

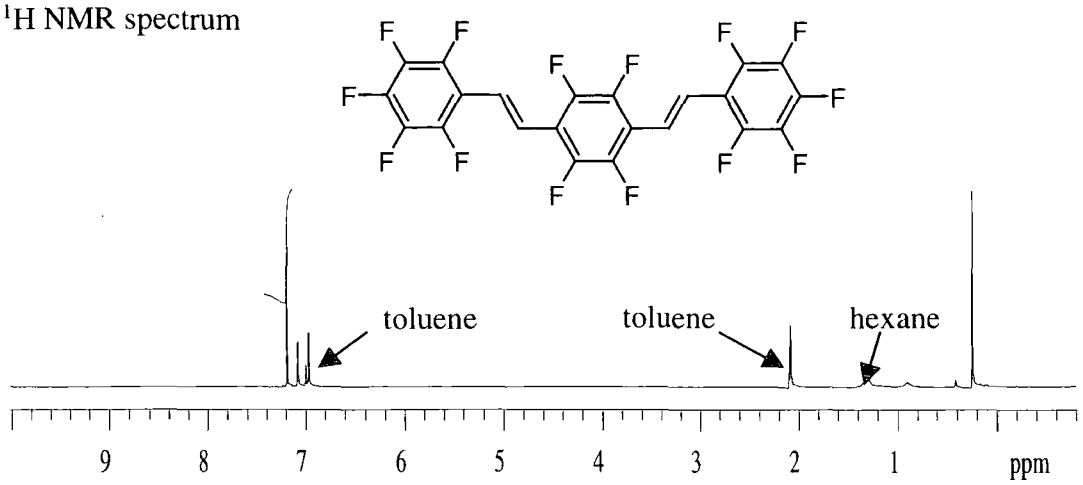

^{13}C NMR spectrum

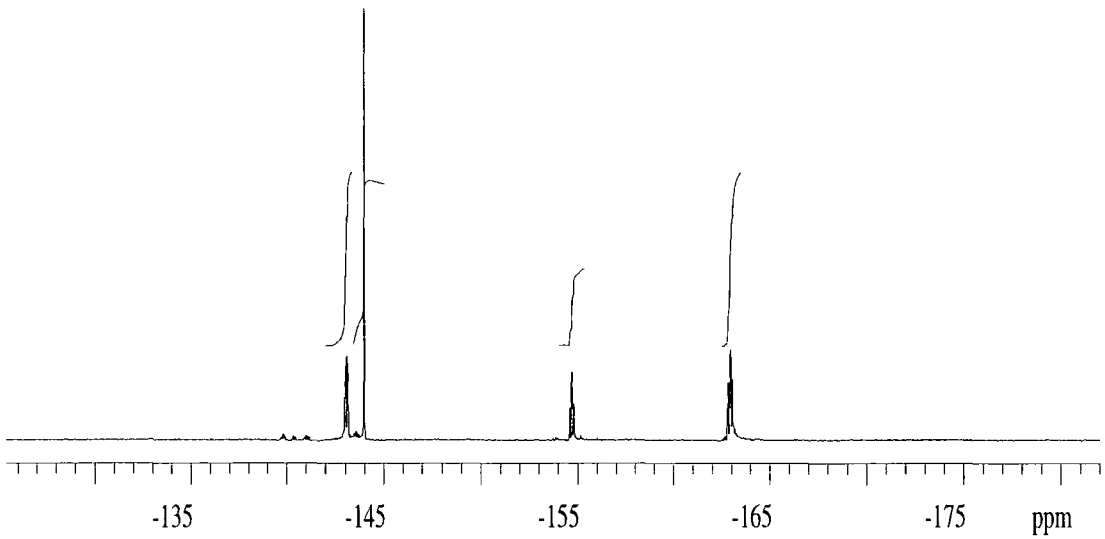

IR spectra of compounds 13 and 30.

The arrows indicate the absorption for fluorinated aromatics.

1,17- Bis(4-methly-2,3,5,6tetrafluorophenyloxy)-3,6,9,12,15-pentaoxaheptadecane (**30**)

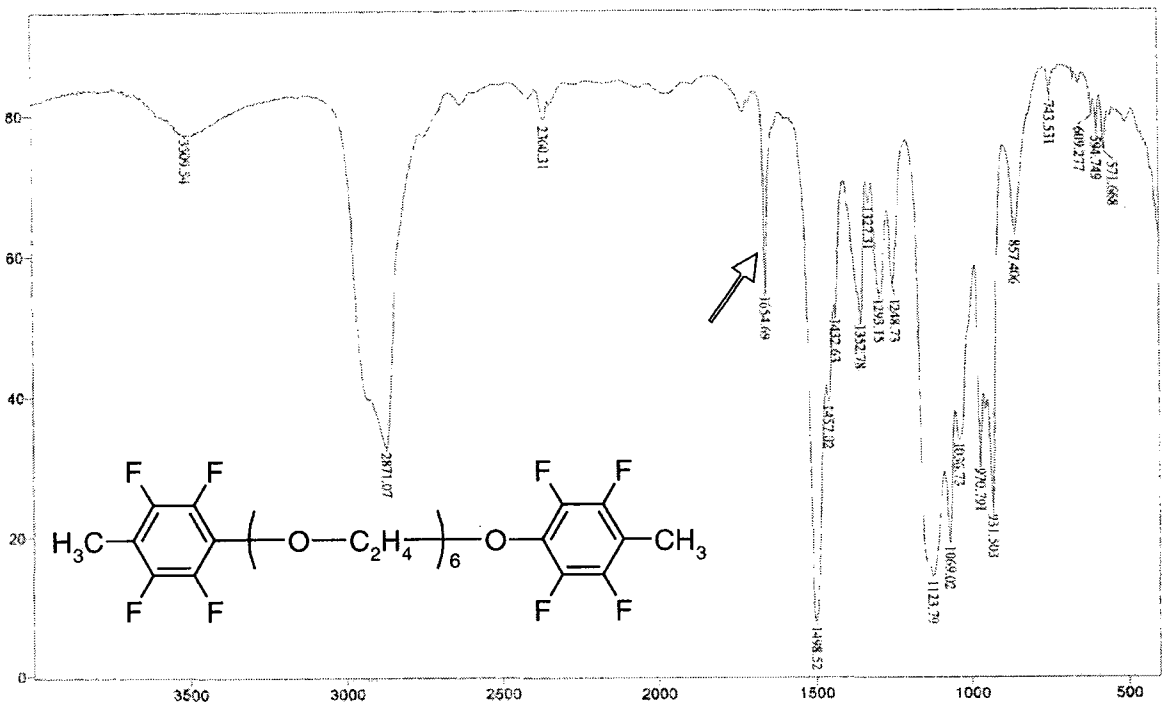

1,17-Bis(4-formyl-2,3,5,6-tetrafluorophenyloxy)-3,6,9,12,15-pentaoxaheptadecane (**13**)

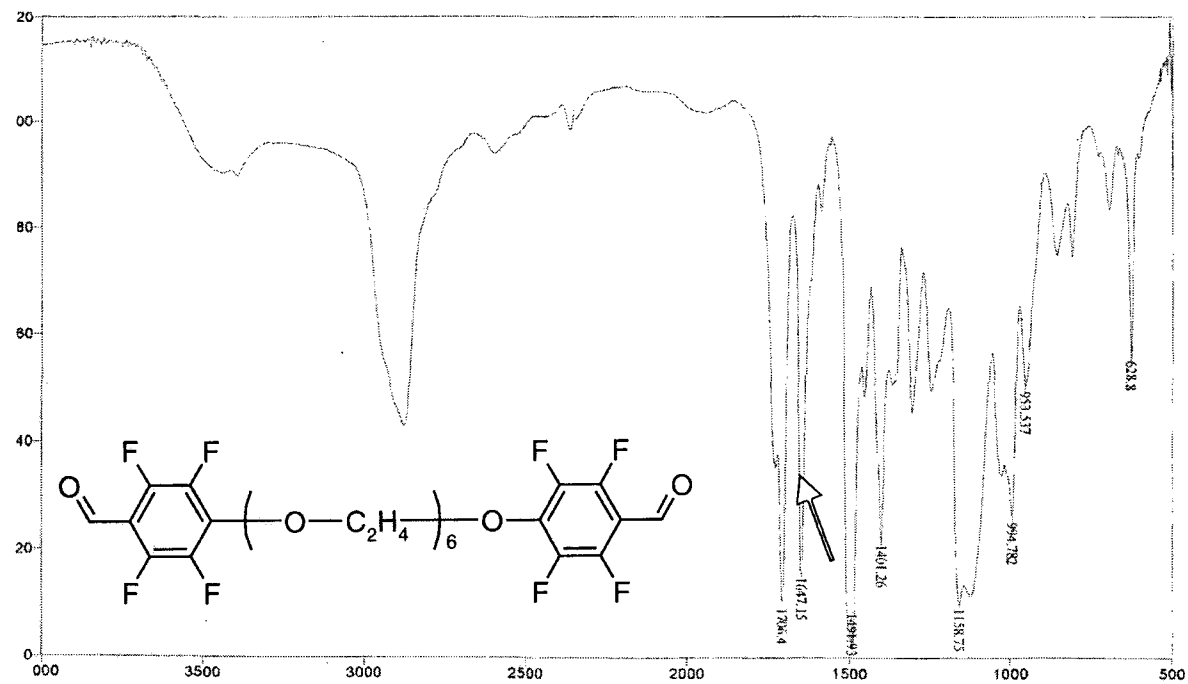

Cyclic voltammetry data

This data was recorded at Cambridge Display Technology (CDT). ITO electrodes were coated with the polymers and the oxidation potential of F-DSB-*block*-SEO *(Figure 1 left)*, H-DSB-*block*-SEO *(Figure 1 right)* and ferrocene *(Figure 2)* were recorded. The potential of ferrocene relative to the vacuum level is 5.3 V.[#] Taking into account solid state effects for the oxidation the IP of the polymers were calculated as:

IP (F-DSB-*block*-SEO) = 6.2 ± 0.1 eV and

IP (H-DSB-*block*-SEO) = 5.5 ± 0.1 eV.

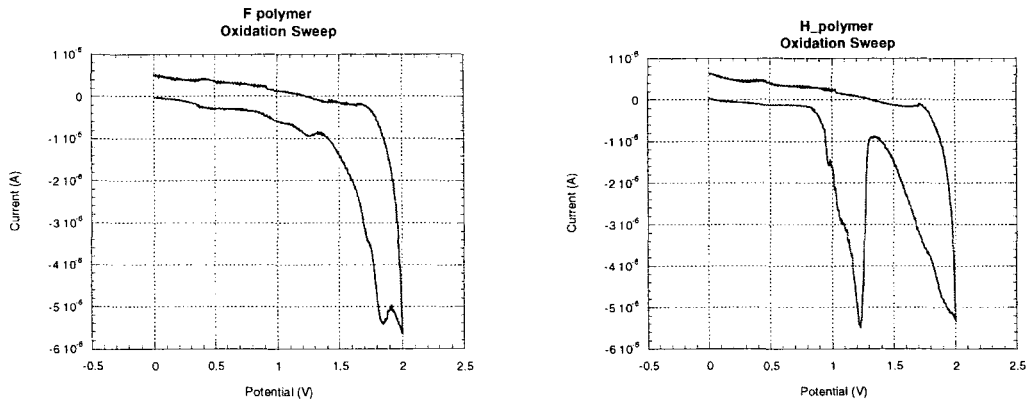

Figure 1 Cyclic voltammetry data for F-DSB-block-SEO (left) and F-DSB-block-SEO (right).

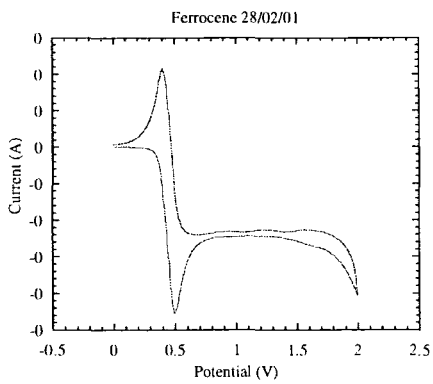

Figure 2 Cyclic voltammetry data for ferrocene.

[#] Renak, M. L.; Bartholomew, G. P.; Wang, S.; Ricatto, P.; Lachicotte, R. J.; Bazan, G. C. *J. Am. Chem. Soc.* **1999**, *121*, 7787

Peter Wilfried Lövenich, Ph.D. thesis, University of Durham, October 2001

List of compounds and abbreviations

No.	compound
2	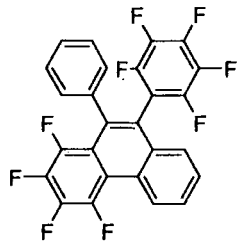
5	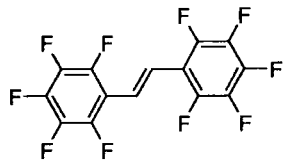
6	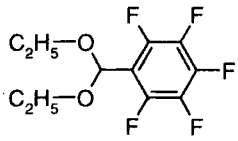
10	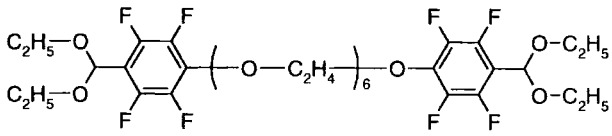
11	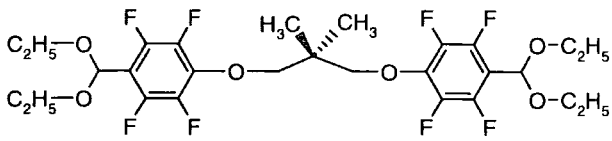
12	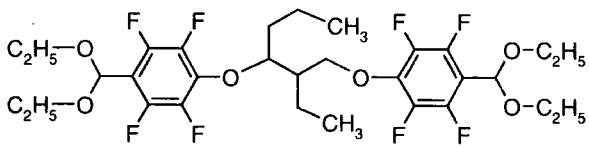
13	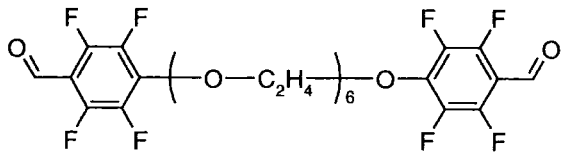
14	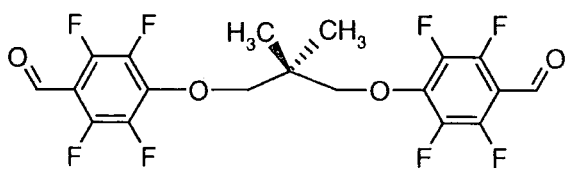
15	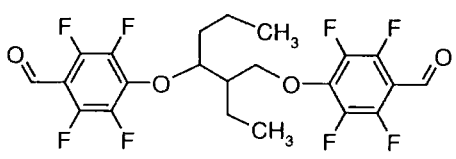

No.	compound
17	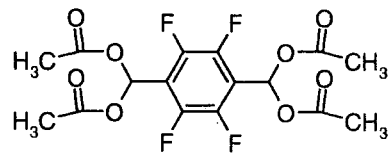
18	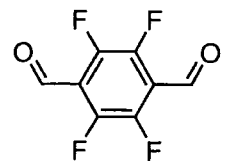
19	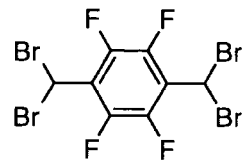
20	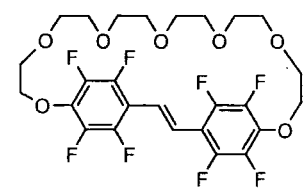
25	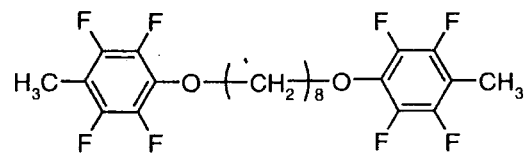
26	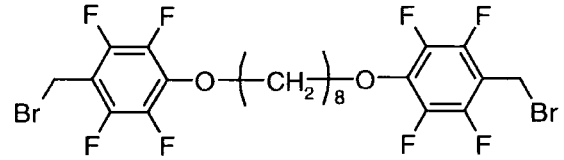
27	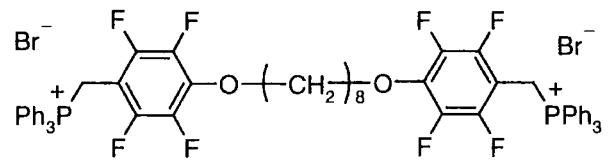
28	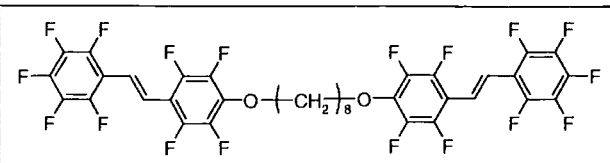
29	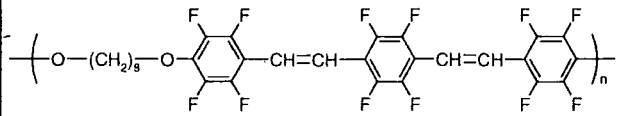

List of compounds and abbreviations

No.	compound
30	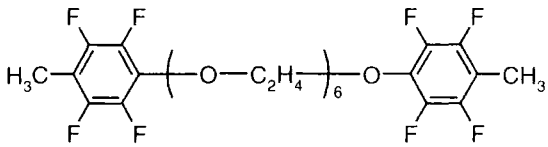
31	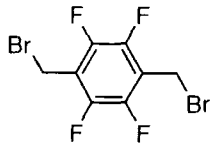
32	
33	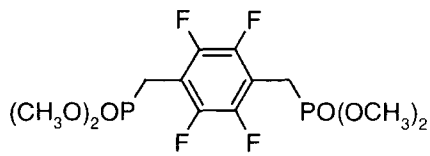
34	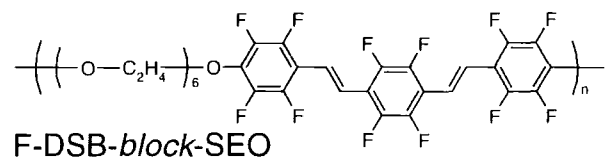 F-DSB-*block*-SEO
35	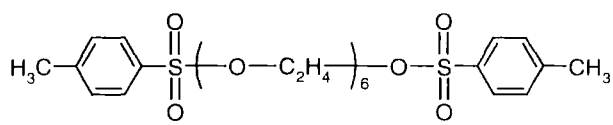
37	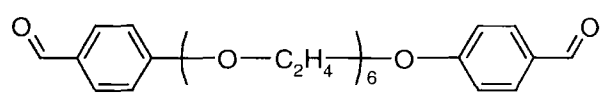

No.	compound
38	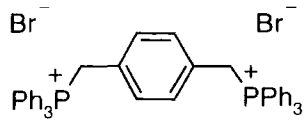
39	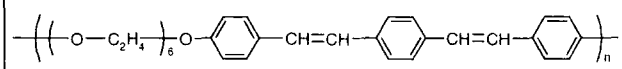 H-DSB-*block*-SEO
41	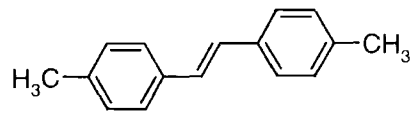
42	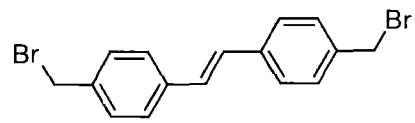
43	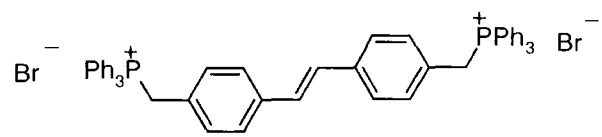
44	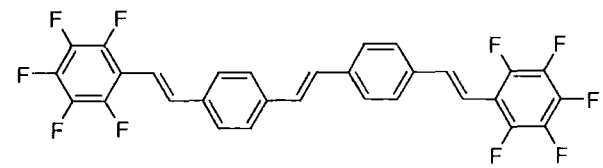
45	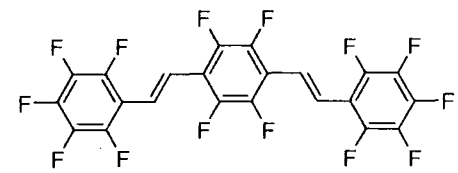

Abbreviations

AFM	atomic force microscopy
AIBN	2,2'-azobis(2-methylpropionitrile)
DCM	dichloromethane
DMF	dimethyl formamide
DSB	1,4-distyrylbenzene
DSS	4,4'-distyrylstilbene
EA	electron affinity
EI	electron impact
EL	electroluminescence
FT	Fourier transform
GC	gas chromatography
GPC	gel permeation chromatography
HOMO	highest occupied molecular orbital
IP	ionisation potential
ITO	indium tin oxide
LEC	light emitting cell
LED	light emitting diode
LUMO	lowest unoccupied molecular orbital
MS	mass spectroscopy
NBS	N-bromosuccinimide
NMR	nuclear magnetic resonance
PA	polyacetylene
PDI	polydispersity index
PEO	poly(ethylene oxide)
PFS	2,3,4,5,6-pentafluorostilbene
PL	photoluminescence
PPV	poly(*p*-phenylene vinylene)
SEO	sexi(ethylene oxide)
THF	tetrahydrofuran